VOLUME 13 (1959) No. 1

NUCLEAR PHYSICS

JOURNAL DEVOTED TO THE EXPERIMENTAL AND THEORETICAL STUDY OF THE FUNDAMENTAL CONSTITUENTS OF MATTER AND THEIR INTERACTIONS

EDITOR: L. ROSENFELD · COPENHAGEN

D. A. BROMLEY, J. A. KUEHNER and E. ALMQVIST, Mechanisms for the $O^{16}(He^3, He^4)O^{15}$ reaction 1

K. J. LE COUTEUR and D. W. LANG, Neutron evaporation and level densities in excited nuclei 32

J. E. DRAPER and A. A. FLEISCHER, Soft gamma rays from Eu^{152} and Eu^{154} following resonance neutron capture 53

B. V. GESHKENBEIN, S. A. NEMIROVSKAYA and A. P. RUDIK, β-decay of RaE . 60

N. NATH, M. A. ROTHMAN, D. M. VAN PATTER and C. E. MANDEVILLE, Inelastic neutron scattering in Mn^{55} 74

C. S. KHURANA and H. S. HANS, Measurements of (n, p), (n, α) and (n, 2n) total cross sections at 14 MeV 88

E. C. CAMPBELL et P. F. FETTWEIS, Mise en évidence de quelques nouveaux états isomériques 92

V. K. RASMUSSEN, F. R. METZGER and C. P. SWANN, Mean life of the first excited state of Na^{23} 95

MARCOS MOSHINSKY, Transformation brackets for harmonic oscillator functions 104

V. I. GOLDANSKY and M. V. KAZARNOVSKY, Intrashell-interaction levels and their excitation by multicharged ions 117

L. COHEN and J. B. WILLIS, Alpha-particle S-state binding energy 125

D. B. FAIRLIE and J. C. POLKINGHORNE, Unstable states and the separable potential model 132

(continued on p. 3 of cover)

NORTH-HOLLAND PUBLISHING COMPANY-AMSTERDAM

October (1) 1959

EDITORIAL BOARD

AUSTRALIA & NEW ZEALAND:	H. Messel (Sydney), M. L. Oliphant (Canberra)
AUSTRIA:	B. Karlik, (Vienna), H. Thirring (Vienna)
BELGIUM:	M. de Hemptinne (Louvain), J. Verhaeghe (Ghent)
CANADA:	G. Volkoff (Vancouver)
DENMARK:	C. Møller (Copenhagen), S. Rozental (Copenhagen)
FINLAND:	L. Simons (Helsinki)
FRANCE:	A. Berthelot (Saclay), S. Gorodetzky (Strasbourg)
GERMANY (DEM. REP.):	G. Hertz (Leipzig)
GERMANY (FED. REP.):	W. Gentner (Freiburg i. B.), J. H. D. Jensen (Heidelberg)
GREAT BRITAIN:	S. Devons (Manchester), T. H. R. Skyrme (Harwell)
HUNGARY:	L. Janossy (Budapest)
INDIA:	H. Bhabha (Bombay), R. Ramanna (Trombay)
IRISH REPUBLIC:	J. McConnell (Maynooth)
ISRAEL:	G. Racah (Jerusalem)
ITALY:	E. Amaldi (Rome)
JAPAN:	S. Kikuchi (Tokyo), S. Tomonaga (Tokyo)
MEXICO:	M. Moshinsky (Mexico)
NETHERLANDS:	H. Brinkman (Groningen), S. R. de Groot (Leiden)
NORWAY:	E. Hylleraas (Oslo), A. Lundby (Oslo), H. Wergeland (Trondheim)
POLAND:	L. Infeld (Warsaw)
PORTUGAL:	J. M. Araújo (Porto), J. R. de Almeida Santos (Coimbra)
SOUTH AMERICA:	G. Beck (Saõ Paulo), J. Leite Lopes (Rio de Janeiro)
SPAIN:	J. M. Otero (Madrid), C. Sanchez del Rio (Madrid)
SWEDEN:	O. Klein (Stockholm), K. Siegbahn (Uppsala), I. Waller (Uppsala)
SWITZERLAND:	P. Huber (Basel), P. Scherrer (Zürich)
U.A.R. & ARAB COUNTRIES:	F. El Bedewi (Alexandria), M. G. Nooh (Cairo)
U.S.A.	H. H. Barschall (Madison, Wisconsin), V. Weisskopf (Cambridge, Mass.)
U.S.S.R.:	M. A. Markov (Moscow), I. S. Shapiro (Moscow), D. V. Skobeltzyn (Moscow)
YUGOSLAVIA:	I. Supek (Zagreb)

CONTRIBUTIONS may be sent to the Editor, Professor L. Rosenfeld, NORDITA, Blegdamsvej 17, Copenhagen Ø, either directly, or preferably through the intermediary of one of the members of the Editorial Board of the country or region in which the author is working. They may be written in English, French or German.

NUCLEAR PHYSICS is published in fortnightly issues. The subscription price per volume of 700 pages is fl 57.00; 114s; $ 15.00. Post-free.

SUBSCRIPTIONS should be sent to the publishers, NORTH-HOLLAND PUBLISHING COMPANY, P.O.Box 103, Amsterdam or to any subscription-agent.

BOOKS FOR REVIEW should be sent to Professor Rosenfeld.

No part of this issue may be reproduced in any form, by print, photoprint, microfilm or any other means without written permission from the publisher. Reprints, photoprints or microfilms are obtainable at cost from the publisher.

Printed in the Netherlands

APPEAL TO CONTRIBUTORS

Many manuscripts are received, especially from the United States, which, while being very carefully typed, do not conform to the typographical and other conventions adopted in this journal. The preparation of these manuscripts for the press entails considerable work for the editorial office. In particular, when no discrimination is made between footnotes and references, the latter have to be re-numbered and re-typed. Also, figures have sometimes to be re-drawn because the labelling contains incorrect unit symbols. The effort made by the authors and their typists to produce neat manuscripts is thus frustrated. This regrettable situation would be easily remedied if the authors would take the slight trouble of conforming to the conventions of the journal and give corresponding instructions to their typists. Sheets containing full Instructions to Contributors are available on request from the publisher or the members of the Editorial Board. Moreover, any issue of the journal gives ample evidence about the details of presentation.

It is superfluous to add that the present appeal is also directed to those contributors who send in manuscripts paying no regard to any style of presentation.

2.C *Nuclear Physics* **13** (1959) 1—31; © *North-Holland Publishing Co., Amsterdam*
Not to be reproduced by photoprint or microfilm without written permission from the publishe

MECHANISMS FOR THE $O^{16}(He^3, He^4)O^{15}$ REACTION

D. A. BROMLEY, J. A. KUEHNER, and E. ALMQVIST
Atomic Energy of Canada Ltd, Chalk River Ontario

Received 3 June 1959

Abstract: Excitation curves for the $O^{16}(He^3\alpha)O^{15}$ and $O^{16}(He^3p)F^{18}$ reactions show pronounced resonance structure in the He^3 energy range from 2.0 to 3.0 MeV. It has been demonstrated that the energy dependence of the alpha particle angular distribution coefficients in the region of the strongest resonance structure requires interference between compound states with angular momentum $\frac{1}{2}$ and $\frac{3}{2}$ and like parity at excitations of 10.44 and 10.46 MeV in Ne^{19}. Total and partial widths for both resonances have been extracted from the data; the He^3 partial width of the $\frac{1}{2}$ resonance is 67 % of the single particle limit. In fitting the experimental data it has been necessary to include the energy dependence of the resonance parameters. Alpha particle angular distributions measured between resonances, in contrast, indicate a direct interaction mechanism for the reaction. A small, relatively constant direct interaction reaction amplitude and a markedly energy dependent compound system amplitude which is dominant in the vicinity of compound system resonances are suggested by these measurements. An upper limit of 0.8 μb has been established for the He^3 capture cross section proceeding through the $\frac{1}{2}$ resonance.

1. Introduction

During the past five years, He^3 induced reactions on many of the light elements have been investigated in a number of laboratories [1]). In contrast to the case of deuteron induced reactions where a direct interaction mechanism has been shown to play a dominant role even at very low incident energies, in the He^3 induced reaction studies no clear picture of the mechanism or mechanisms involved has emerged. A priori it might have been anticipated that $(He^3\alpha)$ and (He^3d) reactions, for example, should be quite similar in their characteristics to the well known (pd) and (dp) pick-up and stripping reactions [2]). The angular momentum coupling situation in (He^3n) and (He^3p) reactions is appreciably more complex since the internal momenta of the transferred pair of nucleons is not uniquely defined. The experimental results currently available at incident He^3 energies less than ≈ 5 MeV suggest that the latter reactions proceed predominantly via a compound system mechanism but with appreciable non-compound amplitudes as well, whereas for incident energies > 5 MeV the non-compound amplitudes dominate the reactions.

Although conceptually simpler, the $(He^3\alpha)$ and (He^3d) reactions have received relatively little experimental study, reflecting the technical diffi-

culties involved in resolving the alpha and deuteron groups of interest from a high background of higher energy protons, of neutrons and of gamma radiation. The reaction $C^{13}(He^3\alpha)C^{12}$ which was investigated in detail by Holmgren *et al.* [3]) at incident energies of 2.0 and 4.5 MeV is a particularly favorable case having a high Q value (15.62 MeV) and a relatively high cross section. The results obtained by these authors showed very pronounced structure in the angular distributions suggestive of direct interaction; Owen and Madansky [5, 6]) have subsequently been extremely successful in

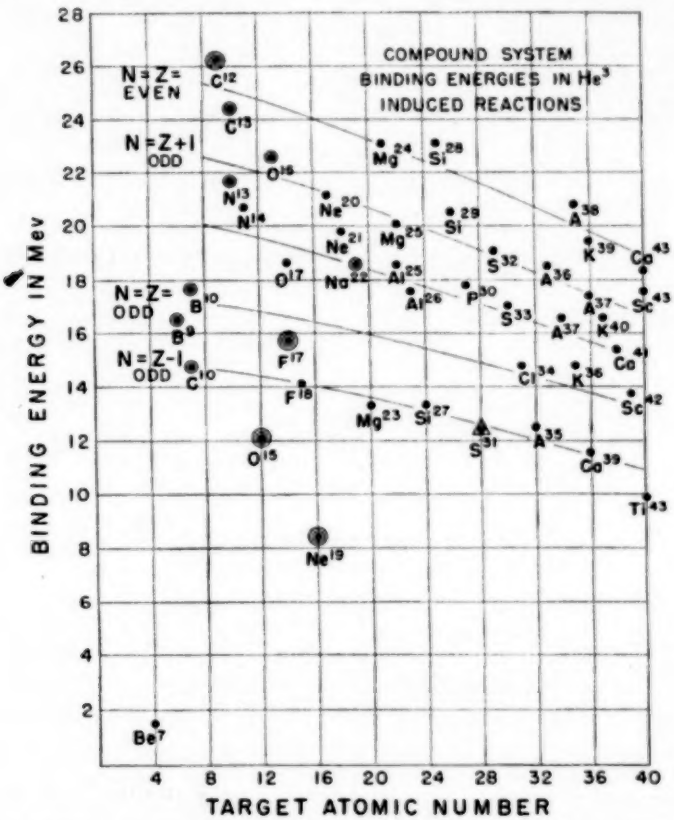

Fig. 1. Binding energies in He^3 induced reactions; the circled points identify reactions which have been studied in this laboratory. Doubly circled points identify systems which have been examined in considerable detail. The curves are drawn simply to identify the various (N, Z) families of compound systems.

fitting these experimental data using a more general formulation of the direct interaction process as will be discussed further later in this paper.

Fig. 1 is a plot of the compound system binding energies for He^3 ions against the target atomic weight [7]); the points are labelled by the appropriate compound nucleus involved. Since the mean binding energy is some 17 MeV it is perhaps not surprising that He^3 reactions are characterized by a relatively larger number of open reaction channels than in the case of proton, deuteron or alpha induced reactions. Not only does this characteristic pro-

vide the background difficulties mentioned previously but also at the excitations involved the density of states is in general much too high to permit the resolution and study of isolated resonances corresponding to individual compound system levels when such a mechanism is involved.

The anomalously low points on this figure are those for the compound systems Be^7 and Ne^{19} corresponding to He^3 bombardment of He^4 and O^{16} respectively. In the former case the excitation is so low (1.584 MeV) that no compound states are available corresponding to low bombarding energies; Holmgren and Johnston [8]) have measured the cross section for non-resonant capture of He^3 by He^4.

In the latter case, the calculated binding energy of 8.416 MeV is sufficiently low that the possibility of finding at least roughly isolated resonances exists. During the course of a series of measurements on the $O^{16}(He^3p\gamma)F^{18}$ reaction in this laboratory, for incident energies from 1.0 to 5.0 MeV [9, 10, 11]) it became clear that such resonances were present; this paper presents the results of a study of this behaviour as reflected in the $O^{16}(He^3\alpha)O^{15}$ ground state reaction [12]). This reaction was considered of particular interest because of its simplicity, not only in terms of a possible direct-interaction interpretation involving a simple nucleon transfer, but also in terms of a detailed compound system formalism since the channel spins in both the initial and final states are restricted to $\frac{1}{2}$. This restriction provides a very great reduction in the complexity of the required analyses as will be demonstrated later in this paper.

An angular momentum and parity assignment of $\frac{1}{2}^-$ has been assumed for the O^{15} ground state. The $N^{14}(dn)O^{15}$ angular distributions demonstrate that formation of the O^{15} ground state requires P-wave proton capture and thus has negative parity [13]). These measurements alone, however, do not distinguish between the spin possibilities $\frac{1}{2}$, $\frac{3}{2}$, $\frac{5}{2}$. The positon decay of O^{15}, on the other hand, has a log *ft* value of 3.57 and an end point of 1.68 MeV [14]). Since the ground state of N^{15} to which this decay occurs has been shown to have $J = \frac{1}{2}$ from optical spectroscopic measurements [15]), this suggests $J = \frac{1}{2}$ for O^{15}; this log *ft* value is in accord with that expected for such a mirror transition. Furthermore the end point of 1.68 MeV falls precisely on the predicted curve of positon end point against $A^{\frac{2}{3}}$ for mirror transitions [16]). This prediction assumes a constant density model with $R_{\text{Coulomb}} = R_0 A^{\frac{1}{3}}$ and suggests $R_0 = 1.45 \times 10^{-13}$ cm.

For incident He^3 energies below 3 MeV the reactions of interest, together with their calculated Q values, [7]) are the following:

$$\begin{aligned} O^{16} + He^3 &\rightarrow Ne^{18} + n - 2.967 \text{ MeV} \\ &\rightarrow F^{18} + p + 2.053 \text{ MeV} \\ &\rightarrow O^{15} + \alpha + 4.976 \text{ MeV} \\ &\rightarrow Ne^{19} + \gamma + 8.416 \text{ MeV}. \end{aligned}$$

For a bombarding energy of 2.40 MeV, for example, as used in much of the work described in this paper, the emergent ground state alpha particle energy varies from 6.93 to 4.26 MeV from a laboratory angle of 0° to one of 180°; the corresponding proton group to the ground state of F^{18} varies from 4.44 to 3.32 MeV over the same angular range. Since absorbers were required to prevent the elastically scattered He^3 beam from entering the detector, the residual alpha particle and proton energy ranges overlapped necessitating a detector which could adequately resolve the alpha group from the proton background peaks.

In the analysis of the data presented herein considerable use has been made of a Datatron computer programme [17]) which carries out the relativistic binary reaction kinematic calculations and in addition automatically corrects the emergent energies and magnetic rigidity values for any given absorbers interposed between the target and detector.

2. Experimental Equipment

2.1. IONIZATION CHAMBER

Fig. 2 is a schematic drawing of the gridded ionization chamber used in these measurements. The active length of the chamber is 11 cm; the photo-

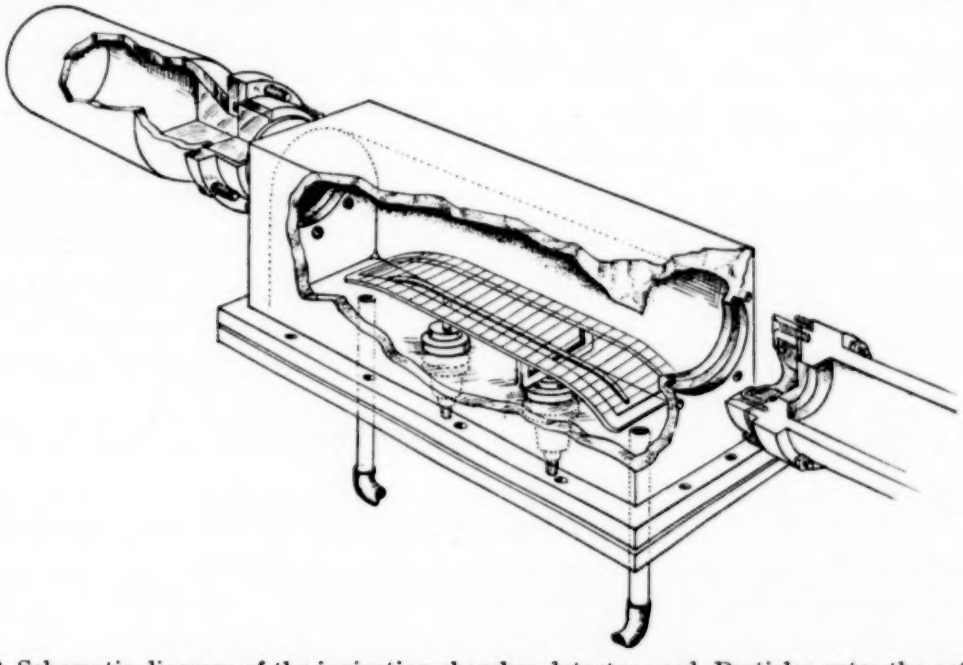

Fig. 2. Schematic diagram of the ionization chamber detector used. Particles enter the active volume through the collimator and window structure on the right and either stop in the chamber or traverse it to strike the CsI crystal detector mounted in the rear wall. The collector, Frish grid and gas handling apertures are as shown. The body of the chamber is machined from brass bar stock; the grid is wound with 0.002 in. stainless steel wire. Indium gaskets are used throughout. Windows of mica or aluminized mylar of areal densities $\approx$ 1 mg/cm^2 have been used in the work reported herein.

multiplier shown at the back end of the chamber volume is part of an anti-coincidence device designed for use in studying heavily ionizing particles which terminate their range in the chamber volume, in the presence of a flux of particles of lesser specific ionization which pass completely through the chamber. This feature was not required in the present measurements. The chamber is designed to operate at gas pressures up to $\approx$ 200 psi but in these measurements was used at atmospheric pressure or slightly below with an entrance window of mica of areal density $\approx$ 1.3 mg/cm^2. The instrumental line width is somewhat better than that illustrated by the spectra in this paper which contain a contribution from the finite target thickness used; using a very thin $\approx$ 50 μg/cm^2 Li^7 target, a full width at half maximum of $\approx$ 0.9 % was obtained for the 10 MeV alpha particles from the $Li^7(He^3\alpha)Li^6$ reaction. In order to achieve this resolution particular care was taken with gas purification and chamber gasketing. Indium metal gaskets have been used throughout; these can be used repeatedly during chamber reassembly or window changing simply by deforming the indium surface prior to assembly.

The technique developed for gas purification involves the use of a large area trap at liquid nitrogen temperatures into which 99.99 % pure tank argon is passed until sufficient argon has liquified to make up the required filling. This liquid argon volume is then connected to a mechanical vacuum pump and the system evacuated for $\approx$ 15 minutes following freezing of the argon until a quasi-equilibrium pressure of $\approx$ 50 mm Hg is attained. 3 % of spectroscopically pure tank methane is added to the previously evacuated chamber and the remaining argon filling is taken from the first fractional boil-off as the argon trap is removed from the liquid nitrogen. With this gas treatment and indium gaskets the chamber characteristics remain constant for periods of several weeks. A detailed study of the impurities present in the tank argon which are removed by this technique and not by the hot calcium circulating system used previously has not been carried out. These impurities appear to vary widely between different tanks of 99.99 % argon even from the same supplier and batch. Fig. 3 is typical of the effects observed using commercial 99.99 % pure argon and a Pu^{240} alpha source.

The collector and Frisch grid voltages were supplied by an Atomic Instrument 512 power supply. Conventional circuitry has been used for amplification of the output pulses: in order to minimize pickup at the microvolt signal levels involved at the collector a ring-of-three feedback loop and output cathode follower buffer is mounted directly on the chamber base plate in a completely closed copper shield can and selected 403B tubes have been used in this preamplifier. Within a given sampling of 20 of these tubes noise levels differing by as much as a factor of 10 have been found. Pulse spectra were displayed on a Goulding 100-channel analyzer [18]).

In all angular distribution measurements a monitor counter at $-145°$ or $-90°$ in the laboratory system was used to normalize the data. This counter employed a CsI crystal detector and has been described previously [19]). Angular distributions were obtained with the ionization chamber attached to a continuous-rotation Clarke target chamber [20]); the angular aperture of the system was $\approx 2°$ and the solid angle 6.7×10^{-4} steradians. A multiple slit collimating system defined the beam spot on target.

In measurements of excitation curves targets on thick backings were used in reflection geometry to allow direct measurement and integration of the He^3 ion beam delivered to the targets. Use of thick targets had the additional

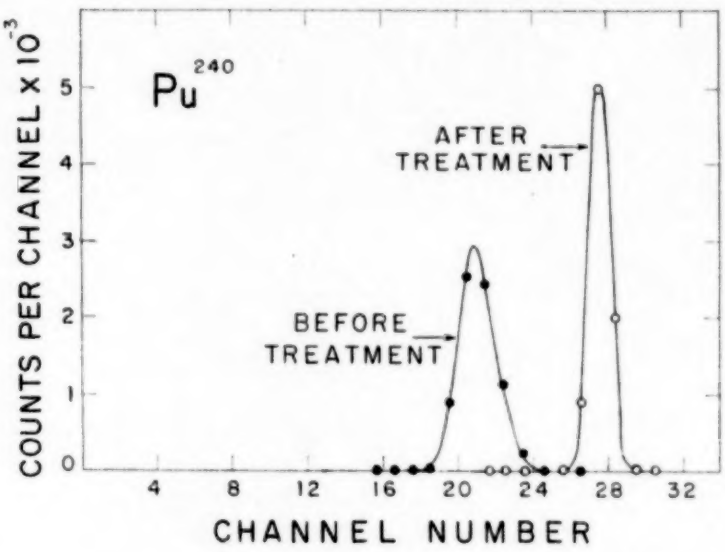

Fig. 3. Chamber response to 5.16 MeV Pu^{240} alpha particles before, and after, the gas treatment described in the text.

advantage of permitting much larger beam intensities which were required to obtain adequate counting statistics in runs of reasonable duration.

2.2. TARGETS

Targets of molybdenum trioxide (MoO_3) and of aluminium oxide (Al_2O_3) have been used in these measurements. MoO_3 targets were prepared by induction of 0.010 in. Mo blanks in oxygen atmospheres and were used in a number of the preliminary measurements of excitation curves using reflection geometry only. These were replaced with Al_2O_3 targets, both unsupported and on Al backings following the development of convenient preparation techniques [21, 22, 23]).

In the production of thin Al_2O_3 films, standard commercial 0.015 in. "2SH" aluminium foil was etched to 0.00075 in. in NaOH and following a distilled water rinse was transferred while wet to an anodizing bath using a

3 % solution of ammonium citrate in distilled water as the electrolyte and a cathode of stainless stell screening. The standard [22]) figure of 13.7 Å of oxide film per volt of applied cell potential was used in obtaining films of the desired thickness. On removal from the anodizing bath, one side of the foil was again exposed to a dilute NaOH solution to remove the Al_2O_3 film and expose the Al metal; following this the Al backing was etched from the remaining Al_2O_3 film using concentrated HCl. Self-supporting films in the range from 300 Å to 4000 Å in thickness were prepared with areas up to 15 cm^2.

The same procedure was used to produce Al_2O_3 films of controlled thickness from 100 Å to 4000 Å on 0.020 Al backings for use in reflection geometry with more intense ion beams than were possible with the self-supporting targets. A 500 Å unsupported foil was found to be stable under bombardment with He^3 ion currents up to 1 μA at 2.5 MeV; currents of 10 μA were used on the supported foils of this thickness.

The foil thicknesses were checked by weighing. Using the data tabulated by Whaling [24]) a 500 Å film of Al_2O_3 represents $\approx$ 20 keV energy loss for a 2.5 MeV He^3 ion.

By examining the yield of reaction alpha particles under identical conditions from a 1000 Å Al_2O_3 target on an 0.020" Al backing and from an identical Al blank, freshly etched with NaOH before mounting, it was found that following the etching an Al_2O_3 film 60 ± 5 Å thick formed spontaneously on the Al surface on exposure to atmospheric oxygen.

For the incident energy range considered herein, measurements on freshly etched Al targets and on cleaned Mo targets showed no evidence for alpha particle groups other than those from the thin oxide layer mentioned above.

2.3. ENERGY CALIBRATION

The energy calibration of the 90° beam analyzing magnet was fixed by examination of the $C^{12}(He^3, n)O^{14}$ reaction in the region of the reaction threshold at 1449.6 ± 3.8 keV [19]). This was carried out using both a thin C^{12} target on 0.010" Ta and the carbon contaminant layer on the O^{16} targets themselves. The equipment used in these measurements has been described previously [19]).

3. Results

3.1. EXCITATION CURVES

Fig. 4 is a typical particle spectrum obtained with the ionization chamber at 90° to the He^3 beam showing the ground state alpha particle group from the $O^{16}(He^3\alpha)O^{15}$ reaction and a number of the proton groups to the low states of F^{18} [10]). At this particular pressure the range of the ground state

proton group exceeds the effective length of the chamber and the corresponding peak is folded back under the $P_{1,2,3,4}$ peak. This group was studied separately by increasing the chamber pressure. Fig. 5 illustrates the effect of reducing the gas pressure in the chamber from 30 psi to 5 psi. At the lower pressures longer range particles completely traverse the chamber and lose a smaller energy in the gas with consequent reduction in the output pulse height. These result in the step in the spectrum at channel 20. The small peak

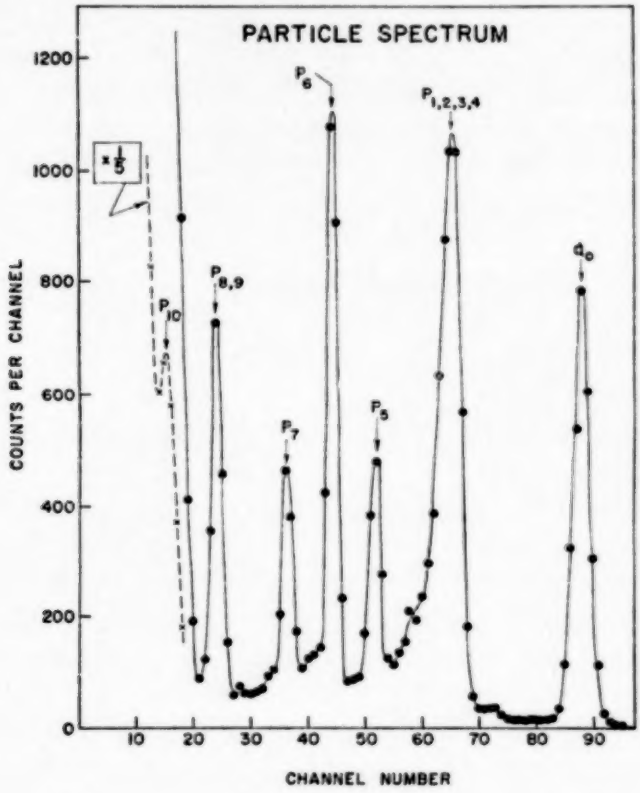

Fig. 4. Typical particle spectrum from an Al_2O_3 target, measured at 90° to the incident 3.10 MeV He^3 beam. The chamber gas pressure used was 30 psi.

in channel 32 corresponds to alpha particles from the $C^{13}(He^3\alpha)C^{12}$ reaction on the carbon target contaminant.

Prior to the detailed measurement of excitation curves a series of measurements were carried out to investigate the effect of target thickness on the experimental curves. Fig. 6 shows the results obtained for the 90° excitation curve in the region of a resonance maximum using 1500, 500 and 150 Å, Al_2O_3 targets. This figure demonstrates that the peak shape remains essentially unchanged in going from a 500 Å ($\approx$ 20 keV) to a 150 Å ($\approx$ 4 keV) target, while use of a 1500 Å ($\approx$ 60 keV) target does distort the shape significantly. As a result of these measurements the excitation curves were

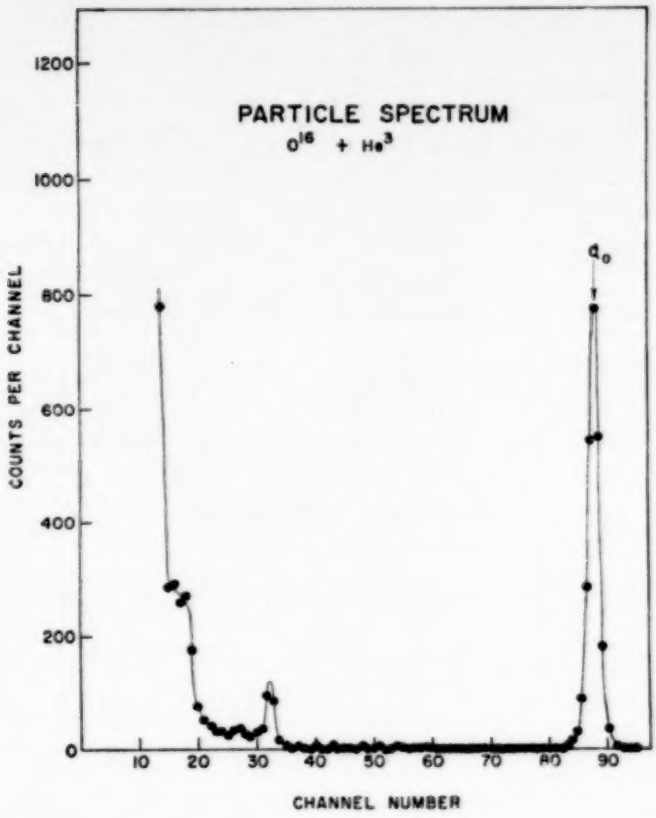

Fig. 5. Typical particle spectrum with 5 psi gas pressure in the ionization chamber; this is to be compared with the results of fig. 4 corresponding to a 30 psi pressure.

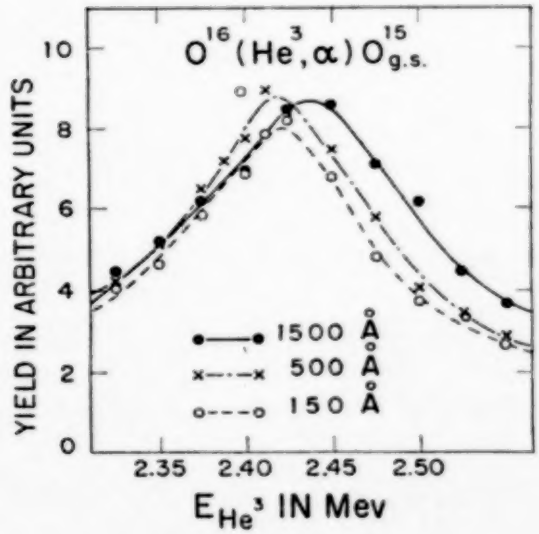

Fig. 6. Alpha particle excitation curve in the region of an $O^{15}(He^3\alpha)O^{16}$ ground state reaction resonance for three different Al_2O_3 target thicknesses as indicated.

obtained using a 500 Å target on a 0.020″ Al backing. Use of this thick backing, reflection geometry and secondary electron suppression electrodes in the target region permitted accurate normalization on the total charge delivered by the beam. As noted previously [19]), this measurement is open to question because of the possible presence of molecular ions of the hydrogen isotopes unless essentially pure He^3 gas is supplied to the ion source of the accelerator and the system has not previously been used to accelerate deuterons. Both conditions were fulfilled.

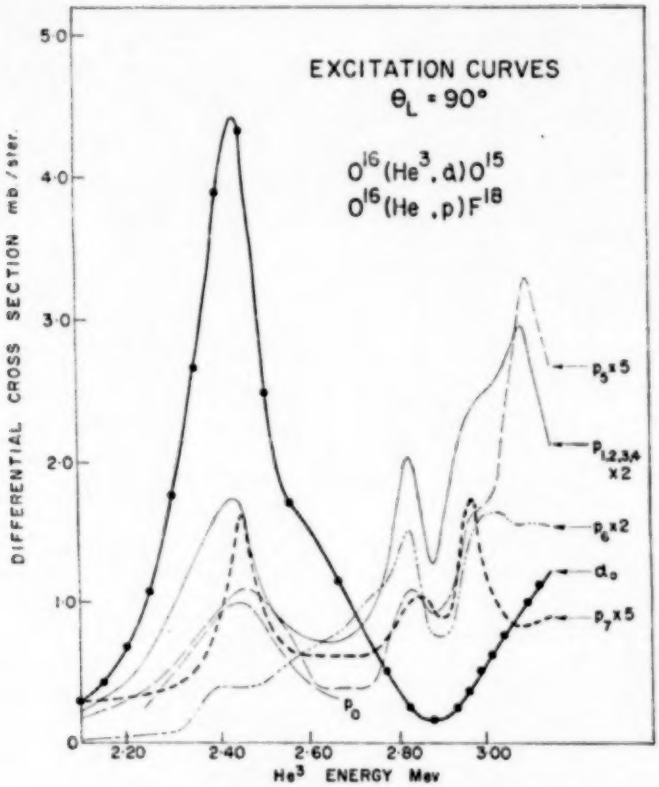

Fig. 7. Excitation curves for alpha particles and protons from the $O^{11}+He^3$ reactions measured at 90° to the incident beam.

Fig. 7 shows the 90° differential excitation curves measured in the He^3 energy range from 2.1 to 3.1 MeV for alpha particles to the ground state of O^{15} from the $O^{16}(He^3\alpha)O^{15}$ reaction and for proton groups to the low states of F^{18} from the $O^{16}(He^3p)F^{18}$ reaction. The absolute cross sections indicated in the ordinate were obtained from the measured target thickness, beam flux and detector solid angle. It should be noted that the proton group corresponding to the 7th level in F^{18} appears to show a narrower resonance width than either the remaining proton groups or the alpha group to the ground state of O^{15}. This narrow resonance is also displaced some 25 keV upward on the bombarding energy scale.

3.2. ANGULAR DISTRIBUTION MEASUREMENTS

Fig. 8 shows typical angular distributions measured at the indicated energies over the pronounced resonance peak shown in the α_0 excitation curve in fig. 6. The experimental accuracy is indicated by the standard deviations shown on the curves. These data have been converted to centre of mass angles and intensities using a standard Datatron computer code; the solid lines drawn through the points are the results obtained by fitting the data to an expansion in Legendre polynomials up to and including the

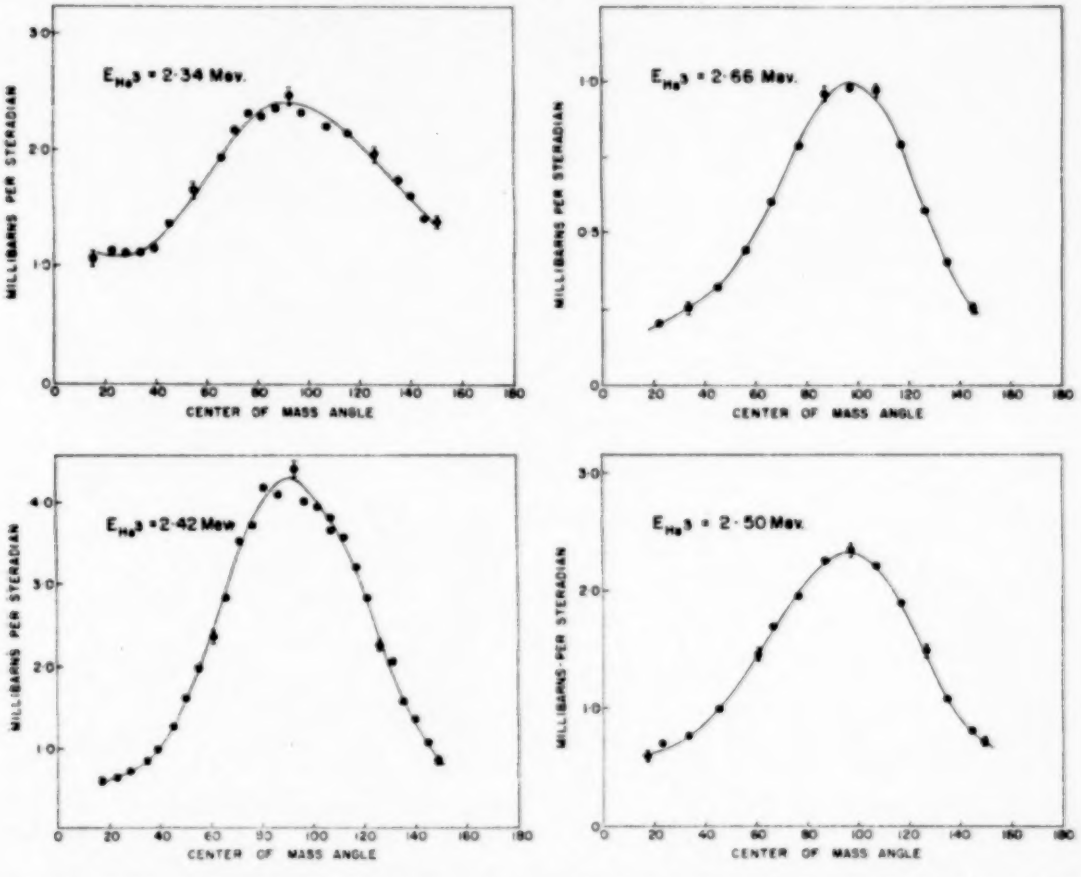

Fig. 8. Typical angular distributions measured in the region of the strong $O^{16}(He^3\alpha)O^{15}$ resonance structure shown in Fig. 7. The experimental data have been corrected to the center of mass angles and intensities and have been fitted to a Legendre polynomial expansion shown by the full lines. The coefficients in these expansions are given in table 1.

eighth order. Table 1 lists the coefficients and their standard deviations as obtained from this least squares fitting procedure. Also included in table 1 is the fit to the angular distribution of fig. 9 measured at a He^3 energy of 2.85 MeV corresponding to the minimum in the excitation curve of fig. 7.

From the angular distributions of fig. 8 and the fits given in table 1 it follows that in the region of the resonance peak the data are represented adequately by including only polynomials up to fourth order. The fits are

TABLE 1

Alpha particle angular distribution: coefficient ratios for Legendre polynomial expansion

E_{He^3} (MeV)	a_1/a_0	a_2/a_0	a_3/a_0	a_4/a_0	a_5/a_0	a_6/a_0	a_7/a_0	a_8/a_0
2.34	-0.08 ± 0.03	-0.55 ± 0.03	0.09 ± 0.03	0.06 ± 0.03	0.11 ± 0.03	0.01 ± 0.03	-0.03 ± 0.03	-0.04 ± 0.03
2.42	-0.06 ± 0.02	-1.13 ± 0.02	0.12 ± 0.03	0.32 ± 0.03	0.02 ± 0.03	-0.00 ± 0.03	-0.04 ± 0.03	-0.02 ± 0.03
2.50	-0.07 ± 0.03	-1.10 ± 0.03	0.15 ± 0.04	0.20 ± 0.04	-0.05 ± 0.04	-0.03 ± 0.04	0.02 ± 0.04	-0.03 ± 0.04
2.66	$-1.0\ \pm0.03$	-1.06 ± 0.03	0.28 ± 0.04	0.29 ± 0.04	-0.14 ± 0.04	-0.03 ± 0.04	0.01 ± 0.04	-0.04 ± 0.04
2.85	-0.37 ± 0.03	0.52 ± 0.05	-0.53 ± 0.05	0.02 ± 0.05	-0.30 ± 0.05	-0.01 ± 0.05	0.11 ± 0.05	0.01 ± 0.05

dominated by a large negative P_2 contribution. The P_1 term is relatively small and is reflected in the angular distributions by a shift of the axes of symmetry from 90° in the centre of mass.

As will be discussed in detail in the following section, the two major resonances corresponding to incident He^3 energies near 2.4 MeV must have the same parity. The presence of odd Legendre polynomials in the angular distribution fits reflects the interference between these resonances and the tails of higher energy ones of opposite parity. There is also a possibility that

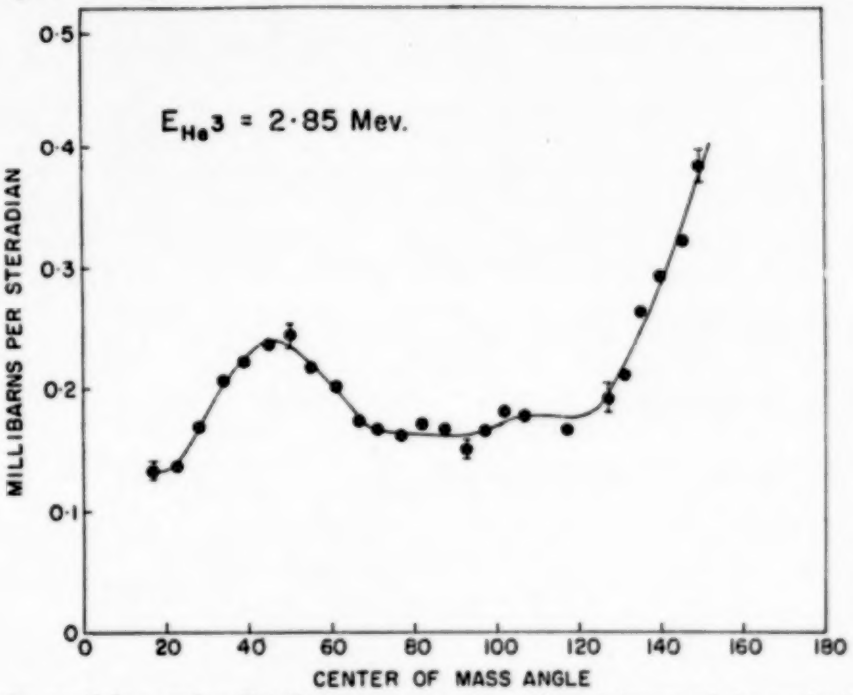

Fig. 9. Alpha particle angular distribution measured at the minimum of the excitation curve shown in fig. 7.

the low angle points in the angular distributions are systematically too high because of a contaminant yield of $O^{16}(He^3, \alpha)O^{15}$ alpha particles from He^3 ions elastically scattered through small angles onto the O^{16} nuclei in the $\approx$ 1 mg/cm² mica window in use on the ion chamber. The resultant asymmetry in the angular distributions would be reflected in an augmented P_3 and higher odd polynomial coefficients; the even polynomial coefficients are relatively less sensitive to this possible systematic error because of the requirement of symmetry with respect to 90° in the centre of mass system.

In order to investigate further the reaction behaviour in the region of the resonance maximum where the P_0, P_2 and P_4 terms dominate, excitation curves similar to those of fig. 7 were measured at laboratory angles of 83°, 119° and 145°. These angles permit the determination of these coefficients with relatively smaller error arising from the neglect of the odd polynomial terms. In particular, since P_3 has a node at 90° and P_4 an antinode, and since the asymmetric contaminant alpha particle contribution referred to pre-

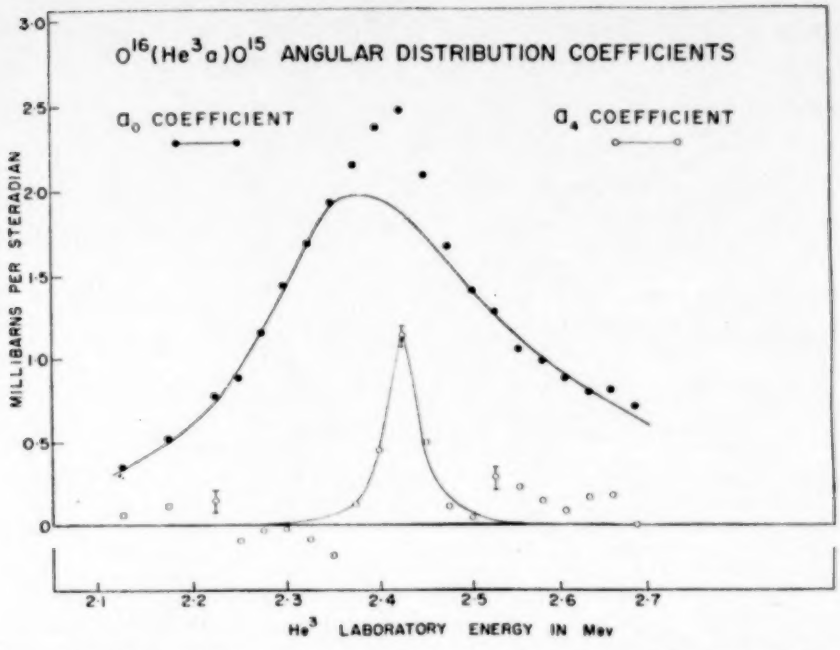

Fig. 10. Legendre polynomial expansion coefficients as functions of the incident He^3 energy in the vicinity of the $O^{16}(He^3\alpha)O^{15}$ resonance structure of fig. 7. The statistical errors are equal to, or less than, the diameter of the solid circles representing the experimental a_0 values; typical statistical errors are indicated on the a_4 data. The solid lines are the fitted curves discussed in the text.

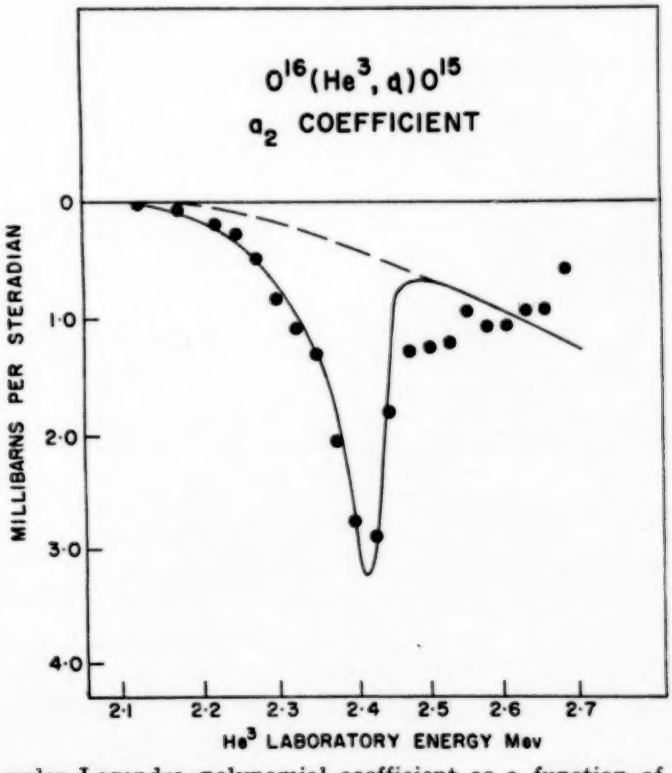

Fig. 11. Second order Legendre polynomial coefficient as a function of the incident He^3 energy. (See fig. 10, caption.) The dashed line represents the assumed contribution from tails of higher resonances as shown in fig. 7. All values are negative.

viously is negligible at large angles, the a_4 coefficient is obtained with minimized error from the neglect of the a_3 terms. From the excitation curve data, the resulting set of simultaneous linear equations

$$W(\theta_j) = \sum_{n=0}^{2} a_{2n} P_{2n}(\cos\theta_j), \quad j = 1, 2, 3 \tag{1}$$

were solved for the coefficients a_{2n} as functions of the incident energy. The results are given as the plotted points in figs. 10 and 11. For the a_0 results the statistical standard deviations are given approximately by the point size; the bars on the figure indicate the same error limits for the a_2 and a_4 results. The cross sections indicated on the ordinate were obtained from the integrated beam flux, the target thickness and the detector solid angle.

In order to examine the effects of ignoring the odd polynomials in this analysis, alpha particle angular distributions measured at incident energies of 2.34, 2.42 and 2.66 MeV, bracketing the resonance peak, were reanalyzed with the computer programme changed to include, first, only even polynomials up to the eight order and, second, only even polynomials up to the fourth order. In table 2 the a_2/a_0 and a_4/a_0 coefficient ratios so obtained are

TABLE 2a, b

Coefficient ratios in the Legendre polynomial expansions to the alpha particle angular distributions from the $O^{16}(He^3\alpha)O^{15}$ reaction

TABLE 2(a)

E_{He^3} (MeV)	$(a_2/a_0)_I$	$(a_2/a_0)_{II}$	$(a_2/a_0)_{III}$	$(a_2/a_0)_{IV}$
2.34	-0.55 ± 0.03	-0.54 ± 0.04	-0.55 ± 0.04	-0.51 ± 0.05
2.42	-1.13 ± 0.02	-1.12 ± 0.03	-1.13 ± 0.03	-1.18 ± 0.05
2.66	-1.06 ± 0.03	-1.02 ± 0.07	-1.03 ± 0.07	-1.14 ± 0.06

TABLE 2(b)

E_{He^3} (MeV)	$(a_4/a_0)_I$	$(a_4/a_0)_{II}$	$(a_4/a_0)_{III}$	$(a_4/a_0)_{IV}$
2.34	0.06 ± 0.03	0.06 ± 0.06	0.07 ± 0.06	-0.04 ± 0.08
2.42	0.32 ± 0.03	0.33 ± 0.04	0.33 ± 0.04	0.42 ± 0.08
2.66	0.29 ± 0.04	0.28 ± 0.08	0.31 ± 0.08	0.23 ± 0.09

The subscripts refer respectively to ratios determined by least squares fitting the angular distributions to expansions including all polynomials up to P_8(I); only even polynomials up to P_8(II); only even polynomials up to P_4(III); and to the ratios determined from the three angle excitation curve data (IV).

listed for comparison with those obtained from the detailed fitting (table 1) of the angular distributions. As indicated in table 2, neglect of the odd polynomials in the latter determination does not introduce a significant systematic error in the a_2/a_0 and a_4/a_0 coefficient ratios.

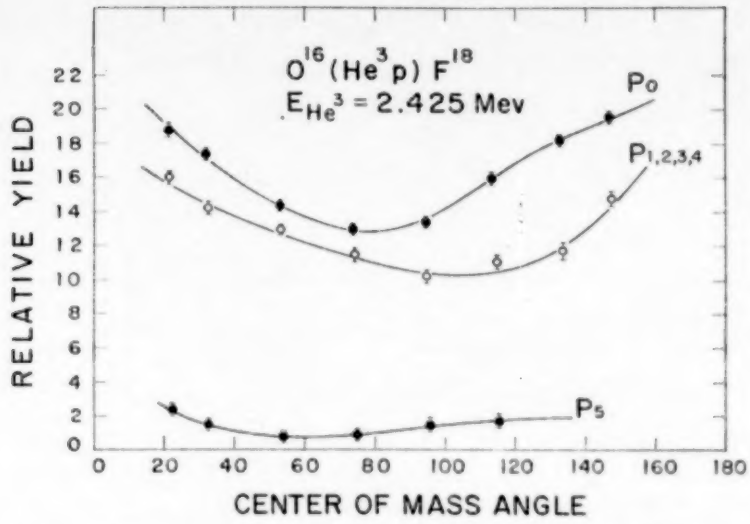

Fig. 12. Angular distributions of proton groups from the $O^{16}(He^3p)F^{18}$ reaction. These have been converted to centre of mass angles and intensities.

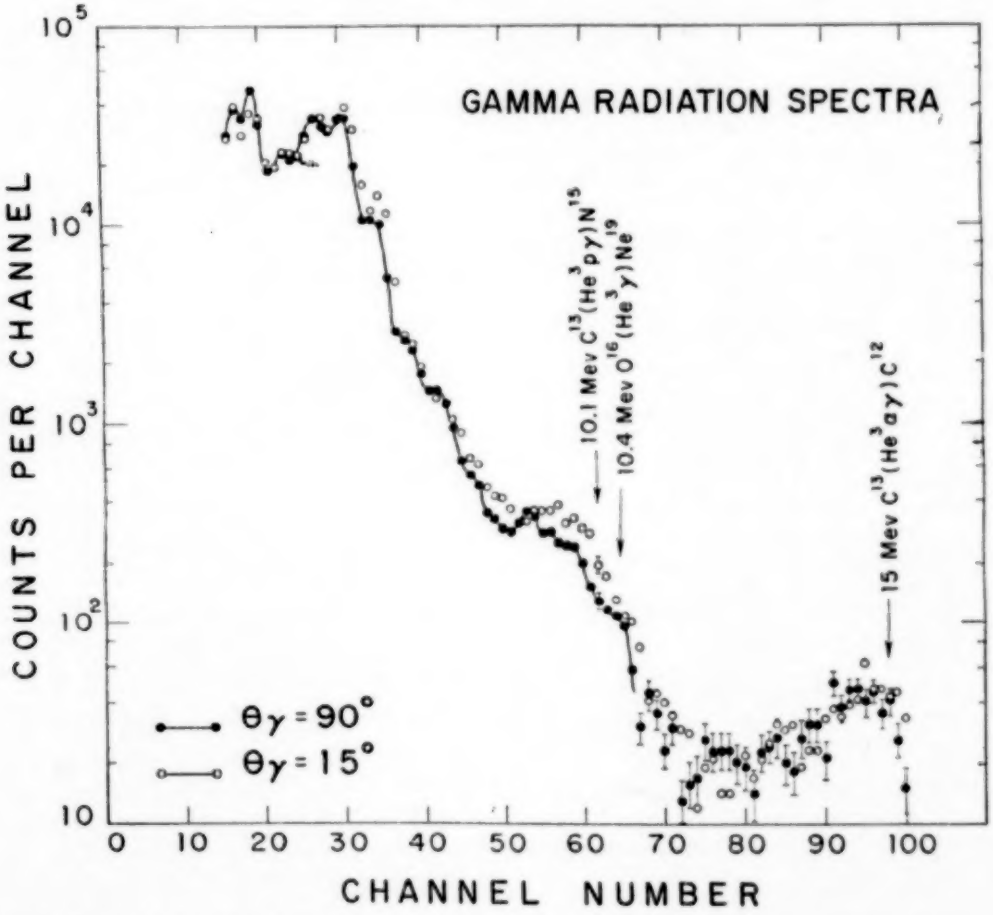

Fig. 13. Gamma radiation from He^3 bombardment of a Al_2O_3 target at an incident energy of 2.42 MeV. The closed and open circles represent data measured at 90° and 15° respectively to the incident beam direction. Two of the contaminant gamma rays are identified on the figure. The higher radiation yield at lower energies results from lower energy transitions in the $C^{13}(He^3p\gamma)N^{15}$, $C^{13}(He^3n\gamma)\,O^{15}$, $O^{16}(He^3\alpha\gamma)O^{15}$, $C^{12}(He^3p\gamma)N^{14}$ and $O^{16}(He^3p\gamma)F^{18}$ reactions.

Following the angular distribution measurements on the $O^{16}(He^3\alpha)O^{15}$ alpha particles, the ionization chamber pressure was increased to permit measurement of selected proton groups from the $O^{16}(He^3p)F^{18}$ reaction proceeding through the same compound states. The results of these measurements are shown in fig. 12.

3.3. CAPTURE GAMMA RADIATION

A search for gamma radiation from the $O^{16}(He^3\gamma)Ne^{19}$ capture reaction was also made using 4000 Å Al_2O_3 targets and 5″ dia. × 4″ deep NaI(Tl) crystal spectrometers [25]). The relevant experimental techniques and apparatus have been described in previous publications [19, 26]). Fig. 13 shows the gamma radiation spectra measured at 90° and 15° to the incident beam using a 2″ aperture lead collimator between the target and detector crystal.

The major experimental difficulty encountered in these studies is that resulting from the carbon contaminant layer which develops on the Al_2O_3 targets. Particular care was taken to minimize this build-up through use of freshly prepared Al_2O_3 targets, auxiliary trapped diffusion pumps on the beam tubing to the target and the target shroud structure maintained at liquid N_2 temperatures [27]) which has also been described previously [26]). The probable sources of the observed radiations are indicated in fig. 13.

4. Discussion

The presence of strong resonance structure in the excitation curve of the $O^{16}+He^3$ reaction as shown for example in fig. 7 implies that compound system formation plays a dominant role in these reactions. The experimental data for the $O^{16}(He^3\alpha)O^{15}$ have been examined in detail in terms of the predictions of the standard compound system, resonance formalism.

4.1. RESONANCE ANALYSES

In this reaction leading to the O^{15} ground state, since the channel spin in both initial and final states is restricted to $\frac{1}{2}$, the orbital momenta of the incident and outgoing particles corresponding to formation and decay of any given compound state are uniquely defined and single valued. Thus each compound system state of total angular momentum J has associated with it a unique pair of orbital angular momenta $(J\pm\frac{1}{2}, J\mp\frac{1}{2})$ for the incident and emergent particles. The upper sign refers to the case where the compound state has positive parity and the lower to that of negative parity. In the analysis, the parity of O^{15} has been taken as odd, as discussed previously in this paper.

As demonstrated in Appendix A, for a reaction involving channel spin $\frac{1}{2}$ for both incident and exit channels and proceeding through a single isolated resonance, it is impossible to obtain negative coefficients in the Legendre polynomial expansion fitted to the angular distributions of the reaction products.

The presence of strong negative P_2 contributions in the angular distributions shown in fig. 8 for alpha particles leading to the ground states of O^{15} then precludes explanation in terms of a single resonance and requires interference between at least two separate resonances.

The general expression for the angular distribution in cases where the l and j values are uniquely correlated, as discussed above, is given for the case of two interfering resonances by Devons and Goldfarb [28]):

$$W(\theta) = \frac{\lambda^2}{4(2I_t+1)(2I_1+1)} \sum_{s_1 s_2} (-1)^{s_1-s_2} \sum_k (-1)^k \times \{Z(l_1 J_1 l_1 J_1; S_1 k) Z(l_2 J_1 l_2 J_1; S_2 k) F_1^2 R_1^2 \quad (2)$$

$$+ Z(l'_1 J_2 l'_1 J_2; S_1 k) Z(l'_2 J_2 l'_2 J_2; S_2 k) F_2^2 R_2^2 \pm 2Z(l_1 J_1 l'_1 J_2; (S_1 k) Z l_2 J_1 l'_2 J_2; S_2 k) \times i^{l_1+l_2-l'_1-l'_2} F_1 F_2 R_1 R_2 \cos \Psi\} P_k(\cos\theta),$$

where by definition

$$R_r^2 = \Gamma^{J_r}_{is_1 l_1} \Gamma^{J_r}_{es_2 l_2}, \quad (3)$$

$$F_r^2 = [(E-E(J_r))^2 + \tfrac{1}{4}\Gamma^2(J_r)]^{-1}, \quad (4)$$

$$\Psi = \psi^{i}_{l'_1} - \phi^{i}_{l'_1} + \psi^{e}_{l'_2} - \phi^{e}_{l'_2} - \psi^{i}_{l_1} + \phi^{i}_{l_1} - \psi^{e}_{l_2} + \phi^{e}_{l_2} + \theta(J_1) - \theta(J_2), \quad (5)$$

$$\theta(J_r) = \tan^{-1} \frac{2(E-E(J_r))}{\Gamma(J_r)}, \quad (6)$$

$$\psi_l^{x} = \sum_{m=1}^{l} \tan^{-1} \eta_x/m, \qquad \eta_x = \frac{ZZ'e^2}{\hbar v_x}, \quad (7)$$

$$\phi_l^{x} = \tan^{-1} \frac{F_l^{x}}{G_l^{x}} + \tan^{-1} \frac{R^{\infty} P_l}{1-R^{\infty} S_l}. \quad (8)$$

Here the index $r = 1,2$ identifies the two compound system levels, $E(J_r)$ is the energy of the incident particle at resonance; the indices i and e identify the incident and emergent particles respectively and primes are used to indicate quantities associated with the second resonance with total angular momentum J_2. F_r is the inverse of the usual resonance energy denominator and R_r^2 is the product of the relevent initial and final partial reaction widths. η is the channel Sommerfeld factor, $\theta(J_r)$ the resonance phase shift and $\psi_l - \phi_l$ is the usual potential phase shift. The second term in the expression for ϕ_l^{x} in eq. (11) may be looked upon as the contribution of distant resonances to the potential scattering phase shift [29]). In the case of nucleons it is this coherent contribution of the distant resonances to the phase shift which changes the hard sphere phase shift into the appropriate optical model phase shift. In the reaction considered here this last term is to be considered as a "distorted wave effect", due to a specifically nuclear potential rather than the Coulomb field, which modifies the potential

scattering. A non-zero R^{∞} would be expected to play an important role in the part of the reaction which proceeds via a direct interaction rather than a compound system mechanism. In eq. (8) the penetrability P_l and the shift factor S_l are defined as

$$P_l = \frac{a}{\lambda} \cdot \frac{1}{F_l^2+G_l^2}\bigg|_{r=a}, \tag{9}$$

$$S_l = \frac{a}{\lambda}\left\{b_l + \frac{F_l F'_l+G_l G'_l}{F_l^2+G_l^2}\right\}\bigg|_{r=a}; \tag{10}$$

S_l is the real part of the logarithmic derivative of the outgoing wave function of unit flux, evaluated at the interaction radius a; the primes denote differentiation with respect to a/λ. The parameter b_l is chosen to make S_l vanish at the resonance energy [29]). P_l is the corresponding imaginary part of this derivative, F_l and G_l are the familiar regular and irregular solutions of the Coulomb equation respectively [30]).

In an attempt to establish the spin assignments to the resonances involved in the $O^{16}(He^3\alpha)O^{15}$ reaction the Legendre polynomial coefficient ratios in $W(\theta)$ as given by eq. (2) were evaluated for $(J_1 J_2)$ possibilities up to and including $J = \frac{7}{2}$. Typical results are presented in fig. 14 which presents the calculated angular distribution coefficient ratios as functions of the channel amplitude ratio ρ, defined as

$$\rho = \frac{F_2 R_2}{F_1 R_1},$$

on a convenient $\tan^{-1}$ scale. Of the $(J_1 J_2)$ possibilities examined only the $(\frac{1}{2}, \frac{5}{2})$ case results in a calculated negative P_2 coefficient of sufficient magnitude to fit the experimental data and a non-zero P_4 coefficient. The results are listed in table 3. From the Z identity of Appendix A it necessarily

TABLE 3

Angular distribution coefficient calculations

J_1	J_2	Remarks
$\frac{1}{2}$	$\frac{3}{2}$	$a_2 > -1.0$; $a_4 \equiv 0$
$\frac{1}{2}$	$\frac{5}{2}$	$a_2 > -1.25$; $0 \mathit{\Gamma} a_4 \leqq 0.8$
$\frac{1}{2}$	$\frac{7}{2}$	$a_2 > 0$
$\frac{3}{2}$	$\frac{5}{2}$	$a_2 \geqq 0.07$
$\frac{3}{2}$	$\frac{7}{2}$	$a_2 \geqq -0.6$
$\frac{5}{2}$	$\frac{7}{2}$	$a_2 \geqq +1.0$

follows that the negative contribution to the P_2 coefficient results entirely from the interference term; consequently the maximum negative value is obtained for $\cos \Psi = 1$. This value has been assumed in these preliminary

calculations and, in particular, applies to the calculations shown in fig. 14; fig. 15 identifies the parameters appearing in eq. (2).

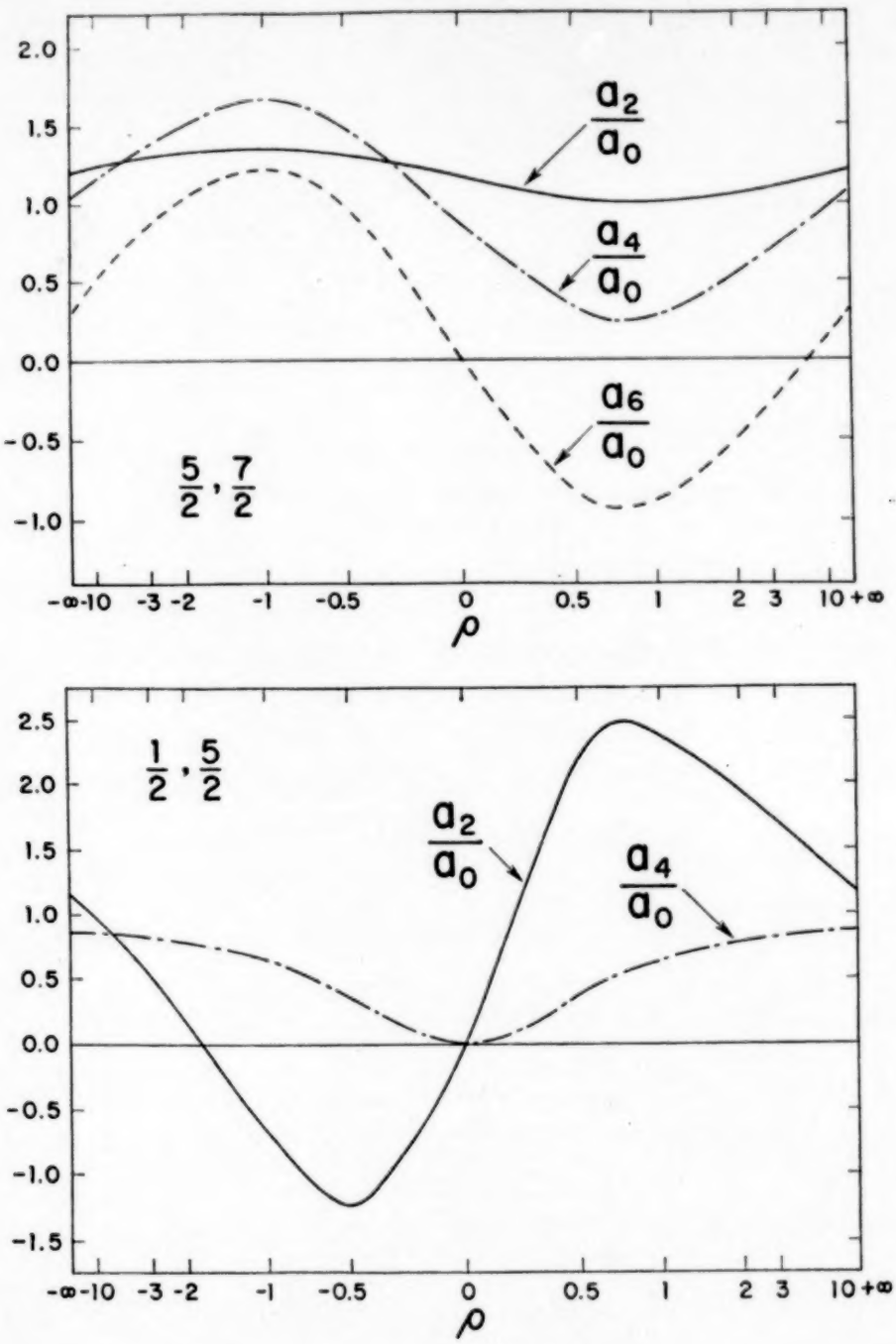

Fig 14. Calculated coefficient ratios for a Legendre polynomial expansion of the angular distributions of alpha particles from the $O^{16}(He^3, \alpha)O^{15}$ reaction as a function of the amplitudes involving the two assumed compound system states. Parts (a) and (b) of the figure present the results for assumed $\frac{5}{2}$, $\frac{7}{2}$ and $\frac{1}{2}$, $\frac{5}{2}$ binary combinations respectively.

Although the parity of these resonances cannot be established from the distribution measurements, the approximate symmetry of the angular

distributions with respect to 90° in the centre of mass system and to a lesser extent the relatively slow variation of the distribution coefficients with energy over the resonance show that the two resonances must have the same parity. In the analysis of the experimental data it has been assumed that this parity is positive although, as will be noted later, no conclusive evidence exists on this point.

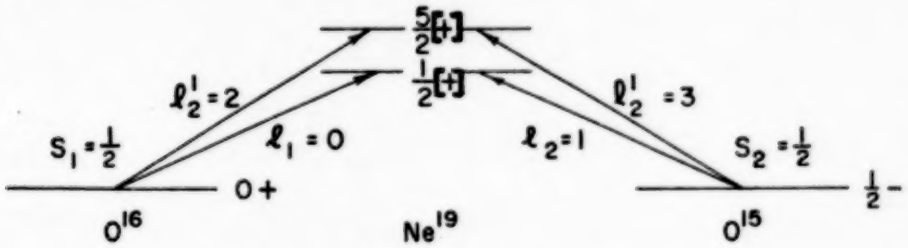

Fig. 15. Schematic representation of the $O^{16}(He^3\alpha)O^{15}$ reaction for incident energies in the vicinity of 2.42 MeV. As discussed in the text, the experimental data do not establish unambiguously the parity of the Ne^{19} states involved.

Taking $J_1 = \frac{1}{2}$ and $J_2 = \frac{5}{2}$, eq. (2) reduces to

$$W(\theta) = \tfrac{1}{8}\lambda^2\{(2F_1^2R_1^2+6F_2^2R_2^2)P_0(\cos\theta) + (\tfrac{48}{7}F_2^2R_2^2 \pm 12F_2R_2F_1R_1\cos\Psi)P_2(\cos\theta)+\tfrac{36}{7}F_2^2R_2^2P_4(\cos\theta)\}. \quad (11)$$

From this it follows that the total reaction cross sections via the $\frac{1}{2}$ and $\frac{5}{2}$ resonances are given by

$$\sigma_1 = 4\pi(a_0)_1 = \pi\lambda^2F_1^2R_1^2 \quad (12)$$

$$\sigma_2 = 4\pi(a_0)_2 = 3\pi\lambda^2F_2^2R_2^2. \quad (13)$$

Furthermore it is clear that the P_4 term in the angular distribution arises only from the $\frac{5}{2}$ resonance. The a_2 coefficient is given by

$$a_2 = \lambda^2F_2^2R_2^2\{\tfrac{6}{7} \pm \tfrac{3}{2}\rho^{-1}\cos\Psi\}. \quad (14)$$

In cases where the resonance widths are relatively small, the resonance widths, the phase shifts, the penetrabilities and the Coulomb phase shifts are all essentially constant over the resonance and the variation of these quantities with the bombarding energy is ordinarily ignored.

With a nuclear radius

$$a = 1.45(A_1^{\frac{1}{3}}+A_2^{\frac{1}{3}})\times 10^{-13}\,\text{cm}, \quad (15)$$

as suggested by alpha scattering data [31]), and a single particle reduced width defined as

$$\gamma_{sp}^2 = \frac{\hbar^2}{\mu a^2}, \quad (16)$$

at the incident and emergent energies involved in the $O^{16}(He^3\alpha_0)O^{15}$ gs

reaction, for alpha particles $\gamma_{sp}^2 = 300$ keV and for He^3 ions $\gamma_{sp}^2 = 420$ keV.

From the angular distribution data of figs. 8, 9 and 12 and the known target thickness, detector efficiencies and beam flux, cross section data has been obtained for both the ($He^3\alpha$) and the (He^3p) reactions on O^{16}. These are the only reaction channels which are energetically allowed for a bombarding energy of 2.40 MeV except for the ($He^3\gamma$) capture reaction which has a negligibly small cross section; this latter reaction will be discussed later in this section. At bombarding energies $E(J_1)$ and $E(J_2)$ eqs. (12) and (13) reduce respectively to

$$\sigma_r^{ge} = 4\pi\lambda^2 \cdot \frac{\Gamma_i^{J_r}\Gamma_e^{J_r}}{[\Gamma(J_r)]^2} \tag{17}$$

where $r = 1, 2$ and the indices i and e refer to the incident and emergent particles as before.

From the a_0 data of fig. 10 a preliminary analysis of the data gave for the $\frac{1}{2}$ resonance

$$\frac{\Gamma_{He^3} \cdot \Gamma_{He^4}}{[\Gamma_{He^3}+\Gamma_{He^4}+\sum\Gamma_{p_j}]^2} = 0.053, \tag{18}$$

where p_j represents a particular proton group, and

$$\frac{\Gamma_{He^3} \cdot \sum\Gamma_{p_j}}{[\Gamma_{He^3}+\Gamma_{He^4}+\sum\Gamma_{p_j}]^2} \approx 0.07. \tag{19}$$

Since the total width was found to be ≈ 350 keV, eq. (18) and (19) may be recast as a quadratic equation for Γ_{He^3} or Γ_{He^4}. One of the solutions is extraneous in that it corresponds to a He^3 reduced width greater than 7 times the single particle limit. The other solution gives the following preliminary set of parameters for the $\frac{1}{2}$ resonance:

$$\Gamma_{He^3} = 50 \text{ keV}, \Gamma_{He^4} = 130 \text{ keV}, \text{ and } \sum\Gamma_{p_j} = 170 \text{ keV}.$$

The observed width Γ and the reduced widths γ^2 are related by

$$\Gamma = 2P_l\gamma^2 \tag{20}$$

where P_l is defined in eq. (9).

Using this expression, the value of $\gamma_{He^3}^2 \approx 0.65\,\gamma_{sp}^2$ (eq. (16)), hence by the usual criterion [32]) that the approximation of energy independent resonance parameters is valid only for $\gamma^2 \lesssim 0.30\,\gamma_{sp}^2$, it follows that in the case of the He^3 widths Thomas shift corrections must be included in the formalism. Fortunately, as will be shown later, this additional complexity is required only for the He^3 width. Furthermore, because of the relatively low He^3 energies involved and the large total width of the resonance structure under study it has been necessary to include the energy variation of the He^3 penetrability over the resonance. The corrections which have been included

modify a number of the definitions and expressions given previously. Where possible, these corrections have been normalized to reference values determined at the individual resonance energy.

In particular, including these corrections modifies the previous definitions of F_r and $\Gamma_{1\mu}$ to the following:

$$F_r^2 = \Big\{[E(J_r)-(S_{i,J_r-\frac{1}{2}}(E)-S_{i,J_r-\frac{1}{2}}[E(J_r)])\gamma^2_{i,J_r-\frac{1}{2}}-E]^2 + \tfrac{1}{4}\left[\frac{P_{i,J_r-\frac{1}{2}}(E)}{P_{i,J_r-\frac{1}{2}}[E(J_r)]}\cdot\Gamma_{i,J_r-\frac{1}{2}}+\Gamma_{e,J_r+\frac{1}{2}}+\sum\Gamma_p\right]^2\Big\}^{-1}, \quad (21)$$

$$\Gamma_{1l} = \frac{2a\gamma_{il}^2}{\lambda_1(1+\mathring{S}_{1l}\gamma_{il}^2)} = \frac{2P_{1l}\gamma_{il}^2}{1+\left(\frac{dS_{1l}}{dE}\right)\gamma_{il}^2} \quad (22)$$

where S_l is defined by eq. (10).

In carrying out the fitting to the data of figs. 10 and 11 an iterative procedure has been employed. In essence this consisted of the following sequence:

(a) Using $(a_0)_1 = \frac{1}{4}\lambda^2 F_1^2 R_1^2$ the curve shown in fig. 10 was fitted to the experimental a_0 data giving $\Gamma_T(J_1) = 355$ keV and $E(J_1) = 2.400\pm0.010$ MeV. From the cross section data quoted previously $\Gamma_{He^3,0} = 50$ keV, $\Gamma_{He^4,1} = 135$ keV, $\sum\Gamma_p = 170$ keV. The first two of these correspond to reduced widths of 281 and 15 keV respectively. These reduced widths are 67 % and 5 % of the corresponding single particle limits. Although, *a priori*, such a large reduced width for the He^3 ions might be considered as evidence for positive parity for the $J = \frac{1}{2}$ resonance, hence S-wave incident He^3 ions, this evidence is extremely weak. At an incident energy of 2.40 MeV the S-wave penetrability in only ≈ 1.6 times that for P waves. It should be noted from eq. (25), that for the interaction radius given by eq. (15), the maximum value which $\Gamma_{He^4,1}$ may have, independent of the magnitude of $\gamma^2_{He^4,1}$ is 250 keV.

(b) By subtracting the fitted curve thus obtained from the experimental points the $(a_0)_2$ contribution was determined as a function of incident energy. By fitting this residual curve with the expression $(a_0)_2 = \frac{3}{4}\lambda^2 F_2^2 R_2^2$, values of $E(J_2) = 2.425\pm0.010$ MeV and $\Gamma_T(J_2) = 45$ keV were obtained after correcting for the 20 keV target thickness. From the $(a_0)_2$ value at resonance,

$$\frac{\Gamma^{J_2}_{He^3,2}\times\Gamma^{J_2}_{He^4,3}}{[\Gamma_{He^3,2}+\Gamma_{He^4,3}+\sum\Gamma_{p_j}]^2} = 5.1\times10^{-3}. \quad (23)$$

As shown in the excitation curves of fig. 7 the proton groups, and in particular p_7, appear to have significant contributions from the $\frac{5}{2}$ resonance.

It has been arbitrarily assumed for fitting purposes that $\Gamma_{He^4,3} = \sum\Gamma_p$ whence $\Gamma_{He^3,2} = 0.45$ keV, $\Gamma_{He^4,3} = \sum\Gamma_p = 0.27$ keV. The first two of these correspond respectively to reduced widths of 11 and 3.5 keV. These are 3 % and 1 % of the corresponding single particle limits. It is gratifying to find that the shapes and locations of the derived a_0 and the a_4 curves in fig. 10 are essentially identical as required by the assumption of $J_1 = \frac{1}{2}$ and $J_2 = \frac{5}{2}$ with the a_4 contribution arising entirely from the $\frac{5}{2}$ resonance.

(c) From $(a_0)_1$ and $(a_0)_2$ values at $E(J_1)$ and $E(J_2)$ respectively and the above total widths it follows that $R_1/R_2 = \pm 23.2$, hence from eq. (14) the predicted a_2 coefficient is given by

$$a_2 = 0.86\lambda^2 F_2^2 R_2^2 \left(1 \pm 40.6 \frac{F_1}{F_2} \cos \Psi\right). \tag{24}$$

The solid curve of fig. 11 was obtained by substituting the widths given above into this equation and adding the dashed ramp shown on the figure empirically to take into account the effects of tails of higher resonances as shown in fig. 7. In obtaining this fit to the a_2 coefficient in the Legendre expansion the negative sign in eq. (24) was used and the required value for the hard sphere phase shift correction,

$$\sum_l \tan^{-1} \frac{R^\infty P_l}{1 - R^\infty S_l},$$

in eq. (8), considered as the only remaining adjustable parameter, was determined to be 1.0 ± 0.1 radians. This value is somewhat larger than would be expected for incident He^3 ions where strong strength function behaviour is not expected and suggests that a direct interaction mechanism is involved in the reaction. Further discussion of this point will be deferred until later in the paper. The measured target thickness of 20 keV was also folded into the calculated fit for presentation with the experimental data in fig. 11.

Although the parameters quoted for the resonances, and summarized in table 4, appear to give an adequate representation of the experimental data, it is not claimed that these parameters constitute a unique set. As an example, it has been found possible to fit the a_0 curve of fig. 10 by ignoring all energy dependent corrections provided that an unrealistically large interaction radius, $a = 2.40(A_1^{\frac{1}{3}} + A_2^{\frac{1}{3}}) \times 10^{-13}$ cm, is assumed. The spin assignments to the resonances are however quite definite as are the total widths; the major source of possible ambiguity is of course in the determination of the relative partial widths. From the value of

$$\frac{R_1}{R_2} = \pm \sqrt{\frac{\Gamma^{(\frac{1}{2})}_{i,\frac{1}{2}0} \Gamma^{(\frac{1}{2})}_{e,\frac{1}{2}1}}{\Gamma^{(\frac{1}{2})}_{i,\frac{1}{2}2} \Gamma^{(\frac{5}{2})}_{e,\frac{1}{2}3}}} \tag{28}$$

of -23.2 required to fit the data of fig. 11, a further check is obtained on the

internal consistency of the fitting. Using the partial widths quoted in table 3 and substituting in the above expression yields $R_1/R_2 = \pm 19.9$. The discrepancy here is not considered serious since it would reflect, for example, a change in the assumed He^3 width for the $\frac{5}{2}$ resonance from 0.45 to ≈ 0.60 keV. From the fact that a negative sign is required for this ratio it is only possible to infer a 180° phase difference between the partial width products for the two resonances.

4.2. REACTION MECHANISM BETWEEN RESONANCES

Fig. 9 shows the alpha particle angular distribution measured at the minimum on the excitation curve of fig. 7 at 2.85 MeV and the appropriate coefficients are given in table 1. The lack of symmetry relative to 90° in the centre of mass system together with the apparent increase in the differential cross section at large angles suggests a direct interaction mechanism although the possibility that this results from interference effects between the tails of several higher resonances with differing parity cannot be excluded.

From the rather meagre experimental evidence available on He^3 induced reaction mechanisms it can be demonstrated [1]) that when the linear momenta involved in the reaction are such that the Huby vector diagram [33]) can close, the angular distributions of outgoing particles, for incident energies $\gtrsim$ 2 MeV show the characteristic features of a forward Butler-type stripping or pick-up process [2]). On the other hand, when the momenta are such that the Huby diagram cannot close, as is characteristically the case for He^3 reactions, because of the high Q values involved, the angular distributions show backward maxima characteristic of the heavy particle or target stripping process as investigated for example by Owen and Madansky [5, 6]).

In the $O^{16}(He^3\alpha)O^{15}$ reaction, P-wave neutron pick-up is required for the direct ground state reaction and in this case the Huby diagram fails to close by a large margin. In the case of the $C^{13}(He^3\alpha)C^{12}$ reaction as studied at 2.0 and 4.5 MeV incident energy [3, 4]), this situation also holds; the angular distributions are characterized by very strong structure and in particular by backward maxima. These data have been fitted with considerable success by Owen and Madansky [6]) using both direct and heavy particle pick-up amplitudes and including the interference between these processes.

This suggests that in the case of the $O^{16}(He^3\alpha)O^{15}$ reaction, between the compound nucleus resonances, the reaction proceeds via such a direct interaction process. The large value of R^{∞} required to fit the angular distribution data constitutes supportive evidence for this suggestion.

4.3. PROTON ANGULAR DISTRIBUTIONS

Fig. 12 shows typical proton angular distributions from the $O^{16}(He^3p\gamma)F^{18}$ reaction. These have been used in determining the magnitudes of the total

cross sections involved as discussed in a previous section. Unfortunately, even with the parameters of the resonances involved in the compound system established, the number of remaining parameters involved in the predicted proton angular distribution [28]) ($\geqq 9$ for $J_{\text{final}} \neq 0$) is too great to allow significant comparison with experiment. This reflects the greater channel spin in the exit channel $S_2 = J \pm \frac{1}{2}$. In the case of $J = 0$, of course the formalism reduces to that considered previously for the ($He^3\alpha$) reaction. Experimentally it has only been possible to resolve the proton groups to the quartet of levels near 1 MeV [11]) in F^{18} (one, and probably two of which have spin 0) from the higher spin members with a high resolution magnetic spectrograph. Because of the much smaller effective detector solid angles involved here, a series of measurements, analogous to those reported herein on the alpha particles, which would be required to establish the resonance parameters for these particular proton emitting channels, was not considered to be justified.

4.4. CAPTURE GAMMA RADIATION

Because of the large He^3 partial width of the $\frac{1}{2}$ resonance at 2.40 MeV it would be expected that the cross section for the capture reaction $O^{16}(He^3\gamma)Ne^{19}$

$$\sigma_{\text{cap}} = \frac{4\pi\lambda^2(2J+1)}{(2i+1)(2I_0+1)} \frac{\Gamma_{He^3} \cdot \Gamma_\gamma}{\Gamma_T^2} \tag{26}$$

might be sufficiently large to allow detection of the gamma radiation involved. From the allowed character of the positon decay of Ne^{19} to the $\frac{1}{2}^+$ ground state of F^{19} ($\log ft = 3.30$) [34]) it follows that the Ne^{19} ground state very probably has $J^\pi = \frac{1}{2}^+$. It would therefore be expected that gamma de-excitation of the state in Ne^{19} at 10.436 MeV corresponding to this resonance should go directly to the ground state via E1 or M1 radiation.

As indicated in fig. 13, however, gamma radiation from He^3 induced reactions on the C^{13} target contaminant tend to mask the region of interest in the gamma spectrum. As a result of the low Q values involved, He^3 reactions on O^{16} and C^{12} give no reaction radiation of energy greater than 5.5 MeV. The C^{13} reactions involved are $C^{13}(He^3n)O^{15}$; $C^{13}(He^3p)N^{15}$ and $C^{13}(He^3\alpha)C^{12}$ with Q values of 7.175, 10.663 and 15.625 MeV respectively. The 15 MeV radiation [35]) from the latter reaction is evident in the spectrum; the highest energy transition from the second of the reactions [36]) listed is thus 10.07 MeV, below the region of interest for He^3 capture. At $E_{He^3} = 2.42$ MeV, only states in O^{15} at excitations below ≈ 9 MeV are energetically accessible via the first of the above listed reactions and the proton binding energy is 7.355 MeV.

From the data of fig. 13 it is not possible to give more than an upper limit

for the cross section for the capture process. From the known target thickness the integrated beam current and the spectrometer efficiency at this energy (0.2 %), as extrapolated from measurements at lower energies [37]), using the calculations of Wolicki *et al.* [38]), an upper limit of 0.8 μb is indicated for the capture cross section. Inserting the experimentally determined values for Γ_{He^3} and Γ_T from table 4 in eq. (26), this cross section corresponds

TABLE 4

Resonance parameters for $O^{16}+He^3$

He^3 bombarding energy	Excitation in Ne^{19}	J	Γ_T (keV)	Γ_{He^3} (keV)	$\frac{\gamma^2_{He^3}}{\gamma^2_{sp}}$	Γ_{He^4} (keV)	$\frac{\gamma^2_{He^4}}{\gamma^2_{sp}}$	$\Sigma\Gamma_p$ (keV)
2.400	10.436	$\frac{1}{2}$	355	50	0.67	135	0.05	170
2.425	10.457	$\frac{5}{2}$	45	0.45	0.03	22.3	0.01	22.3

to a value of $\Gamma_\gamma \approx 0.7$ eV, which would be quite consistent with either an E1 or M1 transition. The Weisskopf widths for these transitions would be 545 and 24 eV respectively and the most probable widths [39]) 17.5 and 3.5 eV.

Because of its lower He^3 widths, the $\frac{5}{2}$ resonance would be expected to have a considerably smaller cross section for gamma de-excitation; in addition, because of the higher J value, if the resonance has positive parity it would be expected that the de-excitation would proceed via cascade transitions through lower levels rather than by a direct E2 transition and if negative parity, the width for direct M2 de-excitation would be expected to be negligible. Because of the background radiation from reactions on C^{13} it was not possible to examine such cascading.

It should be noted that the assumption of pure E1 or M1 radiation from the $J = \frac{1}{2}$ resonance implies an isotropic angular distribution of this radiation whereas in fig. 13 the radiation yield in the region of interest is significantly higher at forward angles. This is taken as evidence that this radiation yield cannot be entirely attributed to transitions from the resonance and thus that the actual capture cross section may be as much as an order of magnitude less than the upper limit quoted.

5. Discussion Summary

In section 4 it has been demonstrated that the data of figs. 10 and 11 on the alpha particle angular distribution coefficients cannot be fitted on the assumption of a single compound system resonance level and that interference between levels of the same parity is required. Of the possibilities involving F, and lower, partial waves in the incident He^3 beam, only the $\frac{1}{2}$, $\frac{5}{2}$ combination of spin assignments is in accord with the data.

Since the He^3 partial width of the $\frac{1}{2}$ resonance is $\approx 67\ \%$ of the corresponding single particle limit the Thomas corrections appearing in the conventional resonance reaction formalism are not negligible; because of the large resonance width and the low He^3 energies involved it has been necessary to include the variation of the He^3 penetrabilities with energy in the analysis. Table 4 lists the resonance parameters resulting from a detailed fitting of the data of figs. 10 and 11, using the corrected energy dependent formalism.

Because of experimental difficulties, only an upper limit on the $(He^3\gamma)$ capture reaction cross section via this $\frac{1}{2}$ resonance has been obtained, equal to 0.8 μb.

6. Conclusions

It has been demonstrated that the $O^{16}(He^3\alpha)O^{15}$ reaction proceeds through relatively well resolved compound system levels at low incident energies. The conventional compound system resonance reaction formalism [40, 28]) with energy dependent parameters necessitated by the large resonance width has been found to give an adequate representation of the experimental data. In fitting the data, the resonance parameters for states in Ne^{19} at 10.44 and 10.46 MeV have been obtained as listed in table 4.

From the behaviour of the angular distributions measured between resonances there is a strong suggestion that a direct interaction mechanism of relatively constant amplitude in the narrow energy range considered ($\approx$ 1 to 3 MeV) underlies the compound system amplitude which shows the strong resonance behaviour and, at the resonances, completely dominates the reaction. This suggestion gains support from the large value of R^∞ required to fit the experimental data. A priori, it might be expected that the direct interaction amplitudes for low incident He^3 energies would be much smaller for the $O^{16}(He^3\alpha)O^{15}$ than for the $C^{13}(He^3\alpha)C^{12}$ reaction because of the greater probability of finding the odd neutron in C^{13} in a state suitable for pick-up by the He^3 ion. The experimental results presented here and those of Holmgren *et al.* [3, 4]) are in agreement with this expectation.

A detailed search for effects resulting from interference between the compound system and direct interaction amplitudes would require a situation with more clearly separated resonances. As illustrated in fig. 1 it is most improbable that such a situation exists in He^3 induced reactions; it may well be that the resonance structure studied here may be quite unique with the exception of higher resonances in the He^3+He^4 reaction corresponding to higher states in Be^7.

The fact that the He^3 reduced partial width of the $\frac{1}{2}$ resonance is such a large fraction (67 %) of the single particle limit is somewhat surprising. It should be borne in mind, of course, that unless the He^3 widths are relatively

large there is a good possibility of missing the resonance in the excitation curves. With only a single example, and the fact that it is somewhat improbable that any extensive measurements are possible on resonances in He^3 induced reactions, it is not possible to do more than comment on this behaviour. The alpha particle reduced partial widths of 5 % and 1 % of the single particle limits for the $\frac{1}{2}$ and $\frac{5}{2}$ resonances respectively are in accord with the systematics of such widths as compiled by Wilkinson [39]) who finds that the distribution in these alpha particle widths centers on $\approx$ 5 % of the single particle limit.

As a result of experimental difficulties involving C^{16} contamination of the O^{16} targets used it is not possible to establish more than an upper limit $\approx$ 1 μb for the cross section for the $(He^3\gamma)$ capture reaction. In general it would be anticipated that these cross sections would be very low because of the high Q values, hence large number of open exit channels in He^3 induced reactions.

Further measurements both on $(He^3\alpha)$ and (He^3d) reactions are needed in order to elucidate the reaction mechanisms involved; particularly at higher bombarding energies where direct interaction amplitudes would be expected to be dominant these reactions, when more fully understood, will provide useful tools in nuclear spectroscopy.

We are indebted to Drs. A. J. Ferguson and E. Vogt for interesting discussions regarding this work and to Mr. W. Woytowich for his assistance in the preparation of the Al_2O_3 targets.

Appendix A

For a resonance reaction with channel spins $\frac{1}{2}$ proceeding through a single resonance J, the angular distribution of the emergent particles is given by [40])

$$W(\theta) = \sum_R Z(l_1 J l_1 J; \tfrac{1}{2}k) Z(l_2 J l_2 J; \tfrac{1}{2}k) P_R(\cos\theta). \qquad \text{(A-1)}$$

From this it follows trivially that for $l_1 = l_2$, it is impossible to obtain negative coefficients in the angular distribution. When $l_1 = J \pm \frac{1}{2}$ and $l_2 = J \mp \frac{1}{2}$ this result is less obvious. However, from the definition of the Z coefficient [41])

$$Z(abcd; ef) = i^{f-a+c}[(2a+1)(2b+1)(2c+1)(2d+1)]^{\frac{1}{2}} \times W(abcd; ef)(ac00|acf0), \qquad \text{(A-2)}$$

and the algebraic expressions for the Racah and Clebsh Gordan coefficients[41]) it follows on substitution that

$$Z(j\pm\tfrac{1}{2}, j, j\pm\tfrac{1}{2}, j; \tfrac{1}{2}k) = (-1)^{3j-\frac{1}{2}k+\frac{1}{2}}\sqrt{2k+1}\ \frac{k!}{(\frac{1}{2}k)!}\ \frac{(\frac{1}{2}[2j+k-1])!}{(\frac{1}{2}[2j-k-1])!}$$
$$\times\sqrt{2j+k+1}\sqrt{\frac{(2j-k)!}{(2j+k-1)!}}. \qquad \text{(A-3)}$$

Thus, in this case also only positive angular distribution coefficients are allowed. It should be noted that this identity

$$Z(b+\tfrac{1}{2}, b, b+\tfrac{1}{2}; ef) \equiv Z(b-\tfrac{1}{2}, b, b-\tfrac{1}{2}, b; ef) \qquad \text{(A-4)}$$

holds only for $e = \frac{1}{2}$, corresponding physically to the case of channel spin $\frac{1}{2}$.

References

1) D. A. Bromley and E. Almqvist, Reports on Progress in Physics (to be published)
2) S. T. Butler, Nuclear Stripping Reactions (John Wiley, 1958)
3) H. D. Holmgren, Phys. Rev. **106** (1957) 100
4) H. D. Holmgren, E. H. Geer, R. L. Johnston and E. A. Wolicki, Phys. Rev. **106** (1957) 102
5) George E. Owen and L. Madansky, Phys. Rev. **105** (1957) 1766
6) G. E. Owen and L. Madansky (to be published).
7) D. A. Bromley and A. R. Rutledge, Nuclear Reaction *Q* Values, Chalk River Report CRP—789 (1958) (unpublished)
8) H. D. Holmgren and R. L. Johnston, Phys. Rev. (to be published)
9) J. A. Kuehner, E. Almqvist and D. A. Bromley, Bull. Am. Phys. Soc. **3** (1958) 27; and to be published
10) D. A. Bromley, J. A. Kuehner and E. Almqvist, Bull. Am. Phys. Soc. **3** (1958) 27; and to be published
11) J. A. Kuehner, E. Almqvist and D. A. Bromley, Phys. Rev. Letters **1** (1958) 260
12) D. A. Bromley, J. A. Kuehner and E. Almqvist, Proceedings of the Paris Conference on Nuclear Structure (1958)
13) Evans, Green and Middleton, Proc. Phys. Soc. A **66** (1953) 108
14) A. Feingold, Revs. Mod. Phys. **23** (1951) 10
15) H. E. Walchli, Oak Ridge Report ORNL—1469 (1953) (unpublished)
16) Evans, The Atomic Nucleus (McGraw-Hill, New York) p. 36
17) D. A. Bromley and B. Miles (to be published)
18) F. S. Goulding, Multichannel Pulse Height Analyzers, National Academy of Science, National Research Council U.S.A. Publication No. 467, p. 86 (1956)
19) D. A. Bromley, E. Almqvist, H. E. Gove, A. E. Litherland, E. B. Paul and A. J. Ferguson, Phys. Rev. **105** (1957) 957
20) R. L. Clarke, Nuclear Instruments **3** (1958) 233
21) K. Strohmaier, Zeits. f. Naturforschg. **6a** (1951) 508
22) L. Harris, J. Opt. Soc. Am. **45** (1955) 26
23) J. R. Young, Phys. Rev. **103** (1956) 292
24) W. Whaling, Handbuch der Physik, Vol. **34** (Springer-Verlag, Berlin, 1958) p. 193
25) R. S. Foote and H. W. Koch, Rev. Sci. Inst. **25** (1954) 746;
A. E. Litherland, E. B. Paul, G. A. Bartholomew and H. E. Gove, Phys. Rev. **102** (1956) 208
26) D. A. Bromley, H. E. Gove, J. A. Kuehner, A. E. Litherland and E. Almqvist, Phys. Rev. in press
27) J. W. Butler and C. R. Gosset, Phys. Rev. **108** (1957) 1473
28) S. Devons and L. J. B. Goldfarb, Handbuch der Physik, Vol. **42** (Springer-Verlag, Berlin, 1957) p. 460

29) E. Vogt, Chapter V of Nuclear Reactions, ed. P. M. Endt and M. Demeur (North-Holland Publishing Co., Amsterdam, 1958)
30) W. T. Sharp, H. E. Gove and E. B. Paul, Graphs of the Coulomb Functions, Chalk River Report TPI—70 (1953) (unpublished)
31) Kerlee, Blair and Farwell, Phys. Rev. **107** (1957) 1343
32) A. M. Lane and R. G. Thomas, Revs. Mod. Phys. **30** (1958) 257
33) R. Huby, Proc. Roy. Soc. A**215** (1952) 385
34) Jones, Phillips, Johnson and Wilkinson, Phys. Rev. **96** (1954) 547
35) E. Almqvist, D. A. Bromley, A. J. Ferguson, H. E. Gove and A. E. Litherland, Phys. Rev. in press
36) F. Ajzenberg-Selove and T. Lauritsen, Revs. Mod. Phys. **27** (1955) 77; and private communication (1958)
37) A. E. Litherland, E. B. Paul, G. A. Bartholomew and H. E. Gove, Phys. Rev. **102** (1956) 208
38) E. A. Wolicki, R. Jastrow and F. Brooks, NRL Report 4833 (1956)
39) D. H. Wilkinson, Proceedings of the Rehovoth Conference on Nuclear Structure (1957), ed. H. J. Lipkin (North Holland Publishing Co., Amsterdam, 1958)
40) J. M. Blatt and L. C. Biedenharn, Revs. Mod. Phys. **24** (1958) 258;
W. T. Sharp, J. M. Kennedy, B. J. Sears and M. G. Hoyle, Chalk River Report CRT—556 (1954) (unpublished)
41) L. C. Biedenharn, J. M. Blatt and M. E. Rose, Revs. Mod. Phys. **24** (1958) 249

2.D *Nuclear Physics* **13** (1959) 32—52; © *North-Holland Publishing Co., Amsterdam*
Not to be reproduced by photoprint or microfilm without written permission from the publisher

NEUTRON EVAPORATION AND LEVEL DENSITIES IN EXCITED NUCLEI

K. J. LE COUTEUR and D. W. LANG
Australian National University, Canberra

Received 11 May 1959

Abstract: The theory of a cascade neutron evaporation process is derived in detail in a form suited to the treatment of highly excited nuclei which have a continuous distribution of excitation energies following a primary direct interaction. The results are found to give good agreement with neutron spectra of nuclei following bombardment with 190 MeV protons observed by Gross. Data from medium energy neutron reactions, thermal energy neutron resonances, and heavy ion reaction experiments are compared. Formulae are derived in an appendix for the effect on the level density of a gap in the single particle level spacing at the Fermi level.

1. Introduction

Since the experimental evidence about the statistical theory of nuclear reactions was analysed [1]) further measurements of neutron evaporation have become available and the density of nuclear levels for slow neutron capture has been measured accurately, so that it is appropriate to consider whether these different types of experiment yield a consistent picture.

We shall first consider high energy neutron evaporation cascades in some detail, because the interpretation is not trivial and recently the energy spectra of neutrons produced by 190 MeV bombardment of six elements have been measured by Gross [2]). The general features of this type of nuclear reaction have recently been reviewed [3]) by one of us. In such experiments each inelastic collision leads to emission of several neutrons with 2 or 3 MeV average energy; so much less than the energy of the primary proton that, when interpreting the evaporation spectrum, the contribution of directly ejected neutrons may be neglected.

Weisskopf's [4]) formula for the distribution of the kinetic energy T of a neutron evaporated from an excited nucleus is

$$n(T)\mathrm{d}T \propto \sigma_c T \mathrm{e}^{-T/\tau}\mathrm{d}T, \qquad (1.1)$$

where σ_c is the capture cross section for the inverse reaction and τ is the "temperature" of the residual nucleus. If U_0 is the initial excitation energy of the nucleus and Q the neutron binding energy, the mean excitation energy of the residual nucleus is $U_0-Q-2\tau$ and τ should correspond to this energy.

However, if U_0 is high enough for several neutrons to be emitted in succession while the temperature falls to zero from the value

$$\tau_m = \tau(U_0 - Q - 2\tau_m) \tag{1.2}$$

which governs the emission of the first neutron, the resultant energy spectrum is of the form

$$\frac{1}{\sigma_c} N(U_0, T)\mathrm{d}T \propto T^{l-1} \mathrm{e}^{-T/\tau_*} \mathrm{d}T/\tau_*{}^l \tag{1.3}$$

(Le Couteur [5]) § 4 or [3]) § 7). In this spectrum the mean and mean square energies are

$$\bar{T} = l\tau_*, \quad \bar{T}^2 = l(l+1)\tau_*{}^2. \tag{1.4}$$

If the excitation energy and temperature are related by a power law

$$U = a\tau^\delta, \tag{1.5}$$

then (ref. [5]) § 4), assuming $T \ll Q$, one obtains formulae for l and τ_*, in particular

$$l \approx \tfrac{16}{11}, \quad \tau_* \approx \tfrac{11}{12}\tau_m \quad \text{for} \quad \delta = 2. \tag{1.6}$$

Gross [2]) analysed his results, plotting $\ln(T^{-5/11} \mathrm{N}(T)/\sigma_c)$ against T (see fig. 9 of ref. [3])) and his measurements were sufficiently accurate to indicate deviations from the straight line plots which would result if equations (1.3) and (1.6) described the spectrum exactly. This discrepancy is not surprising since the 190 MeV protons of Gross experiment generate a small cascade within the nucleus, leading to a broad distribution of excitation energies, whereas (1.3) and (1.6) represent the evaporation spectrum resulting from a unique initial excitation.

In this paper we shall derive the extension of the formula (1.3) to the important practical case of a distribution of initial excitation energies and without the restriction $\tau_m \ll Q$ which is not satisfied in all the relevant experiments.

2. Neutron Evaporation Cascade with U_0 given

The integral equations governing evaporation cascades were formulated in reference [5]); if neutron emission only is considered the resultant energy distribution of particles evaporated in a cascade is determined by

$$N(U_0, T) = n(T) + \int n(T')N(U_0 - Q - T', T)\mathrm{d}T', \tag{2.1}$$

with $n(T)$ given by (1.1). This equation was integrated numerically on Silliac using the (normalized) spectrum (1.1) and $U = a\tau^2$ with $a = 5$, 10 and 20 MeV^{-1}. It was found that the result could be represented with an accuracy of 1 % by formulae like (1.3), which are much more useful than the

numerical integrations since the appropriate value of a is not known, but it is desirable to estimate the parameters in (1.3) more accurately than hitherto.

The average excitation energy removed by each neutron emitted is $Q+2\tau$, but to allow for later inclusion of proton effects we write this as $Q+\alpha\tau$. Thus, the expected number of neutrons emitted when the excitation energy falls by $\mathrm{d}U_0$ is

$$\mathrm{d}n = \mathrm{d}U_0/(Q+\alpha\tau_\mathrm{m}), \tag{2.2}$$

where now

$$\tau_\mathrm{m} = \tau(U_0-Q-\alpha\tau_\mathrm{m}). \tag{2.3}$$

Then, since individual emissions have the energy spectrum (1.1), in which σ_c is independent of U_0 though slightly dependent on T, the approximate solution of (2.1) may be derived as in § 3 of ref. [5]) as

$$N(U_0,T) = \int_{\frac{1}{2}Q}^{U_0} n(T)\,\frac{\mathrm{d}U_0}{Q+\alpha\tau_\mathrm{m}}. \tag{2.4}$$

As this integration cannot be performed explicitly, we work with moments which can be evaluated without further approximation:

$$\int_0^\infty \frac{1}{\sigma_\mathrm{c}} N(U_0, T)\{1, T, T^2, T^3\}\mathrm{d}T = \int_{\frac{1}{2}Q}^{U_0} \frac{\mathrm{d}U}{Q+\alpha\tau_\mathrm{m}}\{1, 2\tau, 6\tau^2, 24\tau^3\}.$$

Therefore,

$$\begin{aligned}
&\int_0^\infty \frac{1}{\sigma_\mathrm{c}} N(U_0, T)(Q+\tfrac{1}{2}\alpha T)\mathrm{d}T = \int_{\frac{1}{2}Q}^{U_0} \mathrm{d}U = U_0-\tfrac{1}{2}Q \\
&\int \frac{1}{\sigma_\mathrm{c}} N(U_0, T)(\tfrac{1}{2}QT+\tfrac{1}{6}\alpha T^2)\mathrm{d}T = \int \tau\mathrm{d}U = \frac{\delta}{\delta+1}(U_0-\tfrac{1}{2}Q)\tau_\mathrm{m} \\
&\int_0^\infty \frac{1}{\sigma_\mathrm{c}} N(U_0, T)(\tfrac{1}{6}QT^2+\tfrac{1}{24}\alpha T^3)\mathrm{d}T = \int \tau^2\mathrm{d}U = \frac{\delta}{\delta+2}(U_0-\tfrac{1}{2}Q)\tau_\mathrm{m}^2,
\end{aligned} \tag{2.5}$$

where δ appears because (1.5) is assumed.

Now if the spectrum $N(U_0, T)$ is represented by (1.3) the moments of (1.3) may be equated to the values (2.5) to determine l and τ_*:

$$\begin{aligned}
Q+\tfrac{1}{2}\alpha l\tau_* &= \frac{(\delta+1)}{2\delta\tau_\mathrm{m}}[Ql\tau_*+\tfrac{1}{3}\alpha l(l+1)\tau_*^2] \\
&= \frac{(\delta+2)}{6\delta\tau_\mathrm{m}^2}\{Q+\tfrac{1}{4}\alpha(l+2)\tau_*\}l(l+1)\tau_*^2,
\end{aligned} \tag{2.6}$$

whence, if we write $x = \alpha\tau_*/Q$,

$$1+\frac{1}{l} = \tfrac{3}{2}\frac{(\delta+1)^2}{\delta(\delta+2)}\{1+\tfrac{1}{3}(l+1)x\}^2\{1+\tfrac{1}{2}lx\}^{-1}\{1+\tfrac{1}{4}(l+2)x\}^{-1} \tag{2.7}$$

and

$$\frac{\tau_m}{\tau}=\frac{\delta+1}{2\delta}l\{1+\tfrac{1}{3}(l+1)x\}/\{1+\tfrac{1}{2}lx\}. \qquad (2.8)$$

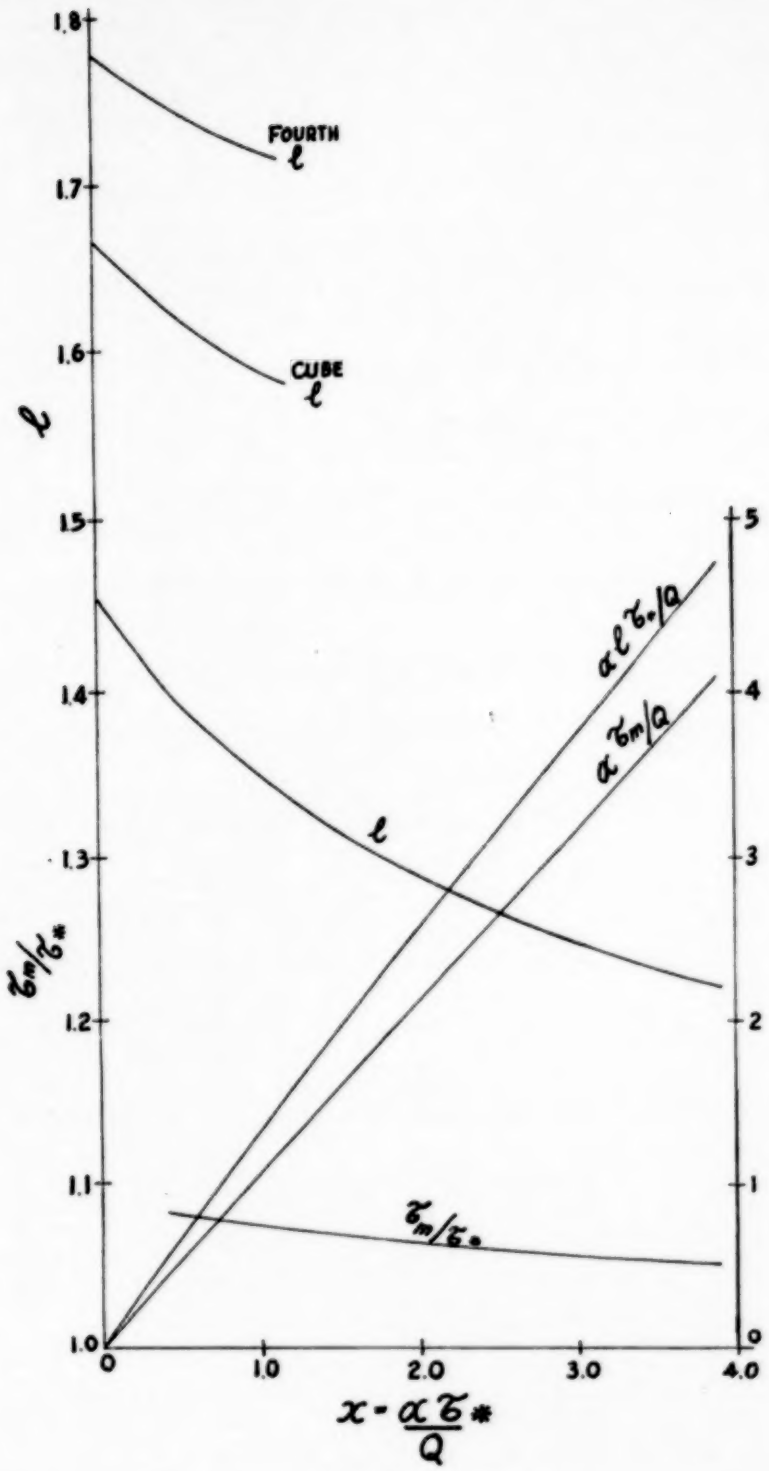

Fig. 1. Values of the exponent l and the ratio τ_m/τ_* (left hand scale), temperature τ_m and the mean neutron energy $l\tau_*$ (right hand scale) as functions of the parameter $\alpha\tau_*/Q$, assuming $U \propto \tau^2$. Values of l for $u \propto \tau^3$ and τ^4 are also presented.

The solutions of equations (2.8, 2.9) are represented graphically in fig. 1, and agree with the rough approximation (1.6) at low temperatures.

The normalization of the spectrum follows from the first of equations (2.5), so that finally

$$N(U_0, T) = \frac{\sigma_c}{\sigma_0} \frac{U_0 - \frac{1}{2}Q}{Q + \frac{1}{2}\alpha l \tau_*} \frac{T^{l-1} e^{-T/\tau_*}}{\Gamma(l) \tau_*{}^l}, \tag{2.9}$$

where σ_0 is the average of σ_c over T. Numerical computations with $\alpha = \delta = 2$ and constant σ_c have verified that the accuracy of (2.10) is within 1 %.

3. Allowance for Proton Emission

The average energy removed by evaporation of a proton is $Q_p + V + 2\tau$, where V is the effective potential barrier height, so if P_n and $P_p = 1 - P_n$ are the respective probabilities of neutron and proton emission the average number of neutrons emitted when the excitation falls by dU is

$$dn_n = dU/(Q_n + 2\tau + (Q_p + V + 2\tau)P_p/P_n) = dU/(Q + \alpha\tau). \tag{3.1}$$

The second form is appropriate because P_p vanishes at $\tau = 0$ and should be considered as an implicit definition of the parameter α, which will subsequently be approximated constant as in (2.2). Also

$$dn_p = \frac{P_p}{P_n} \frac{dU}{Q + \alpha\tau} = \frac{\alpha - 2}{Q_p + V + 2\tau} \frac{\tau dU}{Q + \alpha\tau}. \tag{3.2}$$

The total proton emission in the cascade is then

$$N_p = \frac{\alpha - 2}{Q_p + V + 2\tau} \int \frac{\tau dU}{Q + \alpha\tau} = \frac{1}{2} \frac{\alpha - 2}{Q_p + \bar{T}_p} \bar{T}_n N_n, \tag{3.3}$$

where the slowly varying terms have taken outside the integration. In most of the experiments to be interpreted the number and mean energy $\bar{T}_p$ of evaporated protons is measured so that (3.4) provides an experimental estimate of α as

$$\alpha = 2 + 2N_p(Q_p + \bar{T}_p)/N_n \bar{T}_n. \tag{3.4}$$

TABLE 1

Parameters of Gross [2]) experiment

	U	Au	Ag	Ni	Al
$\bar{T}_n$(Obs) (MeV)		2.4	2.5	2.7	3.0
$\bar{T}_p$(Obs) (MeV)	—	—	9.8	7.4	6.1
N_n(Obs)	9.4	8.0 ±1.6	4.7 ±0.9	2.0 ±0.4	2.1 ±0.4
N_p(Obs)	0	0	0.56 ±0.11	1.10 ±0.22	0.80 ±0.16
Q_n (MeV)	8	8	8	11.5	8
α	2	2	3.7	8.1	5.5
$\alpha\bar{T}/Q$		0.6	1.15	1.89	2.06
l	1.401	1.401	1.361	1.319	1.31
τ_m/τ_*	1.082	1.082	1.076	1.07	1.068

Thus, for Gross' [2]) experiment the values in table 1 are derived, using fig. 1 to derive the values of l and τ_m/τ_* from the observed value of $\alpha l\tau_*/Q = \alpha\bar{T}_n/Q$.

4. Cascade with a Distribution of Initial Excitation Energies

Suppose that the primary collisions leave the nucleus with a distribution of excitation energy $f(U_0)\mathrm{d}U_0$, such as that in fig. 8 of ref. [3]), and let $\sum(T)$ denote the resultant energy distribution of evaporated neutrons. Then

$$\sum(T) = \int f(U_0)\mathrm{d}U_0 N(U_0, T). \tag{4.1}$$

If we represent $\sum$ by a distribution like (1.3),

$$\sum(T)\mathrm{d}T \propto \sigma_c T^{m-1}\mathrm{e}^{-T/\theta}\mathrm{d}T/\theta^m, \tag{4.2}$$

consideration of moments as in § 2 leads to

$$\begin{aligned}\frac{Q+\frac{1}{2}\alpha m\theta}{\langle U_0-\frac{1}{2}Q\rangle} &= \frac{m\theta}{l}\,\frac{Q+\frac{1}{2}\alpha\theta l(m+1)/(l+1)}{\langle (U_0-\frac{1}{2}Q)\tau_*\rangle} \\ &= \frac{m(m+1)}{l(l+1)}\,\theta^2\,\frac{Q+\frac{1}{2}\alpha\theta l(m+2)/(l+2)}{\langle (U_0-\frac{1}{2}Q)\tau_*{}^2\rangle}.\end{aligned} \tag{4.3}$$

In these equations the slow variation of l and τ_*/τ_m with U_0 has perforce been neglected. The expectation values in the denominators stand for

$$\langle U_0-\tfrac{1}{2}Q\rangle = \int f(U_0)(U_0-\tfrac{1}{2}Q)\mathrm{d}U_0 \tag{4.4}$$

$$\begin{aligned}\langle (U_0-\tfrac{1}{2}Q)\tau_*\rangle &= a^{-1/\delta}\,\frac{\tau_*}{\tau_m}\int f(U_0)(U_0-\tfrac{1}{2}Q)(U_0-Q-\alpha\tau_m)^{1/\delta}\mathrm{d}U \\ &= a^{-1/\delta}\,\frac{\tau_*}{\tau_m}\langle (U_0-\tfrac{1}{2}Q)(U_0-Q-\alpha\tau_m)^{1/\delta}\rangle\end{aligned} \tag{4.5}$$

and similarly

$$\langle (U_0-\tfrac{1}{2}Q)\tau_*{}^2\rangle = a^{-2/\delta}\left(\frac{\tau_*}{\tau_m}\right)^2\langle (U_0-\tfrac{1}{2}Q)(U_0-Q-\alpha\tau_m)^{2/\delta}\rangle. \tag{4.6}$$

Define

$$k = \frac{\langle U_0-\frac{1}{2}Q\rangle\langle (U_0-\frac{1}{2}Q)(U_0-Q-\alpha\tau_m)\rangle^{2/\delta}}{\langle (U_0-\frac{1}{2}Q)(U_0-Q-\alpha\tau_m)^{1/\delta}\rangle^2}. \tag{4.7}$$

Then Schwartz's inequality ensures $k \geqq 1$. Equations (4.3) give

$$\frac{l}{m}\,\frac{m+1}{l+1} = \frac{k\left\{1+\frac{1}{2}\alpha\,\dfrac{l(m+1)}{m(l+1)}\,\dfrac{\bar{T}}{Q}\right\}^2}{\left(1+\frac{1}{2}\alpha\,\dfrac{\bar{T}}{Q}\right)\left(1+\frac{1}{2}\alpha\,\dfrac{l}{m}\,\dfrac{m+2}{l+2}\,\dfrac{\bar{T}}{Q}\right)} = k', \tag{4.8}$$

where $\bar{T} = m\theta$ is the mean neutron energy. Formally,

$$1+\frac{1}{m}=\left(1+\frac{1}{l}\right)k'. \tag{4.9}$$

If the distribution of U_0 reduces to a unique value, then $k=1$ and $m=l$, and (4.2) reduces to (2.10). Otherwise, $k-1$ is always small and (4.8) determines k' as

$$k'-1=(k-1)\Big/\left\{1-\frac{k}{(l+2)}\,\frac{\alpha\bar{T}}{(Q+\frac{1}{2}\alpha\bar{T})}\right\}, \tag{4.10}$$

where terms of order $(k-1)/(\alpha\bar{T}/Q)^2$ have been neglected in the denominator. The value of m follows. Using this value of m, θ can be determined graphically from a plot of an experimental spectrum, and a check made that the values found satisfy equations (4.3).

The accuracy of (4.2) has been verified for several typical distributions of U_0 by comparison with the exact machine calculations.

5. The 190 MeV Experiments

Gross [2]) measured neutron spectra from 190 MeV proton bombardment of U, Au, Ag, Ni, Al, C. In the first stage of such a reaction the primary particle generates a small cascade of fast particles within the nucleus, for which we refer to the Monte Carlo calculations [6]) of Metropolis, Bivins, Storm Turkevitch, Miller and Friedlander. These authors plot graphs of the distribution of excitation energy transfered to U, Bi, Ce, Ru, Cu, Al by protons of up to 360 MeV energy. We have calculated the moments of these curves and interpolated them to obtain the values in table 2.

TABLE 2

Moments of the nuclear excitation energy received from 190 MeV protons

	U (MeV)	$(U-4)(U-8)^{\frac{1}{2}}$ (MeV$^{\frac{3}{2}}$)	U^2 (MeV^2)
Al	37.6	246.7	2 399
Ni	53	413	4 380
Cu	55.7	439	6 647
Ag	71.8	632	7 100
Ce	80.5	738	8 056
Au	90	898	10 400
U	95	964	11 640

From these values the moments (4.4), (4.5), (4.6) are easily deduced assuming $\delta=2$, and a first approximation to a, which need not be very accurate since the dependence on a is slight. For each experiment, m can now be determined numerically from (4.9), and then the spectrum (4.2) implies that a plot of $\ln[T^{1-m}/\sigma_c(\sum(T)]$ versus T should yield a straight line of

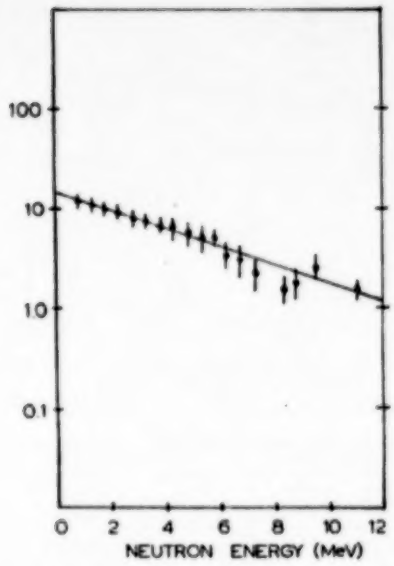

Fig. 2. Logarithmic plot of $\frac{1}{\sigma_c} T^{0.213} \Sigma(T)$ for Al.

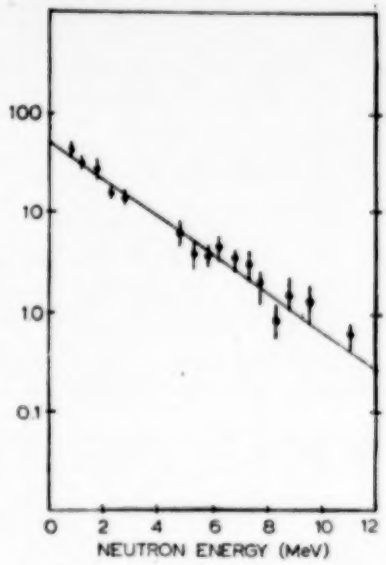

Fig. 3. Logarithmic plot of $\frac{1}{\sigma_c} T^{-0.018} \Sigma(T)$ for Ni.

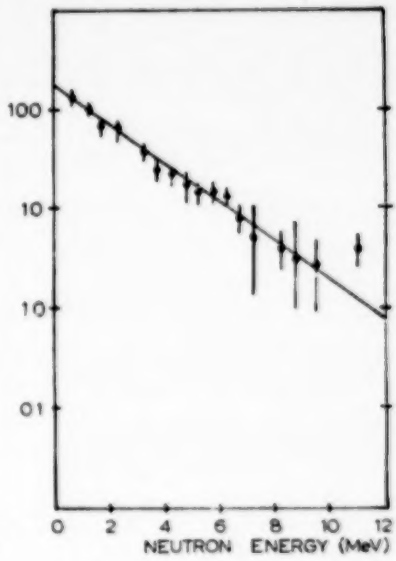

Fig. 4. Logarithmic plot of $\frac{1}{\sigma_c} T^{-0.12} \Sigma(T)$ for Ag.

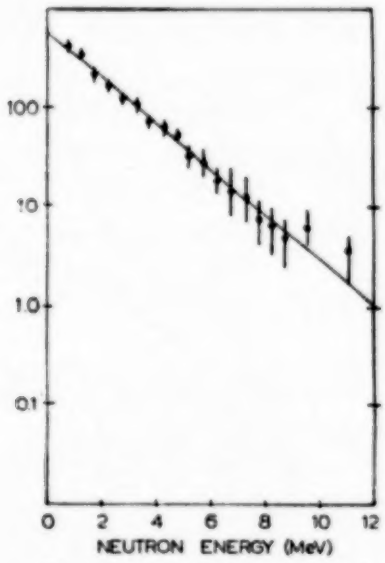

Fig. 5. Logarithmic plot of $\frac{1}{\sigma_c} T^{-0.21} \Sigma(T)$ for Au.

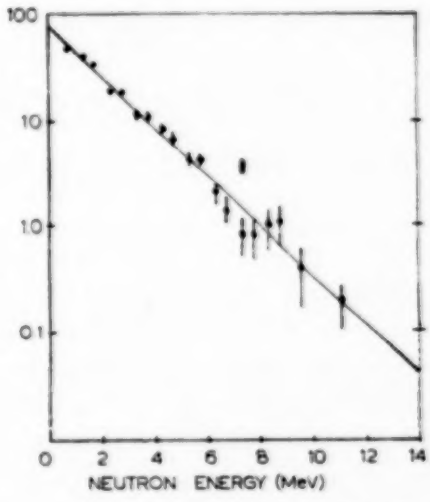

Fig. 6. Logarithmic plot of $\frac{1}{\sigma_c} T^{-0.29} \Sigma(T)$ for U.

slope $1/\theta$, from which the thermodynamic parameter a may be determined. We used Beyster's [7]) optical model calculations of the neutron capture cross section σ_c, which differ very slightly from the results given in Blatt and Weisskopf [8]) as used by Gross [2]). Results for five elements are presented in table 3 and figs. 2 to 6.

The figures show that the spectrum (4.3) represents the observed spectra within the accuracy of observation, and assuming U proportional to τ^2,

TABLE 3

Calculated parameters from Gross' data

	$\langle U-\frac{1}{2}Q\rangle$ (MeV)	$\langle(U-\frac{1}{2}Q)(U-Q-\alpha\tau)^{\frac{1}{2}}\rangle$ (MeV$^{\frac{3}{2}}$)	$\langle(U-\frac{1}{2}Q)(U-Q-\alpha\tau)\rangle$ (MeV^2)	k	k'	m	$1-m$	θ	$a^{-\frac{1}{2}}\left(\frac{\tau_*}{\tau_m}\right)$	a (MeV^{-1})
Al	33.6	184	1 154	1.147	1.29	0.788	0.212	4.6	0.592	2.6
Ni^{58}	47	302	2 126	1.095	1.128	1.018	−0.018	2.3	0.292	10.2
Ag	66	583	5 500	1.068	1.089	1.125	−0.125	2.26	0.292	18
Au	85	846	8 784	1.04	1.05	1.24	−0.24	1.88	0.169	30
U	91	945	10 137	1.03	1.037	1.29	−0.29	1.84	0.165	31

A line drawn through the experimental points gives θ. Then the ratios of the first to the second and the second to the third terms in eq. (4.3) give the ratios of the denominators, from which by use of (4.5) and (4.6) two values for $a^{-\frac{1}{2}}(\tau_*/\tau_m)$ are derived. Taking the mean value, we deduce $U/\tau^2 = a$.

we have inferred the value of U/τ^2 for each element studied. These are plotted in fig. 7.

Of course the results cannot establish that U varies as τ^2 over the range of excitation energy, from about 10 to 150 MeV, involved in each experiment. *However, the spectra suffice to exclude relations like* $U = a\tau^\delta$ with $\delta > 3$. To see this, first consider the extreme assumption that τ is independent of U. Then every neutron is emitted with the spectrum (1.1) with the same τ and so the resultant spectrum has also the form (1.1). Gross' results exclude this possibility by showing that a logarithmic plot of $\sum(T)/T\sigma_c$ does not yield a straight line. Gross' experimental results are sufficiently accurate to show that logarithmic plots of $\sum(T)/T^{5/11}\sigma_c$ all have a common curvature, so that the experiments require $m < \frac{16}{11} = 1.45$ in the spectrum (4.3). But the values of l for $\delta = 3$ and 4 shown in fig. 1 are too large to yield $m < 1.45$ when the calculations of § 4 are carried through; accordingly such large values of δ are excluded. The physical reason is that a temperature variation as $U^{1/\delta}$ with $\delta > 3$ is too slight to yield sufficient modification of the Weisskopf spectrum (1.1).

6. Heavy Ion Experiments

If a nucleus of a light element, e.g. nitrogen or carbon, is accelerated sufficiently to penetrate another nucleus, a compound nucleus can result with an excitation energy made up of the gain in binding energy from fusion (which can be positive or negative) together with the kinetic energy required to bring about fusion. Since neither of these gives rise to a very high energy per nucleon there is some hope that the statistical theory will be immediately applicable to the observed particle emission in the cooling of such a nucleus.

There are, however, two difficulties in such interpretation. The processes of acceleration render it difficult to estimate the ionization and hence the energy of the bombarding nuclei. In the actual collision process breakup of the bombarding nucleus can occur before fusion: such effects are described under the names of "stripping", "grape shot effect" and "evaporation from local hot spots". These will lead to too high temperature if disregarded in cases in which they occur. If in addition the bombarded nucleus is very heavy [9,10]), the prevalence of fission reactions so confuses the interpretation that no reliable estimates of nuclear temperatures have yet been made in this case.

For light target nuclei, Goodman and Need [11]) bombarded beryllium with nitrogen and found that the level density in the various residual nuclei formed could be represented by

$$\rho(E) = \exp\{2[a(E-b)]^{\frac{1}{2}}\} \tag{7.1}$$

and

$$E = a\tau^2+b.$$

The results found are

Reaction product	a (MeV^{-1})	b (MeV)
$\alpha+F^{19}$	1.1	0
$d+Ne^{21}$	1.4	0
$n+Ne^{22}$	2.6	4.9

The wide variation of the parameters over such a small range of atomic mass appears larger than would be expected from pairing energy considerations and could possibly be due to stripping reactions increasing the yield of high energy alphas and deuterons. There is, however, some evidence [12]) against the occurrence of these reactions.

Zucker [13]) bombarded aluminium with nitrogen and found, assuming $b = 0$,

Reaction product	a (MeV^{-1})
$\alpha+A^{37}$	4.1±0.3
$p+K^{40}$	5.0±0.2

These results are plotted in fig. 7.

7. Fermi Gas Model

The simplest theoretical model with which our results may be compared is a Fermi gas of N neutrons and Z protons for which the equation of state is [1])

$$U = \tfrac{1}{6}\pi^2 g t^2 - t \tag{7.1}$$

and the density of states is

$$P(U, N, Z) = \tfrac{1}{12}\left(\frac{6}{g}\right)^{\frac{1}{4}} (U+t)^{-5/4} \exp 2(\tfrac{1}{6}\pi^2 g u)^{\frac{1}{2}}, \tag{7.2}$$

where g is the density of single particle states at the Fermi energy. Since by definition

$$\frac{1}{\tau} = \frac{\mathrm{d}}{\mathrm{d}U}\log P, \tag{7.3}$$

we find a defined by

$$a = \tfrac{1}{6}\pi^2 g = \frac{U}{\tau^2} + \frac{2.5}{\tau}, \tag{7.4}$$

so that at high temperatures, such as obtained in Gross' work, we have the law (1.3). At low temperatures the second term in (7.4) is important.

Newton [14]) has shown that, for excitation energies in the neighbourhood of neutron binding energy, the even-odd dependence of P is sufficiently well represented if the pairing contribution to the binding energy of the ground state is subtracted from the excitation energy before substitution in (7.2).

If the angular momenta of the individual nucleons are combined at random, the number of levels of angular momentum J, including both parities, is derived from (7.2) as

$$\rho(U, N, Z, J) = \frac{2J+1}{\pi^{\frac{1}{2}}(2ct)^{\frac{3}{2}}}\, \mathrm{e}^{-(J+\frac{1}{2})^2/2ct}\, P(U, N, Z), \tag{7.5}$$

where ch^2 can be interpreted as a moment of inertia or related to mean square value of the magnetic quantum number m of individual nucleons by the formula [14])

$$\langle m^2 \rangle g = c. \tag{7.6}$$

Jensen and Luttinger [15]) have shown that the sequence of states in the shell model implies

$$\langle m^2 \rangle \approx 0.146 A^{\frac{5}{3}} \tag{7.7}$$

with about $\pm 10\,\%$ fluctuation due to shell effects. The simplest nuclear models make g and a proportional to A; if $a = \frac{1}{8}A$ MeV^{-1} is adopted, we find

$$c = A^{\frac{5}{3}}/90 \text{ MeV}^{-1}, \tag{7.8}$$

which corresponds to a nuclear moment of inertia ch^2 equal to 0.8 of the rigid body value for a nucleus with root mean square radius $1.22A^{\frac{1}{3}} \times 10^{-13}$ cm.

8. Inelastic Scattering of Low Energy Neutrons

Cranberg and Levin [16]) have used the very accurate "time of flight" method to measure the energy spectra of inelastically scattered neutrons.

Because of the low energy, only one neutron is emitted in each collision and the energy spectra can be directly represented by Weisskopf's equation (1.3) without the intervention of any cascade theory, from which table 4 can be deduced.

TABLE 4

Nuclear temperature from inelastic neutron scattering

Primary energy (MeV)	$^{197}_{79}$Au	$^{181}_{73}$Ta	$^{180}_{74}$W	$^{107}_{47}$Ag
2.45	0.30	0.32	0.36	
3.40	0.45	0.39	0.36	
6.34	0.65	0.50	0.44	0.59

The spectra from the lower bombarding energies are influenced by the individual structure of the low lying nuclear levels. However, Cranberg and Levin show that the spectra from 6.34 MeV bombardment have the Weisskopf shape quite accurately, and only these spectra are used in the subsequent analysis. The values of U/τ^2 calculated, taking for U the mean excitation energy of the residual nucleus (§ 1) after the allowance for the even-odd effect as in § 7, are 10.2, 17.7, 18.7, 11.4 MeV^{-1} for Au, Ta, W, Ag respectively. The second term in (7.4) is significant at the low temperatures and modifies our estimates of a to 14, 22.7, 24.2, 15.5 MeV^{-1}, which are plotted in fig. 7.

9. Inelastic Scattering of 14 MeV Neutrons

Extensive investigations of inelastic scattering of 14 MeV neutrons were made by Graves and Rosen [17]) and later more accurate measurements for Ta and Bi were completed by Rosen and Stewart [18]). The primary energy of 14 MeV ensures that when a true compound nucleus is formed, two neutrons are evaporated in succession. The resultant energy spectra are represented well by (1.3) and (1.6), from which Rosen and Stewart deduced the temperature τ_1, and energy spectrum of the first evaporated neutron and then by subtraction the energy spectrum and temperature τ_2 for the second neutron. Their results are as follows:

	$U_1 = 12$ MeV	$U_2 = 15$ MeV	Derived value of a
Ta	$\tau_1 = 0.95$ MeV	$\tau_2 = 0.46$ MeV	18 MeV^{-1}
Bi	$\tau_2 = 1.05$ MeV	$\tau_2 = 0.53$ MeV	15 MeV^{-1}

The experiment determines only a weighted mean of τ_1 and τ_2 and this specific interpretation is possible only by assuming $U \propto \tau^2$. However for Ta,

the temperature at 3.5 MeV excitation is consistent with Cranberg and Levin's measurement.

The earlier experiments of Graves and Rosen were analysed by Le Couteur [19]) and by Tomasini [20]) and the mean of their values for a derived from (7.4) is plotted on fig. 7.

10. Level Spacings at Neutron Binding Energy

Eighty experimental values of the nuclear level spacing at neutron binding energy were taken from papers of Stolovy and Harvey [21]) and Cameron [22]). It is difficult and possibly misleading to analyse this material by itself

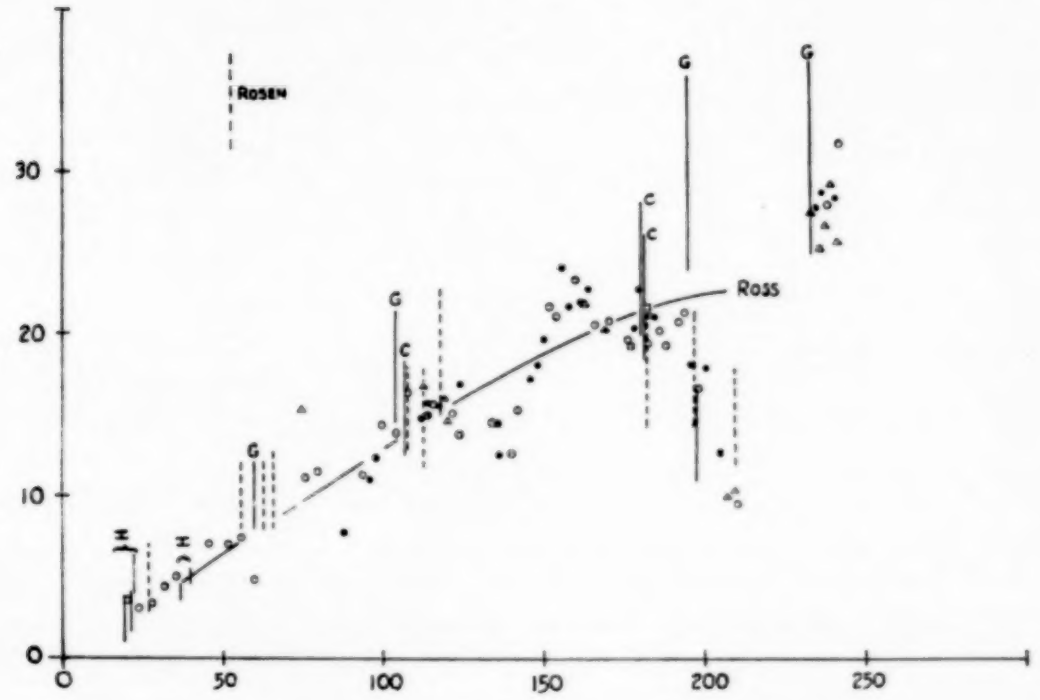

Fig. 7. Estimate of a deduced from experiments of Gross (G) at 190 MeV, Cranberg and Levin (C) at 6 MeV, Rosen and Stewart and Graves and Rosen, and from heavy ion experiments (H), shown with their experimental errors. Values deduced from measured nuclear level spacings at neutron binding energy are shown for comparison (○, ●, △, □). The curve represents Ross' estimate from levels of individual particles in a potential well.

because of the essential dependence of level density on excitation energy and angular momentum, but in terms of a specific model the material is very useful.

We have analysed the spacings in terms of the Fermi gas model through eqs. (7.1) and (7.2) and so obtained a value of g or a for each nucleus. These values are plotted in fig. 7. It is evident that there are strong shell effects,

and the subtraction procedure outlined in § 7 accounts for most of the difference in level density between odd, odd mass and even nuclei.

11. Comparison of Results

Fig. 7 shows that, except in the neighbourhood of closed shells, there is reasonable agreement between the estimates of a derived from nuclear temperatures at high excitation energy, the estimate for level spacing at neutron binding energy, and the estimate from Cranberg's and Levin's work at lower excitation energies. This suggests that between closed shells, the Fermi gas model is an approximation to the nuclear level density valid over a large range of excitation energies. This conclusion is further supported by agreement between our estimate of a or g and the density of single particle states calculated by Ross [23]) from the position of nucleon levels in the potential well models of Ross, Mark and Lawson [24, 25]). Unfortunately the calculations do not extend beyond mass 208 but the dip in Ross' curve for a there results from the method used to average g over the gap in neutron and proton levels at the double closed shell and would presumably not continue up to mass 230.

Near the double closed shell at Pb^{208}, there is sharp decrease in the density of levels at neutron binding energy and this material, considered by itself, has been interpreted [14, 22]) in terms of a reduced value of the single particle level density g, such as indicated by the points in fig. 7. However, the high energy results of Gross show no such tendency, though it is unfortunate that no element closer to the shell than Au was examined. Therefore, we would prefer to interpret the level density near closed shells in terms of a model, illustrated in fig. 8 and discussed in the appendix, which crudely represents the Klinkenberg [26]) level scheme, with a gap of width 2Δ in the spectrum of single particle states and a value for the average density g obtained by interpolation between neighbouring non-magic nuclei. This procedure suggests $a = 25$ MeV^{-1} and $g = 15$ MeV^{-1} near mass 208.

If the density of single particle states is assumed constant outside the gap, the results derived from fig. 8a show that the level density at neutron binding energy is reproduced correctly if the gap has a width of 1 MeV for mass 204 to 210, falling to 0.4 MeV for mass 198 to 195 and to 0.2 MeV for mass 192. The gap of 1 MeV above the double closed shell is less than the distance between the $3p_{\frac{1}{2}}$ and $2g_{\frac{9}{2}}$ levels in the extreme shell model [24, 25]), but as soon as a few particles in the nucleus are excited, the degeneracy of the $g_{\frac{9}{2}}$ states may be removed and our gap 2Δ is perhaps a crude representation of the distance to the lowest of these states.

A distribution of single particle states, like b) in fig. 8, is probably better than a) to represent the situation near a closed shell, where there is a clear gap

between occupied and unoccupied levels at zero temperature, but the degeneracy of the levels concentrates many states near the edges of the gap in such a way that the total number of single particle states is independent of the gap. With model b) the level density at neutron binding energy is reproduced correctly if the gap 2Δ has a width of 1.9 MeV for mass 204 to 210, which is reasonable for the shell model, falling to 0.9 MeV for mass 198 to 195.

Fig. 8 shows that the presence of a gap modifies the temperature τ at all

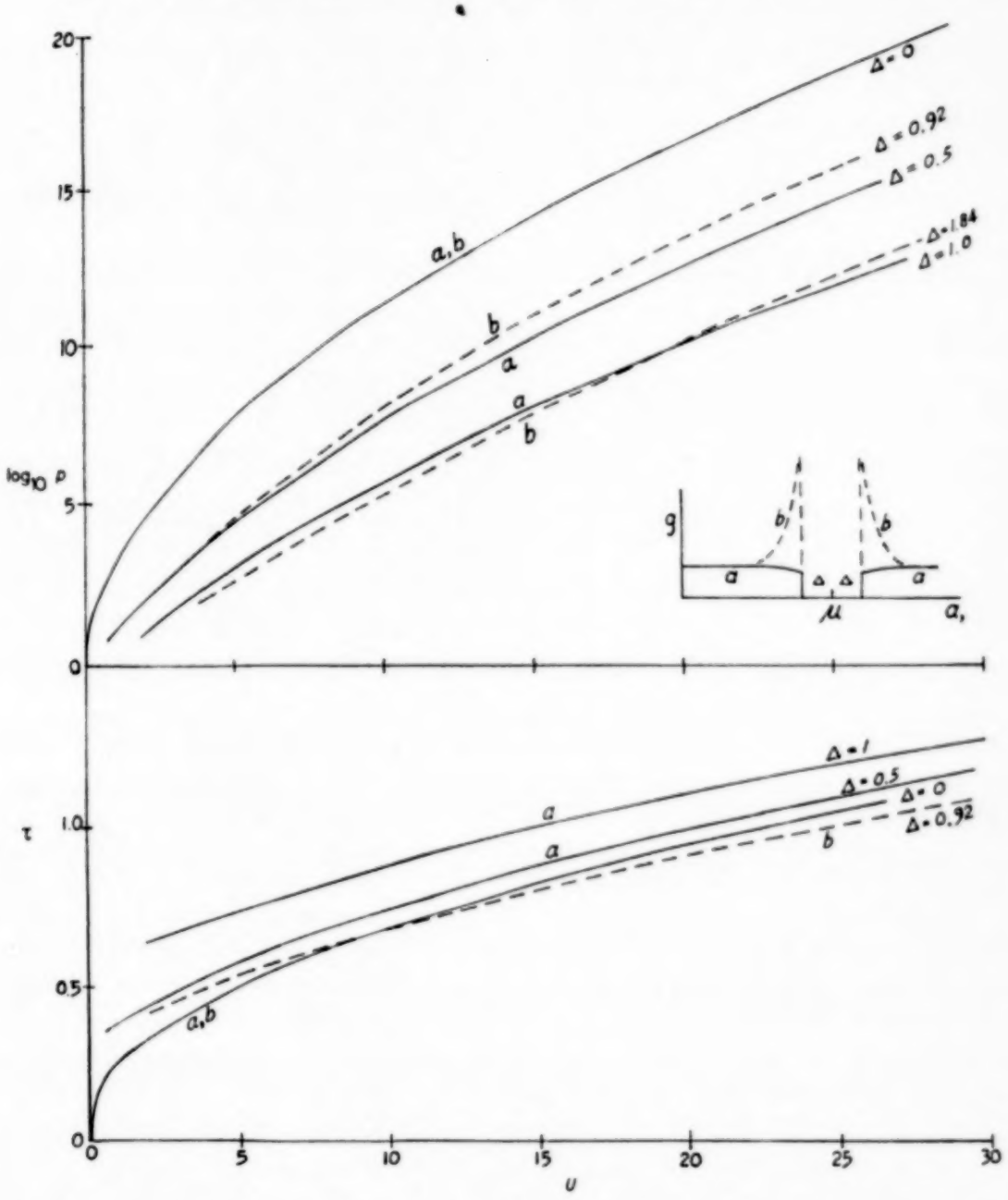

Fig. 8. Effect of a gap, illustrated in the inset, upon the density of levels $P(N, Z, U)$ and temperature τ of a nucleus at excitation energy U. Values refer to $a = 25$ and gaps of half width $\Delta = 0, 0.5, 1$ for model a), $\Delta = 0, 0.92, 1.84$ for model b).

excitation energies considered, but less at high ones. With the values of Δ stated above, the gap increases the temperatures at low excitation energy sufficiently to improve the agreement with the experimental results for Au and Bi stated in § 8 and 9.

The effect of the gaps on the value of U/τ^2 for the Gross experiment with a gold target is slight, because at high excitation the gap has little effect and, as the average number of neutrons emitted in the cascade is eight, by the time low excitations are reached, the nucleus is so far removed from the closed shell that the gap width is negligible. However, it is noteworthy that model b) does slightly reduce the temperature at high excitation, leading to increased values of U/τ^2, so that the rather high value obtained by Gross for Au may have some significance, There would be considerable interest in a repetition of Gross experiment with target nuclei a little heavier than Pb, so that some of the neutrons would be evaporated from the closed shell nucleus.

The low level densities in the neighbourhood of the neutron shell at $A = 140$ may be interpreted in terms of a gap of width 0.7 MeV if model b) is adopted.

It has been suggested [27]), by analogy with theories of superconductivity[28]), that, quite apart from shell effects, the interaction between nuclear particles may produce a gap at the Fermi level in the spectrum of single particle states. The gap width represents a minimum excitation energy of a single particle and may be interpreted as the energy required to separate particles which are paired when the nucleus is in the ground state. This interpretation would suggest a width of about 0.9 MeV in the distorted nuclei around Ta for which the analogy with superconductivity is most appropriate. But with this gap figure 8 indicates a reduction by about a factor 50 on the density of nuclear states at 7 MeV excitation and it would be necessary to increase a from 20 to 28 to retain the observed density of levels for slow neutron capture. Ross' work shows that such a high density of single particle states will not fit into a conventional nuclear potential well. Therefore, we conclude that, if the interactions produce a gap near the Fermi level, the gap must decrease with excitation energy so as to be practically zero at neutron binding energy, and this behaviour would perhaps strengthen the analogy with superconductivity.

Almost any elaboration of the Fermi gas model must have the simple results of § 7 as a high energy limit. Apart from the introduction of a gap, which is certainly required near the closed shells, the effect of pairing interaction between particles has been considered [29, 30]). However, these interactions produce correlations between particles and thus reduce the density of states of the nucleus. Therefore, the values of a derived from the neutron capture data, and shown in fig. 7, are lower limits for such a model. But both

Ross' curve and Gross' experiment suggest that a cannot be increased very much; therefore, the simple Fermi gas must give a fair approximation to the level density at excitations above neutron binding energy. The best values of a or g to use are more conveniently read from fig. 7 than embodied in a formula, but $a = \frac{1}{8}A$ MeV^{-1} is sometimes useful.

By a least squares procedure, applied to c and g independently, Cameron[22]) has fitted the level spacing at neutron binding energy rather more accurately than us. His values of g are less than ours, and accordingly, to find sufficient levels for slow neutron capture, the available states must be concentrated on low angular momenta. This is achieved by adopting a value of the moment of inertia c in (7.5) of about a fifth the rigid body value, which is not very likely.

Finally we remark that we have presented the neutron cascade theory in detail because it would be useful to extend experiments like Gross' and also Cranberg and Levin's to many more elements.

We are indebted to Mrs. B. Nerdal for help with the numerical calculations and to the Nuclear Research Foundation in the University of Sydney for the use of Silliac to solve the integral equations of the neutron cascade.

Appendix

FERMI GAS WITH A GAP

In the notation of the appendix of ref. [1]) the grand partition function for a Fermi gas with individual particle energy levels a_s and b_s for neutrons and protons is

$$-\beta\Phi = \sum_s \log[1+\exp(\zeta_1-\beta a_s)]+\sum_s \log[1+\exp(\zeta_2-\beta b_s)] \qquad \text{(A1)}$$

$$= \sum_{a_s<\mu_1} (\zeta_1-\beta a_s)+\sum_{b_s<\mu_2} (\zeta_2-\beta b_s)+2\int_0^\infty g(\varepsilon)\log(1+e^{-\beta\varepsilon})d\varepsilon \qquad \text{(A.2)}$$

where $\beta = 1/t$, $\zeta_1 = \beta u_1$, $\zeta_2 = \beta\mu_2$; $g(\varepsilon) = g_1(\varepsilon)+g_2(\varepsilon)$ is the sum of the densities of individual neutron states at energies $\mu_1+\varepsilon$ and proton states at energies $\mu_2+\varepsilon$, and we have symmetrized $g(\varepsilon)$ as a function of ε. In the simplest model $g(\varepsilon)$ is treated as a constant; we shall consider two elaborations, illustrated in figs. 8a, b, in which the density g vanishes in a gap extending for a distance Δ on either side of μ.

Model a)

For simplicity the integral in (A1) is taken as

$$\mathcal{I} = \tfrac{1}{6}\pi^2 g e^{-\beta\Delta}, \qquad \text{(A3)}$$

which corresponds exactly to constant $g(\varepsilon)$ if $\Delta = 0$, and if $\Delta > 0$ is an approximation to the case $g(\varepsilon) = g$ for $\varepsilon \gg \Delta$ but $g(\Delta) = \frac{1}{12}\pi^2 g$.

Model b)

In this model the single particle states which are missing from the gap 2Δ are not completely lost to the system as in a), but are displaced to positions just outside the gap in such a way that the total number of single particle states is conserved. A specific model of this kind, taken over from theories of superconductivity [31, 27]), assumes that the attraction between the fermions displaces the levels $\mu \pm \varepsilon_s$ to

$$a_s = \mu \pm (\varepsilon_s^2 + \Delta^2)^{\frac{1}{2}} \tag{A4}$$

and treats $g(\varepsilon)$ as constant. Even though the analogy with superconductivity may not hold, this formula may give a fair representation of the situation in a closed shell nucleus (§ 11). The integral in (A1) becomes

$$2g \int_0^\infty \log(1+e^{-\beta\sqrt{(\varepsilon^2+\Delta^2)}})d\varepsilon \approx \frac{\pi^2 g}{6\beta} e^{-\beta\Delta}(1+72\Delta\beta/\pi^3) \approx \frac{\pi^2 g}{6\beta} e^{-0{\cdot}4(\Delta\beta)^{1.5}}, \tag{A5}$$

and the second approximation, though less accurate than the first, is within 2 % for $t > \frac{1}{2}\Delta$.

With this approximation, the grand partition function for a) or b) may be written

$$-\beta\Phi = \sum \zeta_1 + \zeta_2 - \beta a_s - \beta b_s + \tfrac{1}{6}\pi^2 g e^{-(\delta\beta)^p}, \tag{A6}$$

where $\delta = \Delta$ and $p = 1$ for model a), and $\delta = 0.54\Delta$ and $p = 1.5$ for model b).

The gap Δ must represent some dynamical effect of the interaction between particles and may be expected to decrease with the excitation of the nucleus. This effect can be represented crudely by increasing p in (A6), so as to make Δ decrease as some power of the temperature. The form (A6) incidentally shows that model b) cannot be distinguished from model a) with Δ decreasing as $t^{-\frac{1}{2}}$.

Then, if the ground state energy $\sum(a_s + b_s)$ for $a_s < \mu_1$ and $b_s < \mu_2$ is subtracted from $\partial\beta\Phi/\partial\beta$, the excitation energy is

$$U = \frac{a}{\beta^2} e^{-(\delta\beta)^p}\{1 + p(\delta\beta)^p\}, \tag{A7}$$

where for simplicity, as in (7.4), we write $a = \frac{1}{6}\pi^2 g$.

We require the density of levels for a system of N neutrons and Z protons at excitation U, which is obtained by the usual saddle point multiple integration as

$$P(N, Z, U) = e^s/(-2\pi dU/d\beta)^{\frac{1}{2}}(-2\pi d^2\beta\Phi/d\zeta_1^2)^{\frac{1}{2}}(-2\pi d^2\beta\Phi/d\zeta_2^2)^{\frac{1}{2}}, \tag{A8}$$

$$s = 2at\,\mathrm{e}^{-(\delta\beta)^p}\left(1+\tfrac{1}{2}p(\delta\beta)^p\right). \tag{A9}$$

Eq. (A7) gives

$$-\mathrm{d}U/\mathrm{d}\beta = at^3\mathrm{e}^{-(\delta/t)^p}\{2+p(3-p)(\delta/t)^p+p^2(\delta/t)^{2p}\}.$$

The dispersion $\mathrm{d}^2\beta\Phi/\mathrm{d}\zeta_1^2$ of the number of neutrons in the assembly Φ is reduced by the gap to

$$-\mathrm{d}^2\beta\Phi/\mathrm{d}\zeta_1^2 = \frac{2g_1}{(1+\mathrm{e}^{(\beta\delta)^p})} \tag{A10}$$

which is exact for model a) and approximate for b).

Combining the results, we find

$$P(N, Z, U) = \frac{1+\mathrm{e}^{(\beta\delta)^p}}{2\pi gt}\,\frac{\mathrm{e}^s}{(-2\pi\mathrm{d}U/\mathrm{d}\beta)^{\frac{1}{2}}}. \tag{A11}$$

In the appendix of ref. [1]), it was shown that a succession of single saddle point integrations leads to a slightly more accurate result at low temperatures than the multiple integration (A8), but in the present case that procedure leads to awkward formulae without significant change in the numerical results. Equation (A11) is in convenient form for computation, and on a computer many different models can be studied by simple variation of p. Results are represented in fig. 8.

Of prime importance is the variation of P and S with U, not with t. Eqs. (A7) and (A9) give

$$S^2 = 4aU\,\mathrm{e}^{-(\delta\beta)^p}\left(1+\tfrac{1}{4}p^2(\delta\beta)^{2p}\right)/\left(1+p(\delta\beta)^p\right),$$

thus, at high temperatures,

$$S = 2(aU)^{\frac{1}{2}}-(aU)^{\frac{1}{2}}(\delta\beta)^p \approx 2(aU)^{\frac{1}{2}}-a\delta^p/t^{p-1}. \tag{A12}$$

This formula indicates a qualitative difference between model a), with $p = 1$, in which even at high excitation the gap reduces the level density P by a factor $\exp(a\delta)$ and models like b) with $p > 1$, in which for sufficiently high excitation the level density is gap independent. These tendencies are visible in fig. 8.

Fig. 8 also shows the variation with U of the temperature τ, the inverse logarithmic derivative of P. On models like b) with $p > 1$, the gap slightly lowers τ at high excitation, because P is increasing towards the value for no gap.

References

1) J. M. B. Lang and K. J. Le Couteur, Proc. Phys. Soc. A **67** (1954) 585
2) E. E. Gross, U.C.R.L. **3330** and U.C.R.L. **3337** (1956)
3) K. J. Le Couteur, Nuclear Reactions Vol. 1 (North Holland Publishing Co., Amsterdam, 1958) p. **318**
4) V. F. Weisskopf, Phys. Rev. **52** (1937) 295

5) K. J. Le Couteur, Proc. Phys. Soc. A **65** (1952) 718
6) N. Metropolis, R. Bivins, M. Storm, A. Turkevitch, J. M. Miller and G. Friedlander, Phys. Rev. **110** (1958) 185
7) J. R. Beyster, L. A. 2099
8) J. M. Blatt, and V. F. Weisskopf, Theoretical Nuclear Physics (John Wiley, New York, 1952) 348
9) T. Sikkeland, S. Thompson and A. Ghiorso, Phys. Rev. **112** (1958) 543
10) S. A. Baraboskin, A. S. Karamian and G. N. Flerov, Soviet Physics JETP **5** (1957) 1055
11) C. D. Goodman and J. L. Need, Phys. Rev. **110** (1958) 676
12) D. M. Parfanovich, N. V. Rabin and A. M. Semchinova, Soviet Physics JETP **4** (1957) 99
13) A. Zucker, Nuclear Physics **6** (1958) 420
14) T. D. Newton, Can. Journ. Phys. **34** (1956) 804
15) J. H. D. Jensen and J. M. Luttinger, Phys. Rev. **86** (1952)907
16) J. S. Levin and E. Cranberg, O.R.N.L. 2309 (1958) 84
17) E. R. Graves and L. Rosen, Phys. Rev. **89** (1953)343
18) L. Rosen and L. Stewart, Phys. Rev. **107** (1957) 824
19) K. J. Le Couteur, Rep. Birmingham Conference (1953)
20) A. Tomasini, Nuovo Cimento **12** (1954) 134
21) A. Stolovy and J. A. Harvey, Phys. Rev. **108** (1957) 353
22) A. W. G. Cameron, Can. Journ. Phys. **36** (1958) 1040
23) A. A. Ross, Phys. Rev. **108** (1957) 720
24) A. A. Ross, H. Mark and R. D. Lawson, Phys. Rev. **102** (1956) 1613
25) A. A. Ross, R. D. Lawson and H. Mark, Phys. Rev. **104** (1956) 401
26) P. F. A. Klinkenberg, Revs. Mod. Phys. **24** (1954) 327
27) A. Bohr, B. R. Mottelson and D. Pines, Phys. Rev. **110** (1958) 936
28) N. N. Bogoljubov, Nuovo Cimento **7** (1958) 794
29) T. Ericson, Nuclear Physics **6** (1958) 62
30) K. J. Le Couteur and D. W. Lang, in press
31) J. Bardeen, L. N. Cooper and J. R. Schrieffer, Phys. Rev. **108** (1957) 1175

3.A *Nuclear Physics* **13** (1959) 53—59; © *North-Holland Publishing Co., Amsterdam*
Not to be reproduced by photoprint or microfilm without written permission from the publisher

SOFT GAMMA RAYS FROM Eu^{152} AND Eu^{154} FOLLOWING RESONANCE NEUTRON CAPTURE

J. E. DRAPER and A. A. FLEISCHER
Yale University, New Haven, Connecticut †

Received 29 May 1959

Abstract: The gamma-ray spectra up to 300 keV from the odd Eu^{152} and Eu^{154} have been measured with a NaI(Tl) scintillator following resonance neutron capture in the 0.33, 0.46, 1.06 and 2.46-eV resonances. Absolute intensities are reported for gamma rays of 95 ± 4 keV from Eu^{152} and 74 ± 4 and 95 ± 4 keV from Eu^{154}. The thermal capture spectrum of Eu was reinvestigated with a lead critical absorber, and the resulting value for the contribution of a prompt ($\gtrsim$ 100-μsec delay) $\approx$ 74-keV gamma ray from Eu^{152} is $\gtrsim$ 0.5 photons per 100 captures in elemental Eu. This large discrepancy with the results of Skliarevskii *et al.*, using an unpulsed neutron source, might indicate a new delayed transition.

1. Introduction

Little information is available concerning the transitions and levels in odd nuclei. The reason is that their ground states are usually higher than those of neighbouring isobars, so that they are usually the parents rather than the daughters of radioactive decays. For the same reason, however, they can often be studied via neutron capture gamma rays using odd-proton target nuclei. A number of such spectra have been reported [1]). Those results indicated that for many cases of neutron capture the prominent low energy gamma rays from even nuclei involve the lowest collective levels. Such levels have not been directly identified in odd nuclei. A direct identification will require angular-correlation and internal conversion measurements, but the measurement of gamma-ray spectra constitutes a first step. There is further interest in Eu^{152} because of its use in the important experiment on the helicity of the neutrino [2]).

2. Experimental Results

Most of the experimental techniques have already been reported [1, 3]). The Eu sample was 0.125 $g \cdot cm^{-2}$ of europium oxide of natural isotopic content (purity $> 98.3\,\%$) and was 41 cm^2 in cross-sectional area. The neutron source was the 6.5-MeV electron linear accelerator. For the resonan-

† Research supported by the U. S. Atomic Energy Commission.

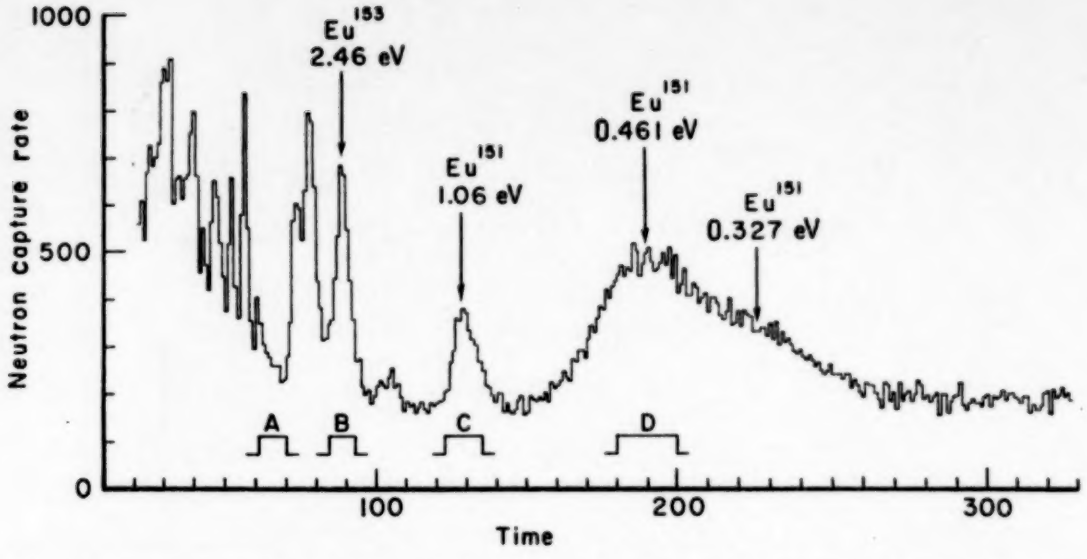

Fig. 1. Count rate from Eu sample vs time (2-μsec channels) after the neutron burst. Gates A, B, C and D were used to investigate individual resonances and background. The sample was 0.125 g · cm^{-2} of europium oxide.

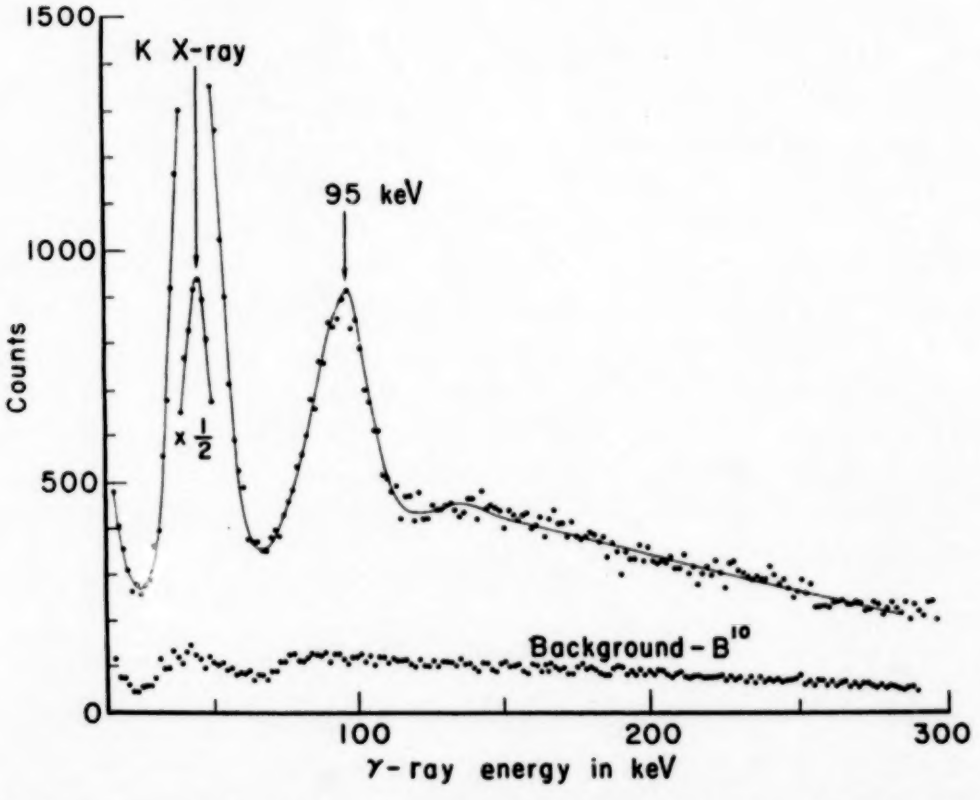

Fig. 2. Europium pulse height spectrum from the 1.06-eV resonance (gate C) producing Eu^{152}. The lower curve is the background (same gate, same neutron monitor count) obtained with thick B^{10} in the neutron beam.

ce capture experiments the sample was placed 3.3 m from the pulsed neutron source and was viewed by a 2.5-in diam by 1.7-in thick NaI(Tl) scintillator. The distance from the sample centre to the near face of the scintillator was 4 in. In fig. 1 the counting rate from the NaI(Tl) scintillator is plotted against the time after the neutron burst. The gamma-ray bias of the NaI(Tl) detector was approximately 50 keV. In order to record the gamma-ray spectrum from an individual resonance, the scintillator pulses were gated into the pulse height analyzer only during one of the time intervals B, C or D.

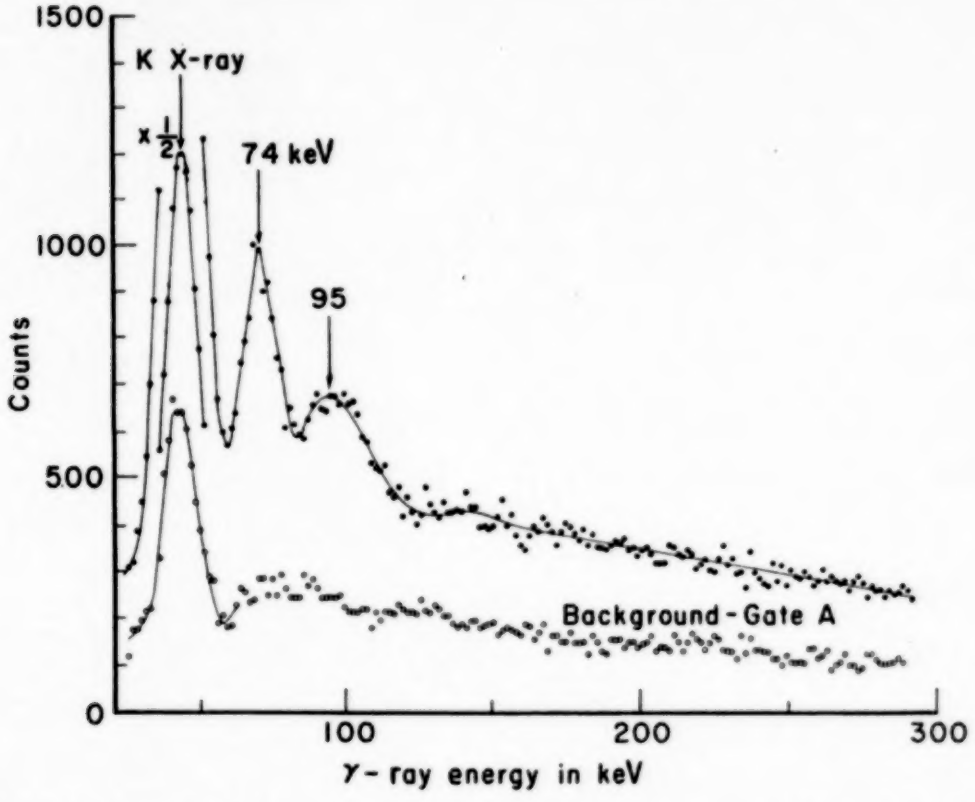

Fig. 3. Europium pulse height spectrum from the 2.46-eV resonance (gate B) producing Eu^{154}. The lower curve is the background between resonances using gate A. The lower curve is normalized to the same gate width and neutron monitor count as the upper curve.

Fig. 2 shows the pulse height spectrum for the 1.06 eV resonance in which neutron capture forms Eu^{152}. The only prominent gamma ray appears at 95 ± 4 keV. The peak at 42 ± 4 keV is presumed to be the K X-ray of Eu following internal conversion or photoelectric absorption of capture gamma rays. The background curve of fig. 2 was obtained with a thick B^{10} absorber ($N\sigma = 1$ at ≈ 100 eV) placed in the neutron beam 40 cm from the Eu sample. Any transitions from activation by fast neutrons or the gamma-ray flash from the accelerator would appear in this background curve. Both curves of fig. 2 were obtained with the same gating interval C and the same number of neutron monitor counts. The spectrum for the combined

0.46-eV and 0.33-eV resonances (gate D) is not shown but is like that of fig. 2.

Fig. 3 is the spectrum for the 2.46 eV resonance (gate B) producing Eu^{154}. Gamma rays appear at 74 ± 4 keV and 95 ± 4 keV in addition to the presumed K X-ray of Eu at 42 ± 4 keV. The background curve in fig. 3 was obtained with gate A, and it is normalized to the same gate width and monitor count as for the top curve of fig. 3. This shows that the structure of figs. 2 and 3 is not caused by an isomer. Because of our pulsed source of neutrons, an isomeric transition would have a half-live $\gtrsim 100$ μsec if it were observable in figs. 2 or 3.

The absolute intensities of these gamma rays were measured by the method previously described [3]) and the results quoted in table 1 include the effects of

TABLE 1

Summary of results

E_0 (eV)	product A	E_γ (keV)	gamma rays per 100 captures	
			isotopic	elemental
0.46	152 [a]	95 ± 4	$26\ \pm4$	
1.06	152	95 ± 4	$22\ \pm4$	
2.46	154	74 ± 4	$12\ \pm3$	
		95 ± 4	6.5 ± 2	
thermal	94 % 152 [a] 6 % 154	95 ± 4		17 ± 3 [b]
		76 ± 4		$\approx 0.5(Eu^{154})$ $\lesssim 0.5(Eu^{152})$

[a] See ref. [4]).
[b] See ref. [1]).

absorption of gamma rays by the Eu sample. The isotopic assignments of the resonances are taken from ref. [4]). The value of Γ_γ/Γ for each of the resonances considered here is greater than 0.98, so transmission measurements reasonably determine the fraction of neutrons captured in each resonance.

In order to obtain further information about the existence of a 71-keV [5]) or 81-keV [6]) prompt gamma ray in Eu^{152}, the same natural Eu sample was used with the method described previously [1]) for the study of thermal neutron capture gamma rays. The resulting spectrum is shown in fig. 4. The intensity of the contribution of the 74-keV photons from Eu^{154} was estimated by assuming that the absolute intensity was the same for resonance capture and thermal capture. Then the 95-keV peak in fig. 4 should be 30 times as intense as the 74-keV contribution from Eu^{154}. This assumption of equal gamma-ray intensities for different neutron energy regions is some-

times erroneous in view of previous results [3]), but it is the only one possible in this case.

In order to emphasize the gamma rays in the energy region 70—87 keV relative to those in the 89—100 keV region a 0.005-in thick Pb critical absorber was placed in the beam of Eu gamma rays at a distance of 40 cm

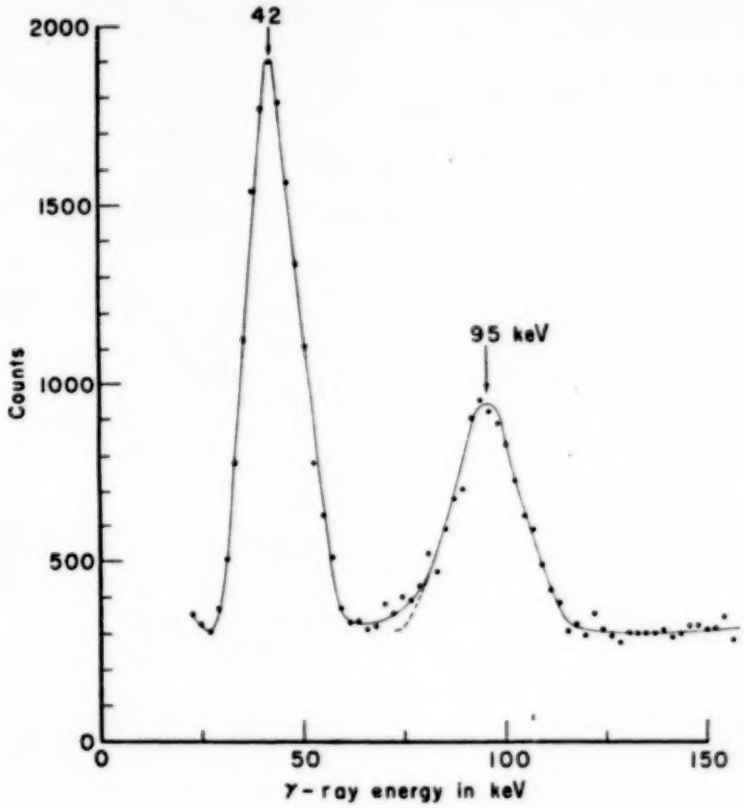

Fig. 4. Europium pulse-height spectrum for thermal neutron capture. The dotted curve is the reflection of the right-hand part of the 95-keV peak about the centre line, indicating the relative absence of pulses in the region of 70—80 keV.

from the scintillator. The resulting spectrum is shown in fig. 5. The expected transmission factor of 0.4 was observed experimentally for the 95-keV peak. The peak indicated at 76 keV in fig. 5 was assumed to have the expected factor of 1.9 enhancement relative to the 95-keV peak after transmission through the Pb sheet. The relative intensities of the peaks in figs. 4 and 5 support this within the limited accuracy of estimation of a 76-keV peak in fig. 4. The shape of the continuum above 110 keV in figs. 2 and 5 indicate several weak low energy transitions in the region. With the available energy resolution it can not be determined whether the structure in fig. 5 near 76 keV is caused by more than one transition.

With the indicated absorber location, the counting rate caused by the 75-keV Pb K X-ray from the photoelectric absorption of the 95-keV photons

would be 0.008 times that from the original 95-keV peak. An estimate of the production of Pb X-rays by the remainder of the gamma rays in the Eu spectrum indicates an increase of the 0.008 to $\approx$ 0.03. The subtraction of this contribution and the estimated contribution from Eu^{154} leaves an upper limit of 0.5 photons per 100 captures in natural Eu for a 76-keV transition

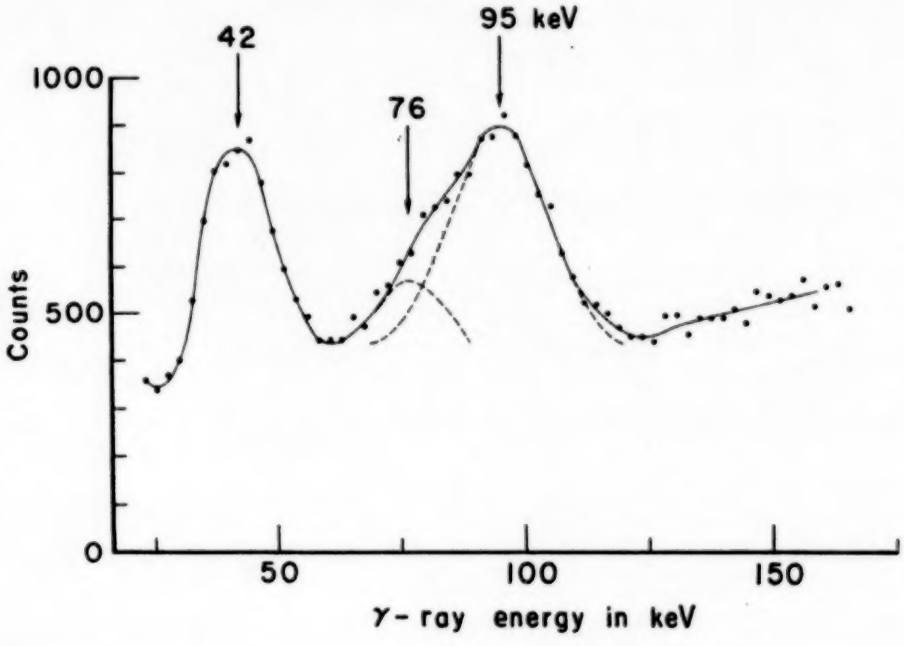

Fig. 5. Similar to fig. 4 but with a 5-mil Pb absorber (K-edge at 88 keV) placed 40 cm from the scintillator to emphasize the 70—87 keV region. The right-hand dotted curve is the 95-keV peak of fig. 4 multiplied by the transmission of the Pb absorber. The left-hand dotted curve is the difference between the other two curves.

in Eu^{152}. This is substantially smaller than the value 4.4 quoted by Skliarevskii *et al.* [5]). The results of Patronis and Marshak [6]) † do not include intensities.

3. Discussion

The results in ref. [1]) have shown that the prominent features of low energy capture gamma rays of many nuclei appear to involve the first few collective levels. The correlation for odd nuclei is unknown because little experimental information about the levels of these nuclei is available, except for the spin of the ground state and sometimes a low-lying isomeric level. Figs. 2 and 3 indicicate somewhat different spectra for $_{63}Eu^{152}_{89}$ and $_{63}Eu^{154}_{91}$. This region of neutron number N is one of rather sudden transition from vibrational to rotational levels in even nuclei [7]). There is no direct evidence here that the observed transitions are collective. The energy ratio of the

† We are grateful to these authors for making their results available to us before publication.

Eu^{154} gamma rays is 1.28 ± 0.07 which is consistent with the ratio $\frac{5}{4}$ expected for a $5 \rightarrow 4 \rightarrow 3$ spin sequence of transitions to the spin 3 ground state [8]) of Eu^{154}. However, this is not regarded as strong evidence.

There appear to be transitions in Eu^{152} and Eu^{154} of nearly the same energies (viz. 95 and possibly 75 keV). However, it would not be expected that they involve levels of the same type and energy in the two nuclei because the relative intensities of the transitions are different by a factor $\lesssim 50$.

In comparing the results of Skliarevskii *et al.* [5]) for thermal capture with those given previously [1]) and in table 1, it is noteworthy that the agreement is good for the intensity of the 95-keV transition, but that there is a factor $\lesssim 4.4$ discrepancy in the intensity of the 76-keV peak. The latter peak is of low intensity and is difficult to measure. However, such a discrepancy if not caused by experimental difficulties would indicate a previously unknown delayed transition with sufficiently long half-life ($\lesssim 100\ \mu$sec) that it would not be observed with our pulsed source of neutrons.

References

1) J. E. Draper, Phys. Rev. **114** (1959) 268 (references to previous work are contained therein)
2) Goldhaber, Grodzins and Sunyar, Phys. Rev. **109** (1958) 1015
3) Draper, Fenstermacher and Schultz, Phys. Rev. **111** (1958) 906;
Fenstermacher, Draper and Bockelman, Nuclear Physics **10** (1959) 386
4) D. J. Hughes and R. B. Schwartz, Neutron Cross Sections, Brookhaven National Laboratory Report BNL-325, Second Edition (U.S. Government Printing Office, Washington, 1958)
5) Skliarevskii, Stepanov and Obiniakov, Atomnaya Energiya **4** 22 (1958)
6) E. T. Patronis Jr. and Harvey Marshak, to be published
7) G. Scharff-Goldhaber, Proceedings of the University of Pittsburgh Conference (June, 1957), unpublished report
8) Abraham, Kedzie and Jeffries, Phys. Rev. **108** (1957) 58

4.A:8.B *Nuclear Physics* **13** (1959) 60—73; © *North-Holland Publishing Co., Amsterdam*

Not to be reproduced by photoprint or microfilm without written permission from the publisher

β-DECAY OF RaE

B. V. GESHKENBEIN, S. A. NEMIROVSKAYA and A. P. RUDIK

U.S.S.R. *Academy of Sciences, Moscow*

Received 10 February 1959

Abstract: Effects due to non-conservation of parity in β-decay of RaE have been considered. Expressions for longitudinal polarization of β-electrons of RaE and angular distribution of β-electrons from an oriented nucleus are obtained, taking into consideration the possibility of time parity non-conservation.

1. Introduction

After it had been found that in a weak interaction space parity is not conserved, the β-decay of RaE was given considerable attention.

In the first place, Lewis [1]), Fujita *et al.* [2]) showed the sensitivity of the beta-ray spectrum of RaE to the possible non-conservation of the time parity. Secondly, Alikhanov made a suggestion supported by experiment[3]) that the longitudinal polarization of β-electrons of RaE is different from v/c and that the amount of this difference in general will depend on a possible violation of the time parity conservation law.

Below, the expression for longitudinal polarization of β-electrons of RaE is given, taking into consideration the possibility of time parity non-conservation.

2. β-Spectrum of RaE

Among the first forbidden transitions, the β-spectrum of RaE (transition $1^- \rightarrow 0^+$) is the only known example of a spectrum the form of which differs from that of allowed-transition spectra. This fact was successfully interpreted in the light of the modern theory of β-decay, which takes into consideration the change of the electron wave function within the nucleus [4–7]). This theory presupposed that time parity in β-decay is conserved.

Below, we shall follow ref. [7]), but we shall take into account the fact that space parity (and possibly, time parity) is not conserved in β-decay. Assumming a two-component neutrino and using the methods of ref. [8]), we have for the correction factor of the β-spectrum of RaE (see Appendix 1) an expression of the form

$$C(Z, R_0, W) = C_0(Z, R_0, W) + \Delta C,$$

where the two terms are given by the following formulae.

For S *and* T *interactions,*

$$C_0(Z, R_0, W) = \bar{M}_1(1+x)^2+\bar{L}_1[\tfrac{1}{3}q^2x^2+y^2+\tfrac{1}{6}q^2+\tfrac{2}{3}qy(x-1) +\bar{N}_1[\tfrac{2}{3}q(x^2-1)+2y(1+x)]+\tfrac{1}{2}\bar{L}_2(2x-1)^2, \quad (1)$$

$$\Delta C = [\bar{M}_1+2\bar{L}_2+\tfrac{1}{3}q^2\bar{L}_1+\tfrac{2}{3}q\bar{N}_1]F^2x^2. \quad (1')$$

Here $\bar{M}_1$, $\bar{L}_1$, $\bar{L}_2$ and $\bar{N}_1$ are functions tabulated in ref.[7]), depending on the total energy of the electron W (expressed in units mc^2). If the change of the electron wave function within the nucleus is not taken into account, $\bar{M}_1 = M_0$, $\bar{L}_1 = L_0$, $\bar{L}_2 = L_1$ and $\bar{N}_1 = N_0$, where the functions M_0, L_0, L_1 and N_0 are determined in refs. [9, 10]).

The two parameters x and y are matrix elements ratios:

$$x = i\frac{g_S\int\beta\mathbf{r}}{g_T\int\beta\boldsymbol{\sigma}\wedge\mathbf{r}}, \qquad y = \frac{\int\beta\boldsymbol{\alpha}}{\int\beta\boldsymbol{\sigma}\wedge\mathbf{r}}.$$

It is supposed that non-conservation of time parity is caused by the complex character of the scalar interaction constant:

$$G_S = g_S(1+iF), \qquad G_T = g_T,$$

where g_S, g_T and F are real quantities.

For V *and* A *interactions,*

$$C_0(Z, R_0, W) = \bar{M}_1(1+x)^2+\bar{L}_1[\tfrac{1}{3}q^2x^2+y^2+\tfrac{1}{6}q^2-\tfrac{2}{3}qy(x-1)] +\bar{N}_1[-\tfrac{2}{3}q(x^2-1)+2y(1+x)]+\tfrac{1}{2}\bar{L}_2(2x-1)^2, \quad (2)$$

$$\Delta C = [\bar{M}_1+\tfrac{1}{2}\bar{L}_2+\tfrac{1}{6}q^2\bar{L}_1+\tfrac{2}{3}q\bar{N}_1]F^2. \quad (2')$$

In the case of V and A interactions x and y are the following ratios of matrix elements:

$$x = i\frac{g_V\int\mathbf{r}}{g_A\int\boldsymbol{\sigma}\wedge\mathbf{r}}, \qquad y = \frac{g_V\int\boldsymbol{\alpha}}{g_A\int\boldsymbol{\sigma}\wedge\mathbf{r}}.$$

Non-conservation of time parity is considered to be caused by the complex character of the axial coupling constant:

$$G_V = g_V, \qquad G_A = g_A(1+iF)$$

(g_V, g_A and F are real).

3. Polarization of β-Electrons of RaE

Let us represent the polarization of β-electrons of RaE in the following way:

$$\langle\boldsymbol{\sigma}\cdot\mathbf{n}\rangle = \frac{D_0(Z, R_0, W)+\Delta D}{C_0(Z, R_0, W)+\Delta C}, \quad (3)$$

where C_0 and ΔC are determined with the help of formulas (1), (1′), (2) and (2′), while D_0 and ΔD are expressed as follows (see appendix 1):

For S *and* T *interactions*,

$$\begin{aligned} D_0(Z, R_0, W) = \sin(\delta_1-\delta_{-1})\{&(\bar{M}_1^2-\bar{M}_{-1}^2)^{\frac{1}{2}}(1+x)^2+(\bar{L}_1^2-\bar{L}_{-1}^2)^{\frac{1}{2}} \\ &\cdot[\tfrac{1}{3}q^2x^2+y^2+\tfrac{1}{6}q^2+\tfrac{2}{3}qy(x-1)]-\tfrac{1}{2}[(\bar{L}_1+\bar{L}_{-1})^{\frac{1}{2}}(\bar{M}_1+\bar{M}_{-1})^{\frac{1}{2}} \\ &+(\bar{L}_1-\bar{L}_{-1})^{\frac{1}{2}}(\bar{M}_1-\bar{M}_{-1})^{\frac{1}{2}}][\tfrac{2}{3}q(x^2-1)+2y(1+x)] \\ &+\tfrac{1}{2}\sin(\delta_2-\delta_{-2})(\bar{L}_2^2-\bar{L}_{-2}^2)^{\frac{1}{2}}(2x-1)^2, \end{aligned} \tag{4}$$

$$\begin{aligned} \Delta D = \sin(\delta_1-\delta_{-1})\{&(\bar{M}_1^2-\bar{M}_{-1}^2)^{\frac{1}{2}}+\tfrac{1}{3}q^2(\bar{L}_1^2-\bar{L}_{-1}^2)^{\frac{1}{2}}-\tfrac{1}{3}q[(\bar{L}_1+\bar{L}_{-1})^{\frac{1}{2}} \\ &\cdot(\bar{M}_1+\bar{M}_{-1})^{\frac{1}{2}}+(\bar{L}_1-\bar{L}_{-1})^{\frac{1}{2}}(\bar{M}_1-\bar{M}_{-1})^{\frac{1}{2}}]F^2x^2+2\sin(\delta_2-\delta_{-2}) \\ &\cdot(\bar{L}_2^2-\bar{L}_{-2}^2)^{\frac{1}{2}}F^2x^2+\cos(\delta_1-\delta_{-1})\{(\bar{L}_1+\bar{L}_{-1})^{\frac{1}{2}}(\bar{M}_1+\bar{M}_{-1})^{\frac{1}{2}} \\ &-(\bar{L}_1-\bar{L}_{-1})^{\frac{1}{2}}(\bar{M}_1-\bar{M}_{-1})^{\frac{1}{2}}\}(y-\tfrac{2}{3}q)Fx; \end{aligned} \tag{4′}$$

for V *and* A *interactions*,

$$\begin{aligned} D_0(Z, R_0, W) = \sin(\delta_1-\delta_{-1})\{&(\bar{M}_1^2-\bar{M}_{-1}^2)^{\frac{1}{2}}(1+x)^2+(\bar{L}_1^2-\bar{L}_{-1}^2)^{\frac{1}{2}} \\ &\cdot[\tfrac{1}{3}q^2x^2+y^2+\tfrac{1}{6}q^2-\tfrac{2}{3}qy(x-1)]-\tfrac{1}{2}[(\bar{L}_1+\bar{L}_{-1})^{\frac{1}{2}}(\bar{M}_1+\bar{M}_{-1})^{\frac{1}{2}} \\ &+(\bar{L}_1-\bar{L}_{-1})^{\frac{1}{2}}(\bar{M}_1-\bar{M}_{-1})^{\frac{1}{2}}][-\tfrac{2}{3}q(x^2-1)+2y(1+x)]\} \\ &+\tfrac{1}{2}\sin(\delta_2-\delta_{-2})(\bar{L}_2^2-\bar{L}_{-2}^2)^{\frac{1}{2}}(2x-1)^2, \end{aligned} \tag{5}$$

$$\begin{aligned} \Delta D = \sin((\delta_1-\delta_{-1})\{&(\bar{M}_1^2-\bar{M}_{-1}^2)^{\frac{1}{2}}+\tfrac{1}{6}q^2(\bar{L}_1^2-\bar{L}_{-1}^2)^{\frac{1}{2}} \\ &-\tfrac{1}{3}q[(\bar{L}_1+\bar{L}_{-1})^{\frac{1}{2}}(\bar{M}_1+\bar{M}_{-1})^{\frac{1}{2}}+(\bar{L}_1-\bar{L}_{-1})^{\frac{1}{2}}(\bar{M}_1-\bar{M}_{-1})^{\frac{1}{2}}]F^2 \\ &+\tfrac{1}{2}\sin(\delta_2-\delta_{-2})(\bar{L}_2^2-\bar{L}_{-2}^2)^{\frac{1}{2}}F^2+\cos(\delta_1-\delta_{-1})[(\bar{L}_1+\bar{L}_{-1})^{\frac{1}{2}}(\bar{M}_1+\bar{M}_{-1})^{\frac{1}{2}} \\ &-(\bar{L}_1-\bar{L}_{-1})^{\frac{1}{2}}(\bar{M}_1-\bar{M}_{-1})^{\frac{1}{2}}](y-\tfrac{2}{3}qx)F. \end{aligned} \tag{5′}$$

In formulas (4′), (4″), (5′) and (5″) all roots are extracted with positive signs. The functions $\bar{M}_{-1}$, $\bar{L}_{-1}$ and $\bar{L}_{-2}$ are given in appendix 2.

We should pay attention to the symmetry existing between functions C_0 and D_0. Indeed, the latter, instead of the quantities $\bar{M}_1$, $\bar{L}_1$, $\bar{L}_2$ and $\bar{N}_1$ present in the expression for C_0, contain respectively:

$$\bar{M}'_1 = (\bar{M}_1^2-\bar{M}_{-1}^2)^{\frac{1}{2}}\sin(\delta_1-\delta_{-1}), \qquad \bar{L}'_1 = (\bar{L}_1^2-\bar{L}_{-1}^2)^{\frac{1}{2}}\sin(\delta_1-\delta_{-1}),$$

$$\bar{L}'_2 = (\bar{L}_2^2-\bar{L}_{-2}^2)^{\frac{1}{2}}\sin(\delta_2-\delta_{-2}),$$

$$\bar{N}'_1 = -\tfrac{1}{2}[(\bar{L}_1+\bar{L}_{-1})^{\frac{1}{2}}(\bar{M}_1+\bar{M}_{-1})^{\frac{1}{2}}+(\bar{L}_1-\bar{L}_{-1})^{\frac{1}{2}}(\bar{M}_1-\bar{M}_{-1})^{\frac{1}{2}}]\sin(\delta_1-\delta_{-1}).$$

As is shown in ref. [11]), if in the expansion of the functions $\bar{M}_1$, $\bar{L}_1$, etc. and $\bar{M}_{-1}$, $\bar{L}_{-1}$, etc. we limit ourselves only to the first powers of pR_0 (and besides, consider that nuclear charge is concentrated at the point, and the electron wave function is constant in the nuclear volume), we get

$$\frac{\bar{M}'_1}{\bar{M}_1} \approx \frac{\bar{L}'_1}{\bar{L}_1} \approx \frac{\bar{L}'_2}{\bar{L}_2} \approx \frac{\bar{N}'_1}{\bar{N}_1} \approx -\frac{v}{c}, \quad \sin(\delta_1-\delta_{-1}) \approx \sin(\delta_2-\delta_{-2}) \approx -1,$$

and we find that the magnitude of the longitudinal polarization of the

β-electrons is equal to $-v/c$. However, in the case of the β-decay of RaE, when the above approximations are not true, the longitudinal polarization of the β-electrons will differ from v/c.

4. Results of Calculations and Discussion

4.1. TIME-PARITY CONSERVED

First, let us consider the case of time parity conservation.

Using values x and y determined in ref. [7]) from the condition of the best fit of the theoretical value of C_0 with the experimental one, we obtain the deviations of the polarization of β-electrons of RaE from v/c for the case of S and T interactions, given in table 1.

TABLE 1

Values of $\langle \boldsymbol{\sigma} \cdot \mathbf{n} \rangle / (-v/c)$ for S and T interactions

W		1.2	1.8	2.4	3.0
x	y				
0.2	18.8	0.53	0.43	0.28	0.13
0.4	22.4	0.67	0.64	0.57	0.44
0.6	25.7	0.71	0.69	0.63	0.50
1.0	32.35	0.76	0.75	0.71	0.62
1.2	35.6	0.77	0.76	0.72	0.65
3.0	64.8	0.80	0.80	0.78	0.75
5.5	104	0.80	0.80	0.77	0.76

For V and A interactions we have determined the range of values x and y for which a satisfactory fit of theoretical and experimental magnitudes of C_0 exists. This range of values, as was expected, appeared to be slightly different from the range obtained for S and T interactions. The resulting values of the deviation of the polarization of β-electrons of RaE from v/c are given in table 2.

TABLE 2

Values of $\langle \boldsymbol{\sigma} \cdot \mathbf{n} \rangle / (-v/c)$ for V and A interactions

W		1.2	1.8	2.4	3.0
x	y				
0.2	19.85	0.83	0.83	0.81	0.76
0.5	24.6	0.80	0.80	0.77	0.70
†1.0	32.35	0.76	0.75	0.71	0.62
1.3	37	0.74	0.73	0.68	0.60
1.7	42.95	0.71	0.68	0.62	0.56
2.0	47.3	0.69	0.65	0.58	0.54

† The above-mentioned formulas for C_0 and D_0 show that for $x = 1$ there is no difference between interactions S and T and interactions V and A.

In principle, the obtained dependence of the polarization of β-electrons of RaE on x makes it possible to determine x unambiguously. The experimental data available at present [3]) (at $W_{\text{kin}} = 125$ and 390 keV, the ratio $\langle\sigma\rangle/(-v/c) = 0.733\pm0.06$ and 0.725 ± 0.06; average value: 0.73 ± 0.04 † are not at variance with the results of theoretical calculation for $x \approx 1.7$ (for V and A interactions) or $x \approx 0.6$ (for S and T interactions).

It is worth mentioning that the dependence of $\langle\sigma\rangle/(-v/c)$ on x is different for the two types of interactions: for interactions S and T, the quantity $\langle\sigma\rangle/(v/c)$ increases with increasing x, while for interactions V and A, it decreases. However, for all interactions, and for any x and y allowing the theoretical and experimental β-spectra of RaE to be reconciled, $\langle\sigma\rangle/(-v/c) \leqq 0.83$.

4.2. POSSIBLE NON-CONSERVATION OF TIME-PARITY

Now, let us estimate the possible non-conservation of time parity in β-decay.

Before we discuss the results of calculation for different permissible values of F, let us explain why it is impossible to reconcile the theoretical and experimental β-spectra of RaE for large values of $F(F \approx 1)$. We base our explanation on the known fact [4]) that the energy dependence $C = C(Z, R_0, W)$ required by experiment can only be obtained as a result of very large interference effects, lowering the value of $C(Z, R_0, W)$ by approximately two orders of magnitude.

Further, let us solve equation $C_{\text{exp}} = C(Z, R_0, W)$ with respect to y, for a certain fixed x. Using (2) and (2′) for V and A interactions we shall have

$$y = \frac{1}{L_1}\left(\varepsilon_0 \pm \sqrt{\varepsilon_0^2 - \varepsilon_1 L_1 + C_{\text{exp}} L_1 - F^2 \varepsilon_2 L_1}\right), \tag{6}$$

where

$$\varepsilon_0 = \tfrac{1}{3}q(x-1)L_1 - (1+x)\bar{N}_1,$$
$$\varepsilon_1 = x^2(\bar{M}_1 + \tfrac{1}{3}q^2 L_1 + 2L_2 - \tfrac{2}{3}q\bar{N}_1) + 2x(\bar{M}_1 - L_2) + \varepsilon_2,$$
$$\varepsilon_2 = \bar{M}_1 + \tfrac{1}{2}L_2 + \tfrac{1}{6}q^2 L_1 + \tfrac{2}{3}q\bar{N}_1.$$

Values of $\varepsilon_0^2 - \varepsilon_1 L_1$ and $\varepsilon_2 L_1$ for different x and w are given in tables 3 and 4.

As has already been mentioned, $L_1 C_{\text{exp}} \approx \varepsilon_0^2 - \varepsilon_1 L_1$. On the other hand, from tables 3 and 4 it is seen that $\varepsilon_0^2 - \varepsilon_1 L_1 \leqq \varepsilon_2 L_1$. Thus, it follows from (6) that F cannot be of order unity (for y is a real quantity). Let us underline the important fact that this argument appears to hold even with such slight changes in the functions L_1, L_2, $\bar{M}_1$ and $\bar{N}_1$ as would allow for inadequate knowledge of the charge distribution within the nucleus, estimation of corrections associated with the third forbidden matrix elements, etc.

† The latest, more precise, data of A. I. Alikhanov, G. P. Eliseyev and V. A. Lyubimov are $\langle\sigma\rangle/(-v/c) = 0.672\pm0.029$, 0.720 ± 0.041, 0.725 ± 0.060 and 0.750 ± 0.051 for $W_{\text{kin}} = 140$, 250, 390 and 600 keV, respectively.

TABLE 3

Values of $(\varepsilon_0^2-\varepsilon_1 L_1)$

x \ W	1.2	1.8	2.4	3.0
0.2	0.37	0.26	0.20	0.20
1.0	1.56	0.98	0.65	0.56
2.0	4.33	2.93	2.36	2.62

TABLE 4

Values of $\varepsilon_2 L_1$

W	1.2	1.8	2.4	3.0
$\varepsilon_2 L_1$	121.70	126.77	130.80	134.38

TABLE 5

Values of $\langle \boldsymbol{\sigma} \cdot \mathbf{n} \rangle / (-v/c)$ for $F = 6\times 10^{-3}$ in the case of interactions V and A

W		1.2		1.8		2.4		3.0	
x	y	$F<0$	$F>0$	$F<0$	$F>0$	$F<0$	$F>0$	$F<0$	$F>0$
0.2	19	0.94	0.67	0.90	0.72	0.89	0.70	0.87	0.68
1.3	36.25	0.86	0.59	0.80	0.61	0.74	0.55	0.69	0.50
1.7	42.4	0.84	0.58	0.77	0.59	0.71	0.53	0.67	0.51

TABLE 6

Values of $\langle \boldsymbol{\sigma} \cdot \mathbf{n} \rangle / (-v/c)$ for $F = 3\times 10^{-3}$, in the case of interactions V and A

W		1.2		1.8		2.4		3.0	
x	y	$F<0$	$F>0$	$F<0$	$F>0$	$F<0$	$F>0$	$F<0$	$F>0$
0.2	19.4	0.89	0.73	0.87	0.76	0.85	0.73	0.81	0.68
1.3	36.55	0.81	0.64	0.76	0.65	0.71	0.59	0.64	0.51
1.9	45.76	0.79	0.62	0.73	0.61	0.67	0.55	0.63	0.53

TABLE 7

Values of $\langle \boldsymbol{\sigma} \cdot \mathbf{n} \rangle / (-v/c)$ for S and T interactions and different F

F^2	W		1.2		1.8		2.4		3.0	
	x	y	$F<0$	$F>0$	$F<0$	$F>0$	$F<0$	$F>0$	$F<0$	$F>0$
10^{-3}	0.4	21.94	0.82	0.47	0.72	0.47	0.62	0.36	0.49	0.23
	0.8	27.96	0.92	0.51	0.84	0.54	0.78	0.49	0.73	0.45
6×10^{-3}	1.2	34.66	0.89	0.61	0.84	0.64	0.80	0.60	0.75	0.55
	2.0	47.20	0.92	0.65	0.88	0.69	0.86	0.67	0.84	0.67
3×10^{-3}	1.2	35.00	0.84	0.66	0.80	0.67	0.75	0.62	0.68	0.54
	3.0	62.65	0.89	0.67	0.85	0.69	0.83	0.66	0.82	0.67

Numerical calculations show, however, that for low values of F ($F^2 < 10^{-2}$) the theoretical β-spectrum of RaE can be satisfactorily reconciled with the experimental one. The values obtained for the longitudinal polarization of β-electrons in the range of permissible values of x and y for $F^2 = 6\times10^{-3}$ and $F^2 = 3\times10^{-3}$, and interactions V and A, are given in tables 5 and 6. As follows from (5′), the polarization appears to be sensitive not only to the magnitude of F^2, but also to the sign of F.

The deviation of the polarization of the β-electrons from v/c for different values of F^2 is given in table 7 (for S and T interactions, values of F^2 up to 10^{-2} appear to be permissible).

The values of the polarization of β-electrons of RaE given in tables 5, 6 and 7 make it possible, on the basis of ref. [3]), to conclude that:

for V *and* A *interactions*, if we assume that time parity in the β-decay is not conserved, the value of the polarization of β-electrons of RaE determined by experiment, for $F^2 = 6\times10^{-3}$ and $F^2 = 3\times10^{-3}$, excludes $F < 0$. With $F > 0$, it is possible to reconcile the results of the calculation and the experiment for $x \approx 0.2$ ($F^2 = 6\times10^{-3}$) or $x \approx 0.7$ ($F^2 = 3\times10^{-3}$);

for S *and* T *interactions*, the value $F^2 = 10^{-2}$, permissible in comparing theoretical and experimental β-spectra of RaE, is excluded by the electron polarization experiments [3]). For $F^2 = 6\times10^{-3}$ and $F^2 = 3\times10^{-3}$, a value $F < 0$ is excluded, and with $F > 0$, there is agreement for any of these values F^2 in the range $x \approx 1.7$.

5. Angular Distribution of β-Electrons from an Oriented RaE Nucleus

Angular distribution of β-electrons from an oriented RaE nucleus may be written down in the following form:

$$I(\theta) = N[C-\tfrac{1}{3}(1-\tfrac{3}{2}\overline{\mu^2})b+b_1\bar{\mu}\cos\theta+(1-\tfrac{3}{2}\overline{\mu^2})b\cos^2\theta], \qquad (7)$$

where θ is the angle between the direction of the nuclear orientation $\mathbf{n}_j$ and the direction of the β-electron $\mathbf{n}$; $\bar{\mu}$ and $\overline{\mu^2}$ are the average values of the spin projection and of the square of the spin projection on the direction $\mathbf{n}_j$ (for a non-oriented nucleus $\bar{\mu} = 0$, $\overline{\mu^2} = \frac{2}{3}$).

The expression for C is given in formulas (1), (1′), (2), (2′); the expressions for b and b_1 are presented in appendix 3; N is a normalization factor.

The value of the asymmetry α is equal to

$$\alpha \equiv \frac{2\left[\int_0^{\frac{1}{2}\pi} I(\theta)\sin\theta\,d\theta - \int_{\frac{1}{2}\pi}^{\pi} I(\theta)\sin\theta\,d\theta\right]}{\int_0^{\pi} I(\theta)\sin\theta\,d\theta} = \frac{b_1}{C}\bar{\mu}.$$

The values obtained for b_1/C in the range of permissible values of x, y and F are given in tables 8, 9 (for A and V interactions) and 10, 11 (for S and T interactions).

TABLE 8

Values of $-b_1/C$ for A and V interactions ($F = 0$)

W		1.2	1.8	2.4	3.0
x	y				
0.2	19.85	0.40	0.58	0.59	0.50
0.5	24.6	0.37	0.59	0.66	0.66
1	32.35	0.31	0.57	0.71	0.79
1.3	37	0.29	0.54	0.72	0.82
1.7	42.95	0.21	0.47	0.67	0.77
2	47.3	0.14	0.38	0.59	0.67

TABLE 9

Values of $-b_1/C$ for A and V interactions and different F

F^2	W		1.2		1.8		2.4		3.0	
	x	y	$F<0$	$F>0$	$F<0$	$F>0$	$F<0$	$F>0$	$F<0$	$F>0$
6×10^{-3}	0.2	19	0.47	0.27	0.68	0.42	0.78	0.40	0.87	0.34
	1.3	36.26	0.28	0.18	0.49	0.45	0.60	0.68	0.58	0.85
	1.7	42.4	0.22	0.13	0.41	0.41	0.53	0.68	0.50	0.86
3×10^{-3}	0.2	19.4	0.44	0.33	0.64	0.48	0.69	0.45	0.70	0.32
	1.3	36.55	0.28	0.22	0.51	0.48	0.64	0.69	0.66	0.84
	1.9	45.76	0.20	0.15	0.41	0.42	0.56	0.68	0.58	0.84

TABLE 10

Values of $-b_1/C$ for S and T interactions ($F = 0$)

W		1.2	1.8	2.4	3.0
x	y				
0.2	18.8	0	0.01	0.18	0.30
0.4	22.4	0.21	0.34	0.37	0.30
0.6	25.7	0.26	0.44	0.53	0.53
1.0	32.35	0.32	0.57	0.71	0.79
1.2	35.6	0.33	0.59	0.75	0.85
3.0	64.8	0.37	0.69	0.89	0.99
5.5	104	0.36	0.69	0.89	0.93

TABLE 11

Values of $-b_1/C$ for S and T interactions and different F

F^2	W		1.2		1.8		2.4		3.0	
	x	y	$F<0$	$F>0$	$F<0$	$F>0$	$F<0$	$F>0$	$F<0$	$F>0$
10×10^{-3}	0.4	21.94	0.23	0.04	0.32	0.11	0.37	0.12	0.38	0.05
	0.8	27.96	0.28	0.12	0.43	0.33	0.50	0.49	0.48	0.60
6×10^{-3}	1.2	34.66	0.32	0.23	0.51	0.54	0.59	0.72	0.54	0.86
	2.0	47.20	0.34	0.28	0.55	0.65	0.62	0.87	0.52	1.00
3×10^{-3}	1.2	35.00	0.32	0.26	0.54	0.54	0.64	0.72	0.62	0.87
	3.0	62.65	0.32	0.29	0.54	0.62	0.60	0.90	0.46	1.00

The authors express their sincere acknowledgement to Academician A. I. Alikhanov for numerous discussions and encouragement in their work, and to B. L. Ioffe and V. A. Lyubimov for their participation in the discussions.

Appendix 1

We shall use the methods of ref. [8]) (designated further by I). Taking into account the finite dimensions of the nucleus, we can write for the electron wave function

$$\psi_{\mathbf{p},\xi}(\mathbf{r}) = \begin{pmatrix} \varphi_{\mathbf{p}} v_\xi \\ \chi_{\mathbf{p}} v_\xi \end{pmatrix} \tag{A1.1}$$

where

$$\begin{aligned} \varphi_{\mathbf{p}} &= \alpha_0 + i\mathbf{p}\cdot\mathbf{r}\alpha_1 + i(\boldsymbol{\sigma}\cdot\mathbf{r})(\boldsymbol{\sigma}\cdot\mathbf{n})\beta_c \\ \chi_{\mathbf{p}} &= [\beta_0 + i\mathbf{p}\cdot\mathbf{r}\beta_1 + i(\boldsymbol{\sigma}\cdot\mathbf{r})(\boldsymbol{\sigma}\cdot\mathbf{n})\alpha_c]\boldsymbol{\sigma}\cdot\mathbf{n}; \end{aligned} \tag{A1.2}$$

$\mathbf{p}$ is the electron momentum, $\mathbf{n} = \mathbf{p}/p$; v_ξ is a two-component unit spinor defining the electron polarization.

The quantities α_i and β_i are chosen in the following form:

$$\begin{aligned} &\alpha_0 = ai e^{-i\delta_{-1}} g_{-1}, \quad \alpha_1 = a\frac{3}{pr} e^{-i\delta_{-2}} g_{-2}, \quad \beta_c = a(e^{-i\delta_1} g_1 - e^{-i\delta_{-2}} g_{-2}), \\ &\beta_0 = a e^{-i\delta_1} f_1, \quad \beta_1 = a\frac{3}{ipr} e^{-i\delta_2} f_2, \quad \alpha_c = a\frac{1}{i}(e^{-i\delta_{-1}} f_1 - e^{-i\delta_2} f_2), \end{aligned} \tag{A1.3}$$

where $a = \sqrt{\pi/2pW}$.

In the course of detailed calculations we used phases given in ref. [12]). These phases are related with those occurring in (A1.3) in the following way:

$$\delta_{-1} = \delta_{\frac{1}{2},-\frac{1}{2}} + \tfrac{1}{2}\pi, \qquad \delta_1 = \delta_{\frac{1}{2},\frac{1}{2}}, \qquad \delta_{-2} = \delta_{\frac{3}{2},-\frac{1}{2}}, \qquad \delta_2 = \delta_{\frac{3}{2},\frac{1}{2}} - \tfrac{1}{2}\pi.$$

Values of $\delta_{\frac{1}{2},-\frac{1}{2}}$, $\delta_{\frac{1}{2},\frac{1}{2}}$, $\delta_{\frac{3}{2},-\frac{1}{2}}$ and $\delta_{\frac{3}{2},\frac{1}{2}}$ are given in the table.

TABLE of phases
($r_0 = 1.2\times10^{-13}$ cm)

W	1.2	1.8	2.4	3.0
$\delta_{\frac{1}{2},\frac{1}{2}}$	0.0208	0.2618	0.3228	0.3604
$\delta_{\frac{1}{2},-\frac{1}{2}}$	0.7647	0.6646	0.6101	0.5713
$\delta_{\frac{3}{2},\frac{1}{2}}$	−0.8175	−0.4438	−0.3643	−0.3204
$\delta_{\frac{3}{2},-\frac{1}{2}}$	−0.3847	−0.2323	−0.2161	−0.2124

The functions $C(Z, R_0, W)$ and $D(Z, R_0, W)$, according to (1.35), will be

$$\begin{aligned} C(Z, R_0, W) &= \lambda_{ik}A_{ik}-\chi_{ik}b_{ik}, \\ D(Z, R_0, W) &= \lambda_{ik}b_{ik}-\chi_{ik}A_{ik}; \\ D(Z, R_0, W) &= D_0(Z, R_0, W)+\Delta D; \qquad \mathbf{B}_{ik} = \mathbf{n}b_{ik}. \end{aligned} \tag{A1.4}$$

After averaging over the neutrino emergence directions, summing over final spin states of the nucleus and averaging over initial spin states of the nucleus, we get, according to (1.32), (1.38) and (1.39), for V and A interactions (it is taken into account that β-decay of RaE proceeds according to the scheme $1^- \to 0^+$) †:

$$\begin{aligned} &A_{0c} = -[C_T-\tfrac{1}{3}qC_b)C_a^*, \qquad b_{0c} = 0; \\ &A_{1c} = 0, \qquad b_{1c} = -\tfrac{1}{3}p|C_a|^2 \\ &A_{01} = 0, \qquad b_{01} = \tfrac{1}{3}p(C_T-\tfrac{1}{3}qC_b)C_a \text{ †}; \\ &A_{cc} = |C_a|^2, \qquad b_{cc} = 0; \\ &A_{11} = \tfrac{1}{3}p^2|C_R|^2+\tfrac{1}{6}p^2|C_T|^2, \qquad b_{11} = 0; \\ &A_{00} = \tfrac{1}{3}q^2|C_R|^2+|C_T|^2+\tfrac{1}{6}q^2|C_T|^2-\tfrac{2}{3}q[\mathrm{Re}\, C_R C_T^*-\mathrm{Im}\, C_T C_T^*]; \qquad b_{00} = 0, \end{aligned} \tag{A1.5}$$

where

$$\mathbf{a} = G_V\int\mathbf{r}-iG_A\int\boldsymbol{\sigma}\wedge\mathbf{r}, \qquad \mathbf{b} = G_V\int\mathbf{r}+iG_A\int\boldsymbol{\sigma}\wedge\mathbf{r},$$
$$\mathbf{R} = G_V\int\mathbf{r}, \qquad \boldsymbol{\tau} = -iG_V\int\boldsymbol{\alpha}, \qquad \mathbf{T} = G_A\int\boldsymbol{\sigma}\wedge\mathbf{r}.$$

Considering that non-conservation of time parity is associated with the A-coupling constant, and introducing the ratios of matrix elements x and y, we can write (in this case, in all A_{ik} and b_{ik} the common factor $g_A^2|\int\boldsymbol{\sigma}\wedge\mathbf{r}|^2$ is omitted; $\int\boldsymbol{\sigma}\wedge\mathbf{r}$ and $\int\boldsymbol{\alpha}$ are pure imaginary, $\int\mathbf{r}$ real)

$$\begin{aligned} &A_{0c} = -[y(1+x)-\tfrac{1}{3}q(x^2-1-F^2)-iF(y-\tfrac{2}{3}qx)], \qquad b_{0c} = 0; \\ &A_{cc} = 0, \qquad b_{1c} = -\tfrac{1}{3}pA_{cc}; \\ &A_{01} = 0, \qquad b_{01} = -\tfrac{1}{3}pA_{0c}; \end{aligned}$$

† We are taking this opportunity of noting that in ref.[8]) there is an error in the determination of $\mathbf{a}$; read $\mathbf{a} = \mathbf{m}-i\mathbf{t}$ (and not $\mathbf{a} = \mathbf{m}+i\mathbf{t}$).

$$A_{cc} = (1+x)^2+F^2, \qquad b_{0c} = 0;$$
$$A_{11} = \tfrac{1}{3}p^2x^2+\tfrac{1}{6}p^2(1+F^2), \qquad b_{11} = 0;$$
$$A_{00} = \tfrac{1}{3}q^2x^2+y^2+\tfrac{1}{6}q^2(1+F^2)-\tfrac{2}{3}q(x-1)y, \qquad b_{00} = 0.$$

Taking into account the fact that for S and T interaction q is substituted for $-q$, and non-conservation of time parity is considered to be connected with the S-coupling constant, we obtain in the same way expressions for A_{ik} and B_{ik} in this case.

Further, in determining λ_{ik} and χ_{ik}, we first establish the relation of the functions $g_{\pm i}$ and $f_{\pm i}$ with the functions L_0, P_0, M_0, Q_0, L_1, P_1 and N_1 [9, 10]). Then, omitting a common factor, we have

$$\lambda_{00} = L_0, \qquad \chi_{00} = (L_0^2-P_0^2)^{\frac{1}{2}} \sin(\delta_{-1}-\delta_1);$$
$$\lambda_{11} = \frac{9}{p^2}L_1, \qquad \chi_{11} = (L_1^2-P_1^2)^{\frac{1}{2}} \sin(\delta_{-2}-\delta_2)$$
$$\lambda_{cc} = M_0+L_1+(M_0-Q_0)^{\frac{1}{2}}(L_1-P_1)^{\frac{1}{2}}\cos(\delta_{-1}-\delta_2)-(M_0+Q_0)^{\frac{1}{2}}(L_1+P_1)^{\frac{1}{2}}\cos(\delta_1-\delta_{-2})$$
$$\chi_{cc} = (M_0^2-Q_0^2)^{\frac{1}{2}} \sin(\delta_{-1}-\delta_1)+(L_1^2-P_1^2)^{\frac{1}{2}} \sin(\delta_{-2}-\delta_2)$$
$$+(L_1-P_1)^{\frac{1}{2}}(M_0+Q_0)^{\frac{1}{2}} \sin(\delta_2-\delta_1)+(L_1+P_1)^{\frac{1}{2}}(M_0-Q_0)^{\frac{1}{2}} \sin(\delta_{-2}-\delta_{-1});$$
$$\lambda_{01} = -\frac{3i}{2p}\{(L_0+P_0)^{\frac{1}{2}}(L_1+P_1)^{\frac{1}{2}}e^{i(\delta_{-1}-\delta_{-2})}+(L_0-P_0)^{\frac{1}{2}}(L_1-P_1)^{\frac{1}{2}}e^{i(\delta_1-\delta_2)}\},$$
$$\chi_{01} = -\frac{3}{2p}\{(L_0+p_0)^{\frac{1}{2}}(L_1-P_1)^{\frac{1}{2}}e^{i(\delta_{-1}-\delta_2)}-(L_0-P_0)^{\frac{1}{2}}(L_1+P_1)^{\frac{1}{2}}e^{i(\delta_1-\delta_{-2})}\}; \quad \text{(A.1.7)}$$
$$\lambda_{0c} = -\tfrac{1}{2}\{2N_0-(L_0+P_0)^{\frac{1}{2}}(L_1-P_1)^{\frac{1}{2}}e^{i(\delta_{-1}-\delta_2)}+(L_0-P_0)^{\frac{1}{2}}(L_1+P_1)^{\frac{1}{2}}e^{i(\delta_1-\delta_{-2})}\},$$
$$\chi_{0c} = \tfrac{1}{2}i\{-(L_0+P_0)^{\frac{1}{2}}(M_0+Q_0)^{\frac{1}{2}}e^{i(\delta_{-1}-\delta_1)}+(L_0-P_0)^{\frac{1}{2}}(M_0-Q_0)^{\frac{1}{2}}e^{-i(\delta_{-1}-\delta_1)}$$
$$+(L_0+P_0)^{\frac{1}{2}}(L_1+P_1)^{\frac{1}{2}}e^{i(\delta_{-1}-\delta_{-2})}+(L_0-P_0)^{\frac{1}{2}}(L_1-P_1)^{\frac{1}{2}}e^{i(\delta_1-\delta_2)}\};$$
$$\lambda_{1c} = \frac{3}{2p}\{-2(L_1^2-P_1^2)^{\frac{1}{2}} \sin(\delta_{-2}-\delta_2)+i(L_1+P_1)^{\frac{1}{2}}(M_0-Q_0)^{\frac{1}{2}}e^{i(\delta_{-2}-\delta_{-1})}$$
$$+i(L_1-p_1)^{\frac{1}{2}}(M_0+Q_0)^{\frac{1}{2}}e^{i(\delta_2-\delta_1)}\},$$
$$\chi_{1c} = \frac{3}{2p}\{(M_0+Q_0)^{\frac{1}{2}}(L_1+P_1)^{\frac{1}{2}}e^{i(\delta_{-2}-\delta_1)}-(M_0-Q_0)^{\frac{1}{2}}(L_1-P_1)^{\frac{1}{2}}e^{i(\delta_2-\delta_{-1})}-2L_1\}.$$

Using the expressions obtained for A_{ik}, b_{ik}, λ_{ik} and χ_{ik}, simple calculations yield the quantities $C(Z, R_0, W)$ and $D(Z, R_0, W)$. In the case of RaE, the following substitution should be made: $M_0 \to \bar{M}_1$, $L_0 \to \bar{L}_1$, $L_1 \to \bar{L}_2$, $N_0 \to \bar{N}_1$, $Q_0 \to -\bar{M}_{-1}$, $P_0 \to -\bar{L}_1$ and $P_1 \to -\bar{L}_2$.

Appendix 2

Using the determination of the functions $\bar{M}_1$, $\bar{L}_1$ and $\bar{L}_2$, it is easy to obtain the following expressions for the functions $\bar{M}_{-1}$, $\bar{L}_{-1}$ and $\bar{L}_{-2}$:

$$\begin{aligned}\bar{M}_{-1} &= \tfrac{1}{2}(X_{-1}^2+Y_1^2)M_1^{(S)}+\tfrac{1}{2}(X_{-1}^2-Y_1^2)M_1^{(L)},\\ \bar{L}_{-1} &= \tfrac{1}{2}(X_1^2+Y_{-1}^2)L_1^{(S)}+\tfrac{1}{2}(X_1^2-Y_{-1}^2)L_1^{(L)},\\ \bar{L}_{-2} &= \tfrac{1}{2}(X_2^2+Y_{-2}^2)L_2^{(S)}+\tfrac{1}{2}(X_2^2-Y_{-2}^2)L_2^{(L)}.\end{aligned} \qquad \text{(A2.1)}$$

The quantities $\bar{M}_{-1}$, $\bar{L}_{-1}$ and $\bar{L}_{-2}$ are given below. They are obtained with the help of functions tabulated in ref. [7]).

TABLE of values $\bar{M}_{-1}$, $\bar{L}_{-1}$ and $\bar{L}_{-2}$ (for $r_0 = 1.17\times10^{-13}$ cm)

W	$\bar{M}_{-1}$	$\bar{L}_{-1}$	$\bar{L}_{-2}$
1.2	104.270	−0.52366	−0.02967
1.8	67.211	−0.34027	−0.07549
2.4	48.663	−0.24878	−0.12031
3.0	37.527	−0.19404	−0.16538

Appendix 3

The function $I(\theta)$, according to (1.35), is of the form

$$I(\theta) = \lambda_{ik}A_{ik}-\chi_{ik}b_{ik}, \qquad \text{(A.3.1)}$$

where A_{ik} and b_{ik} are determined, for V and A interactions, with the help of the following formulas:

$$\begin{aligned}
A_{00} &= \tfrac{1}{3}q^2x^2+y^2+\tfrac{1}{6}q^2(1+F^2)-\tfrac{2}{3}q(x-1)y,\\
b_{00} &= [-\tfrac{1}{3}q^2x+y^2+\tfrac{1}{12}q^2(1+F^2)-\tfrac{2}{3}qy(x-1)]\bar{\mu}\cos\theta;\\
A_{01} &= \tfrac{1}{2}p[y-\tfrac{1}{3}qx+\tfrac{1}{3}q(1+F^2)-iF(y-\tfrac{1}{3}qx)]\bar{\mu}\cos\theta,\\
b_{01} &= [xy-\tfrac{1}{2}y-\tfrac{1}{3}qx^2+\tfrac{1}{2}qx-\tfrac{1}{6}q(1+F^2)+\tfrac{1}{2}iF(y+\tfrac{1}{3}qx)]p(1-\tfrac{3}{2}\overline{\mu^2})\cos^2\theta\\
&\quad+[xy-\tfrac{1}{2}y-\tfrac{1}{3}qx^2+\tfrac{1}{2}qx-\tfrac{1}{6}q(1+F^2)+\tfrac{1}{2}iF(y+\tfrac{1}{3}qx)]\tfrac{1}{2}p\overline{\mu^2}\\
&\quad+\tfrac{1}{2}p[y-\tfrac{1}{3}qx+\tfrac{1}{3}q(1+F^2)-iF(y-\tfrac{1}{3}qx)];\\
A_{0c} &= -y(1+x)+\tfrac{1}{3}q(x^2-1-F^2)+iF(y-\tfrac{2}{3}qx),\\
b_{0c} &= [-y(1+x)+\tfrac{1}{3}q(x^2-1-F^2)+iF(y-\tfrac{2}{3}qx)]\bar{\mu}\cos\theta;\\
A_{11} &= [x^2-\tfrac{1}{4}(1+F^2)](1-\tfrac{3}{2}\overline{\mu^2})p^2\cos^2\theta+\tfrac{1}{2}x^2p^2\overline{\mu^2}+\tfrac{1}{4}(1+F^2)p^2(1-\tfrac{1}{2}\overline{\mu^2}),\\
b_{11} &= \tfrac{1}{4}p^2(1+F^2)\bar{\mu}\cos\theta;\\
A_{1c} &= -\tfrac{1}{2}p(x+1+F^2+iFx)\bar{\mu}\cos\theta,\\
b_{1c} &= p[-x^2-\tfrac{1}{2}x+\tfrac{1}{2}(1+F^2)+\tfrac{3}{2}iFx](1-\tfrac{3}{2}\overline{\mu^2})\cos^2\theta\\
&\quad+\tfrac{1}{2}p[-x^2-\tfrac{1}{2}x+\tfrac{1}{2}(1+F^2)+\tfrac{3}{2}iFx]\overline{\mu^2}-\tfrac{1}{2}p(x+1+F^2+iFx);\\
A_{cc} &= (x+1)^2+F^2, \qquad b_{cc} = [(x+1)^2+F^2]\bar{\mu}\cos\theta.
\end{aligned} \qquad \text{(A3.2)}$$

Using the expressions obtained for A_{ik}, b_{ik}, λ_{ik} and χ_{ik}, we obtain

$$I(\theta) = N[C-\tfrac{1}{3}(1-\tfrac{3}{2}\overline{\mu^2})b+b_1\bar{\mu}\cos\theta+b(1-\tfrac{3}{2}\overline{\mu^2})\cos^2\theta]. \qquad \text{(A3.3)}$$

For V *and* A *interactions,*

$$b = b^{(0)} + \Delta b, \tag{A3.4}$$

$$\begin{aligned} b^{(0)} = {} & \tfrac{3}{4}(2x-1)^2 \bar{L}_2 + 3(xy - \tfrac{1}{2}y - \tfrac{1}{3}qx^2 + \tfrac{1}{2}qx - \tfrac{1}{6}q)[(\bar{L}_1 - \bar{L}_{-1})^{\frac{1}{2}}(\bar{L}_2 + \bar{L}_{-2})^{\frac{1}{2}} \\ & \cdot \cos(\delta_{-1} - \delta_2) - (\bar{L}_1 + \bar{L}_{-1})^{\frac{1}{2}}(\bar{L}_2 - \bar{L}_{-2})^{\frac{1}{2}} \cos(\delta_1 - \delta_{-2})] \\ & + 3(x^2 + \tfrac{1}{2}x - \tfrac{1}{2})[(\bar{M}_1 - \bar{M}_{-1})^{\frac{1}{2}}(\bar{L}_2 - \bar{L}_{-2})^{\frac{1}{2}} \cos(\delta_1 - \delta_{-2}) \\ & - (\bar{M}_1 + \bar{M}_{-1})^{\frac{1}{2}}(\bar{L}_2 + \bar{L}_{-2})^{\frac{1}{2}} \cos(\delta_{-1} - \delta_2)], \end{aligned} \tag{A3.5}$$

$$\begin{aligned} \Delta b = {} & F^2\{\tfrac{3}{4}\bar{L}_2 - \tfrac{1}{2}q[(\bar{L}_1 - \bar{L}_{-1})^{\frac{1}{2}}(\bar{L}_2 + \bar{L}_{-2})^{\frac{1}{2}} \cos(\delta_{-1} - \delta_2) \\ & - (\bar{L}_1 + \bar{L}_{-1})^{\frac{1}{2}}(\bar{L}_2 - \bar{L}_{-2})^{\frac{1}{2}} \cos(\delta_1 - \delta_{-2})] - \tfrac{3}{2}[(\bar{M}_1 - \bar{M}_{-1})^{\frac{1}{2}}(\bar{L}_2 - \bar{L}_{-2})^{\frac{1}{2}} \cos(\delta_1 - \delta_2) \\ & - (\bar{M}_1 + \bar{M}_{-1})^{\frac{1}{2}}(\bar{L}_2 + \bar{L}_{-2})^{\frac{1}{2}} \cos(\delta_{-1} - \delta_2) - \tfrac{3}{2}F\{(y + \tfrac{1}{3}qx)[(\bar{L}_1 - \bar{L}_{-1})^{\frac{1}{2}} \\ & \cdot (\bar{L}_2 + \bar{L}_{-2})^{\frac{1}{2}} \sin(\delta_{-1} - \delta_2) - (\bar{L}_1 + \bar{L}_{-1})^{\frac{1}{2}}(\bar{L}_2 - \bar{L}_{-2})^{\frac{1}{2}} \sin(\delta_1 - \delta_{-2}) \\ & + 3x[(\bar{M}_1 - \bar{M}_{-1})^{\frac{1}{2}}(\bar{L}_2 - \bar{L}_{-2})^{\frac{1}{2}} \sin(\delta_1 - \delta_{-2}) - (\bar{M}_1 + \bar{M}_{-1})^{\frac{1}{2}}(\bar{L}_2 + \bar{L}_{-2})^{\frac{1}{2}} \sin(\delta_{-1} - \delta_2)] \end{aligned} \tag{A3.6}$$

$$b_1 = b_1^{(0)} + \Delta b_1, \tag{A.3.7}$$

$$\begin{aligned} b_1^{(0)} = {} & \{[\tfrac{1}{3}q^2x - y^2 - \tfrac{1}{12}q^2 + \tfrac{2}{3}qy(x-1)](\bar{L}_1^2 - \bar{L}_{-1}^2)^{\frac{1}{2}} + (x+1)[y - \tfrac{1}{3}q(x-1)] \\ & \cdot [(\bar{L}_1 - \bar{L}_{-1})^{\frac{1}{2}}(\bar{M}_1 - \bar{M}_{-1})^{\frac{1}{2}} + (\bar{L}_1 + \bar{L}_{-1})^{\frac{1}{2}}(\bar{M}_1 + \bar{M}_{-1})^{\frac{1}{2}}] - (x+1)^2(\bar{M}_1^2 - \bar{M}_{-1}^2)^{\frac{1}{2}}\} \\ & \cdot \sin(\delta_{-1} - \delta_1) - \tfrac{1}{4}(2x-1)^2(\bar{L}_2^2 - \bar{L}_{-2}^2)^{\frac{1}{2}} \sin(\delta_{-2} - \delta_2) + (-yx + \tfrac{1}{2}y - \tfrac{1}{2}qx + \tfrac{1}{3}qx^2 + \tfrac{1}{6}q) \\ & \cdot [(\bar{L}_1 - \bar{L}_{-1})^{\frac{1}{2}}(\bar{L}_2 - \bar{L}_{-2})^{\frac{1}{2}} \sin(\delta_{-1} - \delta_{-2}) + (\bar{L}_1 + \bar{L}_{-1})^{\frac{1}{2}}(\bar{L}_2 + \bar{L}_{-2})^{\frac{1}{2}} \sin(\delta_1 - \delta_2)] \\ & + (x^2 + \tfrac{1}{2}x - \tfrac{1}{2})[(\bar{L}_2 - \bar{L}_{-2})^{\frac{1}{2}}(\bar{M}_1 + \bar{M}_{-1})^{\frac{1}{2}} \sin(\delta_{-1} - \delta_{-2}) + (\bar{L}_2 + \bar{L}_{-2})^{\frac{1}{2}}(\bar{M}_1 - \bar{M}_{-1})^{\frac{1}{2}} \sin(\delta_1 - \delta_2)], \end{aligned} \tag{A3.8}$$

$$\begin{aligned} \Delta b_1 = {} & F^2\{[-\tfrac{1}{12}q^2(\bar{L}_1^2 - \bar{L}_{-1}^2)^{\frac{1}{2}} + \tfrac{1}{3}q(\bar{L}_1 - \bar{L}_{-1})^{\frac{1}{2}}(\bar{M}_1 - \bar{M}_{-1})^{\frac{1}{2}} \\ & + \tfrac{1}{3}q(\bar{L}_1 + \bar{L}_{-1})^{\frac{1}{2}}(\bar{M}_1 + \bar{M}_{-1})^{\frac{1}{2}} - (\bar{M}_1^2 - \bar{M}_{-1}^2)^{\frac{1}{2}}] \sin(\delta_{-1} - \delta_1) \\ & - \tfrac{1}{4}(\bar{L}_2^2 - \bar{L}_{-2}^2)^{\frac{1}{2}} \sin(\delta_{-2} - \delta_2) + \tfrac{1}{2}[\tfrac{1}{3}q(\bar{L}_1 - \bar{L}_{-1})^{\frac{1}{2}}(\bar{L}_2 - \bar{L}_{-2})^{\frac{1}{2}} \\ & - (\bar{L}_2 - \bar{L}_{-2})^{\frac{1}{2}}(\bar{M}_1 + \bar{M}_{-1})^{\frac{1}{2}}] \sin(\delta_{-1} - \delta_{-2}) + \tfrac{1}{2}[\tfrac{1}{3}q(\bar{L}_1 + \bar{L}_{-1})^{\frac{1}{2}} \\ & \cdot (\bar{L}_2 + \bar{L}_{-2})^{\frac{1}{2}} - (\bar{L}_2 + \bar{L}_{-2})^{\frac{1}{2}}(\bar{M}_1 - \bar{M}_{-1})^{\frac{1}{2}}] \sin(\delta_1 - \delta_2) \\ & + F\{(y - \tfrac{2}{3}qx)[(\bar{L}_1 + \bar{L}_{-1})^{\frac{1}{2}}(\bar{M}_1 + \bar{M}_{-1})^{\frac{1}{2}} - (\bar{L}_1 - \bar{L}_{-1})^{\frac{1}{2}}(\bar{M}_1 - \bar{M}_{-1})^{\frac{1}{2}}] \\ & \cdot \cos(\delta_{-1} - \delta_1) - \tfrac{1}{2}[(y + \tfrac{1}{3}qx)(\bar{L}_1 - \bar{L}_{-1})^{\frac{1}{2}}(\bar{L}_2 - \bar{L}_{-2})^{\frac{1}{2}} \\ & - 3x(\bar{L}_2 - \bar{L}_{-2})^{\frac{1}{2}}(\bar{M}_1 + \bar{M}_{-1})^{\frac{1}{2}}] \cos(\delta_{-1} - \delta_{-2}) - \tfrac{1}{2}[(y + \tfrac{1}{3}qx) \\ & \cdot (\bar{L}_1 + \bar{L}_{-1})^{\frac{1}{2}}(\bar{L}_2 + \bar{L}_{-2})^{\frac{1}{2}} - 3x(\bar{L}_2 + \bar{L}_{-2})^{\frac{1}{2}}(\bar{M}_1 - \bar{M}_{-1})^{\frac{1}{2}}] \cos(\delta_1 - \delta_2). \end{aligned} \tag{A3.9}$$

For S *and* T *interactions,*

$$b = b^{(0)} + \Delta b, \tag{A.3.10}$$

$$\begin{aligned} b^{(0)} = {} & \tfrac{3}{4}(2x-1)^2 \bar{L}_2 + 3(xy - \tfrac{1}{2}y + \tfrac{1}{3}qx^2 - \tfrac{1}{2}qx + \tfrac{1}{6}q)[(\bar{L}_1 - \bar{L}_{-1})^{\frac{1}{2}}(\bar{L}_2 + \bar{L}_{-2})^{\frac{1}{2}} \\ & \cdot \cos(\delta_{-1} - \delta_2) - (\bar{L}_1 + \bar{L}_{-1})^{\frac{1}{2}}(\bar{L}_2 - \bar{L}_{-2})^{\frac{1}{2}} \cos(\delta_1 - \delta_{-2})] + 3(x^2 + \tfrac{1}{2}x - \tfrac{1}{2}) \\ & \cdot [(\bar{M}_1 - \bar{M}_{-1})^{\frac{1}{2}}(\bar{L}_2 - \bar{L}_{-2})^{\frac{1}{2}} \cos(\delta_1 - \delta_{-2}) - (\bar{M}_1 + \bar{M}_{-1})^{\frac{1}{2}}(\bar{L}_2 + \bar{L}_{-2})^{\frac{1}{2}} \cos(\delta_{-1} - \delta_2)], \end{aligned} \tag{A.3.11}$$

$$\begin{aligned}\Delta b = {} & F^2x^2\{3\bar{L}_2+q[(\bar{L}_1-\bar{L}_{-1})^{\frac{1}{2}}(\bar{L}_2+\bar{L}_{-2})^{\frac{1}{2}}\cos(\delta_{-1}-\delta_2)\\ & -(\bar{L}_1+\bar{L}_{-1})^{\frac{1}{2}}(\bar{L}_2-\bar{L}_{-2})^{\frac{1}{2}}\cos(\delta_1-\delta_{-2})]+3(\bar{M}_1-\bar{M}_{-1})^{\frac{1}{2}}(\bar{L}_2-\bar{L}_{-2})^{\frac{1}{2}}\cos(\delta_1-\delta_{-2})\\ & -3(\bar{M}_1+\bar{M}_{-1})^{\frac{1}{2}}(\bar{L}_2+\bar{L}_{-2})^{\frac{1}{2}}\cos(\delta_{-1}-\delta_2)\}+3Fx\{(y-\tfrac{1}{6}q)[(\bar{L}_1-\bar{L}_{-1})^{\frac{1}{2}}(\bar{L}_2+\bar{L}_{-2})^{\frac{1}{2}}\\ & \cdot\sin(\delta_{-1}-\delta_2)-(\bar{L}_1+\bar{L}_{-1})^{\frac{1}{2}}(\bar{L}_2-\bar{L}_{-2})^{\frac{1}{2}}\sin(\delta_1-\delta_{-2})]+\tfrac{3}{2}[(\bar{M}_1-\bar{M}_{-1})^{\frac{1}{2}}(\bar{L}_2-\bar{L}_{-2})^{\frac{1}{2}}\\ & \cdot\sin(\delta_1-\delta_{-2})-(\bar{M}_1+\bar{M}_{-1})^{\frac{1}{2}}(\bar{L}_2+\bar{L}_{-2})^{\frac{1}{2}}\sin(\delta_{-1}-\delta_2)]\};\end{aligned} \tag{A.3.12}$$

$$b_1 = b_1^{(0)}+\Delta b_1, \tag{A.3.13}$$

$$\begin{aligned}b_1^{(0)} = {} & \{[\tfrac{1}{3}q^2x-y^2-\tfrac{1}{12}q^2-\tfrac{2}{3}qy(x-1)](\bar{L}_1^2-\bar{L}_{-1}^2)^{\frac{1}{2}}+[y(x+1)+\tfrac{1}{3}q(x^2-1)]\\ & \cdot[(\bar{L}_1-\bar{L}_{-1})^{\frac{1}{2}}(\bar{M}_1-\bar{M}_{-1})^{\frac{1}{2}}+(\bar{L}_1+\bar{L}_{-1})^{\frac{1}{2}}(\bar{M}_1+\bar{M}_{-1})^{\frac{1}{2}}]-(x+1)^2(\bar{M}_1^2-\bar{M}_{-1}^2)^{\frac{1}{2}}\}\sin(\delta_{-1}-\delta_1)\\ & -\tfrac{1}{4}(2x-1)^2(\bar{L}_2^2-\bar{L}_{-2}^2)^{\frac{1}{2}}\sin(\delta_{-2}-\delta_2)+(-yx+\tfrac{1}{2}y-\tfrac{1}{3}qx^2+\tfrac{1}{2}qx-\tfrac{1}{6}q)\\ & \cdot[(\bar{L}_1-\bar{L}_{-1})^{\frac{1}{2}}(\bar{L}_2-\bar{L}_{-2})^{\frac{1}{2}}\sin(\delta_{-1}-\delta_{-2})+(\bar{L}_1+\bar{L}_{-1})^{\frac{1}{2}}(\bar{L}_2+\bar{L}_{-2})^{\frac{1}{2}}\sin(\delta_1-\delta_2)\\ & +(x^2+\tfrac{1}{2}x-\tfrac{1}{2})[(\bar{L}_2-\bar{L}_{-2})^{\frac{1}{2}}(\bar{M}_1+\bar{M}_{-1})^{\frac{1}{2}}\sin(\delta_{-1}-\delta_{-2})+(\bar{L}_2+\bar{L}_{-2})^{\frac{1}{2}}(\bar{M}_1-\bar{M}_{-1})^{\frac{1}{2}}\sin(\delta_1-\delta_2)],\end{aligned} \tag{A.3.14}$$

$$\begin{aligned}\Delta b_1 = {} & F^2x^2\{[\tfrac{1}{3}q(\bar{L}_1-\bar{L}_{-1})^{\frac{1}{2}}(\bar{M}_1-\bar{M}_{-1})^{\frac{1}{2}}+\tfrac{1}{3}q(\bar{L}_1+\bar{L}_{-1})^{\frac{1}{2}}(\bar{M}_1+\bar{M}_{-1})^{\frac{1}{2}}\\ & -(\bar{M}_1^2-\bar{M}_{-1}^2)^{\frac{1}{2}}]\sin(\delta_{-1}-\delta_1)-(\bar{L}_2^2-\bar{L}_{-2}^2)^{\frac{1}{2}}\sin(\delta_{-2}-\delta_2)+[(\bar{L}_2-\bar{L}_{-2})^{\frac{1}{2}}(\bar{M}_1+\bar{M}_{-1})^{\frac{1}{2}}\\ & -\tfrac{1}{3}q(\bar{L}_1-\bar{L}_{-1})^{\frac{1}{2}}(\bar{L}_2-\bar{L}_{-2})^{\frac{1}{2}}]\sin(\delta_{-1}-\delta_{-2})+[(\bar{L}_2+\bar{L}_{-2})^{\frac{1}{2}}(\bar{M}_1-\bar{M}_{-1})^{\frac{1}{2}}\\ & -\tfrac{1}{3}q(\bar{L}_1+\bar{L}_{-1})^{\frac{1}{2}}(\bar{L}_2+\bar{L}_{-2})^{\frac{1}{2}}]\sin(\delta_1-\delta_2)\}+Fx\{(y-\tfrac{2}{3}q)[(\bar{L}_1+\bar{L}_{-1})^{\frac{1}{2}}(\bar{M}_1+\bar{M}_{-1})^{\frac{1}{2}}\\ & -(\bar{L}_1-\bar{L}_{-1})^{\frac{1}{2}}(\bar{M}_1-\bar{M}_{-1})^{\frac{1}{2}}]\cos(\delta_{-1}-\delta_1)+[(y-\tfrac{1}{6}q)(\bar{L}_1-\bar{L}_{-1})^{\frac{1}{2}}(\bar{L}_2-\bar{L}_{-2})^{\frac{1}{2}}\\ & -\tfrac{3}{2}(\bar{L}_2-\bar{L}_{-2})^{\frac{1}{2}}(\bar{M}_1+\bar{M}_{-1})^{\frac{1}{2}}]\cos(\delta_{-1}-\delta_{-2})+[(y-\tfrac{1}{6}q)(\bar{L}_1+\bar{L}_{-1})^{\frac{1}{2}}(\bar{L}_2+\bar{L}_{-2})^{\frac{1}{2}}\\ & -\tfrac{3}{2}(\bar{L}_2+\bar{L}_{-2})^{\frac{1}{2}}(\bar{M}_1-\bar{M}_{-1})^{\frac{1}{2}}]\cos(\delta_1-\delta_2)\}.\end{aligned} \tag{A.3.15}$$

References

1) R. R. Lewis, Phys. Rev. **108** (1957) 904
2) J. I. Fuzita, M. Yamada, Z. I. Matumoto and S. Nakamura, Phys. Rev. **108** (1957) 1104
3) A. I. Alikhanov, G. P. Yeliseyev and V. A. Lyubimov, JETP **35** (1958) 1061
4) M. Yamada, Prog. Theor. Phys. **10** (1953) 252
5) G. E. Lee-Whiting, Phys. Rev. **97** (1955) 463
6) E. A. Plassman and L. M. Langer, Phys. Rev. **96** (1954) 1593
7) H. Takebe, S. Nakamura and M. Taketani, Prog. Theor. Phys. **14** (1955) 317
8) V. B. Berestetsky, B. L. Ioffe, A. P. Rudik and K. A. Ter-Martirosyan, Nuclear Physics **5** (1958) 464
9) E. J. Konopinsky and G. Uhlenbeck, Phys. Rev. **60** (1941) 308
10) A. M. Smith, Phys. Rev. **82** (1951) 955
11) G. E. Lee-Whiting, Can. Journ. Phys. **36** (1958) 252
12) L. A. Sliv and B. A. Volchok, Tables of Coulomb Phase Shifts and Coulomb Phase Shifts and Amplitudes Taking into Account the Finite Nuclear Size

1.E.4:
2.L:3.A

Nuclear Physics **13** (1959) 74—87; © *North-Holland Publishing Co., Amsterdam*
Not to be reproduced by photoprint or microfilm without written permission from the publisher

INELASTIC NEUTRON SCATTERING IN Mn^{55}

N. NATH †, M. A. ROTHMAN ††, D. M. VAN PATTER and C. E. MANDEVILLE †††
Bartol Research Foundation of the Franklin Institute, Swarthmore, Pa. *

Received 29 May 1959

Abstract: Gamma rays excited by inelastic neutron scattering in Mn^{55} have been studied. Coincidence methods have been used to observe those gamma rays which cascade through the 127 keV first excited state. Branching ratios have been measured for four levels, as well as the cross sections for excitation of each level. Theoretical calculations of the cross section, using a diffuse-edge potential well, give good agreement with the experiment, if appropriate spin values are assigned to each level.

1. Introduction

There have been several studies of the levels in Mn^{55} by means of inelastic neutron scattering [1–5]). The Mn^{55}(p, p′) work of Mazari, Sperduto and Buechner [6]) has more recently provided a definitive level scheme for Mn^{55}.

The presence of this known level scheme made Mn^{55} appear to be a useful subject for testing our gamma-gamma coincidence arrangement, prior to working on lesser-known nuclei. We have essentially repeated the work of Beghian *et al.* [2]) and in so doing have clarified certain ambiguities and have obtained additional information concerning branching ratios and relative yields of gamma rays. Comparison of these results with theory provides suggestions concerning the most likely spin values for the first four excited states.

2. Experimental Arrangement

Fig. 1 shows the experimental arrangement together with a block diagram of the electronics. The analyzed proton beam from the Bartol-ONR Van de Graaff generator produced neutrons in an evaporated lithium target cooled with liquid air. The neutrons were attenuated by Mallory Metal wedges 5″ long. The two wedges and detectors shown were used for the coincidence measurements. For observation of singles spectra only one of the wedges and detectors was kept in place.

† Permanent address: Delhi, India. Now at Louisiana State University, Baton Rouge, La.
†† Now at Project Matterhorn, Princeton University, Princeton, N. J.
††† Now at the University of Alabama, Tuscaloosa, Alabama.
* Assisted by the U.S. Atomic Energy Commission.

The manganese scatterer was a disc $1\frac{3}{4}''$ in diameter and $\frac{1}{4}''$ thick. This is approximately the optimum thickness for measuring coincidences between gamma rays of 130 and 850 keV energy, taking into account self-absorption in the scatterer.

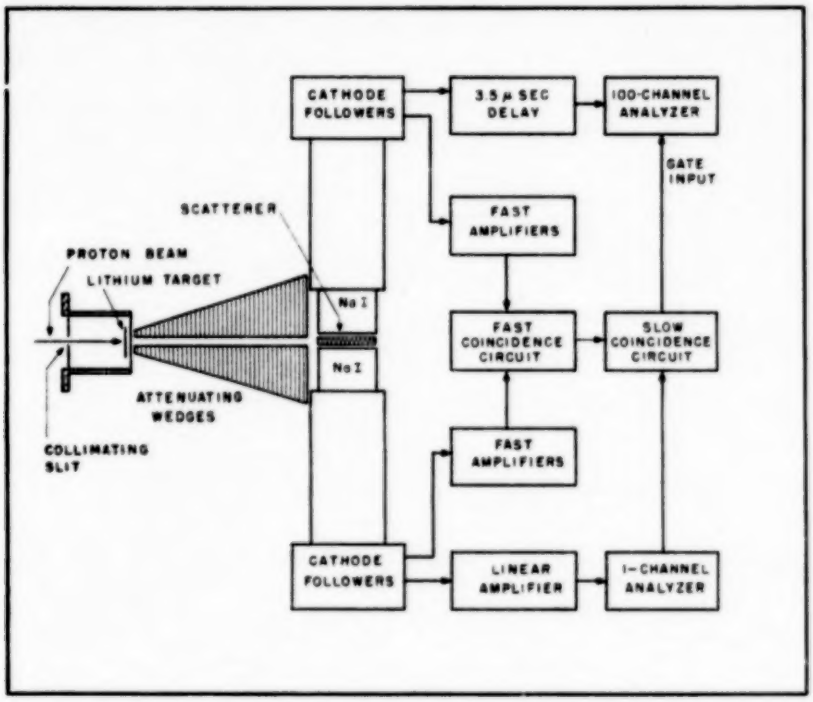

Fig. 1. Apparatus for the detection of gamma-gamma coincidences from inelastic scattering of neutrons.

The block diagram is that of a conventional slow-fast coincidence circuit similar to that described by P. R. Bell [7]). A resolving time of about 30 ns was employed. The NaI crystal used on the 100-channel side was 3.5 cm in diameter and 4 cm long, with a resolution of 8 % for the 662 keV gamma ray from Cs^{137}. Since the single-channel side of the circuit was set on the 127 keV gamma ray from the first excited state of Mn^{55}, the crystal used there was 3 mm thick and 3.5 cm in diameter.

The neutron flux was monitored by a long BF_3 counter located at 90° with respect to the forward direction.

3. Background Effects

The singles and coincidence spectra present different problems. In the singles spectra the background consists of numerous gamma rays from inelastic neutron scattering in iodine, the beta spectrum (25 min half-life) of I^{128}, and a capture gamma ray at about 140 keV, which is prominent at lower neutron bombarding energies. In the present experiment, with such a

small scatterer being used, the background made up over 80 % of the total counting rate. The background spectrum was obtained by using a suitable graphite scatterer.

Since the dead time of the 100-channel analyzer is appreciable, it was necessary to time the runs so that the effective "live time" was the same for both scatterer and background runs.

Since the background has a distinct structure, it is essential that there be no gain shift between runs. Gain shifts in the photomultiplier are minimized by operating the anode at as low a voltage as possible (800—900 V for singles spectra). In some runs corrections were made for the gain shift, which in the worst cases, amounted to about 1 %.

In the coincidence work there are two undesirable background effects which are peculiar to this type of experiment:

(1) A neutron of energy E_n enters the scatterer and undergoes an inelastic collision, producing a gamma ray of energy E_1 and a neutron of energy $E_n - E_1$. The gamma ray goes into one counter and the neutron goes into the other counter, where it undergoes inelastic scattering in the iodine, exciting any of the iodine levels of energy less than $E_n - E_1$. Thus, part of the iodine spectrum will be seen in coincidence with the gamma ray of energy E_1.

(2) A neutron of energy E_n enters the scatterer and undergoes an inelastic collision, producing a gamma ray of energy E_1. The scattered neutron then makes another inelastic collision in the same scattering material, producing another gamma ray of energy E_1, provided that $E_n - E_1 > E_1$, or $E_n > 2E_1$. Thus, any gamma ray will appear in coincidence with itself. In a similar way it is possible to get coincidences between all the combinations of gamma-rays from the levels available in the scattering nucleus. In the case of Mn^{55}, only the gamma-ray from the first excited state gave sufficient intensity to cause difficulty.

In addition there is a background due to chance events, coincidences with capture gamma rays from iodine, and events in which a Compton-scattered gamma ray from one crystal is detected in the other crystal. This latter type of event, as well as multiple scattering events of type (1) may be detected by placing appropriate absorbers between the scatterer and the counter on the 100-channel side.

Multiple scattering of type (2) cannot be eliminated. It is estimated that in the present geometry it amounted to less than 3 % of the single scattering. This effect produces no error in the measurement of branching ratios, because in measuring branching ratios one is concerned with the relative intensities of two gamma rays arising from the same level; how the level is excited is immaterial.

4. Experimental Results

Fig. 2 shows the level scheme of Mn^{55}, with level energies as given by Mazari, Sperduto and Buechner [6]). The gamma ray energies are those obtained by our measurements. No efforts were made to obtain very accurate calibrations, since the level energies were taken as definitive. Where two

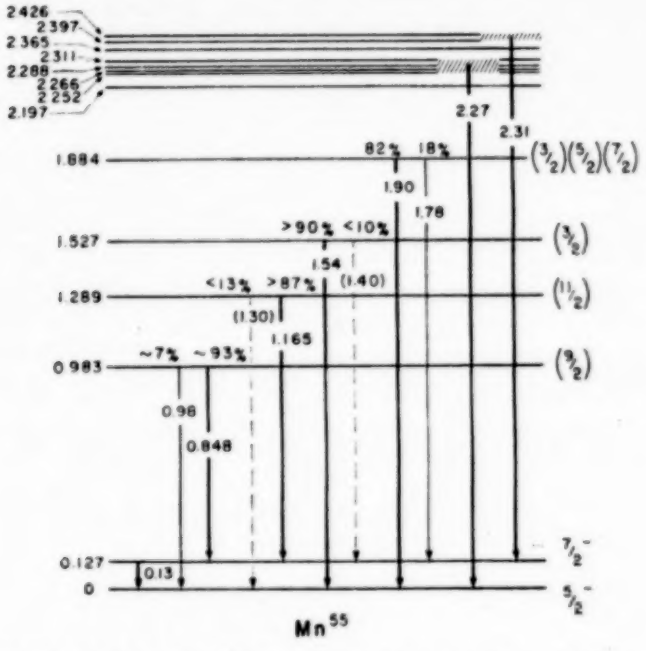

Fig. 2. Level scheme of Mn^{55}, showing spins and branching ratios.

gamma rays arise from the same level, their relative intensities are indicated.

Fig. 3 shows the higher energy end of the singles spectra found at various neutron bombarding energies. From singles spectra alone it would be difficult to determine which gamma rays represented ground state transitions. This is made clear by the coincidence spectra.

The peak seen at 0.98 MeV is actually caused by summing of 0.85 and 0.127 MeV pulses in the sodium iodide crystal. This was demonstrated by inserting a $\frac{1}{16}''$ thick lead absorber between the scatterer and the crystal, whereupon the 0.98 MeV peak was nearly completely wiped out. Measurements of intensities were made either with the absorber, or by correcting the relative intensities for the summing effect.

Fig. 4 shows the spectrum obtained in coincidence with the 127 keV gamma ray, using a neutron energy of 1.25 MeV. The top curve was obtained with no lead absorber; the next curve was obtained with $\frac{3}{8}''$ of lead between the scatterer and the detector on the 100-channel side. This absorber cut down the number of true coincidences, but permitted most of the neutrons through to give a multiple scattering spectrum as described in the previous section. Peaks are seen at approximately 200, 415 and 600 keV, correspond-

ing to iodine gamma rays. The third curve (displaced downward one decade on the scale) represents the difference between the first two curves. This shows that the peaks at 127 and 850 keV persist. The first of these peaks arises from multiple scattering in which the same neutron raises two different nuclei to the 127 keV level. The 850 keV gamma ray represents the cascade transition between the first and second levels of Mn^{55}.

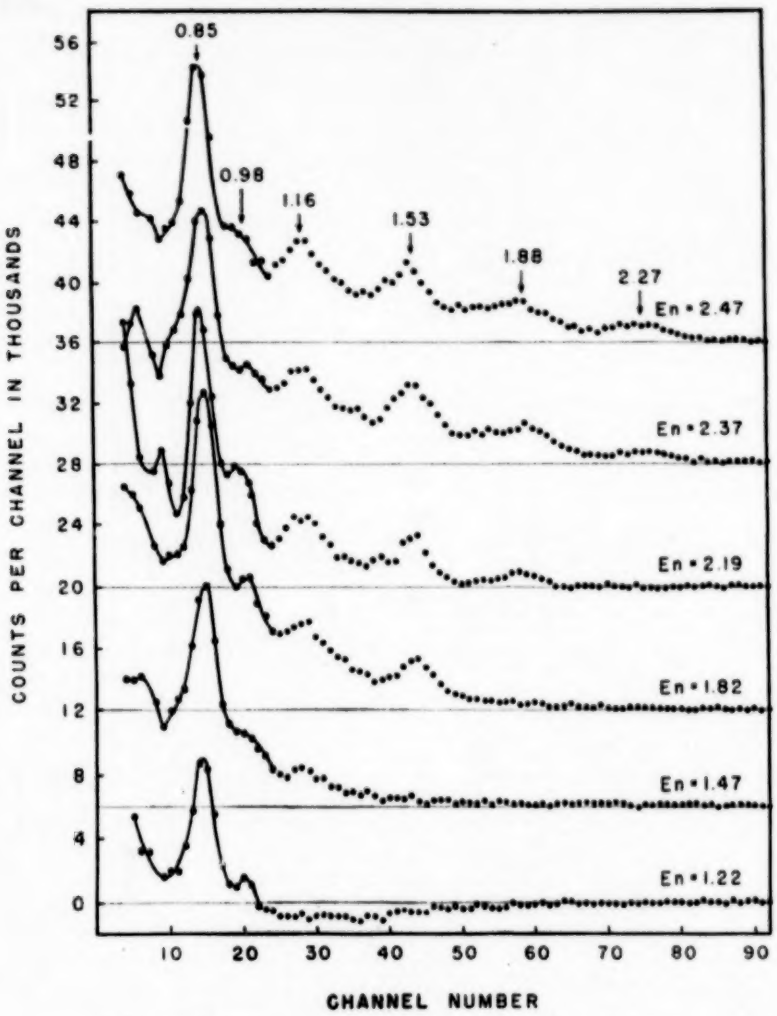

Fig. 3. Gamma ray spectra from Mn^{55} (singles).

Fig. 5 shows the high energy part of the coincidence spectrum, using a neutron energy of 2.5 MeV. In this case $\frac{5}{8}''$ of lead was used as absorber; otherwise the curves are analogous to those of fig. 4.

Fig. 6 gives a comparison between the singles and coincidence spectra at a bombarding energy of 2.5 MeV. (These spectra were taken without the use of lead absorbers.) In the case of the singles spectrum, the background run (with graphite) has been subtracted. No effort has been made to normalize these two curves, since the purpose of this display is to compare the shapes of the two spectra. It is seen that the 0.98, 1.53 and 1.88 MeV peaks do not

appear in the coincidence spectrum, indicating that these represent ground state transitions. It is also clear from a comparison of the shapes that multiple scattering effects introduce little error in this portion of the spectrum.

Table 1 summarizes the gamma rays observed in the singles spectra. Also given are the experimental cross sections for excitation of each level, for a set of bombarding energies varying from 1.22 to 2.47 MeV. These

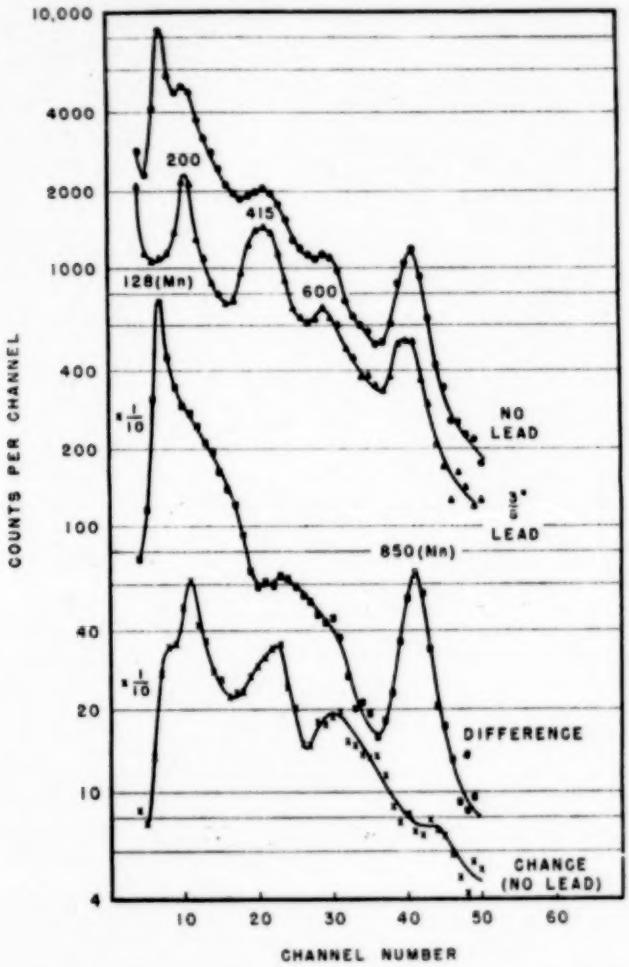

Fig. 4. Coincidences with 127 keV gamma ray from Mn^{55}. $E_n = 1.25$ MeV.

figures were obtained by detailed analysis of the gamma ray spectra, knowing the response of the scintillator to gamma rays of known energy. Corrections were made for crystal efficiency, self-absorption in the Mn scatterer, and sum peak formation.

Table 2 gives the branching ratios obtained for four of the levels. The branching ratio here is defined as I_0/I_1, where I_0 is the number of gamma rays emitted as a result of transitions to the ground state from a given level, and I_1 is the number of gamma rays resulting from transitions to the first excited state. This is related to the number of pulses actually counted through the relationship

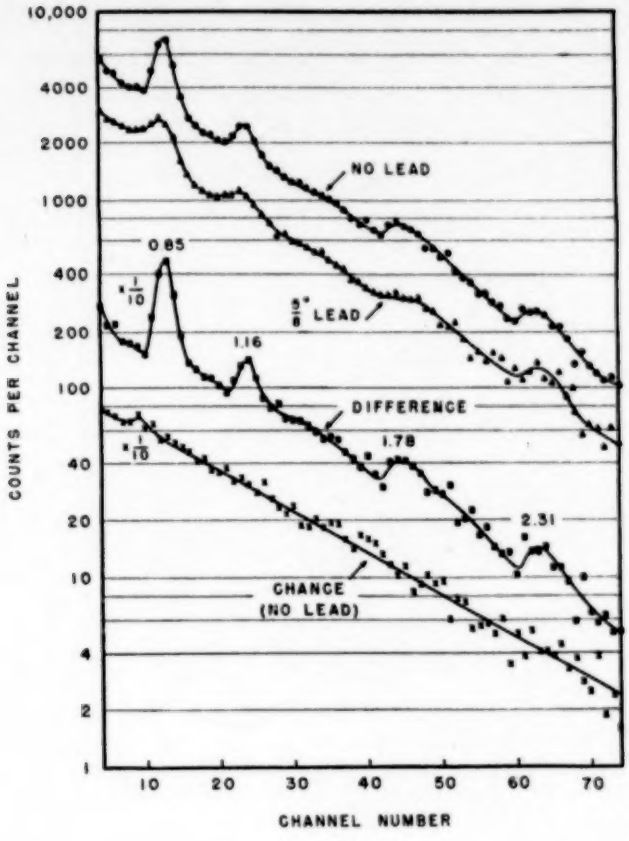

Fig. 5. Coincidences with 127 keV gamma ray from Mn^{55}. $E_n = 2.5$ MeV.

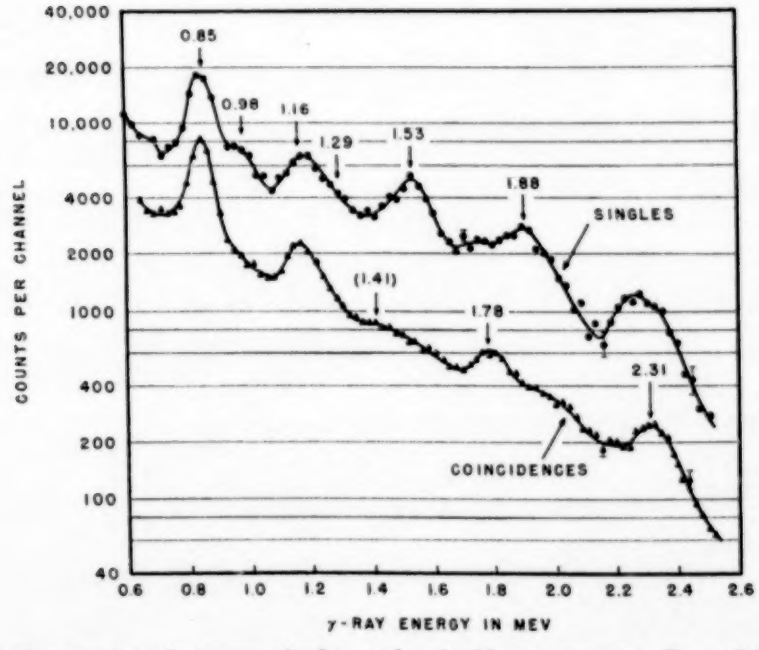

Fig. 6. Comparison between singles and coincidence spectra. $E_n = 2.5$ MeV.

$$\frac{I_0}{I_1}=\frac{N_0\varepsilon_1 T_1}{N_1\varepsilon_0 T_0}, \tag{1}$$

where N_0 and N_1 are the number of counts measured in the photopeak of the corresponding gamma ray, ε is the photopeak efficiency of the detector for the given gamma ray, and T is effectively a transmission coefficient which

TABLE 1

Gamma rays from Mn^{55}

Level	E_γ (observed)	Measured cross section (barns)				
		$E_n = 1.22$	1.48	1.82	2.19	2.47
0.127	0.13	0.73	—	—	—	—
0.983	0.85	0.20	0.29	0.31	0.39	0.31
	0.98					
1.289	1.17		0.08	0.08	0.10	0.08
	1.30					
1.527	1.54			0.16	0.18	0.15
1.884	1.78				0.10	0.14
	1.90					
2.2–2.4	2.3					0.14

Probable error on absolute cross section: 30 %.
Probable error on relative cross sections: 20 %.

TABLE 2

Branching ratios in Mn^{55}

Level (MeV)		0.983	1.289	1.527	1.884
Experimental F		0.93 ±0.03	0.87	0.1	0.18 ±0.05
Experimental I_0/I_1		1/13	1/7	9	3.3——6.7
Level J	Transitions				
$\frac{1}{2}-$	E2/M3	1.83×10^6	8.06×10^5	5.23×10^5	3.06×10^5
$\frac{1}{2}+$	M2/E3	1.07×10^4	4740	3080	1800
$\frac{3}{2}-$	M1/E2	1200	585	390	235
$\frac{3}{2}+$	E1/M2	1.81×10^6	8.69×10^5	5.78×10^5	3.49×10^5
$\frac{5}{2}-$	M1/M1	0.888	0.788	0.756	0.719
$\frac{5}{2}+$	E1/E1	0.888	0.788	0.756	0.719
$\frac{7}{2}-$	M1/M1	1.95	1.73	1.66	1.58
$\frac{7}{2}+$	E1/E1	1.95	1.73	1.66	1.58
$\frac{9}{2}-$	E2/M1	1/533	1/350	1/260	1/179
$\frac{9}{2}+$	M2/E1	$1/7.9\times10^5$	$1/5.2\times10^5$	$1/3.9\times10^5$	$1/2.7\times10^5$
$\frac{11}{2}-$	M3/E2	$1/4.6\times10^5$	$1/3.3\times10^5$	$1/2.5\times10^5$	$1/1.8\times10^5$
$\frac{11}{2}+$	E3/M2	1/2700	1/1900	1/1460	1/1040

This chart tabulates I_0/I_1 calculated from single-particle transition probabilities. Each row corresponds to an assumed level spin, and each column corresponds to the level energy shown above.

takes into account the self-absorption of the gamma rays in the scatterer.

Also shown in table 2 is F, the fraction of gamma rays which go to the first

excited state from the given level. This is related to the branching ratio by

$$F = \frac{I_1}{I_0+I_1} = \frac{1}{1+I_0/I_1}. \tag{2}$$

In favourable cases, I_0/I_1 may be obtained from the singles spectrum alone. The branching ratio for the 0.983 MeV level was obtained by bombarding with 1.21 MeV neutrons, so that only this level was excited. A $\frac{1}{16}''$ thick Pb absorber eliminated summing in the crystal. By comparing spectra made with and without the absorber the actual amount of summing could be measured. It was determined that to correct for summing (when no absorber was used) one had to increase the number of counts in the 0.85 MeV peak by 16 %, while the 0.98 MeV peak was corrected by subtracting the same number of counts.

Because of the fact that one of the gamma rays contributing to the sum is of very low energy, practically all of its spectrum falls into the photopeak. Therefore one can say that, if N_s is the number of counts in the sum photopeak, and ε_{10} is the counting efficiency for the 0.127 MeV gamma ray, then $N_s = I_1\,\varepsilon_1\,\varepsilon_{10} = N_1\varepsilon_{10}$. It is seen that N_s/N_1 is a constant for all the levels which cascade through the first level. Therefore, the same percentage correction for summing applies to all the levels. (It is seen that this procedure also leads to an absolute measure of the crystal efficiency.)

In the case of the higher levels, where the ground state transition was the most prominent, the photopeak of the cascade gamma ray in the singles spectrum, tended to be submerged under the valley of the cross-over gamma ray peak. For this reason it was quite difficult to estimate the intensity of the 1.4 and 1.76 MeV gamma rays in the presence of the more prominent 1.53 and 1.88 MeV peaks.

By making comparisons between the coincidence and the singles spectra a

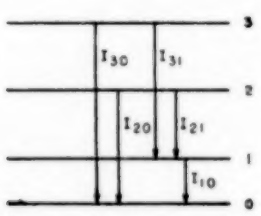

Fig. 7. Nomenclature for gamma ray transitions.

more accurate estimate of the cascades could be made. Using the nomenclature portrayed in fig. 7, it can be shown that

$$\frac{I_{30}}{I_{31}} = \frac{N^c_{21}}{N^c_{31}}\,\frac{N_{30}}{N_{21}}\,\frac{\varepsilon_{31}}{\varepsilon_{30}}\,\frac{T_{31}}{T_{30}}, \tag{3}$$

where, as before, I represents the actual gamma ray intensity, N is the number of counts in the photopeak, ε is the photopeak efficiency, and T is the self-absorption correction. The superscript c refers to coincidence measurements.

From this it is seen that if there is one transition in which the cascade is most prominent (N_{21}), the branching ratio can be obtained for another level in which the cross-over is predominant (N_{30}). In the case of Mn^{55} both the 0.85 and the 1.16 MeV gamma rays were suitable to use as N_{21}.

The 1.4 MeV gamma ray was not really seen, even in the coincidence spectrum. An upper limit was estimated for N_{31}^c in this case. The 1.76 MeV gamma ray was distinctly seen in the coincidence spectrum, so that a fair estimate could be made for its intensity.

The values given in table 2 for I_0/I_0 are averages from a number of measurements. Also shown are the theoretical ratios for each level calculated from the single-particle transition probabilities [8]). The spins for the ground and first excited states were taken as $\frac{5}{2}-$ and $\frac{7}{2}-$, respectively [9]). The ratio I_0/I_1 was calculated for the spin values shown, for each level. Comparison of these theoretical ratios with the experimental ones serves to limit the level spins to one or two possibilities.

For the 0.98 MeV level, a choice of $\frac{9}{2}-$ gives the best agreement, particularly if one expects some enhancement of the E2 transition probability over the single-particle value. This is in agreement with the result of Beghian *et al.* [2]). However, $\frac{11}{2}+$ is not completely ruled out on this evidence alone.

The same conclusions hold for the 1.29 MeV level, since the branching ratio is similar to that of the 0.98 MeV level. An additional possibility here is $\frac{11}{2}-$, since only an upper limit was found for I_0/I.

In the case of the 1.53 MeV level, the 10 % figure for the relative intensity of the 1.4 MeV gamma ray is an extreme upper limit. An upper limit of 5 % would have a good expectation value. $\frac{3}{2}-$ is found to be the most probable spin assignment, although $\frac{1}{2}+$ and $\frac{3}{2}+$ is not completely ruled out on this evidence.

For the 1.88 MeV level, a small change in the theoretical ratio would put $\frac{7}{2}$ (and perhaps $\frac{5}{2}$) within the range of agreement, so that $\frac{3}{2}-$, $\frac{7}{2}$ ($+$ or $-$), and $\frac{5}{2}$ ($+$ or $-$) are possible spin values for this level.

5. Cross Sections

A few measurements of the cross sections for the 0.127 and 0.856 MeV gamma rays have been reported [1, 4, 10]). We have measured the relative intensities of the gamma rays from the first five levels and have compared these with the intensity of the 0.845 MeV gamma rays from iron. The cross section for excitation of this gamma ray was obtained by averaging a num-

ber of previous measurements [4,11,12]). The value taken as a standard for comparison was 0.52 barns at $E_n = 1.21$ MeV.

Yields of gamma rays from Mn were corrected for self-absorption and crystal efficiency according to the expression

$$\sigma = \frac{\sigma' n_c n' B' \varepsilon' T'}{n'_c n B \varepsilon T}, \tag{4}$$

where σ is the cross section for production of the given gamma ray, n_c is the number of counts in the photopeak per unit number of neutron monitor counts (corrected for difference in neutron intensity, between 0° and 90°), n is the number of scattering atoms per cm^3, B is a factor which accounts for the attenuation of incident neutrons in the scatterer, ε is the photopeak efficiency of the crystal, and T is a factor which accounts for the self-absorption of the gamma rays in the scatterer. The unprimed quantities refer to the Mn^{55}, while the primed quantities refer to the iron standard, which was the same shape and size as the manganese piece.

In cases where branching occurs, the yields of the two gamma rays were added up to give the cross section for the excitation of the given level. The yield from each level shows no abrupt rise which might be attributed to cascading from a higher level. Due to the small size of the scatterer, multiple scattering is expected to be less than 3 % of the inelastic scattering.

A figure of approximately 30 % is estimated for the probable error of the absolute cross sections. The value of 0.52 barns used for the iron cross section may be in error by as much as 20 %. Relative cross sections for the various levels in Mn are expected to be more accurate, since they do not involve this uncertainty in the iron standard. The relative cross section for the 0.98 and 1.29 MeV levels is probably good to within 10 % at the lower bombarding energies. As the bombarding energy increases and more levels are excited the spectra become more difficult to analyze and the errors are expected to increase. Furthermore, the efficiency calibration of the NaI crystal is expected to be more in error as the energy of the gamma ray increases. A probable error of 20 % is estimated for relative cross sections at the higher bombarding energies. Fig. 8 shows the cross sections obtained for the second to fifth levels in Mn^{55}.

Fig. 9 shows the results of Hauser-Feshbach calculations of the theoretical cross sections for these same levels. The spins used were $\frac{5}{2}^-$ for the ground state, $\frac{7}{2}^-$ for the first excited state, and the other spins as shown in the figure. The transmission coefficients used in the calculation were obtained from a report by W. S. Emmerich [13]). The nuclear model used is a potential consisting of a constant spherical core of depth V_c and radius R_c to which a diffuse edge has been added of the form $V_c(e^x - x)^{-1}$, where $x = (r - R_c)/\tau$. The diffuseness of the edge is determined by τ. The imaginary part of the

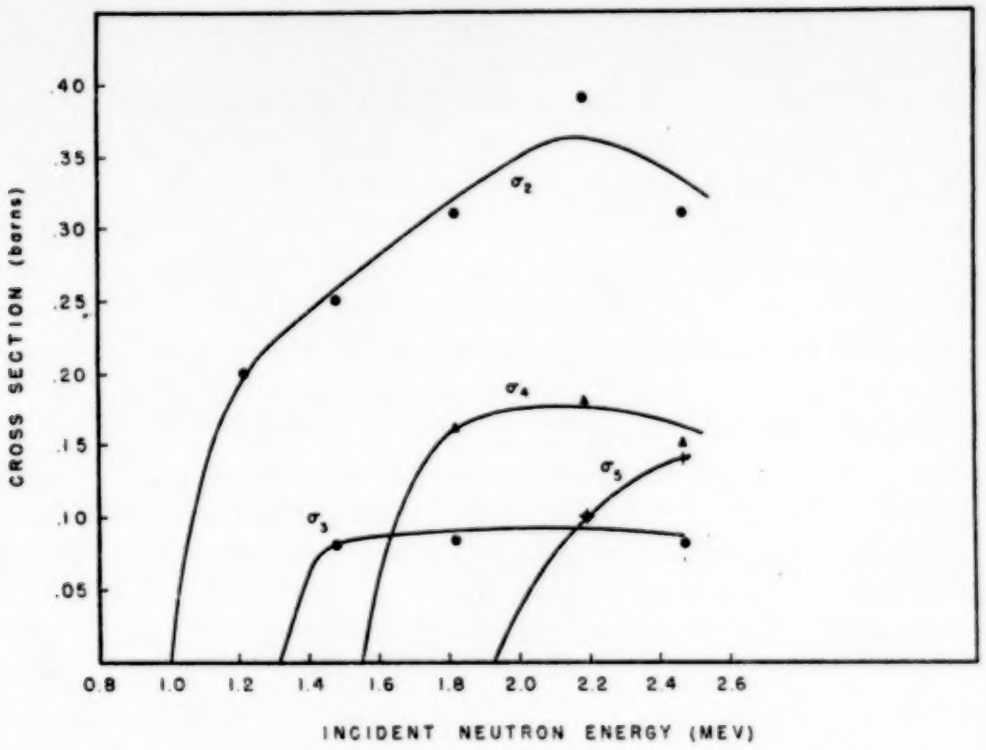

Fig. 8. Experimental inelastic neutron scattering cross sections for Mn^{55}.

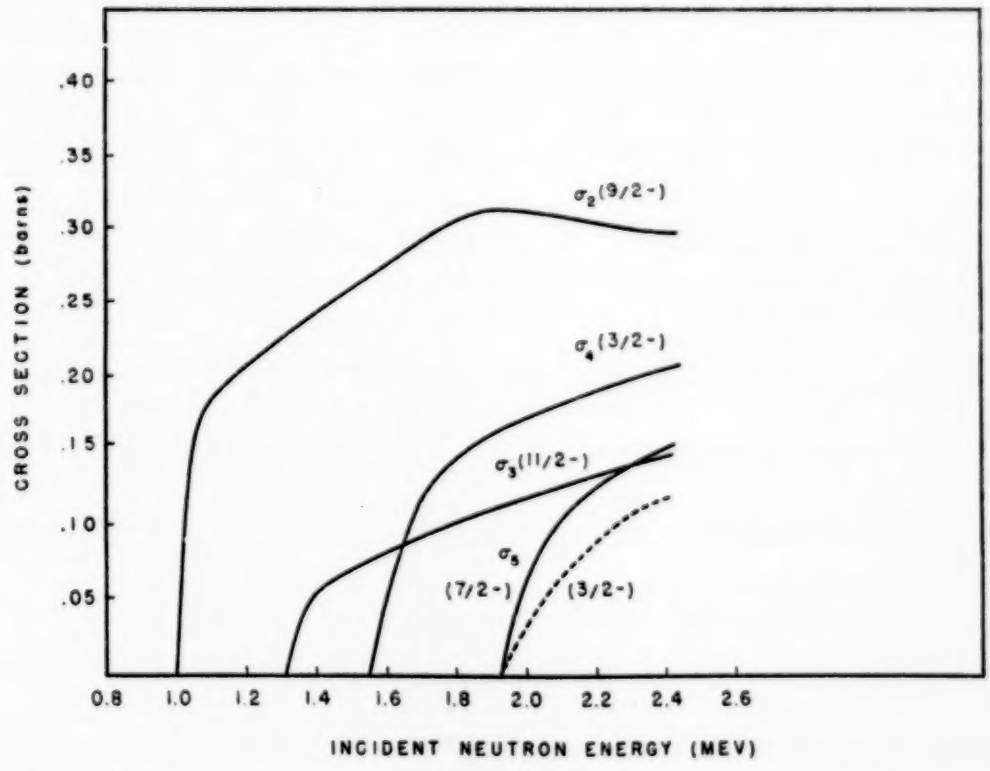

Fig. 9. Theoretical inelastic neutron scattering cross sections for Mn^{55}.

value. The negative parity is somewhat more satisfactory, but the positive parity is not completely ruled out.

For the fifth level, the variation caused by a change of spin is too small, and the experimental errors too large to permit a choice of spin value. It can only be said that the spin probably lies between $\frac{3}{2}$ and $\frac{7}{2}$.

An attempt was made to measure the cross section of the 0.127 MeV level. However, the geometry used in the present experiment is not favourable for the study of such a low-lying state. Use of a thin NaI crystal is required to minimize the background due to neutron scattering in the iodine, as well as interference from higher energy gamma rays. One run made at a bombarding energy of 1.21 MeV yielded a cross section of 0.73 barns, compared with a theoretical value of 0.92 barns. The ratio of cross sections for the first and second excited states was found to be 3.65 from the measurements, and 4.2 from the theoretical calculations. This is a reasonable agreement under the circumstances.

The spins shown in fig. 2 summarize the most probable values as discussed above. The Mn^{55} nucleus has an $(f_{\frac{7}{2}})^{-3}$ configuration. The anomalous ground state spin of $\frac{5}{2}$ is explained in terms of the interaction between the odd $f_{\frac{7}{2}}$ protons [9]). Ford and Levinson also explain it in terms of weak coupling between the extra shell nucleons with collective surface excitations [14]). The latter calculate the order of levels for the present configuration to be potential is taken to be zero in the core and equal to λ times the derivative of the real part with respect to x in the surface region. Values of V_c varied from 44 to 43 MeV in the energy region of interest, λ varied from 0.34 to 0.37, and τ was equal to 0.84, R_c was obtained from the expression $R = R_c + 1.3591 = (1.25A^{\frac{1}{3}} + 0.5) \times 10^{-13}$ cm, where A is the mass number of the nucleus.

The spins used in the calculation were chosen from those mentioned in the previous section as permitted by the branching ratio measurements. Negative parities were used for all the levels, since a change of parity does not introduce much difference in the theoretical cross section.

It is seen that fairly good qualitative agreement can be obtained between the theory and experiment. Previous calculations based on a square, black potential had given cross sections too small by a factor of two. The complex rounded edge potential has been found to give much higher cross sections, because Mn happens to be at the peak of a giant resonance for the even-l waves.

The best agreement for the third level is obtained with the $\frac{11}{2}$ spin as shown. A spin of $\frac{9}{2}$ increases the theoretical cross section by a factor of two. The parity is not identified by this evidence.

For the fourth level, the branching ratio evidence indicates that the spin should be less than $\frac{5}{2}$. The cross sections indicate that $\frac{3}{2}$ is the preferred

$\frac{5}{2}$, $\frac{7}{2}$, $\frac{11}{2}$, $\frac{3}{2}$, $\frac{9}{2}$, $\frac{15}{2}$. This agrees with our measurements except for the location of the $\frac{9}{2}$ level, which we place after the $\frac{7}{2}$ level.

A configuration mixing calculation by Yanagawa [15]) predicts a $\frac{3}{2}$ level at about 1.27 MeV.

The level seen by us at 1.527 MeV may be the single-particle $p_{\frac{3}{2}}$ level which lies above the $f_{\frac{7}{2}}$ shell. This is suggested by a comparison with the $p_{\frac{3}{2}}-f_{\frac{7}{2}}$ spacing in neighbouring odd-mass elements [9]). In Ti^{47} (25 neutrons) this spacing is 1.24 MeV. In Ti^{49} (27 neutrons) the spacing is 1.38 MeV. In the present case of Mn^{55} (25 protons), the spacing between the $\frac{3}{2}$ and $\frac{7}{2}$ levels is 1.40 MeV.

We are grateful to Dr. W. F. G. Swann for his continuing support of this work.

References

1) J. M. Freeman, Phil. Mag. **46** (1955) 12
2) Beghian, Hicks and Milman, Phil. Mag. **1** (1956) 261
3) L. Cranberg and J. S. Levin, Phys. Rev. **103** (1956) 343
4) J. J. van Loef and D. A. Lind, Phys. Rev. **101** (1956) 103
5) F. I. Boley, E. H. Thorndike and A. T. Moffett, Phys. Rev. **110** (1958) 915
6) M. Mazari, A. Sperduto and W. W. Buechner, Phys. Rev. **108** (1957) 103
7) K. Siegbahn, Beta and Gamma Ray Spectroscopy (1955) p. 159
8) *Ibid*, p. 391
9) R. H. Nussbaum, Revs. Mod. Phys. **28** (1956) 423
10) J. B. Guernsey and A. Wattenberg, Phys. Rev. **101** (1956) 1516
11) R. M. Kiehn and C. Goodman, Phys. Rev. **95** (1954) 989
12) R. B. Day, Phys. Rev. **102** (1956) 767
13) W. S. Emmerich, Westinghouse Research Report 6–94511–6–R19 (1958)
14) K. W. Ford and C. Levinson, Phys. Rev. **100** (1955) 1
15) S. Yanagawa, J. Phys. Soc. Japan **13** (1958) 4

2.A.1 *Nuclear Physics* **13** (1959) 88—91; © *North-Holland Publishing Co., Amsterdam*
Not to be reproduced by photoprint or microfilm without written permission from the publisher

MEASUREMENTS OF (n, p), (n, α) AND (n, 2n) TOTAL CROSS SECTIONS AT 14 MeV

C. S. KHURANA † and H. S. HANS
Department of Physics, Muslim University, Aligarh, India

Received 13 June 1959

Abstract: Total cross-sections for the following reactions have been measured at 14 MeV neutron energy: $Al^{27}(n, p)Mg^{27}$(115±10mb); $Al^{27}(n, \alpha)Na^{24}$(111±9mb); $Sb^{123}(n, 2n)Sb^{122}$ (1706±120mb); $Sb^{121}(n, 2n)Sb^{120}$(453±43mb); $Ag^{109}(n, 2n)Ag^{108}$ (619±40mb); $Ag^{109}(n, \alpha)Rh^{106}$(38±6mb); $Sc^{45}(n, 2n)Sc^{44}$ (129±9mb); $Sc^{45}(n, \alpha)K^{42}$(132±8mb); $Ti^{50}(n, p)Sc^{50}$ (147±13mb); $Ti^{49}(n, p)Sc^{49}$(97±16mb).

1. Introduction

At 14 MeV neutron energy (n, p), (n, α) and (n, 2n) are very important reactions. The measurement of their total cross-sections is useful from various considerations. Many measurements of these cross-sections have been earlier reported [1–12]). Attempts have been made by some workers to compare the measured values of these cross-sections with statistical theory and to explain the discrepancy on the basis of direct interaction [13–15]). But because of the large reported errors in the earlier measurements of these cross-sections, such comparison was inconclusive. For example, recent, more precise, measurements of (n, α) cross-sections [6]) at 14 MeV showed a certain regular trend of these cross-sections with atomic weight in contrast to the earlier measurements. Apart from these considerations the knowledge of these cross-sections is desirable, to complete the data of fast neutron cross-sections. With the availability of a 14 MeV neutron source in our laboratory, it has been possible to undertake these measurements.

2. Experimental

Neutrons of 14 MeV energy were obtained from the $T(d, n)He^4$ reaction, using a 130 keV deuteron beam from the Cockcroft-Walton accelerator in our laboratory [17]). The target end, along with arrangement of irradiation of the sample, is shown in fig. 1. Normally a deuteron current of 20 μA was allowed to fall on a Zr—Tr target to get a neutron yield of 10^8n/sec at the target.

† Junior Research Fellow, Ministry of Education, Government of India.

Since the energy and current of the deuteron beam were comparatively low, it was sufficient to cool the tritium target by forced cool air. A ZnS-lucite crystal mounted on a photomultiplier tube was placed at 90° to the

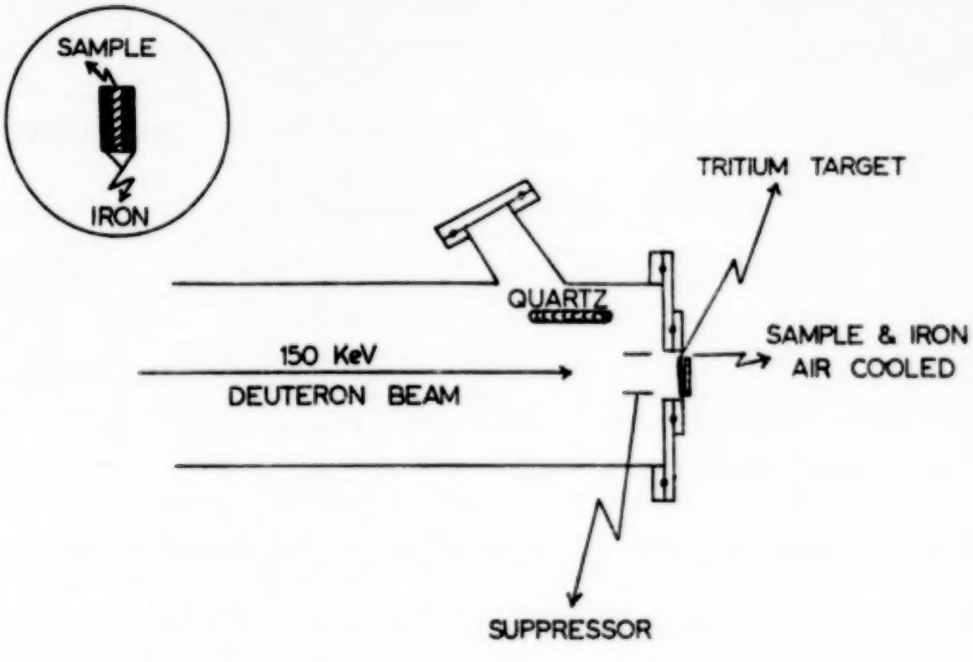

Fig. 1.

deuteron beam to act as a fast neutron monitor. The flux of the neutrons was kept constant during a particular irradiation.

The sample to be irradiated (generally available in powder form) was sandwiched between two cellulose tapes. The area of the sample was kept always equal to 1.5 cm^2, and thickness nearly 20 mg/cm^2. The thickness of the tape was 9 mg/cm^2. The iron samples (available in powder form) were also sandwiched in a similar manner. For irradiation, the sandwiched sample, whose cross-section was to be measured, was placed between the two sandwiches containing iron, as shown in fig. 1. The place of irradiation was the outer side of the brass backing of 0.1 mm thickness, to whose other side the tritium target was fixed. The substances to be irradiated were spectroscopically pure, having a chemical purity of more than 99.9 %.

Because of the low energy of the deuterons, the maximum spread in energy of the neutrons incident on the sample should not be more than 0.5 MeV.

An end window beta-counter of 4 cm diameter, with a mica window of 4.5 mg/cm^2 thickness, was used for measuring the activities of the irradiated samples.

3. Measurements

The cross-section measurements reported here were made relatively to the cross-section for the reaction $Fe^{56}(n, p)Mn^{56}$, for which the standard value of 110 mb, based on the mean of the values of (96.7 ± 12 % mb) by Paul and Clarke [1]) and (124 ± 10 mb) by Forbes [2]), was adopted.

Generally, a sample, along with two iron samples, was irradiated for 30 minutes, after which the activities produced in it, were followed long enough to enable the complete half life curve to be drawn. Since iron, when bombarded by 14 MeV neutrons, yields a nearly pure activity of 156 minutes from the reaction $Fe^{56}(n, p)Mn^{56}$, it was not considered necessary to follow its half life every time. Instead, the counts from the two iron samples were individually measured, after a suitable time, and in the same geometry, for about 20 minutes in each case. However, as a check, the half life curve for Mn^{56} was followed in a couple of cases. The flux incident on the sample was taken to be the mean of the fluxes at the two iron samples. The measurements for a particular sample were repeated many times along with iron, to have good statistics.

The beta-counter was surrounded by about 12 cm of lead from all sides, to reduce the background. Normally, at the time of counting, there was only the cellulose tape of 9 mg/cm^2 between the window of the beta-counter and the sample, amounting to a total thickness of about 33 mg/cm^2, which a beta particle had to traverse before being detected, including the half thickness of the sample.

4. Results

In table 1 are given the cross-sections measured for various reactions. The errors quoted are only the statistical ones. Other errors, judging from the

TABLE 1

(n, p), (n, α) and (n, 2n) cross-sections for 14 MeV neutrons

Reaction	Half life	Cross-section (mb)	Other authors		
			Paul and Clarke [1]) (mb)	Forbes [2]) (mb)	Allan [12]) (mb)
$Al^{27}(n, p)Mg^{27}$	9.5 min	115 ± 10	$52 \pm 10\%$	$79 \pm 7\%$	140 ± 30
$Al^{27}(n, \alpha)Na^{24}$	15.0 h	111 ± 9	$79 \pm 16\%$	$135 \pm 7\%$	116 ± 8
$Sb^{123}(n, 2n)Sb^{122}$	2.8 d	1706 ± 120	$1245 \pm 25\%$	–	–
$Sb^{121}(n, 2n)Sb^{120}$	16.2 min	453 ± 43	$750 \pm 25\%$	–	–
$Ag^{109}(n, 2n)Ag^{108}$	2.3 min	619 ± 40	$311 \pm 50\%$	$1000 \pm 10\%$	–
$Ag^{109}(n, \alpha)Rh^{106}$	140.8 min	38 ± 6	–	–	–
$Sc^{45}(n, 2n)Sc^{44}$	4.01 h	129 ± 9	–	–	–
$Sc^{45}(n, \alpha)K^{42}$	12.4 h	132 ± 8	–	–	–
$Ti^{50}(n, p)Sc^{50}$	1.55 min	147 ± 13	–	–	–
$Ti^{49}(n, p)Sc^{49}$	56.3 min	97 ± 16	–	–	–

reproducibility of the various quantities measured, were considered to be less than 10 %. In some of the cases when measurements have been repeated, an appreciable difference has been found from the values given by other authors, as indicated in the table.

The authors wish to express their sincere thanks to Prof. P. S. Gill, for his active interest and kind encouragement in the course of this work.

References

1) E. B. Paul and R. L. Clarke, Canad. J. Phys. **31** (1953) 267
2) S. G. Forbes, Phys. Rev. **88** (1952) 1309
3) M. E. Battat and F. L. Ribe, Phys. Rev. **89** (1953) 80
4) G. M. Frye, Jr., Phys. Rev. **93** (1954) 1086
5) H. C. Martin, Phys. Rev. **93** (1954) 498
6) H. G. Blossor, C. D. Goodman and T. H. Handley, Phys. Rev. **110** (1958) 531
7) J. B. Marion, R. M. Brugger and R. A. Chapman, Phys. Rev. **101** (1956) 247
8) J. A. Grundle, R. L. Henkel and B. L. Perkins, Phys. Rev. **109** (1958) 425
9) A. H. Armstrong and G. M. Frye, Jr., Phys. Rev. **103** (1956) 335
10) F. L. Ribe, Phys. Rev. **103** (1956) 741
11) J. B. Marion and R. M. Brugger, Phys. Rev. **100** (1955) 69
12) D. L. Allan, Proc. Phys. Soc. A **70** (1957) 195
13) G. Brown and H. Muirhead, Phil. Mag. **2** (1957) 473
14) H. McManus and W. T. Sharp. Statistical aspect of the nucleus. (1955) B.N.L. Report, 68
15) G. Brown, G. C. Morrison, H. Muirhead and W. T. Morton, Phil. Mag. **2** (1957) 785
16) V. F. Weisskopf and D. H. Ewing, Phys. Rev. **57** (1940) 472
17) C. S. Khurana and H. S. Hans, Ind. J. Phys. **32** (1958) 468

1.E.1:
3.A

Nuclear Physics **13** (1959) 92—94; © *North-Holland Publishing Co., Amsterdam*
Not to be reproduced by photoprint or microfilm without written permission from the publisher

MISE EN ÉVIDENCE DE QUELQUES NOUVEAUX ÉTATS ISOMÉRIQUES

E. C. CAMPBELL † et P. F. FETTWEIS
Centre d'Étude de l'Énergie Nucléaire, Mol, Belgique

Reçu le 21 mai 1959

1. Appareillage

Un convoyeur pneumatique rapide a été installé au réacteur BR1 de Mol. Il consiste essentiellement en un tube rectangulaire en aluminium d'une longueur de 6 mètres, menant au centre du réacteur où règne un flux de 10^{12}n/cm^2 · sec. Le porte-échantillon est introduit dans le réacteur par voie pneumatique. Le temps de sortie de l'échantillon, y compris le freinage assurant un positionnement reproductible en face d'un cristal scintillateur NaI(Tl) de $2'' \times 2''$, n'excède pas 0.1 sec.

Le scintillateur est suivi d'une chaîne électronique classique: photomultiplicateur, préamplificateur, sélecteur à un chenal et oscilloscope formant spectromètre gamma. De plus, nous disposons d'un analyseur de temps à 10 chenaux [1]), consistant en une série de 10 échelles rapides dont chacune reçoit les impulsions pendant un temps prédéterminé variable entre 1 msec et 100 sec, de sorte qu'il est possible d'obtenir 10 points de la courbe de décroissance radioactive.

2. Mesures

Les mesures effectuées sont consignées au tableau 1. A titre d'exemple les courbes expérimentales de décroissance du Na^{24m} et du Ga^{72m} sont représentées aux figs. 1 et 2.

Pour distinguer les réactions (n, γ) des autres réactions possibles, nous avons effectué chaque irradiation sans et avec Cd. Pour toutes les réactions, sauf pour le Ba^{135}, l'activité diminue d'un facteur > 2, si l'échantillon est couvert de Cd. Cette atténuation ne peut pas s'expliquer par une absorption des rayons gamma dans le Cd, comme il ressort des mesures effectuées en posant entre l'échantillon activé et le compteur une feuille de Cd de même épaisseur.

† Adresse actuelle: Oak Ridge-National Laboratory, Oak Ridge, Tennessee, U.S.A.

TABLEAU 1

Isotope	Source	Caractéristiques		Références
		$T_{\frac{1}{2}}$ (sec)	E_γ (keV)	
In^{114m}	$In^{113}(n, \gamma)In^{114m}$	2.5	150	Notre travail †
Ir^{194m}	$Ir^{193}(n, \gamma)Ir^{194m}$	0.05	90	Notre travail †
Hf^{178m}	$Hf^{177}(n, \gamma)Hf^{178m}$	3.5	440, 330	Notre travail †
	$Ta^{178} \xrightarrow{E.C.} Hf^{178m}$	4.8		[2]
Ga^{72m}	$Ga^{71}(n, \gamma)Ga^{72m}$	0.040 ± 0.002	≈ 90	Notre travail
Ba^{135m}	Réaction probable: $Ba^{135}(n, n')Ba^{135m}$	0.33 ± 0.03	≈ 800, ≈ 700	Notre travail
Na^{24m}	$Ne^{24} \xrightarrow{\beta^-} Na^{24m}$	$0.005 < T_{\frac{1}{2}} < 0.05$	472	[3]
	$Na^{23}(d, p)Na^{24m}$	0.0199 ± 0.0007		[4]
	$Na^{23}(n, \gamma)Na^{24m}$	0.020 ± 0.002		Notre travail
Yb^{175}	$Yb^{174}(n, \gamma)Yb^{175m}$	0.067 ± 0.004	455	Notre travail
Yb^{177}	$Yb^{176}(n, \gamma)Yb^{177m}$	6.5 ± 0.5	212, 104	Notre travail † et ref. [5]

† Ces activités avaient été décelées à Oak-Ridge par E. C. Campbell, M. Goodrich et J. Kahn, mais l'identification de l'isotope responsable n'avait pas été faite. Celle-ci a été obtenue par activation d'isotopes séparés, fournis par ORNL.

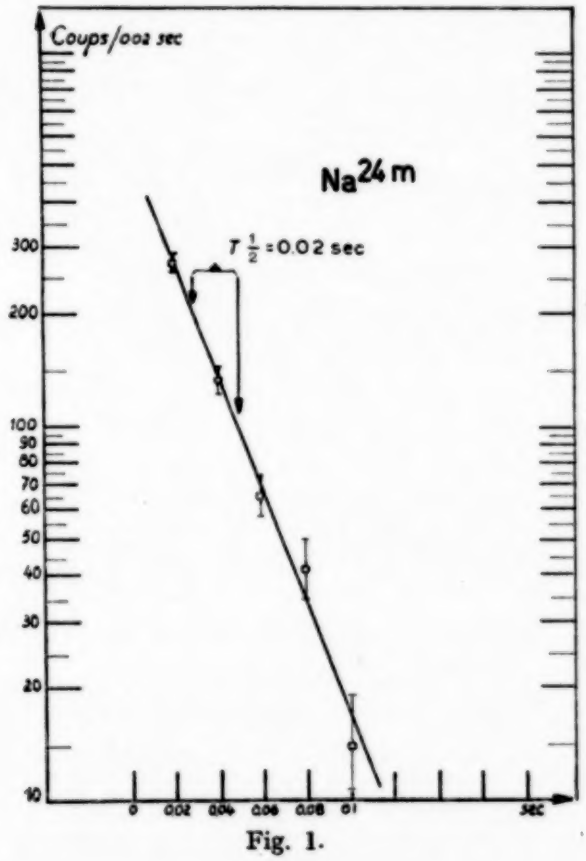

Fig. 1.

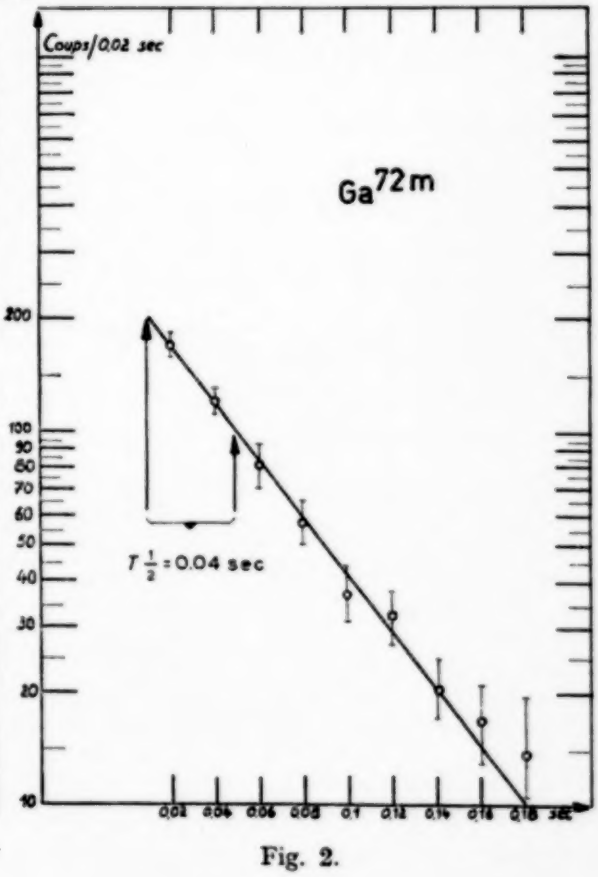

Fig. 2.

Signalons que le niveau isomérique de As^{75m} [6]) est encore visible avec notre appareil, ce qui indique que sa limite de sensibilité se situe aux environs de 15 msec.

Enfin nous n'apercevons pas l'isomère In^{114m}($T_{\frac{1}{2}} = 0.042 \pm 0.05$ sec, $E_\gamma = 311 \pm 5$ keV) signalé par R. B. Duffield et S. H. Vegors Jr. [7]) et mis en évidence par la réaction $In^{115}(\gamma, n)^{114m}$. Cet isomère a été également vu par la réaction Cd(p, n)In^{m} [8]). Duffield et Vegors basent leur interprétation isotopique sur des considérations d'intensité. La non-apparition de cet isomère par réaction (n, γ) d'une part, et l'existence d'un autre état isomérique dans In^{114} mis en évidence par isotopes séparés d'autre part, laisse supposer que l'isomère de 0.042 sec est dû plutôt à la réaction $In^{113}(\gamma, n)In^{112m}$ [9]).

L'étude détaillée de ces niveaux se poursuit au moyen d'un analyseur rapide de hauteurs d'impulsion à 20 chenaux, type Baird Atomic Model 520.

En présentant ce travail, nous remercions MM. J. Goens et M. Nève de Mévergnies pour l'intérêt constant qu'ils ont témoigné envers cette étude, ainsi que M. M. Demeur, pour les discussions fructueuses que nous avons pu avoir avec lui.

Bibliographie

1) J. Delhove et E. Gourski, Colloque International sur l'Électronique Nucléaire, Paris (16—20 sept. 1958), session 8.2
2) F. F. Felber, F. S. Stephens Jr. et Frank Asaro, J. Inorg. Nucl. Chem. **7** (1958) 153
3) B. J. Dropesky et A. W. Schardt, Phys. Rev. **102** (1956) 426
4) A. W. Schardt et A. Goodman, Bull. Am. Phys. Soc. **4** (1959) 56
5) E. der Mateosian and M. Goldhaber, Phys. Rev. **76** (1949) 187
6) A. W. Schardt, Phys. Rev. **108** (1957) 398
7) R. B. Duffield and S. H. Vegors, Phys. Rev. **112** (1958) 1558
8) O. I. Leipunsky, A. M. Morozov, Iu V. Makarov and P. A. Iampolsky, JETP **32** (1957) 339; Sov. Phys. JETP **5** (1957) 305
9) K. Way and G. L. McGinnis, communication privée

1.E.4:
2.L:3.A

Nuclear Physics **13** (1959) 95—103; © *North-Holland Publishing Co., Amsterdam*
Not to be reproduced by photoprint or microfilm without written permission from the publisher

MEAN LIFE OF THE FIRST EXCITED STATE OF Na^{23}

V. K. RASMUSSEN, F. R. METZGER and C. P. SWANN

Bartol Research Foundation of the Franklin Institute, Swarthmore, Pennsylvania †

Received 1 June 1959

Abstract: The nuclear resonant scattering by sodium of the 440 keV γ-radiation from Na^{23}(p, p′) has been investigated. From the self-absorption of the resonance radiation the mean life of the first excited state of Na^{23} is found to be $(1.8^{+0.4}_{-0.3}) \times 10^{-12}$ sec. The E2 partial life of this level has previously been measured by Coulomb excitation, and the E2/M1 amplitude ratio δ is then 0.056. The theoretical ratio of 151° to 115° nuclear resonant scattering is either 1.06 or 1.20, depending on whether δ is positive or negative. The experimental ratio is 1.10 ± 0.04 suggesting that δ is positive.

1. Introduction

Previous measurements of the mean life of the 440-keV level of Na^{23} have given an upper limit of 2.5×10^{-11} sec [1]), and a range of 10^{-13}—10^{-12} sec [2]). This level is strongly excited in the Na^{23} (p, p′) reaction, so that its mean life should be measurable by the nuclear resonance fluorescence techniques previously described [3, 4, 5, 6]). For lifetimes appreciably longer than 10^{-13} sec the use of solid targets (experimentally the simplest procedure with sodium) involves the complication that the excited nuclei lose a large part of the recoil velocity imparted to them in the charged-particle reaction before they decay. The original velocity gives a Doppler broadening of the γ-radiation that is large compared to that necessary to compensate for nuclear recoil in γ-ray emission and absorption, (and very large compared to the γ-ray width of the nuclear level). A reduction of the broadening, down to the point where it just compensates for nuclear recoil in γ-emission and absorption is then advantageous from an experimental point of view because the number of γ-rays of the correct energy for resonant scattering is increased. The mean life (or scattering cross-section) is, however, then obtainable only from a self-absorption measurement since it is not feasible to calculate or measure (in an independent experiment) the velocity loss of the recoil nuclei with the required accuracy and detail.

The partial lifetime for electric quadrupole excitation of this level, as found by Coulomb excitation measurements, is 5.6×10^{-10} sec [7]) and the spin of the excited state is given as $\frac{5}{2}$ [8, 9, 10]). A mixed M1—E2 transition is

† Assisted by the joint program of the U.S. Office of Naval Research and the Atomic Energy commission.

therefore indicated. For this spin and range of mixing ratios it is found that the angular distribution of the resonance radiation will depend appreciably on whether the M1 and E2 amplitudes have the same or opposite signs, so that the sign might be experimentally determinable.

2. Experimental Method and Details

The experimental procedures were similar to those used in previous measurements [3, 4, 5, 6]), and only details of special importance will be mentioned here.

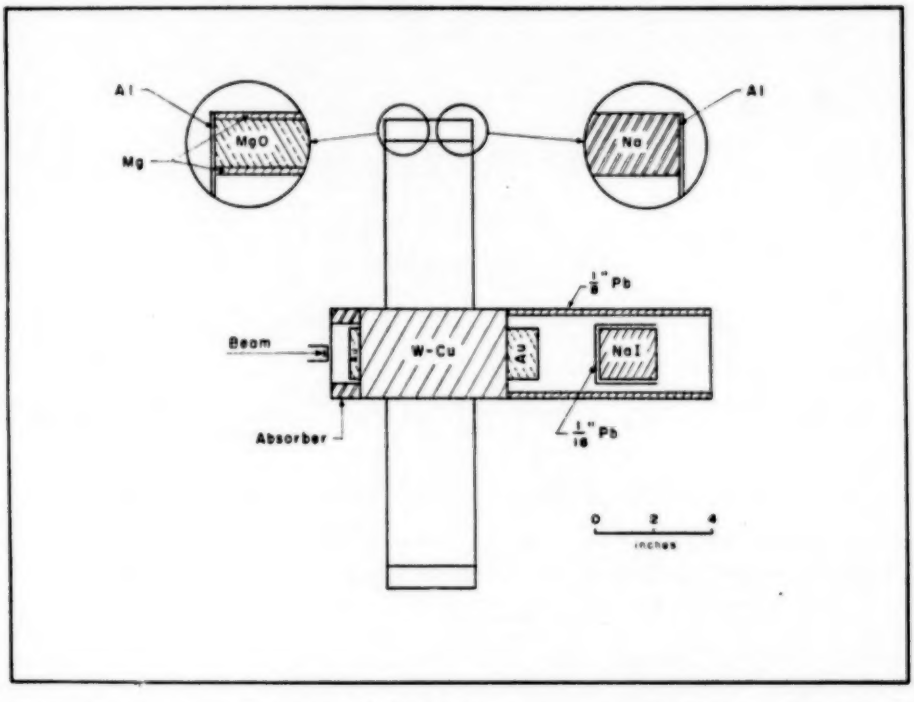

Fig. 1. Ring geometry used in the self-absorption measurement. The inserts show details of construction of the sodium and magnesium scatterers.

At the proton energy used, 2.78 MeV, a thick sodium metal target gives of the order of 10^8 440-keV photons per microcoulomb. For the self-absorption measurements, it was necessary to limit the beam to 2.5 μA to avoid melting the sodium, and even then the targets deteriorated to the point where they had to be replaced after a few hours of bombardment. For the angular distribution measurements, an improved target assembly in which the sodium was melted, in vacuum, in a brass or steel cup which subsequently formed the end closure of the machine vacuum system, gave much longer target life at currents up to 4 μA.

An upper limit to the proton bombarding energy was set by the increasing relative yield of 1.63-MeV γ-rays from the $Na^{23}(p, \alpha)Ne^{20}$ reaction, which

interferred with detection of the resonance-scattered 440-keV radiation through the production of annihilation radiation and through Compton scattering at scattering angles smaller than 115°. To compensate for these effects, it was necessary to match the sodium scatterer and the comparison scatterer for both Compton scattering and pair production, i.e., for both Z and Z^2.

The experimental arrangements used are shown in figs. 1 and 2. The sodium scatterers were made by pressing weighed chunks of the metal into $3'' \times 3'' \times \frac{3}{4}''$ or $3'' \times 1'' \times \frac{3}{4}''$ blocks, and bending the blocks to the required radius. These blocks were then taped to rings cut from 0.015" aluminium. To pre-

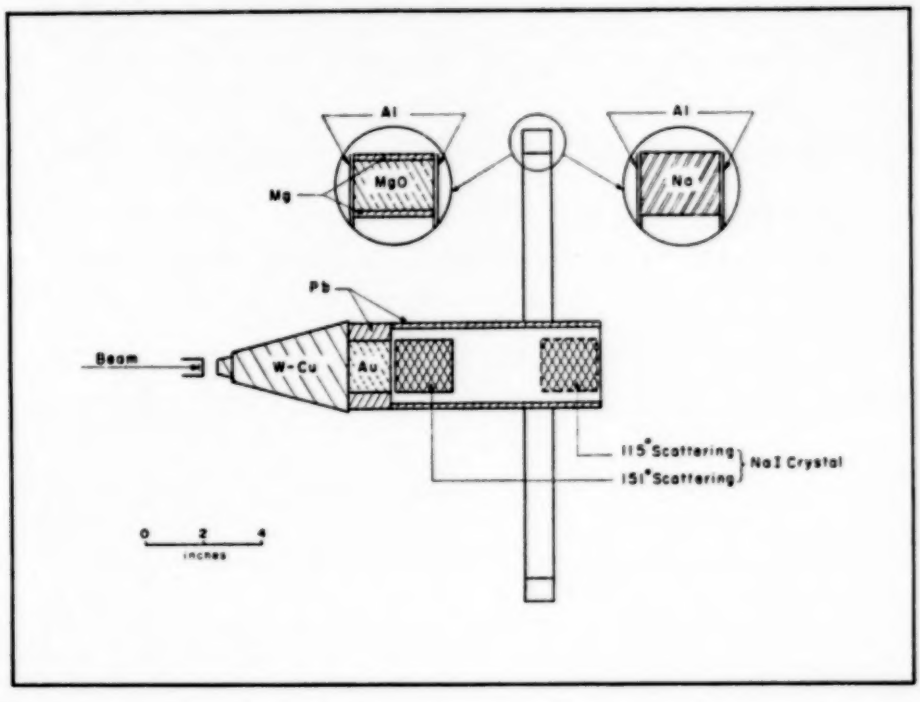

Fig. 2. Ring geometry used in the angular distribution measurement. The inserts show details of construction of the sodium and magnesium scatterers. The two alternate positions of the NaI counter are shown.

serve the sodium, it was found to be sufficient to dip it in hot ceresin wax and then wrap it in 0.0005" Saran foil †. Althoug a spotty white oxide deposit appeared on the surface of the sodium fairly soon, no change in weight was observed after several months. The Mg—MgO scatterers were made by filling a ring-shaped container, with inner and outer walls of 0.079" Mg and top and bottom of 0.015" Al with the proper weight of MgO. It will be noted that although the gross matching is exact, in the sense that a photon passing radially through the scatterer will have equal probabilities for pair production or Compton scattering for Na and for the Mg—MgO mixture used, it is

† A proprietary plastic foil produced by the Dow Chemical Co., Midland, Michigan, U.S.A.

only approximate when the weighting of various parts of the scatterer by geometric factors is considered. When the matching of these scatterers for effects of the 1.6 MeV radiation was checked by using the $Ne^{20}(p, p')$ reaction with neon gas being contained in a cell, as in ref. [4]), small changes in the amount of MgO were found to be required. Matching for effects of 400-keV γ-radiation other than resonant scattering was checked with a 20mC Au^{198} source.

The Na absorber and the comparison Mg—MgO absorber were made in essentially the same way as the scatterers.

The relative sensitivity of the NaI counter assembly for photons scattered from different parts of the scatterer was measured using the 440 keV γ-ray from Tl^{202}.

3. Results

3.1. SELF-ABSORPTION MEASUREMENT

The various spectra obtained with the 3" long scatterer are shown in fig. 3. The difference in the shape of the Compton edge with the $Ne^{20}+p$ γ-ray

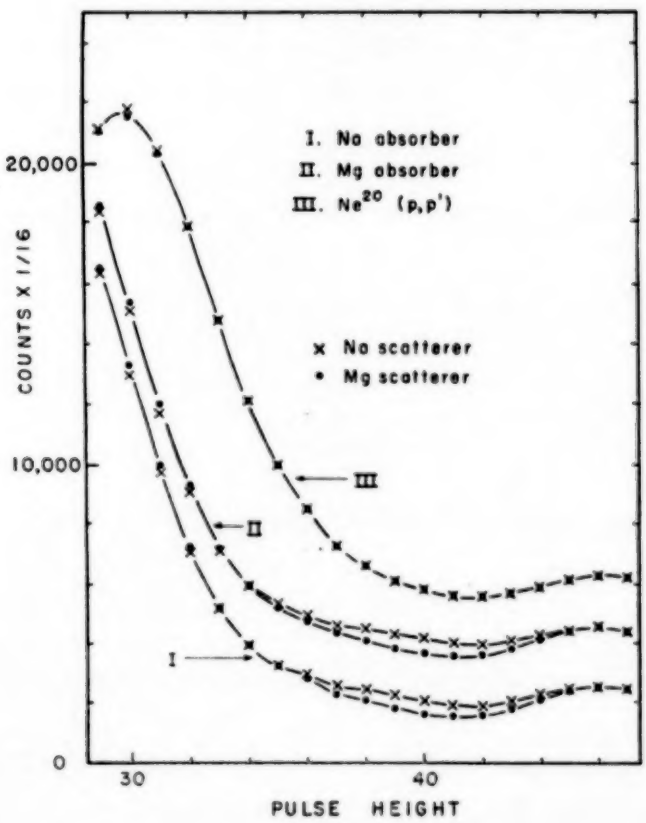

Fig. 3. Pulse-height spectra obtained in the self-absorption measurement. Pulse height 40 corresponds approximately to an energy of 440 keV. The pair of curves labelled "II" has been shifted up by 2000 counts, and the pair labelled "III" by 4000 counts, for clarity.

source and the Na^{23}+p source results from the difference in the geometry — for the gas target, the γ-rays come from a line source 1″ long, but the sodium target gives almost a point source. Some difference in the amount of annihilation radiation is also indicated and is not unexpected, for the same reason.

The corresponding Na minus Mg—MgO difference curves are shown in fig. 4 where the shape of the solid curve is that observed for the 440 keV γ-ray from Tl^{202}. The sum of the counts from pulse height 38 to 42 was taken as representing the resonance scattering effect. The negative effect in the region of the Compton edge is attributed to small, and probably systematic rather than random, errors in placement of the scatterers, and the resultant shift of the Compton edge. This was verified by shifting the Mg—MgO scatterer 0.12 in. toward the target which gave a counting rate change in the lower channels $\approx$ 10 times the negative effect of fig. 4, but reassuringly, no appreciable change for the resonance region, i.e., pulse height 38 to 42.

A further source of error in the energy region just below 440 keV may be ruled out. It is based on the observation that Mg^{25} has levels at 1.61, 0.98, and 0.58 MeV [11]). The nominally 1.63-MeV γ's from Ne^{20} may be Doppler-shifted enough in the Na^{23}(p, α) reaction to overlap the Mg^{25} level, but not enough in the Ne^{20}(p, p′) reaction to overlap. If the resonance-excited Mg^{25} level then decayed partially by cascade through the 0.98 and 0.58 MeV levels, the Mg scatterer would show a peak at 0.4 MeV for the Na^{23}(p, α) source, but not for the Ne^{20}(p, p′) source. This possibility is rejected by noting that this Mg^{25} level decays predominantly ($> 96\,\%$) to the ground state [11]) while a rough check at 1.6 MeV γ-energy with the Na^{23}(p, α) reaction showed no difference between the scattering by Mg and by Na, with errors small enough to rule out any contribution at 400 keV.

In order to calculate the lifetime from the self-absorption data, one must know the relative number of photons of resonance energy arriving at various sections of the scatterer. This was measured using the geometry of fig. 1 and the 1″ scatterers shown in fig. 2 in three positions covering the indicated position of the 3-inch scatterer and the two contiguous positions. Within the statistical errors of $\approx 10\,\%$, the intensity of the resonance scattering at the various positions was consistent with isotropy of the radiation of resonant energy, as would be expected from the large slowing-down noted below, and exact isotropy was assumed in further calculations.

The data of fig. 4 corresponds to a resonance transmission of ($82 \pm 2.5\,\%$) by the sodium absorber and a ratio of $\Gamma/\Delta = 5.3 \times 10^{-4}$. A Debye temperature for sodium of 150° K [12]) gives an effective temperature of 305° K [13]) and a thermal width of $\Delta = 0.689$ eV. Then $\Gamma = 3.65 \times 10^{-4}$ eV and the mean life $\tau = (1.8^{+0.4}_{-0.3}) \times 10^{-12}$ sec., where the error given is predominantly statistical in origin. The statistical weight factor used was for the spin sequence $\frac{3}{2} - \frac{5}{2} - \frac{3}{2}$.

Comparison of this result with the apparent scattering cross-section, as obtained from the number of resonant-scattered photons, shows that there is an effective slowing down by a factor of 6.5, i.e., the Doppler broad-

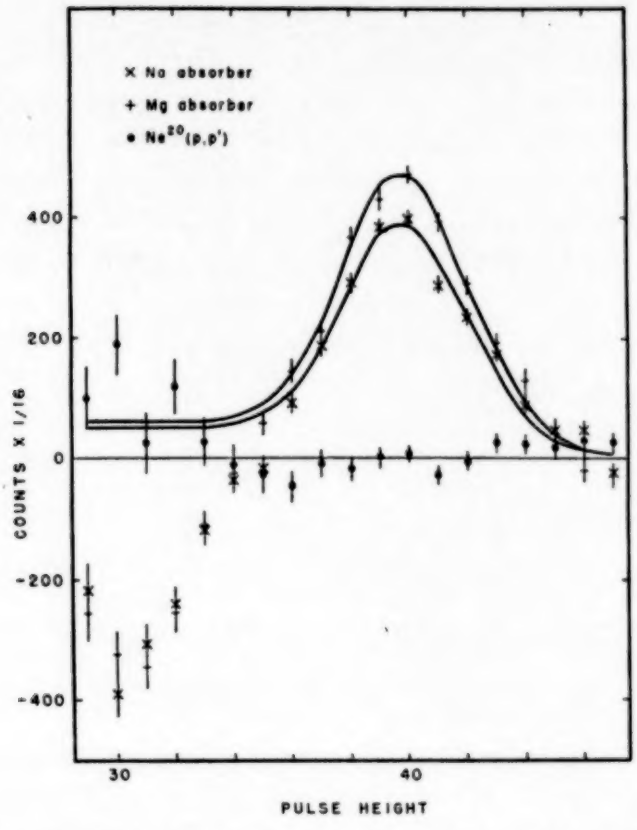

Fig. 4. Sodium scatterer-magnesium scatterer differences from the data shown in fig. 3. The shape of the solid curves is that observed with the 440-keV γ-ray from Tl^{202} adjusted slightly in pulse height to match the experimental points (it is *not* to be inferred that a precise comparison of the energies of these two γ-rays has been obtained). The negative differences at lower pulse heights result from small errors in the placement of the scatterers, as explained in the text. The sum of counts from pulse height 38 to 42 is taken to be proportional to the resonance effect.

ening of the radiation from $Na^{23}(p, p')$ is only 400 eV instead of the 2600 eV expected from the initial recoil velocities.

3.2. ANGULAR DISTRIBUTION

The arrangement used for the angular distribution measurement is shown in fig. 2. The smallest practical scattering angle is set by effects of the Compton-scattered 1.6 MeV radiation at about 115°, and the largest is set by intensity considerations at about 150°. One of the two sets of data obtained is shown in fig. 5. After correction for geometric factors, etc., one obtains an experimental intensity ratio for 151° scattering to 115° scattering of 1.10 ± 0.04.

From our mean life for this level and from the Coulomb excitation results,

the ratio δ^2 of the E2 partial width to the M1 partial width is $\frac{1}{320}$. Errors are not given for the Coulomb excitation work, but are presumably at least as large as in the present case, so that the error in the ratio is perhaps 30 %

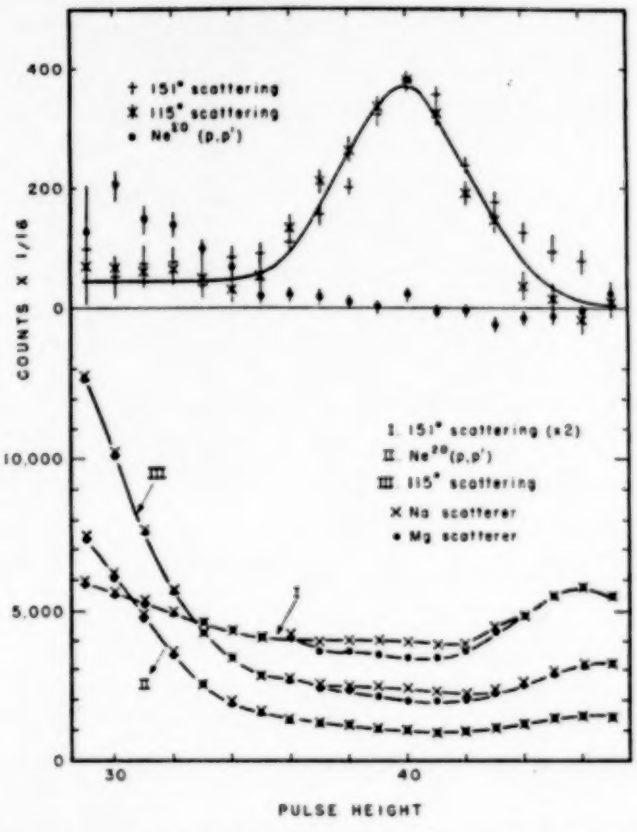

Fig. 5. Pulse height spectra and Na—Mg differences from the angular distribution measurement The 115° and 151° scattering data in the difference curve have been normalized to give the same sums for pulse height 38 to 42.

or larger. Writing the angular correlation for resonance scattering as

$$1+A_2P_2(\cos\theta)+A_4P_4(\cos\theta)$$

and taking the spin sequence as $\frac{3}{2}—\frac{5}{2}—\frac{3}{2}$, one finds $A_4 \approx 0$ and either $A_2{}^+ = 0.070^{-0.009}_{+0.010}$ or $A_2{}^- = 0.229^{+0.013}_{-0.016}$, where the superscripts indicate, in the notation of Biedenhorn and Rose[14]), whether the ratio of the amplitudes is positive or negative. After a small correction for the finite angular resolution, the predicted ratio of the 151° scattered intensity to the 115° intensity is found to be either 1.06 ± 0.005 or $1.20^{+0.012}_{-0.014}$. The experimental ratio is seen to indicate that the E2 and M1 amplitudes have the same sign (positive ratio), although the possibility of their having opposite signs is not ruled out. It may be noted that doubling the error in δ^2 roughly doubles the error in A_2.

Although the spin of the 440-keV level of Na^{23} seems to be established as $\frac{5}{2}$, our measured angular correlation is also consistent with $\frac{3}{2}$. For this case,

our mean life would be 1.2×10^{-12} sec and the angular correlation coefficients would be $A_2^+ = 0.21$ and $A_2^- = 0.11$.

4. Discussion

Paul and Montague [15]) have used the unified model to calculate the properties of the Na^{23} nucleus. What they refer to as a "first trial" fit gives τ(M1) for the 440-keV level as 4×10^{-13} sec, which is not too far from the experimental value of 18×10^{-13} sec. The single-particle Weisskopf formula[16]) also predicts 4×10^{-13} sec, taking $r_0 = 1.4\times10^{-13}$ cm, and ignoring the statistical weight factor. It is not expected that there will be any difficulty in reconciling theory and experiment for this particular transition.

Note added in proof: Since this paper was submitted, results of another measurement by resonance fluorescence of the lifetime of the first excited state of Na^{23} have been published by Booth *et al.*[17]). Their value of $(1.5\pm0.3)\times10^{-10}$ sec is in disagreement with the work of refs.[1]) and [2]) and, considering the value of the E2/M1 mixing ratio they give, with the Coulomb excitation results of ref.[8]), as well as with the present work.

Booth *et al.* used the Na^{23} γ-ray as excited in the decay of Ne^{23}. Aside from the unattractive proposal that two close levels of Na^{23}, one excited in β-decay and the other in the (p, p') reaction, are involved, two aspects of their experiment may be questioned. First, it is assumed, and is essential to their result, that the Ne^{23} is in the gaseous state so that it is free to recoil from the β-decay without hindrance or collision during the γ-lifetime. But they apparently did not use any carrier gas, and the amount of Ne^{23} involved is so exceedingly small that one should certainly determine what fraction of it is adsorbed on the walls of the container. Second, they apparently did not make a correction for self-absorption of the resonance radiation. Our measured value of 18 % absorption for an average path length of about 1.5 cm of Na implies that for their 5 cm scatterers the correction would be large.

We may also remark that for a 10^{-10} sec lifetime we would observe no resonance scattering, especially with our solid targets.

References

1) C. P. Swann and W. C. Porter, Bull. Am. Phys. Soc. **1** (1956) 29
2) R. W. Krone, A. Everett and S. S. Hanna, Bull. Am. Phys. Soc. **1** (1956) 329
3) C. P. Swann and F. R. Metzger, Phys. Rev. **108** (1957) 982
4) V. K. Rasmussen, F. R. Metzger and C. P. Swann, Phys. Rev. **110** (1958) 154
5) F. R. Metzger, C. P. Swann and V. K. Rasmussen, Phys. Rev. **110** (1958) 906
6) C. P. Swann, V. K. Rasmussen and F. R. Metzger, Phys. Rev. **114** (1959) 862
7) K. Alder, A. Bohr, T. Huus, B. Mottelson and A. Winther, Revs. Mod. Phys. **28** (1956) 432

8) G. M. Temmer and N. P. Heydenburg, Phys. Rev. **104** (1956) 989
9) W. G. Read and R. W. Krone, Phys. Rev. **104** (1956) 1018
10) R. Berenbaum, J. H. Towle and J. H. Matthews, Proc. Phys. Soc. A **69** (1956) 858
11) P. M. Endt and C. M. Braams, Revs. Mod. Phys. **29** (1957) 683
12) Jules deLaunay in Solid State Physics, edited by F. Seitz and D. Turnbull (Academic Press, Inc., New York, 1956) Vol. 2
13) W. E. Lamb, Phys. Rev. **55** (1939) 190
14) L. C. Biedenhorn and M. E. Rose, Revs. Mod. Phys. **25** (1953) 729
15) E. B. Paul and J. H. Montague, Nuclear Physics **5** (1958) 61
16) J. M. Blatt and V. F. Weisskopf, Theoretical Nuclear Physics, (John Wiley and Sons, New York, 1952) p. 627
17) Booth, Hutchinson, Segar, Shute and White, Nuclear Physics **11** (1959) 341

1.D.1. *Nuclear Physics* **13** (1959) 104—116; © *North-Holland Publishing Co., Amsterdam*
Not to be reproduced by photoprint or microfilm without written permission from the publisher

TRANSFORMATION BRACKETS FOR HARMONIC OSCILLATOR FUNCTIONS

MARCOS MOSHINSKY

Instituto de Física, Universidad de México, e Instituto Nacional de la Investigación Científica, México D.F., †

Received 23 May 1959

Abstract: We define the transformation brackets connecting the wave functions for two particles in an harmonic oscillator common potential with the wave functions given in terms of the relative and centre of mass coordinates of the two particles. With the help of these brackets we show that all matrix elements for the interaction potentials in nuclear shell theory can be given directly in terms of Talmi integrals. We obtain recurrence relations and explicit algebraic expressions for the transformation brackets that will permit their numerical evaluation.

1. Introduction

The increased importance acquired by the nuclear shell model [1]) in the past decade, has served as a spur to develop mathematical methods that would simplify the evaluation of the matrix elements involved in this model. It is well known [1]) that all matrix elements for the interaction forces can be reduced to two particle interaction matrix elements [1]), and that these, in turn, can be evaluated in terms of Slater coefficients by the standard methods of atomic spectroscopy. The evaluation of the Slater coefficients in nuclear shell theory is more troublesome than in atomic spectroscopy, as there are more types of forces and these are not yet very well defined. It was shown by Talmi [2]) that when the common potential of the nucleons is of the harmonic oscillator type, the evaluation of the Slater coefficients simplifies considerably. The method of Talmi supplemented by Thieberger's [3]) tables, as well as by other more recent developments [4]), is widely used in nuclear shell theory calculations.

In the Talmi method [2]) one could say that the evaluation of the matrix elements is given in two steps: a) The matrix element is reduced to Slater coefficients by means of the standard methods of Racah [5]) and b) the Slater coefficients are evaluated assuming an harmonic oscillator common potential, taking advantage of the relations between the wave functions for two

† This paper was initiated during a short stay of the author at Princeton University as an Alfred P. Sloan Research Fellow. The author wishes to express his thanks to these institutions.

nucleons in this potential, with the wave functions associated with the relative and centre of mass coordinates for the same two nucleons.

In the present paper we show that by introducing a transformation bracket connecting the two nucleon wave function to the relative and centre of mass wave function, the two nucleon matrix elements are given directly in terms of Talmi radial integrals, without the intermediate step of the Slater coefficients. Furthermore, we indicate how the transformation brackets, in combination with fractional parentage coefficients, reduce any matrix element in nuclear shell theory to Talmi integrals. Finally, we give recurrence relations and explicit expressions for the transformation brackets, which will permit their numerical evaluation.

We start by introducing the hamiltonian for two nucleons in a harmonic oscillator potential of frequency ω as

$$H = \tfrac{1}{2}(p_1^2/m)+\tfrac{1}{2}m\omega^2 r_1^2+\tfrac{1}{2}(p_2^2/m)+\tfrac{1}{2}m\omega^2 r_2^2 \tag{1}$$

where $\mathbf{r}_1$, $\mathbf{r}_2$ and $\mathbf{p}_1$, $\mathbf{p}_2$ are the coordinates and momenta of the two nucleons and m their mass. We now introduce the relative coordinate $\mathbf{r}$ and the centre of mass coordinate $\mathbf{R}$ by the definitions

$$\mathbf{r} = \frac{1}{\sqrt{2}}(\mathbf{r}_1-\mathbf{r}_2), \quad \mathbf{R} = \frac{1}{\sqrt{2}}(\mathbf{r}_1+\mathbf{r}_2). \tag{2}$$

These definitions will have the advantage over the customary ones [2,3] that the harmonic oscillator functions will have the same form for all the coordinates involved. The corresponding momenta are

$$\mathbf{p} = \frac{1}{\sqrt{2}}(\mathbf{p}_1-\mathbf{p}_2), \quad \mathbf{P} = \frac{1}{\sqrt{2}}(\mathbf{p}_1+\mathbf{p}_2), \tag{3}$$

so that the hamiltonian can also be written as

$$H = \tfrac{1}{2}(p^2/m)+\tfrac{1}{2}m\omega^2 r^2+\tfrac{1}{2}(P^2/m)+\tfrac{1}{2}m\omega^2 R^2. \tag{4}$$

The angular momenta associated with the different coordinates will be designated by $\mathbf{l}_1$, $\mathbf{l}_2$, $\mathbf{l}$, $\mathbf{L}$ and from (2) and (3) we see that

$$\mathbf{l}_1+\mathbf{l}_2 = \mathbf{l}+\mathbf{L} = \boldsymbol{\lambda}, \tag{5}$$

where $\boldsymbol{\lambda}$ stands for the vector representing the total angular momentum of the two particles.

The wave function for a single harmonic oscillator will be given by

$$\mathscr{R}_{nl}(r)Y_{lm}(\theta, \varphi) \tag{6}$$

where Y_{lm} are spherical harmonics and $\mathscr{R}_{nl}(r)$ the radial functions. In what follows we shall always assume that r is given in units of

$$(\hbar/m\omega)^{\frac{1}{2}}, \tag{7}$$

so that the radial function takes the form

$$\mathscr{R}_{nl}(r) = [2(n!)/\Gamma(n+l+\tfrac{3}{2})]^{\frac{1}{2}} r^l \exp(-\tfrac{1}{2}r^2) L_n^{l+\frac{1}{2}}(r^2), \tag{8}$$

where $L_n^{l+\frac{1}{2}}$ is a Laguerre polynomial as defined in Magnus and Oberhettinger's book [6]), and Γ is a gamma function. The energy associated with this wave function in units of $\hbar\omega$ is

$$E_{nl} = 2n+l+\tfrac{3}{2}. \tag{9}$$

As $\boldsymbol{\lambda}$ commutes with the hamiltonian, we can construct eigenfunctions of H, λ^2, λ_z starting either from (1) or (4), to obtain the eigenkets

$$|n_1l_1, n_2l_2, \lambda\mu\rangle = \sum_{m_1m_2} \langle l_1l_2m_1m_2|\lambda\mu\rangle \mathscr{R}_{n_1l_1}(r_1)Y_{l_1m_1}(\theta_1, \varphi_1)\mathscr{R}_{n_2l_2}(r_2)Y_{l_2m_2}(\theta_2, \varphi_2), \tag{10}$$

$$|nl, NL, \lambda\mu\rangle = \sum_{mM} \langle lLmM|\lambda\mu\rangle \mathscr{R}_{nl}(r)Y_{lm}(\theta, \varphi)\mathscr{R}_{NL}(R)Y_{LM}(\Theta, \Phi), \tag{11}$$

where $\langle l_1l_2m_1m_2|\lambda\mu\rangle$, etc., are Clebsch-Gordan coefficients.

The brackets we are interested in are those connecting (10) and (11), i.e.

$$|n_1l_1, n_2l_2, \lambda\mu\rangle = \sum_{nlNL} |nl, NL, \lambda\mu\rangle\langle nl, NL, \lambda|n_1l_1, n_2l_2, \lambda\rangle. \tag{12}$$

As is well known [5]), the bracket in (12) is independent of the magnetic quantum number μ, and this parameter was therefore not included in the bracket. Because of conservation of energy the bracket will only be different from zero if the following relation is satisfied:

$$2n_1+l_1+2n_2+l_2 = 2n+l+2N+L. \tag{13}$$

As all the parameters in (13) are non-negative integers, it is clear that the summation involved in (12) is a finite one. The condition (13) guarantees also the conservation of parity in the wave function as

$$(-1)^{l_1+l_2} = (-1)^{l+L}. \tag{14}$$

In the next section we shall show how the brackets defined in (12) can be used to determine the matrix elements for different types of nuclear forces.

2. Matrix Elements for Nuclear Forces

2.1. CENTRAL FORCES

Let us consider first a central interaction $V(r)$ between the two nucleons. Using (12) we see that a general matrix element could be written as

$$\langle n_1l_1, n_2l_2, \lambda\mu|V(r)|n'_1l'_1, n'_2l'_2, \lambda'\mu'\rangle = \sum_{nlNL} \sum_{n'l'N'L'} \{\langle n_1l_1, n_2l_2, \lambda|nl, NL, \lambda\rangle\langle n'l', N'L', \lambda'|n'_1l'_1, n'_2l'_2, \lambda'\rangle \langle nl, NL, \lambda\mu|V(r)|n'l', N'L', \lambda'\mu'\rangle\}. \tag{15}$$

But as $V(r)$ depends only on the magnitude of the relative coordinates, we have

$$\langle nl, NL, \lambda\mu|V(r)|n'l', N'L', \lambda'\mu'\rangle = \langle nl||V(r)||n'l'\rangle\, \delta_{ll'}\delta_{NN'}\delta_{LL'}\delta_{\lambda\lambda'}\delta_{\mu\mu'}, \tag{16}$$

where

$$\langle nl||V(r)||n'l'\rangle = \int_0^\infty \mathscr{R}_{nl}(r)V(r)\mathscr{R}_{n'l'}(r)r^2\mathrm{d}r. \tag{17}$$

From the relation (13) we also see that

$$n'-n = n'_1-n_1+n'_2-n_2+\tfrac{1}{2}(l'_1+l'_2-l_1-l_2) \tag{18}$$

where, because of parity considerations, the term in the parenthesis of (18) must be even.

Substituting (16) in (15) we obtain

$$\begin{aligned}\langle n_1l_1, n_2l_2, \lambda\mu|V(r)|n'_1l'_1, n'_2l'_2, \lambda\mu\rangle \\ = \sum_{nlNL}\{\langle nl, NL, \lambda|n_1l_1, n_2l_2, \lambda\rangle\langle n'l, NL, \lambda|n'_1l'_1, n'_2l'_2, \lambda\rangle \\ \langle nl||V(r)||n'l\rangle\}\end{aligned} \tag{19}$$

where n' and n are related by (18), and we have used the fact that the brackets are real, as shown in the following sections, to invert the order in the first bracket.

Using the explicit expressions [6]) for the Laguerre polynomials, the matrix elements (17) can be given in terms of the Talmi integrals

$$I_p = [2/\Gamma(p+\tfrac{3}{2})]\int_0^\infty r^{2p}\exp(-r^2)V(r)r^2\mathrm{d}r. \tag{20}$$

It is clear, therefore, that a matrix element for central forces could be directly determined in terms of Talmi integrals provided that the transformation brackets involved in (19) were available.

2.2. SPIN-ORBIT COUPLING FORCES

For forces of the type

$$V_{ls} = V(r)\mathbf{l}\cdot\mathbf{S} \tag{21a}$$

where

$$\mathbf{l} = \mathbf{r}\times\mathbf{p}, \quad \mathbf{S} = \tfrac{1}{2}(\boldsymbol{\sigma}_1+\boldsymbol{\sigma}_2), \tag{21b}$$

the matrix elements in LS coupling can be easily obtained [7]) once

$$\langle n_1l_1, n_2l_2, \lambda||V(r)\mathbf{l}||n'_1l'_1, n'_2l'_2, \lambda'\rangle, \tag{22}$$

is known. Using (12), we see that to determine (22) we need the matrix element

$$\begin{aligned}\langle nl, NL, \lambda||V(r)\mathbf{l}||n'l', NL, \lambda'\rangle \\ = (-1)^{L+1-l'-\lambda}\langle nl||V(r)\mathbf{l}||n'l'\rangle[(2\lambda+1)(2\lambda'+1)]^{\frac{1}{2}}W(ll'\lambda\lambda'; 1L),\end{aligned} \tag{23}$$

where W stands for a Racah coefficient, and the right hand side of (23) is due to the fact that $V(r)\mathbf{l}$ is a Racah tensor [5]) of order one depending only on the relative coordinate. It is also well known [5]) that

$$\langle nl||V(r)\mathbf{l}||n'l'\rangle = \delta_{ll'}\langle nl||V(r)||n'l'\rangle[l(l+1)(2l+1)]^{\frac{1}{2}}, \tag{24}$$

where $\langle nl||V(r)||n'l'\rangle$ is given by (17). Collecting terms we see that the

matrix element (22) becomes

$$\langle n_1 l_1, n_2 l_2, \lambda || V(r)\mathbf{1} || n'_1 l'_1, n'_2 l'_2, \lambda' \rangle$$
$$= \sum_{nlNL} \{\langle nl, NL, \lambda | n_1 l_1, n_2 l_2, \lambda \rangle \langle n' l, NL, \lambda' | n'_1 l'_1, n'_2 l'_2, \lambda' \rangle \quad (25)$$
$$\langle nl || V(r) || n' l \rangle [l(l+1)(2l+1)(2\lambda+1)(2\lambda'+1)]^{\frac{1}{2}} (-1)^{L+1-l-\lambda} W(ll\lambda\lambda'; 1L)\},$$

where the relation between n' and n is again given by (18).

2.3. TENSOR FORCES

The tensor forces can be written in the form [7])

$$V_T = V(r)(\tfrac{32}{5}\pi)^{\frac{1}{2}} \mathbf{Y}_2 \cdot \mathbf{X}_2, \quad (26a)$$

where $\mathbf{Y}_2$ represents a Racah tensor whose components are the spherical harmonics $Y_{2m}(\theta, \varphi)$, and the $m = 0$ components of the Racah tensor $\mathbf{X}_2$ is

$$X_{20} = \frac{1}{\sqrt{2}} (3S_z^2 - S^2), \quad (26b)$$

with $\mathbf{S}$ given by (21b).

The matrix elements in LS coupling for tensor forces can be easily obtained[7]) once

$$\langle n_1 l_1, n_2 l_2, \lambda || V(r) \mathbf{Y}_2(\theta, \varphi) || n'_1 l'_1, n'_2 l'_2, \lambda' \rangle \quad (27)$$

is known.

Using (12), we see that to determine (27) we need the matrix element [5])

$$\langle nl, NL, \lambda || V(r) \mathbf{Y}_2(\theta, \varphi) || n' l', NL, \lambda' \rangle$$
$$= (-1)^{L+2-l'-\lambda} \langle nl || V(r) \mathbf{Y}_2(\theta, \varphi) || n' l' \rangle [(2\lambda+1)(2\lambda'+1)]^{\frac{1}{2}} W(ll'\lambda\lambda'; 2L) \quad (28)$$

where in turn [5])

$$\langle nl || V(r) \mathbf{Y}_2(\theta, \varphi) || n' l' \rangle = \langle nl || V(r) || n' l' \rangle [5(2l+1)/4\pi]^{\frac{1}{2}} \langle l200 | l'0 \rangle. \quad (29)$$

Collecting terms, we find that the matrix element (27) becomes

$$\langle n_1 l_1, n_2 l_2, \lambda || V(r) \mathbf{Y}_2(\theta, \varphi) || n'_1 l'_1, n'_2 l'_2, \lambda' \rangle$$
$$= \sum_{nlNL} \sum_{n'l'} \{\langle nl, NL, \lambda | n_1 l_1, n_2 l_2, \lambda \rangle \langle n' l', NL, \lambda' | n'_1 l'_1, n'_2 l'_2, \lambda' \rangle \quad (30)$$
$$\langle nl || V(r) || n' l' \rangle (-1)^{L-\lambda-l'} [(2\lambda+1)(2\lambda'+1)(2l+1)(\tfrac{5}{4}\pi)]^{\frac{1}{2}} \langle l200 | l'0 \rangle$$
$$W(ll'\lambda\lambda'; 2L)\},$$

where l' is restricted to

$$l' = l \pm 2, l, \quad (31a)$$

and n' is given by the relation

$$n' = n + (n'_1 + n'_2 - n_1 - n_2) + \tfrac{1}{2}(l'_1 + l'_2 - l_1 - l_2) + \tfrac{1}{2}(l - l'). \quad (31b)$$

2.4. j—j COUPLING

In the previous subsections we analyzed with the help of the transformation brackets the matrix elements for nuclear forces in LS coupling. To

illustrate the corresponding procedure in j—j coupling, we consider a diagonal matrix element for a central force, and from the relations between the wave functions in j—j coupling and LS coupling [8]), as well as from (19), we immediately obtain

$$\langle n_1 l_1 \tfrac{1}{2}, j_1; n_2 l_2 \tfrac{1}{2}, j_2; J|V(r)|n_1 l_1 \tfrac{1}{2}, j_1; n_2 l_2 \tfrac{1}{2}, j_2; J\rangle$$
$$= \sum_{\lambda S n l N L} \Bigg\{ (2\lambda+1)(2S+1)(2j_1+1)(2j_2+1) \left[\begin{Bmatrix} l_1 & \frac{1}{2} & j_1 \\ l_2 & \frac{1}{2} & j_2 \\ \lambda & S & J \end{Bmatrix} \right]^2 \quad (32)$$
$$[\langle nl, NL, \lambda | n_1 l_1, n_2 l_2, \lambda\rangle]^2 \langle nl||V(r)||nl\rangle \Bigg\},$$

where the curly bracket represents a $9j$ coefficient [8]), and the last factor is given by (17). Similar expressions will hold for other types of forces.

2.5. MATRIX ELEMENTS FOR MORE THAN TWO PARTICLES

Let us consider a system of p identical particles in the $n_1 l_1 j_1$ shell, and assume a central force interaction between them of the form

$$\sum_{i<j=1}^{p} V(r_{ij}). \quad (33)$$

Then, as is well known [9]), the diagonal matrix element for the interaction potential is given by

$$\langle (n_1 l_1 \tfrac{1}{2} j_1)^p \alpha J M | \sum_{i<j=1}^{p} V(r_{ij}) | (n_1 l_1 \tfrac{1}{2} j_1)^p \alpha J M\rangle$$
$$= \tfrac{1}{2} p(p-1) \sum_{\alpha'' J'' J'} \{ [\langle (j_1)^2 J', (j_1)^{p-2} \alpha'' J'', J | \} (j_1)^p \alpha J\rangle]^2 \quad (34)$$
$$\langle n_1 l_1 \tfrac{1}{2}, j_1; n_1 l_1 \tfrac{1}{2}, j_1; J'|V(r)|n_1 l_1 \tfrac{1}{2}, j_1; n_1 l_1 \tfrac{1}{2}, j_1; J'\rangle \},$$

where α, α'' are additional quantum numbers necessary to specify the states of p and $p-2$ particles respectively, and the first term in the right hand side of (34) is a fractional parentage coefficient in which J' is restricted to even values that satisfy the triangular relation $(J' J'' J)$. The matrix element on the right hand side of (34) is a particular case of (32) when $n_2 = n_1$ etc., so that the matrix elements for p particles in a shell are given directly in terms of Talmi integrals and of coefficients which are combinations of fractional parentage coefficients and transformations brackets.

In the previous subsections we have shown that if the transformation brackets

$$\langle nl, NL, \lambda | n_1 l_1, n_2 l_2, \lambda\rangle, \quad (35)$$

were available, the coefficients of the Talmi integrals in the explicit expressions for all types of matrix elements, could be tabulated in a direct

fashion. In the next sections we obtain recurrence relations and explicit expression for the brackets.

3. Recurrence Relations

It is well known [1,2]) that for the energy levels of interest in nuclear shell theory n_1, n_2 are restricted to the values n_1, $n_2 = 0, 1, 2, 3$. It seems therefore convenient to obtain recurrence relations for the brackets (35) in such a way that a bracket with arbitrary n_1, n_2 could be obtained from the bracket with $n_1 = n_2 = 0$. In this section we shall derive the recurrence relations, while in the next section we obtain the explicit expression for the bracket in which $n_1 = n_2 = 0$.

Let us consider the ket $|n_1+1l_1, n_2l_2, \lambda\mu\rangle$. From the recurrence relations for Laguerre polynomials [10])

$$L_{n+1}^{l+\frac{1}{2}}(r^2) = (n+1)^{-1}[(2n+l+\tfrac{3}{2})-r^2]L_n^{l+\frac{1}{2}}(r^2)-(n+1)^{-1}(n+l+\tfrac{1}{2})L_{n-1}^{l+\frac{1}{2}}(r^2), \quad (36)$$

and the form (8) of the radial function we obtain

$$|n_1+1l_1, n_2l_2, \lambda\mu\rangle = [(n_1+1)(n_1+l_1+\tfrac{3}{2})]^{-\frac{1}{2}}[(2n_1+l_1+\tfrac{3}{2})-r_1^2]|n_1l_1, n_2l_2, \lambda\mu\rangle - [n_1(n_1+l_1+\tfrac{1}{2})]^{\frac{1}{2}}[(n_1+1)(n_1+l_1+\tfrac{3}{2})]^{-\frac{1}{2}}|n_1-1l_1, n_2l_2, \lambda\mu\rangle. \quad (37)$$

If we multiply both sides of (37) by the bra $\langle nl, NL, \lambda\mu|$ we see that the left hand side of (37) will be zero unless

$$2n+l+2N+L = 2n_1+l_1+2n_2+l_2+2. \quad (38)$$

For bras that satisfy (38) the brackets on the right hand side of (37) will be zero, so we are left with

$$\begin{aligned}\langle nl, NL, \lambda|n_1+1l_1, n_2l_2, \lambda\rangle &= [(n_1+1)(n_1+l_1+\tfrac{3}{2})]^{-\frac{1}{2}}\langle nl, NL, \lambda\mu|-r_1^2|n_1l_1, n_2l_2, \lambda\mu\rangle \\ &= [(n_1+1)(n_1+l_1+\tfrac{3}{2})]^{-\frac{1}{2}}\sum_{n'l'N'L'}\{\langle nl, NL, \lambda\mu|-r_1^2|n'l', N'L', \lambda\mu\rangle \\ &\cdot \langle n'l', N'L', \lambda|n_1l_1, n_2l_2, \lambda\rangle\}.\end{aligned} \quad (39)$$

To evaluate the matrix element in (39), we recall that from (2)

$$r_1^2 = \tfrac{1}{2}(r^2+R^2+2\mathbf{R}\cdot\mathbf{r}). \quad (40)$$

Using the standard methods of Racah [5]) we give the matrix elements in table 1 for all the values of n', l', N', L', consistent with the energy conservation rule

$$2n+l+2N+L = 2n'+l'+2N'+L'+2, \quad (41)$$

and the selection rules in the radial integrals, where these integrals were evaluated using (36) and the recurrence relation for Laguerre polynomials [10])

$$r^2 L_n^{l+\frac{3}{2}}(r^2) = (n+l+\tfrac{3}{2})L_n^{l+\frac{1}{2}}(r^2) - (n+1)L_{n+1}^{l+\frac{1}{2}}(r^2). \tag{42}$$

If we had started with the ket $|n_1 l_1,\ n_2+1 l_2,\ \lambda\mu\rangle$ we would have got the same expression (39), only with the first factor changed to index 2 instead of index 1, and the matrix element of $-r_2^2$ instead that of $-r_1^2$. As

$$r_2^2 = \tfrac{1}{2}(r^2 + R^2 - 2\mathbf{R}\cdot\mathbf{r}) \tag{43}$$

the table for the matrix element of $-r_2^2$ would be the same table 1, but with the last four lines (that correspond to the matrix element of $\mathbf{R}\cdot\mathbf{r}$) with their signs changed.

TABLE 1

Matrix elements of $(-r_1^2)$

n'	l'	N'	L'	$\langle nl, NL, \lambda \vert -r_1^2 \vert n'l', N'L', \lambda\rangle$
$n-1$	l	N	L	$\tfrac{1}{2}[n(n+l+\tfrac{1}{2})]^{\frac{1}{2}}$
n	l	$N-1$	L	$\tfrac{1}{2}[N(N+L+\tfrac{1}{2})]^{\frac{1}{2}}$
$n-1$	$l+1$	$N-1$	$L+1$	$[nN(l+1)(L+1)]^{\frac{1}{2}}(-1)^{\lambda+L+l}W(ll+1LL+1;1\lambda)$
$n-1$	$l+1$	N	$L-1$	$[n(N+L+\tfrac{1}{2})(l+1)L]^{\frac{1}{2}}(-1)^{\lambda+L+l}W(ll+1LL-1;1\lambda)$
n	$l-1$	$N-1$	$L+1$	$[(n+l+\tfrac{1}{2})Nl(L+1)]^{\frac{1}{2}}(-1)^{\lambda+L+l}W(ll-1LL+1;1\lambda)$
n	$l-1$	N	$L-1$	$[(n+l+\tfrac{1}{2})(N+L+\tfrac{1}{2})lL]^{\frac{1}{2}}(-1)^{\lambda+L+l}W(ll-1LL-1;1\lambda)$

From table 1 and the considerations of the previous section, we see that we could determine straightforwardly the brackets for arbitrary n_1, n_2 once the brackets with $n_1 = n_2 = 0$ are given.

4. The Bracket $\langle nl, NL, \lambda \vert 0l_1, 0l_2, \lambda\rangle$

For the brackets with $n_1 = n_2 = 0$ we shall give explicit expressions rather than recurrence relations. To derive these expressions we shall need a formula for the translation of multipole fields [11]). This formula concerns the development of the multipole field $r^l Y_{lm}(\theta, \varphi)$ when the vector $\mathbf{r}$, of spherical coordinates (r, θ, φ) is represented by

$$\mathbf{r} = \mathbf{r}' - \mathbf{r}'' \tag{44}$$

where the spherical coordinates of $\mathbf{r}'$ and $\mathbf{r}''$ are given by (r', θ', φ') and $(r'', \theta'', \varphi'')$ respectively. As the multipole field is a solution of the Laplace equation, we see from (44) that

$$\nabla'^2 r^l Y_{lm}(\theta, \varphi) = 0, \quad \nabla''^2 r^l Y_{lm}(\theta, \varphi) = 0, \tag{45}$$

so $r^l Y_{lm}(\theta, \varphi)$ should be expanded in terms of multipole fields in $\mathbf{r}'$, $\mathbf{r}''$. Furthermore, the multipole fields are basis for the representation of the rotation group [5]). Combining these two facts we see immediately that

$$r^l Y_{lm}(\theta, \varphi)$$
$$= \sum_{l', l''=0}^{l} \delta_{l'+l'', l} G(l'l''l) \sum_{m'm''} \langle l'l''m'm''|lm\rangle r'^{l'} Y_{l'm'}(\theta', \varphi') r''^{l''} Y_{l''m''}(\theta'', \varphi'') \tag{46}$$

where $G(l'l''l)$ is a coefficient to be determined. Assuming now that $\theta' = \theta'' = 0$, we see from (44) that $\theta = 0$ and $r = r' - r''$, so that (46) becomes

$$[(2l+1)4\pi]^{\frac{1}{2}}(r'-r'')^l$$
$$= \sum_{l', l''=0}^{l} \delta_{l'+l'', l} G(l'l''l) \langle l'l''00|l0\rangle [(2l'+1)(2l''+1)]^{\frac{1}{2}} r'^{l'} r''^{l''}. \tag{47}$$

As (47) is valid for any r', r'' we obtain, using the explicit expression [5]) for Clebsch Gordan coefficients, that [11])

$$G(l'l''l) = (-1)^{l''}(4\pi)^{\frac{1}{2}}[(2l+1)!]^{\frac{1}{2}}[(2l'+1)!(2l''+1)!]^{-\frac{1}{2}}. \tag{48}$$

Let us now consider the ket $|0l_1, 0l_2, \lambda\mu\rangle$. From the definition of the Laguerre polynomials we have [6, 10])

$$L_0^{l+\frac{1}{2}}(r^2) = 1 \tag{49}$$

so from (8) and (10) we obtain

$$|0l_1, 0l_2, \lambda\mu\rangle = 2[\Gamma(l_1+\tfrac{3}{2})\Gamma(l_2+\tfrac{3}{2})]^{-\frac{1}{2}} \exp[-\tfrac{1}{2}(r_1^2+r_2^2)]|l_1 l_2 \lambda\mu\rangle \tag{50}$$

where $|l_1 l_2 \lambda\mu\rangle$ stands for

$$|l_1 l_2 \lambda\mu\rangle = \sum_{m_1 m_2} \langle l_1 l_2 m_1 m_2|\lambda\mu\rangle r_1^{l_1} Y_{l_1 m_1}(\theta_1, \varphi_1) r_2^{l_2} Y_{l_2 m_2}(\theta_2, \varphi_2). \tag{51}$$

From (2) we have

$$\mathbf{r}_1 = \frac{1}{\sqrt{2}}\mathbf{R} + \frac{1}{\sqrt{2}}\mathbf{r}, \quad \mathbf{r}_2 = \frac{1}{\sqrt{2}}\mathbf{R} - \frac{1}{\sqrt{2}}\mathbf{r}. \tag{52}$$

Applying (46) to the multipole fields in (51), and using the relation [12])

$$Y_{l'm'}(\theta, \varphi) Y_{l''m''}(\theta, \varphi) = \sum_{l,m} H(l'l''l) \langle l'l''m'm''|lm\rangle Y_{lm}(\theta, \varphi), \tag{53}$$

where

$$H(l'l''l) = [(2l'+1)(2l''+1)/4\pi(2l+1)]^{\frac{1}{2}} \langle l'l''00|l0\rangle, \tag{54}$$

as well as the relation that reduces the summation of products of Clebsch-Gordan coefficients to $9j$ coefficients [13]), we obtain

$$|l_1 l_2 \lambda\mu\rangle = 2^{-\frac{1}{2}(l_1+l_2)} \sum_{L,l} \sum_{l'L'l''L''} \Big\{ (-1)^{l'} \delta_{L'+l',l_1} \delta_{L''+l'',l_2}$$
$$G(L'l'l_1) G(L''l''l_2) H(l'l''l) H(L'L''L)$$
$$[(2L+1)(2l+1)(2l_1+1)(2l_2+1)]^{\frac{1}{2}} \begin{Bmatrix} l' & l'' & l \\ L' & L'' & L \\ l_1 & l_2 & \lambda \end{Bmatrix} \tag{55}$$
$$r^{l'+l''-l} R^{L'+L''-L} [\sum_{M,m} \langle lLmM|\lambda\mu\rangle r^l Y_{lm}(\theta,\varphi) R^L Y_{LM}(\Theta,\Phi)] \Big\}.$$

From (54) we see that $l'+l''-l$, $L'+L''-L$ are non-negative even numbers, so that using the expansion formula of a power of the variable in terms of Laguerre polynomials † we have

$$(r^2)^{\frac{1}{2}(l'+l''-l)} = \sum_{n=0}^{\frac{1}{2}(l'+l''-l)} \frac{(-1)^n [\frac{1}{2}(l'+l''-l)]!}{[\frac{1}{2}(l'+l''-l)-n]!} \frac{\Gamma[\frac{1}{2}(l'+l''+l+3)]}{\Gamma(n+l+\frac{3}{2})} L_n^{l+\frac{1}{2}}(r^2) \tag{56}$$

and a similar expression for $R^{L'+L''-L}$. As the arguments of the factorials must always be non-negative, we see from (56) and the corresponding expression for R that

$$\begin{aligned} l'+l''-l-2n &\geqq 0, \\ L'+L''-L-2N &\geqq 0. \end{aligned} \tag{57}$$

Adding these two expressions, we obtain from the Kronecker deltas in (55), that

$$l_1+l_2-l-2n-L-2N \geqq 0. \tag{58}$$

But, from the conservation of energy relation (13), we see that (58) is actually zero, so that in (57) both expressions must be zero. Therefore, when introducing (56) and the corresponding formula for R in (55), we can include the Kronecker deltas

$$\delta_{l'+l'',2n+l}, \quad \delta_{L'+L'',2N+L}. \tag{59}$$

Going now back to (50), where we replace $|l_1 l_2 \lambda\mu\rangle$ by its explicit expression in terms of (55), (56) etc., and comparing with the ket (11) as well as with the form (8) of the radial function, it is seen straightforwardly that

$$\langle nl, NL, \lambda | 0l_1, 0l_2, \lambda\rangle = \left[\frac{(2l+1)(2L+1)(2l_1+1)(2l_2+1)}{\Gamma(l_1+\frac{3}{2})\Gamma(l_2+\frac{3}{2}) n! \Gamma(n+l+\frac{3}{2}) N! \Gamma(N+L+\frac{3}{2})} \right]^{\frac{1}{2}}$$
$$2^{-\frac{1}{2}(l_1+l_2)} \sum_{l'L'l''L''} \Big\{ (-1)^{l'} \delta_{L'+l',l_1} \delta_{L''+l'',l_2} \delta_{l'+l'',2n+l} \delta_{L'+L'',2N+L} \tag{60}$$
$$G(L'l'l_1) G(L''l''l_2) H(l'l''l) H(L'L''L)$$
$$\begin{Bmatrix} l' & l'' & l \\ L' & L'' & L \\ l_1 & l_2 & \lambda \end{Bmatrix} (-1)^n [\tfrac{1}{2}(l'+l''-l)]! \Gamma[\tfrac{1}{2}(l'+l''+l+3)]$$
$$(-1)^N [\tfrac{1}{2}(L'+L''-L)]! \Gamma[\tfrac{1}{2}(L'+L''+L+3)] \Big\}.$$

† To obtain this formula we use the relation $L_n^{-n}(x) = (-1)^n (n!)^{-1} x^n$ and the expansion of $L_n^{\alpha}(x)$ in terms of $L_m^{\beta}(x)$.

The expression (60) gives then the explicit evaluation of the transformation bracket when $n_1 = n_2 = 0$. The Kronecker deltas in (60) reduce the quadruple summation to a single sum (the $\delta_{L'+L'',\,2N+L}$ is a consequence of the other three δ's and of (13)), but we have in the summation $9j$ coefficients not readily available. We shall use the definition of the $9j$ coefficients in terms of Racah coefficients to simplify the expression (60) for the transformation brackets. It is well known that [13])

$$\begin{Bmatrix} l' & l'' & l \\ L' & L'' & L \\ l_1 & l_2 & \lambda \end{Bmatrix} = (-1)^k \begin{Bmatrix} l & l'' & l' \\ L & L'' & L' \\ \lambda & l_2 & l_1 \end{Bmatrix}$$

$$= \sum_x (2x+1)(-1)^{l+L-\lambda} W(lLl_1l_2;\lambda x) W(l''L''xL;l_2L') W(l'L'lx;l_1l'') \quad (61)$$

where k stands for the sum of all nine coefficients. From (60) we see that $l'+L' = l_1$, $l''+L'' = l_2$, so that the last two Racah coefficients appearing in (61) are expressed as simple products of factorials [14]). Substituting (61) in (60), making use of the explicit form of all factors in (60), and defining

$$q = l_1+l''-l' = l_2+L'-L'' \quad (62)$$

we obtain

$$\langle nl, NL, \lambda | 0l_1, 0l_2, \lambda \rangle$$

$$= \left[\frac{l_1!\, l_2!}{(2l_1)!(2l_2)!} \frac{(2l+1)(2L+1)}{2^{l+L}} \frac{(n+l)!}{n!(2n+2l+1)!} \frac{(N+L)!}{N!(2N+2L+1)!}\right]^{\frac{1}{2}} \quad (63)$$

$$(-1)^{n+l+L-\lambda} \sum_x \{(2x+1) A(l_1l, l_2L, x) W(lLl_1l_2;\lambda x)\},$$

where W is a Racah coefficient, and A is defined by

$$A(l_1l, l_2L, x)$$

$$= \left[\frac{(l_1+l+x+1)!(l_1+l-x)!(l_1+x-l)!}{(l+x-l_1)!}\right]^{\frac{1}{2}} \left[\frac{(l_2+L+x+1)!(l_2+L-x)!(l_2+x-L)!}{(L+x-l_2)!}\right]^{\frac{1}{2}} \quad (64)$$

$$\sum_q \left\{(-1)^{\frac{1}{2}(l+q-l_1)} \frac{(l+q-l_1)!}{[\frac{1}{2}(l+q-l_1)]![\frac{1}{2}(l+l_1-q)]!} \frac{1}{(q-x)!(q+x+1)!} \frac{(L+q-l_2)!}{[\frac{1}{2}(L+q-l_2)]![\frac{1}{2}(L+l_2-q)]!}\right\}.$$

From (62) we see that

$$l+q-l_1 = l''-l'+l \quad (65)$$

and as from (54) the right hand side is even, we conclude that the summation over q is restricted to those non-negative integer values of q for which $l+q-l_1$ is even and the arguments of the factorials are non-negative integers. The restrictions on x are given by the Racah coefficient, i.e.

$$|l-l_1| \leqq x \leqq l+l_1, \quad |L-l_2| \leqq x \leqq L+l_2. \quad (66)$$

In (63) we have then an explicit expression for the bracket with $n_1 = n_2 = 0$. Combining these results with the recurrence relations of the previous

section, we could evaluate explicitly any transformation bracket for the harmonic oscillator wave functions.

5. Discussion

In section 2 we indicated the application of the transformation brackets to the evaluation of matrix elements for different types of forces, where these matrix elements in turn are of interest in the problems of energy levels, configuration mixing, etc., of nuclear shell theory. To determine the matrix elements, the brackets must be available in numerical form, and we shall estimate the number of brackets we need to tabulate.

We first note that from the definition (10) and (11) of the eigenkets and the relation (2), the brackets have the following symmetry properties:

$$\langle nl, NL, \lambda | n_1 l_1, n_2 l_2, \lambda \rangle = (-1)^{L-\lambda} \langle nl, NL, \lambda | n_2 l_2, n_1 l_1, \lambda \rangle$$
$$= (-1)^{l_1-\lambda} \langle NL, nl, \lambda | n_1 l_1, n_2 l_2, \lambda \rangle = (-1)^{l_1+l} \langle NL, nl, \lambda | n_2 l_2, n_1 l_1, \lambda \rangle. \quad (67)$$

We can therefore restrict our evaluation to brackets in which

$$l_2 \geqq l_1, \quad L \geqq l. \quad (68)$$

Furthermore, in nuclear shell theory we are only interested in states in which [15])

$$2n_1+l_1 \leqq 6, \quad 2n_2+l_2 \leqq 6, \quad (69)$$

so that we have the restrictions

$$0 \leqq n_1, n_2 \leqq 3, \quad 0 \leqq l_1, l_2 \leqq 6. \quad (70)$$

Let us now consider brackets in which n_1, n_2 are given and define ρ and σ as

$$\rho = 2n_1+l_1+2n_2+l_2, \quad (71)$$

$$\sigma = l+L. \quad (72)$$

For a given σ and with the restriction (68), the number of possible pairs of values for l, L are given by $F(\sigma)$ where

$$F(\sigma) = \begin{cases} \frac{1}{2}(\sigma+2) & \text{if } \sigma \text{ is even,} \\ \frac{1}{2}(\sigma+1) & \text{if } \sigma \text{ is odd.} \end{cases} \quad (73)$$

Furthermore, from (11) and (68) we have

$$L-l \leqq \lambda \leqq L+l, \quad (74)$$

so that for a given l the number of possible values of λ is $2l+1$. Combining this with (73) we see that for a given σ the number of possible values of l, L, λ is $F^2(\sigma)$. Finally, from (13) we have $n+N = \frac{1}{2}(\rho-\sigma)$, so the number of possible pairs of values of n, N with ρ, σ given is

$$\tfrac{1}{2}(\rho-\sigma)+1. \quad (75)$$

From (13) and (14) we see that $\sigma \leqq \rho$ and $\rho-\sigma$ is even, and the above

analysis shows that the number of kets $|nl, NL, \lambda\rangle$ where $L \geqq l$ and ρ is fixed, is

$$U(\rho) = \sum_{\substack{\sigma=0 \\ \rho-\sigma \text{ even}}}^{\rho} \{F^2(\sigma)[\tfrac{1}{2}(\rho-\sigma)+1]\}. \tag{76}$$

If n_1, n_2 are given we see from (71) that the number of possible pairs of values for l_1, l_2 is

$$F(\rho)-(n_1+n_2), \tag{77}$$

so that the total number of brackets becomes

$$\mathcal{N}(n_1, n_2) = \sum_{\rho=2(n_1+n_2)}^{12} \{[F(\rho)-(n_1+n_2)]U(\rho)\}. \tag{78}$$

From (78) we have, for $n_1 = n_2 = 0$, the number of brackets $\mathcal{N}(0, 0) = 6300$. Considering all the possibilities $n_1, n_2 = 0, 1, 2, 3$ allowed by (70), the total number of brackets is 49 680. This number is still reasonable for tabulation, particularly as it is probable that there are, besides (67), other symmetry properties which establish relations between the brackets. A general tabulation is planned using the 650 IBM machine of the University of Mexico.

The author is indebted to Prof. V. Bargman and Dr. W. T. Sharp for helpful discussions and to Mr. D. Dillenburg for checking the calculations.

References

1) J. P. Elliot and A. M. Lane, The nuclear shell model, in Handbuch der Physik, Vol. **39** (Springer-Verlag, Berlin-Göttingen-Heidelberg, 1957) pp. 241—410
2) I. Talmi, Helv. Phys. Acta **25** (1952) 185
3) R. Thieberger, Nuclear Physics **2** (1956/57) 533
4) K. W. Ford and E. J. Konopinski, Nuclear Physics **9** (1958/59) 218
5) G. Racah, Phys. Rev. **62** (1942) 438
6) W. Magnus and F. Oberhettinger, Special functions of mathematical physics (Chelsea Publishing Company, New York 1949)pp. 84, 85
7) M. Moshinsky, Nuclear Physics **8** (1958) 19
8) H. Matsunobu and H. Takebe, Progr. Theoret. Phys. **14** (1955) 589
9) G. Racah, Phys. Rev. **63** (1943) 367;
C. Schwartz and A. de Shalit, Phys. Rev. **94** (1954) 1257
10) Erdélyi *et al.*, Higher transcendental functions, Vol. 2, (McGraw-Hill, New York, 1953) pp. 188—192
11) M. Moshinsky and E. Salz, (to be published)
12) M. E. Rose, Elementary theory of angular momentum (John Wiley and Sons, New York, 1957) p. 61
13) H. A. Jahn and J. Hope, Phys. Rev. **93** (1954) 318
14) Biedenharn, Blatt and Rose, Revs. Mod. Phys. **24** (1952) 249
15) J. P. Elliot and A. M. Lane, loc. cit. p. 251

1.D.1:
2.L

Nuclear Physics **13** (1959) 117—124; © *North-Holland Publishing Co., Amsterdam*
Not to be reproduced by photoprint or microfilm without written permission from the publisher

INTRASHELL-INTERACTION LEVELS AND THEIR EXCITATION BY MULTICHARGED IONS

V. I. GOLDANSKY and M. V. KAZARNOVSKY

P. N. Lebedev Physical Institute, USSR Academy of Sciences, Moscow

Received 20 March 1959

Abstract: On the basis of the shell model of the nucleus one may anticipate the existence of the whole series of hitherto unknown nuclear levels arising from the interaction of nucleons in a given shell. Many of these levels possess angular momenta which strongly differ from those of the ground state, although their energy above the ground state is sufficiently low. The most efficient method of excitation of such levels would seem to be by bombardment of nuclei with multicharged ions. The theory of excitation of low-lying levels by inelastic scattering of complex nuclei is considered. New cases of nuclear isomerism may be produced by low energy E2-transitions between intrashell-interaction levels.

1. Intrashell-Interaction Levels

As is well known, excited electron energy levels in atoms can arise not only from the removal of an electron from one shell to another but also as a result of different arrangements of a given number of electrons in unfilled shells. Some examples are the $^1D_2$, $^3P_{2,1,0}$ and $^1S_0$ levels which appear when two p-electrons are in the outer shell.

The energy difference of such intrashell-interaction levels is not large (≈ 1 eV) and is approximately an order of magnitude smaller than the energy difference of electrons belonging to different shells.

On the basis of the shell model, which satisfactorily describes a number of properties of spherical nuclei at low excitation energies, it would seem reasonable to assume that in such nuclei, along with levels due to removals of nucleons between different shells, there should also be levels which are due to the interaction of nucleons within a given shell [1]).

Possible values of the total angular momenta of such levels for various numbers of nucleons in shells with $j = \frac{3}{2}$ to $\frac{11}{2}$ are enumerated in table 1 †. If there are only two or three nucleons (or holes) in the shell, all the levels indicated in the corresponding rows of table 1 can be excited by displacing

† This table, with some corrections, is taken from the book of M. Goeppert-Mayer and J. H. D. Jensen, Elementary Theory of Nuclear Shells, four levels omitted in it have been included by us. It may be mentioned here that the levels for O^{18} (but not for O^{16}), Ne^{20} and Kr^{84} presented in ref. [1]) were written down without taking account of the Pauli principle. Only even j should be retained, and this corresponds to E2 but not to M1 transitions between the levels of these nuclei.

TABLE 1

Total angular momenta of intrashell-interaction levels for shells with $j = \frac{3}{2}$ to $\frac{11}{2}$

j	number of nucleons	total angular momenta of levels †	number of levels
$\frac{3}{2}$	1 (or 3)	$\underline{\frac{3}{2}}$	1
	2	$2, \underline{0}$	2
$\frac{5}{2}$	1 (or 5)	$\underline{\frac{5}{2}}$	1
	2 (or 4)	$4, 2, \underline{0}$	3
	3	$\frac{9}{2}, \underline{\frac{5}{2}}, \frac{3}{2}$	3
$\frac{7}{2}$	1 (or 7)	$\underline{\frac{7}{2}}$	1
	2 (or 6)	$6, 4, 2, \underline{0}$	4
	3 (or 5)	$\frac{15}{2}, \frac{11}{2}, \frac{9}{2}, \underline{\frac{7}{2}}, \frac{5}{2}, \frac{3}{2}$	6
	4	$8, 6, 5, 4, 4, 2, 2, \underline{0}$	8
$\frac{9}{2}$	1 (or 9)	$\underline{\frac{9}{2}}$	1
	2 (or 8)	$8, 6, 4, 2, \underline{0}$	5
	3 (or 7)	$\frac{21}{2}, \frac{17}{2}, \frac{15}{2}, \frac{13}{2}, \frac{11}{2}, \frac{9}{2}, \underline{\frac{9}{2}}, \frac{7}{2}, \frac{5}{2}, \frac{3}{2}$	10
	4 (or 6)	$12, 10, 9, 8, 8, 7, 6, 6, 6, 5, 4, 4, 4, 3, 2, 2, 0, \underline{0}$	18
	5	$\frac{25}{2}, \frac{21}{2}, \frac{19}{2}, \frac{17}{2}, \frac{17}{2}, \frac{15}{2}, \frac{15}{2}, \frac{13}{2}, \frac{13}{2}, \frac{11}{2}, \frac{11}{2}, \frac{9}{2}, \frac{9}{2}, \underline{\frac{9}{2}}, \frac{7}{2}, \frac{7}{2},$ $\frac{5}{2}, \frac{5}{2}, \frac{3}{2}, \frac{1}{2}$	20
$\frac{11}{2}$	1 (or 11)	$\underline{\frac{11}{2}}$	1
	2 (or 10)	$10, 8, 6, 4, 2, \underline{0}$	6
	3 (or 9)	$\frac{27}{2}, \frac{23}{2}, \frac{21}{2}, \frac{19}{2}, \frac{17}{2}, \frac{15}{2}, \frac{15}{2}, \frac{13}{2}, \frac{11}{2}, \underline{\frac{11}{2}}, \frac{9}{2}, \frac{9}{2}, \frac{7}{2}, \frac{5}{2}, \frac{3}{2}$	15
	4 (or 8)	$16, 14, 13, 12, 12, 11, 10, 10, 10, 9, 9, 8, 8, 8, 8, 7, 7, 6, 6, 6, 6,$ $5, 5, 4, 4, 4, 4, 3, 2, 2, 2, 0, \underline{0}$	33
	5 (or 7)	$\frac{35}{2}, \frac{31}{2}, \frac{29}{2}, \frac{27}{2}, \frac{27}{2}, \frac{25}{2}, \frac{25}{2}, \frac{23}{2}, \frac{23}{2}, \frac{23}{2}, \frac{21}{2}, \frac{21}{2}, \frac{21}{2}, \frac{19}{2}, \frac{19}{2},$ $\frac{19}{2}, \frac{19}{2}, \frac{17}{2}, \frac{17}{2}, \frac{17}{2}, \frac{17}{2}, \frac{15}{2}, \frac{15}{2}, \frac{15}{2}, \frac{15}{2}, \frac{15}{2}, \frac{13}{2}, \frac{13}{2}, \frac{13}{2}, \frac{13}{2},$ $\frac{11}{2}, \frac{11}{2}, \frac{11}{2}, \frac{11}{2}, \underline{\frac{11}{2}}, \frac{9}{2}, \frac{9}{2}, \frac{9}{2}, \frac{9}{2}, \frac{7}{2}, \frac{7}{2}, \frac{7}{2}, \frac{7}{2}, \frac{5}{2}, \frac{5}{2}, \frac{5}{2}, \frac{3}{2}, \frac{3}{2}, \frac{1}{2}$	49
	6	$18, 16, 15, 14, 14, 13, 13, 12, 12, 12, 12, 11, 11, 10, 10, 10, 10, 10,$ $9, 9, 9, 9, 8, 8, 8, 8, 8, 8, 7, 7, 7, 7, 6, 6, 6, 6, 6, 6, 6, 5, 5, 5, 4, 4,$ $4, 4, 4, 4, 3, 3, 3, 2, 2, 2, 2, 0, 0, \underline{0}$	58

† The ground-state angular momentum is underlined.

only one nucleon (hole) within a given shell. If, however, there are four or more nucleons in the shell, single-nucleon removals will produce only those levels which occur for at most two or three nucleons in the shell, according

as the shell contains an even or odd number of nucleons. The other levels can only arise from a combination of single and multiple-nucleon removals. For example, single-nucleon removals from the ground state (with a total angular momentum $J = 0$) of a four-nucleon configuration in a shell with $j = \frac{9}{2}$ cannot lead to the appearance of levels with angular momenta 9, 10 or 12.

It should be mentioned that excited states similar to those considered in the present work are observed in odd nuclei [2]). However, these states arise from different ways of coupling the angular momenta of the odd proton and the odd neutron.

The excitation energy differences of the various intrashell-interaction levels enumerated in table 1 probably amount to tens and hundreds of keV. However, owing to the necessity of unpairing the nucleons, the excitation energy of the first of these levels may be appreciably higher ($\gtrsim$ 1 MeV). Thus, not all the "fine" structure of the intrashell levels may necessarily be located below the shell-to-shell removal levels, as is the case for rotational levels. The first shell-to-shell removal level may either lie below the intrashell level group (if the energy of this removal is smaller than the unpairing energy) or fall within the limits of this level group. This circumstance, however, cannot change the general pattern of transitions between the intrashell-interaction levels. Such transitions should involve the emission of E2 or M1 radiation or of conversion electrons. The life-times with respect to E2 transitions between levels corresponding to single-nucleon removal, computed for energy differences of 20—100 keV (without taking account of internal conversion), is $\tau \approx (6\times 10^{-4}\text{—}2)A^{-\frac{4}{3}}$ sec. Account of electron conversion reduces the value of τ by 2—3 orders of magnitude. It is evident, nevertheless, that even if conversion is taken into account, it should be quite possible to detect an essentially new class of isomeric transitions, namely E2 transitions between the intrashell-interaction levels. It can be seen from table 1 that such E2 transitions are most probable in shells containing two nucleons (or holes).

2. Methods of Excitation of Intrashell-Interaction Levels

Although the angular momenta of intrashell-interaction levels may differ strongly from those of the ground-state, the excitation energies of the intrashell levels are usually relatively small.

This circumstance determines the specificity of excitation of these levels; thus, neither bombardment of nuclei by elementary particles, nor β-decay or γ-ray emission from a different type of level, can effectively lead to the appearance of the most characteristic intrashell levels (those possessing large angular momenta).

For example, in order to induce the comparatively small change of angular momentum $\Delta j = 4$, such as the formation of $O^{18*}(J = 4)$ in the inelastic scattering of neutrons, it is necessary to bombard the O^{18} nuclei with neutrons possessing an energy of the order of tens of MeV (corresponding to the condition $R_{O^{18}} \approx 4\lambda_n$). Evidently, various other types of nuclear reactions will then predominate and excitation of intrashell levels will be very improbable. Hence, the most efficient method for excitation of intrashell levels is apparently (as noted in ref. [1])) to make complex nuclei collide, that is, to bombard nuclei with multicharged ions possessing sufficiently large angular momenta in the outer neutron shells †. The following examples of such ions may be cited:

$$_8O^{18}(d_{\frac{5}{2}}^2 \text{ neutrons}),\quad _{10}Ne^{20}(d_{\frac{5}{2}}^2),\quad _{18}A^{40}(f_{\frac{7}{2}}^2),\quad _{36}Kr^{83}(g_{\frac{9}{2}}^7),\quad _{36}Kr^{84}(g_{\frac{9}{2}}^8).$$

Intrashell levels can be excited by inelastic scattering, e.g.

$$\underset{(0^+)}{_{18}A^{40}} + \underset{(\frac{9}{2}^+)}{_{36}Kr^{83}} \rightarrow \underset{(6^+)}{_{18}A^{40*}} + \underset{(\frac{21}{2})}{_{36}Kr^{83*}},$$

as well as in some neutron transfer processes of the type

$$\underset{(\frac{9}{2}^+)}{_{36}Kr^{83}} + \underset{(\frac{9}{2}^+)}{_{38}Sr^{87}} \rightarrow \underset{(8^+)}{_{36}Kr^{84*}} + \underset{(8^+)}{_{38}Sr^{86*}}.$$

Neutron-transfer processes have been studied theoretically in sufficient detail in a number of papers [4,5]); however, the possibility of excitation of intrashell and other levels of the residual nucleus was not considered. We shall consider here the excitation of intrashell levels by inelastic scattering of complex nuclei.

In ref. [1]) an interaction between complex nuclei 1 and 2 was considered which involved a real exchange of two neutrons, one of them being transferred from nucleus 1 to nucleus 2, the second being transferred in the opposite direction. The cross section for this neutron-exchange interaction turns out to be proportional to the exponential factor

$$W = \exp\left\{-\frac{2}{\hbar}\frac{Z_1 Z_2 e^2}{E_0}(\sqrt{2mI_1}+\sqrt{2mI_2})\right\}, \qquad (1)$$

where Z_1 and Z_2 are the nuclear charges, I_1 and I_2 the neutron binding energies in nuclei 1 and 2, m the neutron mass and E_0 the energy of relative motion of the nuclei. Calculations of the exponential term for neutron exchange were carried out in ref. [1]) in exactly the same manner as the computations of neutron transfer from one complex nucleus to another performed by

† It is possible that fission fragments contain nuclei with excited intrashell-interaction levels.

E. M. Lifshitz [4]). The pre-exponential factor was estimated by comparing Lifshitz's formula with the experimental data on neutron transfer in N^{14} nuclei. Formula (1) can be rewritten as follows:

$$W = \exp\{-2R(\kappa_1+\kappa_2)\} \tag{2}$$

where $R = Z_1 Z_2 e^2/E_0$ is the minimum distance between the centres of the colliding nuclei in classical Coulomb scattering, and $\kappa_i = (2mI_i/\hbar^2)^{\frac{1}{2}}$ is the reciprocal relaxation length of the wave function of a neutron of binding energy I_i outside the nucleus. Similar expressions for the probability of excitation by single-nucleon transitions should hold not only in the case of real exchange of neutrons, but also when account is taken of possible virtual processes, the only difference being that in the latter case, instead of I_1 and I_2 one should introduce I and I^*, which are respectively the neutron binding energy in the ground-state and the excited nuclear state. Indeed, formula (2) can then be interpreted as the exponential factor of the square modulus of the matrix element for the transition of a neutron from state 1 (with energy I) to a state 2 (with energy I^*), induced by a perturbation localized at a distance R from the nucleus.

As mentioned in ref. [1]), the finite dimensions of the nuclei were not taken into account in the deduction of eq. (1). In order to take this factor into account, R should be replaced by $R-\rho$ in eq. (2), ρ being the sum of the radii of the colliding nuclei. Moreover, no account was taken, in ref. [1]), of the fact that the process under consideration is essentially a non-adiabatic one, since it can proceed only if the relative velocity of the colliding nuclei is sufficient for them to spend part of their energy in excitation of the neutron. The probability of this process should therefore decrease exponentially with increasing product of the collision time $t_0 \approx R/v$ and the transition frequency $\omega = (I-I^*)/\hbar$, just as in the case of Coulomb excitation. In the semi-classical approximation, i.e. when the colliding nuclei are assumed to move along a classical Coulomb trajectory, the probability for excitation of the nucleus is proportional to the square modulus of

$$M = \int_{-\infty}^{\infty} e^{i\omega t}\, dt\, \mu[\mathbf{r}(t)],$$

where $\mu[\mathbf{r}(t)]$ is the matrix element for a transition of the nucleus from ground state to excited state, the transition being induced by a perturbation produced by the second nucleus located at a distance $\mathbf{r}$ from the first one. In order to evaluate this integral, it is convenient to change from the variable t to a new variable w in accordance with the formula

$$t = \frac{R}{2v_0}(\varepsilon \sinh w + w),$$

where R is the minimum distance between the colliding nuclei, v_0 the relative

velocity at infinity and $\varepsilon = 1/\sin\frac{1}{2}\theta$, θ being the deflection angle. Then, for a Coulomb trajectory,

$$r = \sqrt{x^2+y^2+z^2} = \tfrac{1}{2}R(\varepsilon\cosh w+1),$$

$$x = \tfrac{1}{2}R(\cosh w+\varepsilon), \quad y = \tfrac{1}{2}R(\varepsilon^2-1)^{\frac{1}{2}}\sinh w, \quad z = 0,$$

and if

$$\mu(\mathbf{r}) = \exp\{-r(\kappa+\kappa^*)\}f(\mathbf{r}),$$

where

$$\kappa = \sqrt{\frac{2mI}{\hbar^2}}, \qquad \kappa^* = \sqrt{\frac{2mI^*}{\hbar^2}}$$

and $f(\mathbf{r})$ is some power of $\mathbf{r}$ or any other function of $\mathbf{r}$ more smoothly varying than the exponential, we obtain

$$M = \int_{-\infty}^{+\infty} e^{\frac{1}{2}i\frac{\omega R}{v_0}(\varepsilon\sinh w+w)-\frac{1}{2}(\kappa+\kappa^*)R(\varepsilon\cosh w+1)}\chi(w)\mathrm{d}w,$$

where $\chi(w)$ is also a relatively smoothly varying function of w. If $\frac{1}{2}(\kappa+\kappa^*)R$ or $\frac{1}{2}\omega R/v_0$ are large, this integral can be estimated by the saddle point method: it is proportional to $\exp[\varphi(w_0)]$, where w_0 is the saddle point of the function

$$\varphi(w) = \tfrac{1}{2}i\frac{\omega R}{v_0}(\varepsilon\sinh w+w)-\tfrac{1}{2}(\kappa+\kappa^*)R(\varepsilon\cosh w+1),$$

i.e. the point at which $\partial\varphi(w)/\partial w = 0$. Evidently, the main contribution to the cross section arises from head-on collisions, when ε is close to 1. It is easy to show that in this case

$$|M|^2 \approx \exp\left\{-2(R-\rho)(\kappa+\kappa^*)-\frac{2R\omega}{v_0}\tan^{-1}\frac{\omega}{v_0(\kappa+\kappa^*)}\right\}. \qquad (3)$$

Here, the finite size of the nucleus was taken into account by replacing $R(\kappa+\kappa^*)$ by $(R-\rho)(\kappa+\kappa^*)$.

In the case of Coulomb excitation, the transition matrix element does not contain the exponential factor $\exp\{-r(\kappa+\kappa^*)\}$ and the expression for $|M|^2$ can formally be derived from (3) by putting $\kappa = \kappa^* = 0$. As a result, we obtain the familiar expression [6]) $|M|^2 \approx \exp\{-\pi R\omega/v_0\}$. If $\omega/v_0(\kappa+\kappa^*)$ is small, then

$$|M|^2 \approx \exp\left\{-2(R-\rho)(\kappa+\kappa^*)-2R\frac{\omega^2}{v_0^2(\kappa+\kappa^*)}\right\}.$$

The effects due to the finite size of the nucleus and to non-adiabaticity can only partially compensate each other, as the first of these contributes to the cross section a coefficient which is independent of the energy of the colliding nuclei, whereas the second yields a coefficient which decreases exponentially at small energies.

By applying eq. (3) one can write the cross section for excitation of neutron

levels in the nucleus in the form

$$\sigma_{\text{exc}} = \sigma^0_{\text{exc}} \exp\left\{-2(R-\rho)(\kappa+\kappa^*) - 2R\frac{\omega}{v_0}\tan^{-1}\frac{\omega}{v_0(\kappa+\kappa^*)}\right\}, \qquad (4)$$

where σ^0_{exc} is a relatively weak function of energy and, in order of magnitude, is equal to the geometrical cross section.

On the other hand, it can be shown by similar reasoning that the cross section for neutron transfer from one nucleus (with neutron binding energy I_1) to another (the binding energy of the neutron in the residual nucleus being I_2) can be written for $I_2 < I_1$, in the form

$$\sigma_{\text{tr}} = \sigma^0_{\text{tr}} \exp\left\{-2(R-\rho)\kappa_2 - 2R\frac{\omega'}{v_0}\tan^{-1}\frac{\omega'}{v_0\kappa_2}\right\},$$

where

$$\kappa_2 = \sqrt{2mI_2}, \quad \omega' = (I_1-I_2)/\hbar$$

and σ^0_{tr}, in order of magnitude, is equal to σ^0_{exc} for the final nucleus. Thus, the excitation cross section for a nucleus with N neutrons and Z protons is

$$\begin{aligned}\sigma_{\text{exc}}(N, Z) \approx \sigma_{\text{tr}}(N-1, Z) \exp\Big\{&-2(R-\rho)\kappa(N, Z)\\ &-2R\frac{I(N, Z)-I^*(N, Z)}{\hbar v_0}\tan^{-1}\frac{I(N, Z)-I^*(N, Z)}{\hbar v_0[\kappa(N, Z)+\kappa^*(N, Z)]}\\ &+2R\frac{I(N-1, Z)-I(N, Z)}{\hbar v_0}\tan^{-1}\frac{I(N-1, Z)-I(N, Z)}{\hbar v_0[\kappa(N-1, Z)+\kappa(N, Z)]}\Big\}\end{aligned} \qquad (5)$$

where σ_{exc} and σ_{tr} should be referred to equal velocities of relative motion.

3. Conclusions

1) A level series due to the intrashell-interaction of nucleons may be assumed to exist in spherical nuclei. These levels for shells with $j = \frac{3}{2}$ to $\frac{11}{2}$ are enumerated in table 1.

2) Many of the intrashell levels should differ strongly with respect to total angular momentum, having at the same time only a small difference in their excitation energies. A result of this may be the appearance of peculiar E2 isomeric transitions.

3) One of the most effective ways of exciting intrashell levels with large angular momenta is to exploit the interaction of complex nuclei; this can be done by bombarding nuclei with multicharged ions.

4) As was already suggested in ref. [1]), the order of magnitude of the cross sections for such processes can be estimated by considering the mechanism of direct neutron exchange between the colliding nuclei, since, even when

possible virtual processes are taken into account, the binding energy of the neutron still enters the exponent twice, viz. in the ground-state and in the excited state of the nucleus.

In conclusion the authors express their appreciation to A. S. Davydov for valuable discussions.

References

1) V. I. Goldansky, Nuclear Physics **9** (1959) 551; JETP **36** (1959) 526
2) L. V. Groshev and A. M. Demidov, Atomnaja Energija **3** (1957) 91
3) V. Weisskopf, Phys. Rev. **83** (1951) 1073
4) E. M. Lifshitz, JETP **9** (1939) 1
5) G. Breit and M. E. Ebel, Phys. Rev. **103** (1956) 679
6) K. A. Ter-Martirosian, JETP **22** (1952) 284

1.E.2 *Nuclear Physics* **13** (1959) 125—131; © *North-Holland Publishing Co., Amsterdam*
Not to be reproduced by photoprint or microfilm without written permission from the publisher

ALPHA-PARTICLE S-STATE BINDING ENERGY

L. COHEN and J. B. WILLIS
Mathematics Department, University of Southampton

Received 5 June 1959

Abstract: A variational calculation has been made of the principal S-state contribution to the binding energy of the alpha-particle using a Yukawa interaction and a radial wave-function of the form $\exp(-\mu \Sigma_{i<j} r_{ij})$. The results show a substantial improvement on earlier calculations with a radial wave-function of the form $\exp[-\mu(\Sigma_{i<j} r_{ij}^2)^{\frac{1}{2}}]$. The methods used are such that extension to include hard-core interactions would be very straightforward. Monte-Carlo methods are used to evaluate the integrals.

1. Introduction

In a direct variational calculation of the binding energy of the alpha-particle when hard core interactions are present, the wave-functions must be expressed in terms of interparticle distances, since the wave-function is required to vanish when any interparticle distance becomes less than the hard-core radius. In the present paper, central interactions are used which do not contain hard cores, but the techniques are developed in a way which may easily be extended to deal with central hard-core interactions. The further extension to non-central forces involves a fuller classification of alpha-particle states and it is hoped to deal with this more general problem in a later paper.

There are twelve position coordinates for the four particles. The centre of gravity takes care of three, and there are three Euler angles defining the orientation of the nucleus in space. This leaves six coordinates describing the tetrahedron formed by the four particles. These can be taken as the six interparticle distances $r_{ij}(i, j = 1, 2, 3, 4)$. (The correspondence between possible tetrahedra and interparticle distances is 2—1, since a reflection in a face of the tetrahedron cannot in general be obtained by a rotation of the tetrahedron. A further two-valued coordinate should strictly be introduced, but can be suppressed since the Hamiltonian is clearly invariant under these reflections.)

A similar situation arises in the case of triton. There the three interparticle distances satisfy the triangular inequality, and by a suitable transformation several authors have been able to evaluate analytically the integrals arising in a variational calculation (e.g. Pease and Feshbach [1])). The inequalities satisfied by the interparticle distances in the alpha-particle case

are more involved, analytic evaluation has not been possible, and numerical integration of the six-dimensional integrals was found to be necessary.

In the triton case, it is well known that a trial wave function containing a factor of the form $\exp(-\mu\sum r_{ij})$ gives much better results for the binding energy than one containing $\exp[-\mu(\sum r_{ij}^2)^{\frac{1}{2}})]$. In the present paper a similar comparison is made for alpha-particle S-state wave functions.

2. Coordinate System

A convenient choice of axes can be made in the following manner. If A_1, A_2, A_3, A_4 are the positions of the four nucleons, then A_1A_2 is taken as the z-axis and the plane $A_1A_2A_3$ as the xz-plane. (This specification is clearly not invariant under permutations of the nucleons, and a more sophisticated specification will probably have to be made before it is possible to provide a full classification of alpha-particle wave functions.) A_1, A_2 are assumed to be protons, A_3, A_4 neutrons. Denote the interparticle distances A_1A_2, A_1A_3, A_1A_4 by r_1, r_2, r_3 respectively, and let the spherical polar coordinates of A_3, A_4 be $(r_2, \psi, 0)$ and (r_3, θ, ϕ) respectively. If r_4, r_5, r_6 denote the interparticle distances A_2A_3, A_2A_4, A_3A_4, then

$$\begin{aligned} r_4^2 &= r_1^2+r_2^2-2r_1r_2\cos\psi, \\ r_5^2 &= r_1^2+r_3^2-2r_1r_3\cos\theta, \\ r_6^2 &= r_2^2+r_3^2-2r_2r_3\,(\cos\theta\cos\psi+\sin\theta\sin\psi\cos\phi). \end{aligned}$$

The limits on θ, ψ are that

$$0 \leqq \theta \leqq \pi, \quad 0 \leqq \psi \leqq \pi,$$

so that

$$|r_1-r_2| \leqq r_4 \leqq r_1+r_2; \quad |r_1-r_3| \leqq r_5 \leqq r_1+r_3. \tag{1}$$

We further impose the restriction that $0 \leqq \phi \leqq \pi$ (this is equivalent to neglecting reflections as mentioned in the introduction). Then

$$(r_6)_{\min} \leqq r_6 \leqq (r_6)_{\max} \tag{2}$$

where

$$\begin{aligned} (r_6)_{\min}^2 &= r_2^2+r_3^2-2r_2r_3\cos(\theta-\psi), \\ (r_6)_{\max}^2 &= r_2^2+r_3^2-2r_2r_3\cos(\theta+\psi). \end{aligned} \tag{3}$$

The volume element in terms of the polar angles is clearly

$$d\tau = 8\pi^2 r_1^2 r_2^2 r_3^2 \sin\psi \sin\theta \, dr_1 dr_2 dr_3 d\psi \, d\theta \, d\phi.$$

In terms of interparticle distances alone, this can be transformed to

$$d\tau = \frac{16\pi^2 r_1 r_2 r_3 r_4 r_5 r_6 \, dr_1 dr_2 dr_3 dr_4 dr_5 dr_6}{r_1[r_6^2-(r_6)_{\min}^2]^{\frac{1}{2}}[(r_6)_{\max}^2-r_6^2]^{\frac{1}{2}}}. \tag{4}$$

The limits to be imposed on the variables are given by equations (1) and (2), and by $0 \leqq r_i \leqq \infty$ $(i = 1, 2, 3)$.

3. Kinetic Energy Operator

When the wave function is independent of the Euler angles, the kinetic energy operator simplifies considerably. If ∇_i^2 is the Laplacean operator corresponding to the i^{th} nucleon, and $\mathbf{r}_{ij}$ is the vector displacement from A_i to A_j, we have

$$\sum_{i=1}^{4} \nabla_i^2 \Phi_S = 2 \sum_{i<j} \left(\frac{\partial^2 \Phi_S}{\partial r_{ij}^2} + \frac{2}{r_{ij}} \frac{\partial \Phi_S}{\partial r_{ij}} \right) + 2 \sum_{i;j<k} \frac{\mathbf{r}_{ij} \cdot \mathbf{r}_{ik}}{r_{ij} r_{ik}} \frac{\partial^2 \Phi_S}{\partial r_{ij} \partial r_{ik}} \tag{5}$$

The last summation is over all i and over $j < k (\neq i)$; i.e. it consists of twelve terms, contributions coming from every pair of interparticle distances which meet at a nucleon.

The simplest way of obtaining this result is by direct transformation of the kinetic operator in eq. (21) of Abraham, Cohen and Roberts [2]) neglecting derivatives with respect to Euler angles.

4. Wave Functions and Matrix Elements

In this paper we are concerned only with the principal S-state binding energy and accordingly the wave function is assumed to be of the form

$$\Phi_S = qR$$

where

$$R = N \exp(-\mu \sum_{i<j} r_{ij}),$$

$$q = \tfrac{1}{2}[\alpha(1)\beta(2) - \alpha(2)\beta(1)][\alpha(3)\beta(4) - \alpha(4)\beta(3)],$$

α, β denoting the spin functions with spin up and spin down, and μ a variational parameter. The normalisation constant N is given by

$$\frac{1}{N^2} = \int \exp(-2\mu \sum_{i<j} r_{ij}) \mathrm{d}\tau.$$

The interaction used is the central part of the interaction used by Abraham, Cohen and Roberts [2]), and is of the form

$$V_{12} = -\frac{\hbar^2 \lambda}{M r_c^2} [1 - \tfrac{1}{2}g + \tfrac{1}{2}g(\boldsymbol{\sigma}_1 \cdot \boldsymbol{\sigma}_2)] \frac{\mathrm{e}^{-(r_{12}/r_c)}}{(r_{12}/r_c)}. \tag{6}$$

This makes possible a direct comparison between the wave function defined above, and the wave function containing

$$R = N \exp[-\mu (\sum_{i<j} r_{ij}^2)^{\frac{1}{2}}]$$

used in the earlier calculations The total Hamiltonian for the system is

$$\mathscr{H} = -\frac{\hbar^2}{2M} \sum_{i=1}^{4} \nabla_i^2 + \sum_{i<i} V_{ij} + \frac{e^2}{r_{12}},$$

the last term being the Coulomb energy operator.

The principal S-state binding energy is then written as

$$\langle \Phi_s | \mathscr{H} | \Phi_s \rangle = -\frac{\hbar^2}{4Mr_c^2} E + \text{Coulomb energy}.$$

If a transformation is made to non-dimensional variables by the substitution $\mu r_i = x_i (i = 1, \ldots, 6)$, the following expression can be obtained for E in terms of $\kappa = \mu r_c$:

$$E = [-2\kappa^2 I_T + 4\lambda(1-g) I_V(\kappa)]/I_N, \tag{7}$$

where

$$I_N = \int \exp\left(-2 \sum_{i=1}^{6} x_i\right) d\tau_x,$$

$$I_T = \int [4 \sum_i (1/x_i) - 12 - 2 \sum (\text{cosines})] \exp(-2 \sum x_i) d\tau_x,$$

$$I_V(\kappa) = \int \sum_i \frac{\exp(-x_i/\kappa)}{(x_i/\kappa)} \exp(-2 \sum x_i) d\tau_x.$$

In addition the Coulomb energy is given by

$$\text{Coulomb energy} = e^2 \mu \int \frac{1}{x_1} \exp(-2 \sum x_i) d\tau_x / I_N.$$

In these expressions $d\tau_x$ denotes the volume element of eq. (4) with x_i replacing the r_i, the limits satisfied by the x_i being of the same form as those satisfied by the r_i.

The cosines occurring in I_T are the cosines of the twelve angles between any pair of adjacent edges of the tetrahedron formed by the four nucleons.

5. Evaluation of the Integrals

It has not been possible to evaluate the integrals analytically and numerical techniques have had to be used. Classical methods, combining Gauss and Gauss-Laguerre quadrature, are satisfactory if the integrands are smooth. When the integrals arising in the present problem are expressed in the form required for the application of classical quadrature, the integrands involve $|x_1 - x_2|$ and $|x_1 - x_3|$ because of the lower limits for x_4 and x_5. It would have been possible to remove these moduli from the integrands by dividing up the ranges of integration suitably, but this would have trebled the number of integrations to be performed. Furthermore, error analysis in the quadrature of multiple integrals is extremely difficult. Eventually Monte-Carlo methods were used (see e.g. ref.[3])). The awkward lower limits for x_4 and x_5 could easily be taken into account by a rejection technique, but experience showed that it was more efficient to include the limits directly by a simple transformation, the moduli then appearing in the integrand.

The experience gained in a preliminary investigation of the numerical integration of the three-dimensional integrals occurring in the evaluation of the triton binding energy was drawn on rather heavily. The use of antithetic variates [4]), for example, required a fairly simple type of distribution function (i.e. one whose cumulative distribution function could easily be inverted), and it turned out to be more efficient to do a straightforward Monte-Carlo calculation with more complicated distribution functions. A brief discussion of the method finally adopted is given in the Appendix, and a fuller account will be given elsewhere.

An important problem in the use of Monte-Carlo methods is to obtain as small a variance as is practicable, since the error goes down only as the square root of the number of points used. All calculations were carried out on the Pegasus computer at Southampton. In the method eventually used, about 40 000 points were taken and gave a possible error (twice the standard deviation) of two per cent in the value of each integral, and the total machine time required for the final run was about 40 hours. The possible error in the binding energy was then about five per cent.

6. Results and Conclusions

The binding energy was calculated for several of the sets of parameters used by Abraham, Cohen and Roberts [2]) where the S-state binding energy was obtained using the radial wave function $\exp[-\mu(\sum r_{ij}^2)^{\frac{1}{2}}]$. Their results are given in the column headed $\varepsilon^{(1)}$ of the table below. The parameters η and η/τ in the table are proportional to the ranges of the central and tensor parts of the interaction and are as defined in Feshbach and Schwinger [5]). The column headed $\varepsilon^{(2)}$ is the S-state binding energy obtained in the present calculations, and κ_0 is the value of κ for which the binding energy is a maximum (obtained by graphical interpolation).

η	η/τ	$\varepsilon^{(1)}$ (MeV)	κ_0	$\varepsilon^{(2)}$ (MeV)
0.313	0.492	27.3	0.70	34.2
	0.355	9.6	0.56	14.6
	0.320	2.4	0.45	5.7
0.275	0.492	31.9	0.69	40.5
	0.355	10.0	0.52	15.7
	0.320	2.0	0.43	6.0
0.256	0.355	11.2	0.53	17.8
	0.320	1.9	0.43	6.4

The main conclusion shown in the table is that the radial wave-function used in the present paper brings about a substantial increase in the calcu-

lated value of the binding energy. The increase is in fact about equal to that due to the introduction of the principal D-state in the earlier calculations. The Coulomb energy is virtually unaltered.

A very rough comparison of the sizes of the nucleus in the two calculations can be made by comparing $\sqrt{6}\mu r_c$ in the earlier work with $6\mu r_c$ in the present work. The results suggest that the radius of the nucleus is slightly lower in the present case.

Appendix

The integrals that occur are of the form

$$I = \int_0^\infty \mathrm{d}x_1 \int_0^\infty \mathrm{d}x_2 \int_0^\infty \mathrm{d}x_3 \int_{|x_1-x_2|}^{x_1+x_2} \mathrm{d}x_4 \int_{|x_1-x_3|}^{x_1+x_3} \mathrm{d}x_5 \int_{(x_6)_{\min}}^{(x_6)_{\max}} \mathrm{d}x_6\, g(x_1, \ldots, x_6)$$
$$\times \exp\left(-2\sum_i x_i\right) x_2 x_3 x_4 x_5 x_6 / (x_6^2 - (x_6)_{\min}^2)^{\frac{1}{2}} ((x_6)_{\max}^2 - x_6^2)^{\frac{1}{2}},$$

where $(x_6)_{\min}$, $(x_6)_{\max}$ are defined in equations (3). We rewrite this as

$$I = \frac{\pi}{512} \int \ldots \int g(x_1, \ldots, x_6)\, \mathrm{e}^{-2x_6} x_5$$
$$[F_2(x_1+x_2) - F_2(|x_1-x_2|)][F_1(x_1+x_3) - F_1(|x_1-x_3|)]$$
$$\times \prod_i f_i(x_i)\mathrm{d}x_i$$

where

$$f_1(x_1) = 2\mathrm{e}^{-2x_1},$$
$$f_2(x_2) = 4x_2\mathrm{e}^{-2x_2}, \quad f_3(x_3) = 4x_3\mathrm{e}^{-2x_3},$$
$$f_4(x_4) = 4x_4\mathrm{e}^{-2x_4}/[F_2(x_1+x_2) - F_2(|x_1-x_2|)],$$
$$f_5(x_5) = 2\mathrm{e}^{-2x_5}/[F_1(x_1+x_3) - F_1(|x_1-x_3|)],$$
$$f_6(x_6) = (2/\pi)x_6/[x_6^2 - (x_6)_{\min}^2]^{\frac{1}{2}}[(x_6)_{\max}^2 - x_6^2]^{\frac{1}{2}},$$
$$F_1(x) = \int_0^x 2\mathrm{e}^{-2x}\mathrm{d}x, \quad F_2(x) = \int_0^x 4x\mathrm{e}^{-2x}\mathrm{d}x.$$

The $f_i(x_i)$ are distribution functions normalised over the appropriate ranges of the x_i. Values of the x_i distributed in the correct way were obtained either by the "direct" method or by use of the "rejection" technique (Butler [3]) from pseudo-random numbers uniformly distributed in the range (0, 1). The pseudo-random numbers themselves were generated by a congruential process.

For example, x_6 can be expressed in terms of the variable ξ lying in range (0, 1) by means of the transformation

$$x_6^2 = (x_6)_{\min}^2 \cos^2(\tfrac{1}{2}\pi\xi) + (x_6)_{\max}^2 \sin^2(\tfrac{1}{2}\pi\xi).$$

The rest of the integrand was then evaluated at each set of the x_i so obtained.

References

1) R. L. Pease and H. Feshbach, Phys. Rev. **88** (1952) 945
2) G. Abraham, L. Cohen and A. S. Roberts, Proc. Phys. Soc. **68** (1955) 265
3) Symposium on Monte Carlo Methods (Wiley, 1956); in particular the article by J. W. Butler, p. 249
4) J. M. Hammersley and K. W. Morton, Proc. Camb. Phil. Soc. A **52** (1956) 449
5) H. Feshbach and J. Schwinger, Phys. Rev. **84** (1952) 194

7.A *Nuclear Physics* **13** (1959) 132—135; © *North-Holland Publishing Co., Amsterdam*
Not to be reproduced by photoprint or microfilm without written permission from the publisher

UNSTABLE STATES AND THE SEPARABLE POTENTIAL MODEL

D. B. FAIRLIE
Pembroke College, Cambridge
and
J. C. POLKINGHORNE
Trinity College, Cambridge

Received 25 June 1959

Abstract: A model based on a separable potential is investigated and it is shown that the unstable states can be associated with poles of the continuation of the scattering amplitude into the second Riemann sheet.

1. Introduction

The problem of the description of unstable states has recently aroused a considerable amount of discussion [1–5]). In particular several authors [3–5]) have shown that Peierls' conjecture [6]) that these states should be associated with poles of the propagator when this is continued into its multiple Riemann sheets is true for the Lee model. In view of the interest of this result it may be worthwhile to establish it for another and rather different model. In this paper we consider several different particles interacting through a separable potential. The bound states that can exist when the particles only interact with themselves can become unstable when an interaction is introduced linking different particles. This behaviour is shown to be reflected mathematically in the appearance of a pole in the second Riemann sheet of the scattering amplitude. In the weak coupling limit the real and imaginary parts of this pole are related in the expected manner to the mass and lifetime of the unstable state.

The model that we consider is, of course, just a simple quantal system. However, the problem of the description of unstable states is common to the whole of quantum mechanics and is not restricted to quantum field theory. In contrast with the Lee model the states that become unstable are produced by the interaction and do not need for their description a separate dynamical entity such as the V-particle field.

The separable potential model has already been used to discuss the solutions of the Low equation [7, 8]) and has been used recently by Lee and Klein [9]) to discuss scattering resonances. The latter discussion is closely related to

the work of this paper. Indeed, unstable states and resonances are but two different aspects of the result of the appearance of poles in the second sheet of the scattering amplitude.

2. The Reciprocal Low Equation

We consider a non-relativistic system with free Hamiltonian H_0 and total Hamiltonian $H = H_0+V$. We shall suppose that the eigenstates of H_0 are simply states describing different types of particles:

$$H_0|k, \alpha\rangle = E_k{}^{\alpha}|k, \alpha\rangle, \tag{1}$$

where k is the momentum and α denotes the type of particle. The eigenstates of H will consist of the corresponding incoming wave states:

$$H|k^+, \alpha\rangle = E_k{}^{\alpha}|k^+, \alpha\rangle \tag{2}$$

together with possible bound states. The interaction Hamiltonian V is supposed to be separable:

$$\langle k', \beta|V|k, \alpha\rangle = \lambda g_\beta{}^* g_\alpha V_\beta{}^*(k')V_\alpha(k). \tag{3}$$

In (3) it is convenient to choose standard functions of the momenta, $V_\alpha(k)$, and to determine the strengths of the interactions by the coupling constants, g_α. The factor λ is $+1$ or -1 according as the self interaction of particles is to be repulsive or attractive.

The form of (3) enables us to define a scattering amplitude by the equation

$$\langle k'^+, \beta|V|k, \alpha\rangle = g_\beta{}^* V_\beta{}^*(k')g_\alpha V_\alpha(k)h_\beta(k'); \tag{4}$$

$h_\beta(k')$ is the amplitude for elastic scattering of the β-type particles. The amplitudes for inelastic scattering (change of particle type) are trivially related to the elastic amplitudes for the separable potential case and are of no interest to us in this paper.

As usual the theory is most readily solved by considering the inverse of $h_\beta(k)$ and forming the reciprocal Low equation [8]). A straightforward calculation yields

$$H_\beta(k) = \frac{1}{h_\beta(k)} = \lambda+\sum_\alpha \int \mathrm{d}k' \, \frac{|g_\alpha|^2|V_\alpha(k')|^2}{E_{k'}^{\alpha}-E_k{}^{\beta}-i\varepsilon}. \tag{5}$$

3. Bound States and Unstable States

We consider for simplicity a system in which there are just two types of particle and initially suppose that $g_1 \neq 0$, $g_2 = 0$. Then, the first type of particle interacts with itself and if the interaction is attractive ($\lambda = -1$) and sufficiently strong a bound state can exist. It is convenient to define the function

$$H_1(z) = -1+\int \mathrm{d}k' \frac{|g_1|^2|V_1{}^2(k')|}{E^1_{k'}-z}, \tag{6}$$

which is an analytic function of the complex variable z in the complex plane cut along the real axis from $E_0{}^1$ (the minimum value of $E_k{}^1$) to $+\infty$. The inverse scattering amplitude $H_1(k)$ is given by the limit of $H_1(z)$ as $z \to E_k$ from above the real axis. Consideration of the imaginary part of $H_1(z)$ shows that $H_1(z)$ can only vanish on the real axis off the cut. The vanishing of $H_1(z)$ gives a pole in the scattering amplitude which would correspond to the existence of a bound state. The bound state energy is given by the (unique) root E of the equation

$$-1+\int \mathrm{d}k' \frac{|g_1|^2|V_1{}^2(k')|}{E^1_{k'}-E} = 0. \tag{7}$$

This equation can also be derived from the Schrödinger equation for the system.

Suppose now that g_2 is no longer zero. The interaction couples particles of the first and second types, and if $E > E_0{}^2$ (the minimum value of $E^2_{k'}$), so that the original bound state of the first particle lies in the continuum of energy eigenstates of the second type of particle, we expect that the bound state now becomes unstable. This is indeed the case. Eq. (6) is replaced by

$$H_1(z) = -1+\int \mathrm{d}k' \frac{|g_1|^2|V_1{}^2(k')|}{E^1_{k'}-z} + \int \mathrm{d}k' \frac{|g_2|^2|V_2{}^2(k')|}{E^2_{k'}-z} \tag{8}$$

and the cut now extends from $E_0{}^2$ to $+\infty$. Therefore, there is no longer a zero at E, and if g_2 is sufficiently small and $E_0{}^2$ and E sufficiently separated, it is easy to see that there is no longer a bound state.

If we assume† that $\sum_{E_{k'}{}^2=E}|V_2{}^2(k')|$ is an analytic function $V(E)$ of the energy E, we can continue $H_1(z)$ across the cut from $E_0{}^2$ to $E_0{}^1$ into the second Riemann sheet by the equation

$$H'_1(z) = H_1(z)+2\pi i|g_2|^2V(z). \tag{9}$$

In the weak coupling approximation (g_2 small), there is then a zero in the second sheet at $x-iy$ where

$$-1+\int \mathrm{d}k' \frac{|g_1|^2|(V_1{}^2(k')|}{E^1_{k'}-x} + \mathrm{P}\int \mathrm{d}k' \frac{|g_2|^2|V_2{}^2(k')|}{E^2_{k'}-x} = 0, \tag{10}$$

$$y = \frac{\pi|g_2|^2V(x)}{\int \mathrm{d}k' \dfrac{|g_1|^2|V_1{}^2(k')|}{(E^1_{k'}-x)^2}}. \tag{11}$$

This gives a pole in the second sheet of the continuation of the scattering amplitude.

† Cf. the discussion of Lévy [5]) on this point for the Lee model.

As in the case of the Lee model [5]), if a continuation is made across the cut from E_0^1 to $+\infty$ into the third Riemann sheet, a spurious pole is found whose imaginary part does not go to zero as g_2 tends to zero.

One of us (D. B. F.) wishes to thank the Department of Scientific and Industrial Research for a maintenance grant.

References

1) V. Glaser and G. Källén, Nuclear Physics **2** (1956) 706
2) P. T. Matthews and A. Salam, Phys. Rev. **112** (1958) 283
3) H. Araki, Y. Munakata, M. Kawaguchi and T. Gôto, Progr. Theor. Phys. **17** (1957) 419
4) G. Höhler, Zeits. f. Phys. **152** (1958) 546
5) M. Lévy, Nuovo Cimento **13** (1959) 115
6) R. E. Peierls, Proceedings of the 1954 Glasgow Conference (Pergamon Press, 1955) p. 296
7) R. Haag, Nuovo Cimento **5** (1957) 203
8) D. B. Fairlie and J. C. Polkinghorne, Nuovo Cimento **8** (1958) 555
9) B. W. Lee and A. Klein, to be published

4.A:6.B *Nuclear Physics* **13** (1959) 136—139; © *North-Holland Publishing Co., Amsterdam*
Not to be reproduced by photoprint or microfilm without written permission from the publisher

RELATIVISTIC COULOMB WAVE FUNCTION WITH DEFINITE ASYMPTOTIC MOMENTUM AND POLARIZATION

A. DELOFF
Institute for Nuclear Research, Warsaw

Received 23 March 1959

Abstract: A relativistic Coulomb wave function with definite asymptotic momentum is given in the form of an operator A acting on a plane wave spinor u.

1. Introduction

The Dirac equation with Coulomb potential has been solved so far only in the *jlm* representation [1]). In some problems, and especially those in which polarized electrons are involved, the function ψ_{jlm} is very inconvenient because it does not describe particles in a definite momentum and polarization state. Recently [2]), the author attempted to find the relativistic wave function $\psi(\mathbf{r}, \mathbf{p}, \sigma)$, with definite asymptotic momentum $\mathbf{p}$ and polarization σ, which could be applied to the β-decay theory. However, the wave function given in ref. [2]) is not exact since it contains some multipole expansions in which only terms necessary for allowed and first forbidden transitions have been kept.

In this note we give a Coulomb wave function in an exact and much simpler form $A(\mathbf{r}, \mathbf{p})u(\mathbf{p}, \sigma)$, where the operator $A(\mathbf{r}, \mathbf{p})$ is built up of Dirac matrices and acts on a plane wave spinor. This wave function is very convenient for the evaluation of matrix elements by the usual method of projection operators and traces.

2. Theory

Let us expand the unknown function $\psi(\mathbf{r}, \mathbf{p}, \sigma)$ in a complete set of spherical waves [2]):

$$\overset{\text{in}}{\psi}{}^{\text{out}}(\mathbf{r}, \mathbf{p}, \sigma) = \sum_{k,\mu} a_{k\mu}(\mathbf{p}, \sigma) \mathrm{e}^{\mp i\Delta_k} \psi_{k\mu} \tag{1}$$

where $k = \pm 1, \pm 2, \ldots$ determines j and l ($j = |k| - \frac{1}{2}$, $l = j + \frac{1}{2}k/|k|$), and Δ_k is the Coulomb phase shift given in ref. [1]):

$$\Delta_k = \delta_k(Z) - \delta_k(0),$$

$$\delta_k = -\arg \Gamma(\gamma + i\eta) + \tfrac{1}{2} \arg \frac{-k + i\eta\,(m/W)}{\gamma + i\eta} - \tfrac{1}{2}\pi\gamma + \eta \log 2pr,$$

$$\eta = Ze^2 W/p, \quad \gamma = \sqrt{k^2 - (Ze^2)^2}.$$

By "in" and "out" we denote wave functions having the asymptotic behaviour of a plane wave plus an ingoing or outgoing spherical wave. We take the spherical wave function as in ref. [3]):

$$\psi_{k\mu} = \begin{pmatrix} g_k \chi_k{}^{\mu} \\ i f_k \chi_{-k}^{\mu} \end{pmatrix},$$

where the spherical spinors $\chi_k{}^{\mu}(\hat{\mathbf{r}})$ (where $\hat{\mathbf{r}} = \mathbf{r}/r$) are defined in ref. [1]) and the radial Dirac solutions g_k and f_k are defined as in ref. [3]).

The unknown coefficients $a_{k\mu}(\mathbf{p}, \sigma)$ can easily be found by putting the potential equal to zero. In this case the left side of (1) is the usual plane wave and on the right side the following alterations should be introduced:

$$\begin{aligned} &\Delta_k \to 0, \\ &g_k \to \mathring{g}_k = [p^2(W+m)/\pi W]^{\frac{1}{2}} S_k j_{l(k)}(pr), \\ &f_k \to \mathring{f}_k = [p^2(W-m)/\pi W]^{\frac{1}{2}} j_{l(-k)}(pr), \end{aligned} \tag{2}$$

where $S_k = k/|k|$, $j_{l(\pm k)}(pr)$ is the spherical Bessel function, W and p are energy and momentum. Taking the above substitutions into account we have, instead of (1),

$$(2\pi)^{-\frac{3}{2}} u(\mathbf{p}, \sigma) e^{i\mathbf{p}\cdot\mathbf{r}} \equiv (2\pi)^{-\frac{3}{2}} N \begin{pmatrix} \chi_{\frac{1}{2}}{}^{\sigma} \\ \dfrac{\boldsymbol{\sigma}\cdot\mathbf{p}}{W+m} \chi_{\frac{1}{2}}{}^{\sigma} \end{pmatrix} e^{i\mathbf{p}\cdot\mathbf{r}} = \sum_{k,\mu} a_{k\mu}(\mathbf{p}, \sigma) \begin{pmatrix} \mathring{g}_k \chi_k{}^{\mu} \\ i\mathring{f}_k \chi_{-k}^{\mu} \end{pmatrix}, \tag{3}$$

where $N = [(W+m)/2W]^{\frac{1}{2}}$ and $\chi_{\frac{1}{2}}{}^{\sigma}$ are Pauli spinors.

We can determine $a_{k\mu}(\mathbf{p}, \sigma)$ by considering only one of the spinors on both sides of eq. (3), for example the upper one. Multiplying the upper part of (3) by $\chi_k{}^{\mu\dagger}$ from the left and integrating over angles and summing over the spin variable we obtain, using the orthogonality of $\chi_k{}^{\mu}$,

$$\mathring{g}_k a_{k\mu}(\mathbf{p}, \sigma) = N(2\pi)^{-\frac{3}{2}} \int e^{i\mathbf{p}\cdot\mathbf{r}} (\chi_k{}^{\mu}, \chi_{\frac{1}{2}}{}^{\sigma}) d\Omega. \tag{4}$$

Expanding the exponent in (4) into spherical harmonics the integration can easily be performed and we have for $a_{k\mu}(\mathbf{p}, \sigma)$ two equivalent expressions:

$$a_{k\mu}(\mathbf{p}, \sigma) = p^{-1} i^{l(k)} S_k (\chi_k{}^{\mu}(\hat{\mathbf{p}}), \chi_{\frac{1}{2}}{}^{\sigma}), \tag{5}$$

$$a_{k\mu}(\mathbf{p}, \sigma) = -p^{-1} i^{l(k)} S_k \left(\chi_{-k}^{\mu}(\hat{\mathbf{p}}), \frac{\boldsymbol{\sigma}\cdot\mathbf{p}}{p} \chi_{\frac{1}{2}}{}^{\sigma} \right), \tag{6}$$

where the spherical spinors $\chi_k{}^{\mu}$ now depend on $\hat{\mathbf{p}} = \mathbf{p}/p$. Formula (6) can be obtained from (5) with the help of the useful relation [1])

$$\frac{\boldsymbol{\sigma}\cdot\mathbf{p}}{p} \chi_k{}^{\mu}(\hat{\mathbf{p}}) = -\chi_{-k}^{\mu}(\hat{\mathbf{p}}). \tag{7}$$

Inserting expressions (5) and (6) into (1) we may express the wave function $\overset{\text{in}}{\psi}{}^{\text{out}}(\mathbf{r}, \mathbf{p}, \sigma)$ in the form of an operator acting on a plane wave spinor:

$$\overset{\text{in}}{\psi}{}^{\text{out}}(\mathbf{r}, \mathbf{p}, \sigma) = \frac{1}{p} \sum_{k\mu} i^{lk} S_k e^{\mp i\Delta_k} \begin{pmatrix} g_k \chi_k{}^{\mu}(\hat{\mathbf{r}}) \chi_k{}^{\mu\dagger}(\hat{\mathbf{p}}) & 0 \\ 0 & -if_k \dfrac{W+m}{p} \chi_{-k}^{\mu}(\hat{\mathbf{r}}) \chi_{-k}^{\mu\dagger}(\hat{\mathbf{p}}) \end{pmatrix} \begin{pmatrix} \chi_{\frac{1}{2}}{}^{\sigma} \\ \dfrac{\boldsymbol{\sigma} \cdot \mathbf{p}}{W+m} \chi_{\frac{1}{2}}{}^{\sigma} \end{pmatrix}. \quad (8)$$

The expressions $\sum_\mu \chi_k{}^{\mu} \chi_k{}^{\mu\dagger}$ and $\sum_\mu \chi_{-k}^{\mu} \chi_{-k}^{\mu\dagger}$, which are 2×2 matrices, can be written as linear combinations of Pauli $\boldsymbol{\sigma}$ matrices:

$$\sum_\mu \chi_k{}^{\mu}(\hat{\mathbf{r}}) \chi_k{}^{\mu\dagger}(\hat{\mathbf{p}}) = A_k + B_k \boldsymbol{\sigma} \cdot \hat{\mathbf{r}}\, \boldsymbol{\sigma} \cdot \hat{\mathbf{p}}. \quad (9)$$

$$\sum_\mu \chi_{-k}^{\mu}(\hat{\mathbf{r}}) \chi_{-k}^{\mu\dagger}(\hat{\mathbf{p}}) = A_k \boldsymbol{\sigma} \cdot \hat{\mathbf{r}}\, \boldsymbol{\sigma} \cdot \hat{\mathbf{p}} + B_k, \quad (10)$$

where A_k and B_k are scalar functions depending on the angle θ between the vectors $\mathbf{r}$ and $\mathbf{p}$. Taking the traces of the matrices given by (9) and (10), and using some orthogonality relations of the Clebsch-Gordan coefficients occurring in $\chi_k{}^{\mu}$, we obtain two algebraic equations for A_k and B_k:

$$\begin{aligned} A_k + B_k \cos\theta &= \frac{|k|}{4\pi} P_l(\cos\theta), \\ A_k \cos\theta + B_k &= \frac{|k|}{4\pi} P_{\bar{l}}(\cos\theta), \end{aligned} \quad (11)$$

where $\bar{l} \equiv l(-k)$. Introducing the derivatives $P'_l(\cos\theta) \equiv \mathrm{d}P_l(\cos\theta)/\mathrm{d}\cos\theta$ of the Legendre polynomials, we can write A_k and B_k in a compact form:

$$\begin{aligned} 4\pi A_k &= -S_k P'_{\bar{l}}(\cos\theta), \\ 4\pi B_k &= S_k P'_l(\cos\theta). \end{aligned} \quad (12)$$

Taking into account equations (9), (10) and (12), we get from (8), if we introduce the normalized plane wave spinor $u(\mathbf{p}, \sigma)$ given by (3),

$$\overset{\text{in}}{\psi}{}^{\text{out}}(\mathbf{r}, \mathbf{p}, \sigma) = \frac{(2W)^{\frac{1}{2}}}{4\pi p} \sum_k i^l e^{\mp i\Delta_k} \left\{ \tfrac{1}{2}(1+\beta)[-P'_{\bar{l}} + P'_l\, \boldsymbol{\alpha} \cdot \hat{\mathbf{r}}\, \boldsymbol{\alpha} \cdot \hat{\mathbf{p}}] \frac{g_k}{(W+m)^{\frac{1}{2}}} \right.$$
$$\left. -\tfrac{1}{2}(1-\beta)[P'_l - P'_{\bar{l}}\, \boldsymbol{\alpha} \cdot \hat{\mathbf{r}}\, \boldsymbol{\alpha} \cdot \hat{\mathbf{p}}] \frac{if_k}{(W-m)^{\frac{1}{2}}} \right\} u(\mathbf{p}, \sigma). \quad (13)$$

We can eliminate from the formula (13) the operator $\boldsymbol{\alpha} \cdot \mathbf{p}$ by making use of the fact that $u(\mathbf{p}, \sigma)$ is a solution of the free Dirac equation. The wave function $\overset{\text{in}}{\psi}{}^{\text{out}}(\mathbf{r}, \mathbf{p}\, \sigma)$, will then contain only the operators 1, β, $\boldsymbol{\alpha} \cdot \hat{\mathbf{r}}$, $\boldsymbol{\alpha} \cdot \hat{\mathbf{r}}\beta$:

$$\overset{\text{in}}{\psi}{}^{\text{out}}(\mathbf{r}, \mathbf{p}, \sigma) = \frac{(2W)^{\frac{1}{2}}}{8\pi p} \sum_k i^l e^{\mp i\Delta_k} \left\{ -\left[\frac{g_k P'_{\bar{l}}}{(W+m)^{\frac{1}{2}}} + \frac{if_k P'_l}{(W-m)^{\frac{1}{2}}} \right] - \beta \left[\frac{g_k P'_{\bar{l}}}{(W+m)^{\frac{1}{2}}} - \frac{if_k P'_l}{(W-m)^{\frac{1}{2}}} \right] \right.$$
$$\left. + \boldsymbol{\alpha} \cdot \hat{\mathbf{r}} \left[\frac{g_k P'_l}{(W-m)^{\frac{1}{2}}} + \frac{if_k P'_{\bar{l}}}{(W+m)^{\frac{1}{2}}} \right] + \boldsymbol{\alpha} \cdot \hat{\mathbf{r}}\, \beta \left[\frac{-g_k P'_l}{(W-m)^{\frac{1}{2}}} + \frac{if_k P'_{\bar{l}}}{(W+m)^{\frac{1}{2}}} \right] \right\} u(\mathbf{p}, \sigma). \quad (14)$$

It is remarkable that if we multiply the right side of (14) by $-\boldsymbol{\alpha}\cdot\hat{\mathbf{r}}$ and interchange g_k and if_k, the wave function $\overset{\text{in}}{\psi}{}^{\text{out}}(\mathbf{r}, \mathbf{p}, \sigma)$ remains unaltered. This is a consequence of the following identity, based on the relation (7):

$$-\boldsymbol{\alpha}\cdot\hat{\mathbf{r}}\begin{pmatrix} if_k\chi_k{}^{\mu} \\ g_k\,\chi^{\mu}_{-k}\end{pmatrix} = \begin{pmatrix} g_k\,\chi_k{}^{\mu} \\ if_k\chi^{\mu}_{-k}\end{pmatrix}. \tag{15}$$

Taking the above identity into account, we can replace $\psi_{k\mu}$ by the left side of (15) already in our starting formula (1).

The wave function obtained by the author in ref. [2]) was just that resulting from formula (14) when only terms proportional to P'_1 and P'_2 are kept.

The author is much indebted to B. Kuchowicz for helpful discussions.

References

1) Rose, Biedenharn and Arfken, Phys. Rev. **85** (1952) 5
2) A. Deloff, Bull. Ac. Pol. Sc. **6** (1958) 327
3) T. Kotani, Progr. Theor. Phys. **14** (1955) 379

7.B *Nuclear Physics* **13** (1959) 140—149; © *North-Holland Publishing Co., Amsterdam*
Not to be reproduced by photoprint or microfilm without written permission from the publisher

ON THE CORRESPONDENCE PRINCIPLE IN QUANTUM ELECTRODYNAMICS

G. M. PROSPERI and A. SCOTTI

Istituto Nazionale di Fisica Nucleare, Sezione di Milano

and

Istituto di Scienze Fisiche dell'Università degli Studi di Milano

Received 27 April 1959

Abstract: In this paper we start from a simplified version of quantum electrodynamics: precisely, we describe the charged particles by means of a quantized Schrödinger field $\psi(\mathbf{x}, t)$ interacting with a quantized and an external electromagnetic field.

We introduce the operator $q_k(t) = \mathrm{d}_3\mathbf{x}\, x_k \psi^+\psi$ and study the time evolution of its expectation value $\langle q_k \rangle = \langle \Psi | q_k | \Psi \rangle$ for a state $|\Psi\rangle$ with only one incoming charged particle and a certain initial condition on the radiation field.

Under the assumption that the indeterminacies Δq_k and $\Delta \dot{q}_k$ be negligible and the gradients of the external field be sufficiently small, we find that $\langle q_k \rangle$ obeys a third order differential equation which coincides with the classical non-relativistic equation of motion of Lorentz.

1. Introduction

Let us consider the equations of motion of a charged particle in an electromagnetic field generated by a given source in classical electrodynamics:

$$m_0 \ddot{x}^\mu = F^{\mu\nu} \dot{x}_\nu \qquad (F^{\mu\nu}_{|\nu} = j^\mu). \tag{1}$$

These equations are derived essentially from results of experiments in which charged particles interact at distances which are great compared to their dimensions. The effects of the interaction of the particle with its own field are here neglected. As is well known, to describe these effects one generalizes eq. (1) by introducing into the right-hand side not only the field generated by other particles $F^{(\mathrm{ext})\mu\nu}$, but also the field generated by the particle itself $F^{(\mathrm{self})\mu\nu}$, thus giving the interactions at very short distances (such as those which come into play when one wants to study the reaction of the particle on itself) the same formal structure as those at great distances. Dirac succeeded in this way in re-expressing $F^{(\mathrm{self})\mu\nu}$ by means of the dynamical variables of the particle and obtained the following equation [1]):

$$(m_0 + m_{\mathrm{em}})\ddot{x}^\mu - \frac{e^2}{6\pi c^3}\left(\dddot{x}^\mu + \frac{\dot{x}^\mu \dot{x}^\nu}{c^2}\dddot{x}_\nu\right) = \frac{e}{c} F^{(\mathrm{ext})\mu\nu}\dot{x}_\nu. \tag{2}$$

This equation is the relativistic generalization of that previously deduced

in an analogous way by Lorentz in non-relativistic electrodynamics [2]):

$$(m_0+m_{\mathrm{em}})\ddot{\mathbf{q}}-\frac{e^2}{6\pi c^3}\dddot{\mathbf{q}}=\mathbf{E}^{(\mathrm{ext})}(\mathbf{q})+\frac{e}{c}\dot{\mathbf{q}}\wedge\mathbf{H}^{(\mathrm{ext})}(\mathbf{q}). \tag{3}$$

The quantity m_{em} is divergent and can be written symbolically in the following way, for the case of eq. (3):

$$m_{\mathrm{em}}=\frac{e^2}{6\pi c^2}\int \mathrm{d}_3\mathbf{r}\,\frac{\delta(\mathbf{r})}{r}. \tag{4}$$

In elementary quantum mechanics, the motion of a charged particle is described by relativistic equations such as the Klein-Gordon or Dirac equations and the electromagnetic field is treated as a given classical function of the space-time coordinates. In second quantization, charged particles are described as quanta of a field $\psi(\mathbf{x}, t)$ which obeys equations formally identical to those of the first quantization; the electromagnetic field is now also quantized and its sources are the densities of charge and current expressed through the field $\psi(\mathbf{x}, t)$: in this way the interaction of a charged particle with itself is automatically included in the theory.

The passage from the former to the latter formulation of quantum theory appears in this way as the result of a formal generalization analagous to the one made in classical theory in passing from eq. (1), in which there are no reaction terms, to eq. (2). But while it has been shown [3]) that the equations of the first quantization in the classical limit (that is to say when the indeterminacy of the position and momentum of the particle, and the intensity and gradient of the external electromagnetic field, are such as to allow the description of the particle as a mass point) go over into eq. (1), it is not a priori clear what happens when one makes the corresponding limit starting from the complete electrodynamics in second quantization.

This problem has never been treated in its full generality. Some authors [4, 5]) † studied a simplified version, starting from a theory in which the electromagnetic field is quantized, but the charged particle is described in first quantization and in the non-relativistic approximation. With the aim of studying the formal aspects of this problem in second quantization, we shall now treat it in describing the charged particles by means of a quantized field which satisfies the non-relativistic Schroedinger equation. Having defined a suitable position operator, we study its expectation value in a state corresponding to one incoming electron and a certain initial condition for the electromagnetic field: this quantity, which under reasonable assumptions about the state just mentioned, can be thought of as the classical position of the charged particle, is found to obey the equation (3) of Lorentz. The only approximation made in deriving this result consists in neglecting expectation

† C.f. in this connection refs. [6–10]).

values of powers greater than one of the time derivatives of the position operator, and is physically equivalent to that made by Lorentz [2]) in deducing eq. (3). On the other hand, in the complete relativistic case, owing to the appearance of virtual pairs, some simplifications characteristic of the model studied here are no longer present and one would not obtain eq. (2) of Dirac. We hope to return to this problem in a future paper.

2. Field Equations and Definition of State

In the Heisenberg picture and in the Lorentz gauge (which we will use throughout the following) the equations of motion for the Schroedinger field and the electromagnetic potentials are

$$\frac{1}{2m_0}\sum_1^3{}_k\left(\frac{\hbar}{i}\frac{\partial}{\partial x_k}-\frac{e}{c}A_k(\mathbf{x},t)\right)^2\psi(\mathbf{x},t)+eA_0(\mathbf{x},t)\psi(\mathbf{x},t)=i\hbar\frac{\partial\psi(\mathbf{x},t)}{\partial t},$$

$$\Box A_\mu^{(\mathrm{rad})}(\mathbf{x},t)=-j_\mu(\mathbf{x},t), \tag{5}$$

$$A_\mu(\mathbf{x},t)=A_\mu^{(\mathrm{ext})}(\mathbf{x},t)+A_\mu^{(\mathrm{rad})}(\mathbf{x},t)\quad(\mu=1,2,3,4;\ A_4=iA_0),$$

where

$$j_k(\mathbf{x},t)=\frac{e}{mc}\left[\frac{\hbar}{2i}\left(\psi^+(\mathbf{x},t)\frac{\partial}{\partial x_k}\psi(\mathbf{x},t)-\frac{\partial}{\partial x_k}\psi^+(\mathbf{x},t)\psi(\mathbf{x},t)\right)-\frac{e}{c}A_k(\mathbf{x},t)\psi^+\psi\right]$$

$$=j_k^{(0)}(\mathbf{x},t)-\frac{e^2}{mc^2}A_k(\mathbf{x},t)\psi^+(\mathbf{x},t)\psi(\mathbf{x},t), \tag{6}$$

$$\frac{1}{i}j_4=\rho(\mathbf{x},t)=e\psi^+(\mathbf{x},t)\psi(\mathbf{x},t), \tag{7}$$

$$\frac{\partial}{\partial x_\mu}j_\mu=\operatorname{div}\mathbf{j}(\mathbf{x},t)+\frac{1}{c}\frac{\partial\rho(\mathbf{x},t)}{\partial t}=0. \tag{8}$$

The non-vanishing commutators of the field operators (for definiteness the charged particles are supposed to be fermions) are the following:

$$\{\psi(\mathbf{x},t),\psi^+(\mathbf{x}',t)\}=\delta(\mathbf{x}-\mathbf{x}'), \tag{9}$$

$$\left[A_k^{(\mathrm{rad})}(\mathbf{x},t),\frac{1}{c^2}\frac{\partial A_k^{(\mathrm{rad})}(\mathbf{x}',t)}{\partial t}\right]=\left[A_0^{(\mathrm{rad})}(\mathbf{x},t),\frac{1}{c^2}\frac{\partial A_0^{(\mathrm{rad})}(\mathbf{x}',t)}{\partial t}\right]=i\hbar\delta(\mathbf{x}-\mathbf{x}'). \tag{10}$$

Eqs. (5) can be re-written in the following integral form:

$$\psi(\mathbf{x},t)=\psi^{(\mathrm{in})}(\mathbf{x},t)+\int \mathrm{d}_3\mathbf{x}'\,\mathrm{d}t'K_{\mathrm{ret}}(\mathbf{x}-\mathbf{x}',t-t')\phi(\mathbf{x}',t'), \tag{11}$$

$$A_\mu^{(\mathrm{rad})}(\mathbf{x},t)=A_\mu^{(\mathrm{in})}+\frac{1}{4\pi}\int \mathrm{d}_3\mathbf{x}'\,\frac{j_\mu\left(\mathbf{x}',t-\dfrac{|\mathbf{x}-\mathbf{x}'|}{c}\right)}{|\mathbf{x}-\mathbf{x}'|}, \tag{12}$$

where

$$\left(-\frac{\hbar^2}{2m_0}\Delta_2 - i\hbar\frac{\partial}{\partial t}\right)K_{\text{ret}}(\mathbf{x}-\mathbf{x}', t-t') = \delta(\mathbf{x}-\mathbf{x}')\delta(t-t'),$$

$$K_{\text{ret}}(\mathbf{x}-\mathbf{x}', t-t') = 0 \quad \text{for} \quad t < t',$$

$$\phi(\mathbf{x}, t) = -\frac{1}{2m_0}\sum_1^3{}_k\left[\frac{e^2}{c^2}A_k{}^2(\mathbf{x}, t) - \frac{e}{c}\frac{\hbar}{i}\frac{\partial A_k(\mathbf{x}, t)}{\partial x_k} - \frac{2e}{c}A_k(\mathbf{x}, t)\frac{\partial}{\partial x_k}\right]\psi(\mathbf{x}, t)$$
$$-eA_0(\mathbf{x}, t)\psi(\mathbf{x}, t);$$

$\psi^{(\text{in})}(\mathbf{x}, t)$ and $A_\mu{}^{(\text{in})}(\mathbf{x}, t)$ represent the so-called incoming field and satisfy the free field equations. The operators $\psi^{(\text{in})+}$ and $\psi^{(\text{in})}$ create and annihilate, respectively, states with one incoming particle, the negative and positive frequency part of the operators $A_\mu{}^{(\text{in})}$ create and annihilate, respectively, states with one incoming photon.

As is well known, in this theory the physical and the bare vacuum coincide, a physical state with photons only coincides with the corresponding bare state, a state with an incoming electron and a certain state of the incoming electromagnetic field is in general a superposition of states with a bare particle and different numbers of photons and can be expressed in the following way:

$$|\Psi\rangle = \sum_{n=0}^{\infty}\sum_1^4{}_{\lambda_1\ldots\lambda_n}\int \varphi_n(\mathbf{z}, \mathbf{k}_1\lambda_1, \ldots, \mathbf{k}_n\lambda_n)|\mathbf{z}, \mathbf{k}_1\lambda_1, \ldots, \mathbf{k}_n\lambda_n, t\rangle \mathrm{d}_3\mathbf{z}\mathrm{d}_3\mathbf{k}_1 \ldots \mathrm{d}_3\mathbf{k}_n \quad (13)$$

where

$$|\mathbf{z}, \mathbf{k}_1\lambda_1, \ldots, \mathbf{k}_n\lambda_n, t\rangle = \psi^+(\mathbf{z}, t)a^+(\mathbf{k}_1\lambda_1, t)\ldots a^+(k_n\lambda_n, t)|0\rangle,$$

$$a^+(k\lambda, t) = \frac{1}{c}\sum_1^4{}_\mu e_\mu{}^{(\lambda)}\int \mathrm{d}_3\mathbf{x}\left(u_k\frac{\partial A_\mu}{\partial t} - \frac{\partial u_k}{\partial t}A_\mu\right), \quad u_k(\mathbf{x}, t) = \frac{1}{(2\pi\hbar)^{\frac{3}{2}}}\frac{1}{\sqrt{2|\mathbf{k}|}}\mathrm{e}^{i(\mathbf{k}\cdot\mathbf{x}-|\mathbf{k}|ct)},$$

is a state with a bare particle localized in $\mathbf{z}$ and n photons in the states $\mathbf{k}_1\lambda_1, \ldots, \mathbf{k}_n\lambda_n$ at time t. For short we shall write in the following

$$|\Psi\rangle = \int \mathrm{d}_3\mathbf{z}\mathrm{d}\alpha\varphi(\mathbf{z}, \alpha, t)|\mathbf{z}, \alpha, t\rangle. \quad (13')$$

The state (13) is to be further determined by means of a condition analagous to the classical one according to which the radiation field has to go to zero for $t \to -\infty$ (retarded potentials); we shall discuss this condition in subsection 3.2.

3. Equation of Motion for Mean Barycentre of Fermion Field

Let us now introduce the operator

$$q_k(t) = \frac{1}{e}\int \mathrm{d}_3\mathbf{x}\, x_k\, \rho(\mathbf{x}, t): \quad (14)$$

it represents the barycentre of the charge distribution of the Schroedinger

field. For brevity let us put $\langle q_k \rangle = \langle \Psi | q_k | \Psi \rangle$. Supposing that in the time interval of interest the state $|\Psi\rangle$ satisfies the conditions

$$\Delta q_k = \sqrt{\langle q_k{}^2 - \langle q_k \rangle^2 \rangle} \ll \delta q_k, \qquad \Delta \dot{q}_k = \sqrt{\langle \dot{q}_k{}^2 - \langle \dot{q}_k{}^2 \rangle \rangle} \ll \delta \dot{q}_k, \quad (15)$$

where δq_k and $\delta \dot{q}_k$ characterize the accuracy with which q_k and $\dot{q}_k$ are determined, we shall consider $\langle \mathbf{q} \rangle$ as the "classical" position of the particle, and deduce a differential equation for this quantity.

From the continuity equation we obtain

$$\dot{q}_k(t) = \frac{c}{e} \int \mathrm{d}_3\mathbf{x}\, j_k(\mathbf{x}, t), \quad (16)$$

$$\overset{(n)}{q}_k(t) = \frac{c}{e} \int \mathrm{d}_3\mathbf{x} \frac{\partial^{n-1} j_k(\mathbf{x}, t)}{\partial t^{n-1}}. \quad (17)$$

From eq. (5), in a way formally identical to that used in first quantization for the mean value of the position [3]), we get

$$\begin{aligned} m_0 \ddot{q}_k(t) = &\int \mathrm{d}_3\mathbf{x} [\rho(\mathbf{x}, t) E_k{}^{(\mathrm{rad})}(\mathbf{x}, t) + (\mathbf{j}(\mathbf{x}, t) \wedge \mathbf{H}^{(\mathrm{rad})}(\mathbf{x}, t))_k] \quad (18) \\ &+ \int \mathrm{d}_3\mathbf{x} [\rho(\mathbf{x}, t) E_k{}^{(\mathrm{ext})}(\mathbf{x}, t) + (\mathbf{j}(\mathbf{x}, t) \wedge \mathbf{H}^{(\mathrm{ext})}(\mathbf{x}, t))_k]. \end{aligned}$$

The evaluation of the expectation value of the second term can be carried out very easily and will be discussed in subsection 3.3. The main point, therefore, is the study of the expectation value of the first term.

Expanding (12) in a series of powers of the retardation parameter $|\mathbf{x}-\mathbf{x}'|/c$, we may write

$$\begin{aligned} A_0{}^{(\mathrm{rad})}(\mathbf{x}, t) &= A_0{}^{(\mathrm{in})}(\mathbf{x}, t) + A_0{}^{(\mathrm{ret})}(\mathbf{x}, t) \\ &= A_0{}^{(\mathrm{in})}(\mathbf{x}, t) + \frac{1}{4\pi} \sum_{n=0}^{\infty} (-1)^n \frac{1}{n! c^n} \int \mathrm{d}_3\mathbf{x}' \frac{\partial^n \rho(\mathbf{x}', t)}{\partial t^n} |\mathbf{x}-\mathbf{x}'|^{-1}, \\ \mathbf{A}^{(\mathrm{rad})}(\mathbf{x}, t) &= \mathbf{A}^{(\mathrm{in})}(\mathbf{x}, t) + \mathbf{A}^{(\mathrm{ret})}(\mathbf{x}, t) \\ &= \mathbf{A}^{(\mathrm{in})}(\mathbf{x}, t) + \frac{1}{4\pi} \sum_{n=0}^{\infty} \frac{(-1)^n}{n! c^n} \int \mathrm{d}_3\mathbf{x}' \frac{\partial^n \mathbf{j}(\mathbf{x}', t)}{\partial t^n} |\mathbf{x}-\mathbf{x}'|^{n-1}. \end{aligned} \quad (19)$$

3.1. CONTRIBUTION FROM RETARDED POTENTIALS

For a state $|\Psi\rangle$ of the above-mentioned structure one easily verifies that the following relation holds true (see appendix 1):

$$\mathbf{j}(\mathbf{x}, t)|\Psi\rangle = \frac{1}{2c} \{\rho(\mathbf{x}, t), \dot{q}_k\} |\Psi\rangle. \quad (20)$$

Making use of the continuity equation, we have then

$$\frac{\partial \rho(\mathbf{x}, t)}{\partial t} |\Psi\rangle = -\tfrac{1}{2} \sum_k \left\{ \frac{\partial \rho(\mathbf{x}, t)}{\partial x_k}, \dot{q}_k \right\} |\Psi\rangle. \quad (21)$$

Differentiating n times these relations, we get

$$\frac{\partial^n j_k(\mathbf{x},t)}{\partial t^n}|\Psi\rangle = \tfrac{1}{2}\frac{1}{c}\{\rho(\mathbf{x},t),\overset{(n+1)}{q_k}(t)\}|\Psi\rangle + \mathrm{O}(\overset{(r)\,(s)}{q\;q})|\Psi\rangle \qquad (n>0),$$
$$\frac{\partial^n \rho(\mathbf{x},t)}{\partial t^n}|\Psi\rangle = -\tfrac{1}{2}\sum_k\left\{\frac{\partial\rho(\mathbf{x},t)}{\partial x_k},\overset{(n)}{q_k}(t)\right\}|\Psi\rangle + \mathrm{O}(\overset{(r)\,(s)}{q\;q})|\Psi\rangle \qquad (n>1), \tag{22}$$

where $\mathrm{O}(\overset{(r)\,(s)}{q\;q})$ is an operator at least of the second order in the time derivative of $\mathbf{q}(t)$. Expectation values of operators of this type will always be neglected in the following: this closely corresponds to what is done in classical theory in deriving eq. (3) (see ref.[2])). Taking into account (19), (20), (21), (22), we have

$$\left\langle \int \mathrm{d}_3\mathbf{x}\,\mathbf{j}(\mathbf{x},t)\wedge \mathrm{rot}\,\mathbf{A}^{(\mathrm{ret})}(\mathbf{x},t)\right\rangle$$
$$= \frac{1}{4\pi}\sum_{n=0}^{\infty}\frac{(-1)^n}{c^n n!}\int \mathrm{d}_3\mathbf{x}\int \mathrm{d}_3\mathbf{x}'\left\langle \mathbf{j}(\mathbf{x},t)\wedge\left(\mathrm{grad}|\mathbf{x}-\mathbf{x}'|^{n-1}\wedge\frac{\partial^n\mathbf{j}(\mathbf{x}',t)}{\partial t^n}\right)\right\rangle \tag{23}$$
$$= \langle \mathrm{O}(\overset{(r)\,(s)}{q\;q})\rangle \approx 0,$$

$$\left\langle \frac{1}{c}\int \mathrm{d}_3\mathbf{x}\rho(\mathbf{x},t)\frac{\partial A_k^{(\mathrm{ret})}(\mathbf{x},t)}{\partial t}\right\rangle$$
$$= \frac{1}{4\pi}\sum_{n=0}^{\infty}\frac{(-1)^n}{c^{n+1}n!}\int \mathrm{d}_3\mathbf{x}\int \mathrm{d}_3\mathbf{x}'\left\langle \rho(\mathbf{x},t)\frac{\partial^{n+1}j_k(\mathbf{x}',t)}{\partial t^{n+1}}\right\rangle|\mathbf{x}-\mathbf{x}'|^{n-1} \tag{24}$$
$$= \frac{1}{4\pi}\sum_{n=0}^{\infty}\frac{(-1)^n}{2c^{n+2}n!}\int \mathrm{d}_3\mathbf{x}\int \mathrm{d}_3\mathbf{x}'\langle\rho(\mathbf{x},t)\{\rho(\mathbf{x}',t),\overset{(n+2)}{q_k}\}\rangle|\mathbf{x}-\mathbf{x}'|^{n-1} + \langle \mathrm{O}(\overset{(r)\,(s)}{q\;q})\rangle,$$

$$\left\langle \int \mathrm{d}_3\mathbf{x}\,\rho(\mathbf{x},t)\frac{\partial A_0^{(\mathrm{ret})}(\mathbf{x},t)}{\partial x_k}\right\rangle$$
$$= -\frac{1}{4\pi}\int \mathrm{d}_3\mathbf{x}\int \mathrm{d}_3\mathbf{x}'\langle\rho(\mathbf{x},t)\rho(\mathbf{x}',t)\rangle(x_k-x'_k)|\mathbf{x}-\mathbf{x}'|^{-3} \tag{25}$$
$$-\frac{1}{4\pi}\sum_{n=1}^{\infty}(-1)^n\frac{n-1}{2n!\,c^n}\sum_1^3{}_r\int \mathrm{d}_3\mathbf{x}\int \mathrm{d}_3\mathbf{x}'(x_k-x'_k)|\mathbf{x}-\mathbf{x}'|^{-3}\left\langle \rho(\mathbf{x},t)\left\{\frac{\partial\rho(\mathbf{x}',t)}{\partial x'_r},\overset{(n)}{q_k}(t)\right\}\right\rangle$$
$$+\langle \mathrm{O}(\overset{(r)\,(s)}{q\;q})\rangle.$$

(The term with $n=0$ in (23) is not divergent but zero for symmetry reasons; the term with $n=1$ is also zero.)

Use will be made of the following equations (see appendix 2):

$$\int \mathrm{d}_3\mathbf{x}\int \mathrm{d}_3\mathbf{x}'\langle\rho(\mathbf{x},t)[\rho(\mathbf{x}',t),\dot{q}_k(t)]\rangle|\mathbf{x}-\mathbf{x}'|^p = 0 \qquad (p\geqq -1), \tag{26}$$

$$\sum_r\int \mathrm{d}_3\mathbf{x}\int \mathrm{d}_3\mathbf{x}'\left\langle \rho(\mathbf{x},t)\left[\frac{\partial\rho(\mathbf{x}',t)}{\partial x'_r},\dot{q}_r(t)\right]\right\rangle(x_k-x'_k)|\mathbf{x}-\mathbf{x}'|^{p'} = 0 \quad (p'\geqq -3), \tag{26'}$$

and of those which can be deduced for $p \geqq 0$, $p' \geqq -1$ by differentiating these n times:

$$\int d_3\mathbf{x} \int d_3\mathbf{x}' \langle \rho(\mathbf{x}, t)[\rho(\mathbf{x}', t), \overset{(n)}{q_k}(t)]\rangle |\mathbf{x}-\mathbf{x}'|^p = \langle O(\overset{(r)}{q}\,\overset{(s)}{q})\rangle \approx 0, \tag{27}$$

$$\int d_3\mathbf{x} \int d_3\mathbf{x}' \sum_r \left\langle \rho(\mathbf{x}, t)\left[\frac{\partial \rho(\mathbf{x}', t)}{\partial x'_r}, \overset{(n)}{q_k}(t)\right]\right\rangle (x_k - x'_k)|\mathbf{x}-\mathbf{x}'|^{p'} = \langle O(\overset{(r)}{q}\,\overset{(s)}{q})\rangle \approx 0. \tag{27'}$$

We now notice that

$$\langle \mathbf{z}', \alpha', t | \int d_3\mathbf{x} \int d_3\mathbf{x}' \rho(\mathbf{x}, t)\rho(\mathbf{x}', t) \overset{(n+2)}{q}(t) |\mathbf{x}-\mathbf{x}'|^{n-1} | \mathbf{z}'', \alpha'', t\rangle$$

$$= e^2 \int d_3\mathbf{x} \int d_3\mathbf{x}' \delta(\mathbf{z}'-\mathbf{x})\delta(\mathbf{z}'-\mathbf{x}')|\mathbf{x}-\mathbf{x}'|^{n-1} \langle \mathbf{z}', \alpha', t | \overset{(n+2)}{q}(t) | \mathbf{z}'', \alpha'', t\rangle$$

$$= e^2 \int d_3\mathbf{x}' \delta(\mathbf{z}'-\mathbf{x}')|\mathbf{z}'-\mathbf{x}'|^{n-1} \langle \mathbf{z}', \alpha', t | \overset{(n+2)}{q}(t) | \mathbf{z}'', \alpha'', t\rangle$$

$$= e^2 \int d_3\mathbf{r}\, \delta(\mathbf{r}) r^{n-1} \langle \mathbf{z}', \alpha', t | \overset{(n+2)}{q}(t) | \mathbf{z}'', \alpha'', t\rangle.$$

Making use of (27) (27'), we have then

$$\tfrac{1}{2} \int d_3\mathbf{x} \int d_3\mathbf{x}' \langle \rho(\mathbf{x}, t)\{\rho(\mathbf{x}', t), \overset{(n+2)}{q}(t)\}\rangle |\mathbf{x}-\mathbf{x}'|^{n-1}$$

$$\approx \int d_3\mathbf{x} \int d_3\mathbf{x}' \langle \rho(\mathbf{x}, t)\rho(\mathbf{x}', t) \overset{(n+2)}{q}(t)\rangle |\mathbf{x}-\mathbf{x}'|^{n-1}$$

$$= e^2 \int d_3\mathbf{r}\, \delta(\mathbf{r}) r^{n-1} \langle \overset{(n+2)}{q}(t)\rangle = \begin{cases} e^2 \int d_3\mathbf{r} \dfrac{\delta(\mathbf{r})}{r} \langle \ddot{q}\rangle & \text{for } n = 0 \\ e^2 \langle \ddot{q}\rangle & \text{for } n = 1 \\ 0 & \text{for } n > 1. \end{cases}$$

And analogously, making use of (25') (26'), we obtain

$$\int d_3\mathbf{x} \int d_3\mathbf{x}' \langle \rho(\mathbf{x}, t)\rho(\mathbf{x}', t)\rangle (x_k - x_{k'})|\mathbf{x}-\mathbf{x}'|^{-3} = e^2 \int d_3\mathbf{r}\, r_k r^{-3} \delta(\mathbf{r}) = 0$$

$$\tfrac{1}{2} \sum_1^3{}_{k'} \int d_3\mathbf{x} \int d_3\mathbf{x}' \left\langle \rho(\mathbf{x}, t)\left\{\frac{\partial \rho(\mathbf{x}', t)}{\partial x'_k}, \overset{(n)}{q_{k'}}(t)\right\}\right\rangle (x_k - x'_k)|\mathbf{x}-\mathbf{x}'|^{n-3}$$

$$\approx \sum_1^3{}_{k'} \int d_3\mathbf{x} \int d_3\mathbf{x}' \left\langle \rho(\mathbf{x}, t) \frac{\partial \rho(\mathbf{x}', t)}{\partial x'_{k'}} \overset{(n)}{q_{k'}}(t)\right\rangle (x_k - x'_k)|\mathbf{x}-\mathbf{x}'|^{n-3}$$

$$= e^2 \sum_1^3{}_{k'} \int d_3\mathbf{r} \left(\delta_{kk'} + (n-3)\frac{r_k r_{k'}}{r^2}\right) r^{n-3} \delta(\mathbf{r}) \langle \overset{(n)}{q_{k'}}\rangle$$

$$= \tfrac{1}{3} e^2 n \int d_3\mathbf{r}\, r^{n-3} \delta(\mathbf{r}) \langle \overset{(n)}{q_k}(t)\rangle$$

$$= \begin{cases} \frac{2}{3} e^2 \int d_3\mathbf{r} \dfrac{\delta(\mathbf{r})}{r} \langle \ddot{q}\rangle & \text{for } n = 2 \\ e^2 \langle \dddot{q}_k\rangle & \text{for } n = 3 \\ 0 & \text{for } n > 3. \end{cases}$$

Thus, we obtain

$$\left\langle \int \mathrm{d}_3\mathbf{x}\,\rho(\mathbf{x},t)\left(\frac{1}{c}\frac{\partial A_k^{(\mathrm{ret})}(\mathbf{x},t)}{\partial t}+\frac{\partial A_0^{(\mathrm{ret})}(\mathbf{x},t)}{\partial x_k}\right)\right\rangle$$
$$\approx -\frac{e^2}{6\pi c^2}\int \mathrm{d}_3\mathbf{r}\,\frac{\delta(\mathbf{r})}{r}\langle\ddot{q}_k(t)\rangle+\frac{e^2}{6\pi c^3}\langle\dddot{q}_k(t)\rangle.$$

3.2. CONDITION ON INCOMING ELECTROMAGNETIC FIELD

Let us now consider the terms

$$\left\langle \int \mathrm{d}_3\mathbf{x}(\rho(\mathbf{x},t)\mathbf{E}^{(\mathrm{in})}(\mathbf{x},t)+\mathbf{j}(\mathbf{x},t)\wedge\mathbf{H}^{(\mathrm{in})}(\mathbf{x},t))\right\rangle. \tag{28}$$

Classically they are not present owing to the initial condition on the electromagnetic field:

$$\mathbf{E}^{(\mathrm{in})}=\mathbf{H}^{(\mathrm{in})}=0. \tag{29}$$

From the point of view of quantum theory a very natural condition seems to be the following:

$$A_\mu^{(\mathrm{in})(+)}|\Psi\rangle=0; \tag{30}$$

it corresponds to an initial state with no incoming photons. With such a condition we have

$$\langle\mathbf{E}^{(\mathrm{in})}(\mathbf{x},t)\rangle=\langle\mathbf{H}^{(\mathrm{in})}(\mathbf{x},t)\rangle=0. \tag{31}$$

Unfortunately, however, if (30) is satisfied the term (28) becomes divergent. On physical grounds, one expects instead this term to be zero: the complete study of this point is connected with the renormalization of the Schroedinger field; we shall not discuss it further at the moment, but intend to deal with it in a separate paper. In the following, we shall assume that the term (28) can be neglected. We then finally obtain

$$\left\langle \int \mathrm{d}_3\mathbf{x}\,\rho(\mathbf{x},t)\left(\frac{1}{c}\frac{\partial A_k^{(\mathrm{rad})}(\mathbf{x},t)}{\partial t}+\frac{\partial A_0^{(\mathrm{rad})}(\mathbf{x},t)}{\partial x_k}\right)\right\rangle$$
$$\approx -\frac{e^2}{6\pi c^2}\int \mathrm{d}_3\mathbf{r}\,\frac{\delta(\mathbf{r})}{r}\langle\dot{q}_k(t)\rangle+\frac{e^2}{6\pi c^3}\langle\dddot{q}_k(t)\rangle.$$

3.3. CONTRIBUTION FROM EXTERNAL FIELD

Eq. (20), taking into account the results obtained in the previous subsections, becomes

$$(m+m_{\mathrm{em}})\langle\ddot{q}_k(t)\rangle-\frac{e^2}{6\pi c^3}\langle\dddot{q}_k(t)\rangle$$
$$=\int \mathrm{d}_3\mathbf{x}\left[-\langle\rho(\mathbf{x},t)\rangle\left(\frac{\partial A_0^{(\mathrm{ext})}}{\partial x_k}+\frac{1}{c}\frac{\partial A_k^{(\mathrm{ext})}}{\partial t}\right)+(\langle\mathbf{j}(\mathbf{x}t)\rangle\wedge\mathrm{rot}\,\mathbf{A}^{(\mathrm{ext})}(\mathbf{x},t))_k\right],$$

with

$$m_{\mathrm{em}} = \frac{e^2}{6\pi c^2} \int \mathrm{d}_3 \mathbf{r}\, \frac{\delta(\mathbf{r})}{r}.$$

We have

$$\langle j_k(\mathbf{x}, t)\rangle = \tfrac{1}{2}\langle\{\rho(\mathbf{x}, t), \dot{q}_k(t)\}\rangle \approx \langle \dot{q}_k(t)\rangle\langle\rho(\mathbf{x}, t)\rangle.$$

If we now assume

$$\frac{1}{E_r^{(\mathrm{ext})}} \frac{\partial E_r^{(\mathrm{ext})}}{\partial x_k} \ll \frac{1}{\Delta q_k}, \qquad \frac{1}{H_r^{(\mathrm{ext})}} \frac{\partial H_r^{(\mathrm{ext})}}{\partial x_k} \ll \frac{1}{\Delta q_k},$$

remembering that for states such as (13) one has

$$\langle (q_k - \langle q_k\rangle)^2\rangle = \int (x_k - \langle q_k\rangle)^2 \langle\rho(\mathbf{x}, t)\rangle \mathrm{d}_3\mathbf{x},$$

we may write

$$m\langle\ddot{\mathbf{q}}\rangle - \frac{e^2}{6\pi c^3}\langle\dddot{\mathbf{q}}\rangle = e\left(\mathbf{E}^{(\mathrm{ext})}(\langle\mathbf{q}\rangle, t) + \frac{1}{c}\langle\dot{\mathbf{q}}\rangle \wedge \mathbf{H}^{(\mathrm{ext})}(\langle\mathbf{q}\rangle, t)\right), \tag{32}$$

$$m = m_0 + m_{\mathrm{em}}.$$

This equation indeed coincides with the equation (3) of Lorentz, as was also the case for the simpler versions of the problem studied in refs. [4,5]). The conditions imposed on the state (13) would need further examination; in particular, in connection with conditions (15), see ref. [11]) and the bibliography there quoted, and also ref. [12]).

We wish to thank Profs. P. Caldirola, A. Loinger and P. Bocchieri for stimulating discussions on the subject.

Appendix I

To prove eq. (20) we notice that

$$\rho(\mathbf{x}, t)|\Psi\rangle = e\psi^+(\mathbf{x}, t)\psi(\mathbf{x}, t)|\Psi\rangle = e\int \mathrm{d}\alpha\, \varphi^*(\mathbf{x}, \alpha, t)\varphi(\mathbf{x}, \alpha, t)|\mathbf{x}, \alpha; t\rangle,$$

$$j_k^{(0)}(\mathbf{x}, t)|\Psi\rangle = \frac{e\hbar}{2mic}\left(\psi^+(\mathbf{x}, t)\frac{\partial\psi(\mathbf{x}, t)}{\partial x_k} - \frac{\partial\psi^+(\mathbf{x}, t)}{\partial x_k}\psi(\mathbf{x}, t)\right)|\Psi\rangle$$

$$= \frac{e\hbar}{2mic}\int \mathrm{d}\alpha \left(\frac{\partial\varphi(\mathbf{x}, \alpha, t)}{\partial x_k} - \varphi(\mathbf{x}, \alpha, t)\frac{\partial}{\partial x_k}\right)|\mathbf{x}, \alpha; t\rangle,$$

whence

$$\frac{1}{c}\rho(\mathbf{x}, t)\int \mathrm{d}_3\mathbf{x}'\, j_k^{(0)}(\mathbf{x}', t)|\Psi\rangle = \frac{e\hbar}{mic}\int \mathrm{d}\alpha \frac{\partial\varphi(\mathbf{x}, \alpha, t)}{\partial x_k}|\mathbf{x}, \alpha; t\rangle,$$

$$-\frac{1}{c}\int \mathrm{d}_3\mathbf{x}'\, j_k^{(0)}(\mathbf{x}', t)\rho(\mathbf{x}, t)|\Psi\rangle = -\frac{e\hbar}{mic}\int \mathrm{d}\alpha\, \varphi(\mathbf{x}, \alpha, t)\frac{\partial}{\partial x_k}|\mathbf{x}, \alpha; t\rangle,$$

$$\frac{1}{2c}\{\rho(\mathbf{x}, t)\int \mathrm{d}_3\mathbf{x}' j_k^{(0)}(\mathbf{x}', t)\}|\Psi\rangle = j_k^{(0)}(\mathbf{x}, t)|\Psi\rangle.$$

Furthermore,

$$[\rho(\mathbf{x}', t), \psi^+(\mathbf{x}'', t)\psi(\mathbf{x}'', t)A_k(\mathbf{x}'', t)] = 0.$$

Appendix II

To prove eq. (26) we notice that

$$\int \mathrm{d}_3\mathbf{x}''[\rho(\mathbf{x}, t), j_k^{(0)}(\mathbf{x}'', t)]$$

$$= \frac{e\hbar}{imc}\int \mathrm{d}_3\mathbf{x}'' \frac{\partial\delta(\mathbf{x}-\mathbf{x}'')}{\partial x''_k}(\psi^+(\mathbf{x}', t)\psi(\mathbf{x}'', t)+\psi^+(\mathbf{x}'', t)\psi(\mathbf{x}', t))$$

$$\langle \mathbf{z}', \alpha'; t| \int \mathrm{d}_3\mathbf{x} \int \mathrm{d}_3\mathbf{x}' \int \mathrm{d}_3\mathbf{x}''\rho(\mathbf{x}, t)[\rho(\mathbf{x}', t), j_k^{(0)}(\mathbf{x}'', t)]|\mathbf{x}-\mathbf{x}'|^p|\mathbf{z}'', \alpha''; t\rangle$$

$$= \int \mathrm{d}_3\mathbf{x}'|\mathbf{z}'-\mathbf{x}'|^p\left(\frac{\partial\delta(\mathbf{x}'-\mathbf{x}'')}{\partial x'_k}\delta(\mathbf{x}'-\mathbf{z}')+\frac{\partial\delta(\mathbf{x}'-\mathbf{z}')}{\partial x'_k}\delta(\mathbf{x}'-\mathbf{z}'')\right)\delta(\alpha'-\alpha'')$$

$$= p\delta(\alpha'-\alpha'')\delta(\mathbf{z}'-\mathbf{z}'')\int \mathrm{d}_3\mathbf{x}'|\mathbf{z}-\mathbf{x}'|^{p-2}(z'_k-x'_k)\delta(\mathbf{x}'-\mathbf{z}') = 0.$$

Similarly, to prove eq. (26′) we notice that

$$\langle \mathbf{z}', \alpha'; t| \sum_r \int \mathrm{d}_3\mathbf{x} \int \mathrm{d}_3\mathbf{x}' \int \mathrm{d}_3\mathbf{x}''\rho(\mathbf{x}, t)\frac{\partial}{\partial x'_r}[\rho(\mathbf{x}', t), j_r(\mathbf{x}'', t)]$$

$$\cdot (x_k-x'_k)|\mathbf{x}-\mathbf{x}'|^{p'}|\mathbf{z}'', \alpha''; t\rangle$$

$$= \sum_r \int \mathrm{d}_3\mathbf{x}'(\mathbf{z}'_k-x'_k)|\mathbf{z}'-\mathbf{x}'|^{p'}$$

$$\frac{\partial}{\partial x'_r}\left(\frac{\partial\delta(\mathbf{x}'-\mathbf{z}'')}{\partial x'_r}\delta(\mathbf{x}'-\mathbf{z}')+\frac{\partial\delta(\mathbf{x}'-\mathbf{z}')}{\partial x'_r}\delta(\mathbf{x}'-\mathbf{z}'')\,\delta(\alpha'-\alpha'')\right.$$

$$= \delta(\alpha'-\alpha'')\delta(\mathbf{z}'-\mathbf{z}'')\sum_r \int \mathrm{d}_3\mathbf{x}'\frac{\partial^2}{\partial x'^2_r}[(z'_k-x'_k)|\mathbf{z}'-\mathbf{x}'|^{p'}]\delta(\mathbf{x}'-\mathbf{z}') = 0.$$

References

1) P. A. M. Dirac, Proc. Roy. Soc. A **167** (1938) 148
2) H. E. Lorentz, The theory of Electrons (Teubner 1909, Dover reprint 1952) p. 252 ff
3) W. Pauli, Die Allgemeinen Prinzipien der Wellenmechanik in Handbuch der Physik **5/1** (1958) 164 and 28
4) G. Morpurgo, Nuovo Cimento **9** (1952) 808
5) A. Loinger, Nuovo Cimento **2** (1955) 561
6) H. E. Kramers, Collected Scientific Papers (North-Holland Publishing Co. Amsterdam, 1956) p. 845 ff
7) Van Kampen, Mat. Fys. Medd. Dan Vid. Selsk. **26**, No. 15 (1951)
8) H. Steinwedel, Ann. der Physik **15** (1955) 207;
K. McVoy and H. Steinwedel, Nuclear Physics **1** (1956) 164
9) E. D. Enz, Nuovo Cimento Suppl. **3** (1956) 363
10) Wildermuth and K. Baumann, Nuclear Physics **3** (1957) 612
11) Van Kampen, Physica **24** (1958) 545
12) F. E. Norton and W. K. R. Watson, Bull. Am. Phys. Soc. **4** (1959) 29 (JA7, JA8); and preprint

7.C:8.C *Nuclear Physics* **13** (1959) 150—155; © *North-Holland Publishing Co., Amsterdam*
Not to be reproduced by photoprint or microfilm without written permission from the publisher

ON THE BOSON MASS RENORMALIZATION CONSTANTS IN PSEUDOSCALAR MESON THEORY

JOHN W. MOFFAT
RIAS, *Baltimore* 12, *Maryland, U.S.A.*

Received 22 May 1959

Abstract: The purpose of this paper is to investigate the significance of Lehmann's theorem, which states that for pseudoscalar mesons $\delta m^2 \leqq 0$. This theorem prevents us from ascribing the meson mass to self-mass effects alone. By including a $\lambda\phi^4$ term in the Lagrangian it is proved that Lehmann's theorem is no longer necessarily fulfilled. On the basis of this conclusion one can no longer exclude the possibility that the mass of the meson in the absence of interaction is zero, and that the ϕ^4 coupling produces most of the observable meson mass. However, in view of the singular behaviour of the modified propagator, the vacuum expectation value $\langle\phi^2\rangle_0$ is divergent and δm^2 appears to be either infinite or indeterminate.

1. Introduction

Salam and Tiomno [1]) have recently conjectured that the calculation of self-mass effects using second order perturbation theory may not be too misleading. On the basis of this conjecture they calculated the nucleon-electron mass ratio. It was assumed in the mass ratio that the bare mass (the same for both particles) is vanishingly small. This corresponds to the assumption that in the absence of interaction the leptons, nucleons and hyperons reduce to the same fundamental bare mass. The observed fermion mass spectrum is related to the same couplings responsible for the dynamical interactions and the production of the particles.

Lehmann [2]) has shown, without the use of perturbation theory, that $\delta m^2 \leqq 0$ (δm^2 is the meson self-mass). As this theorem is obtained by using a rigorous procedure based on the axioms of local field theory, its consequences are of obvious importance. The theorem prevents us from extending the Salam-Tiomno conjecture to bosons, because in order to maintain positive masses we must choose $m_0^2 > \delta m^2$, where m_0^2 is the mass of the boson in the absence of interaction. This indicates that we cannot treat π- and K-mesons as elementary particles, but should consider them instead as composite structures. Thus Lehmann's theorem suggests that the meson mass spectrum is due to an intrinsic mass and not to the couplings responsible for the interaction.

It will be shown in the following that if a $\lambda\phi^4$ term is included in the

Lagrangian, the condition $\delta m^2 \leqq 0$ is no longer required to hold. Consequently, we cannot rule out the possibility, on the basis of renormalization theory, that the π-meson is an elementary particle. We are in a position to conjecture that the meson bare mass is zero, and that the ϕ^4 term provides the mesons with their mass.

2. Vacuum Expectation Values

To make the discussion complete, we shall briefly outline in this section Lehmann's [2]) procedure including, however, a $\lambda\phi^4$ term in the formalism. We shall consider the pseudoscalar coupling of a real meson field $\phi(x)$ and a spinor field $\psi(x)$. Let us introduce the renormalized Heisenberg variables

$$\begin{aligned} \psi(x) &= Z_2^{-\frac{1}{2}}\psi_u(x), \qquad \phi(x) = Z_3^{-\frac{1}{2}}\phi_u(x); \\ g &= Z_1^{-1}Z_2Z_3^{\frac{1}{2}}g_0, \quad m^2 = m_0^2+\delta m^2, \\ M &= M_0+\delta M, \end{aligned} \tag{1}$$

where m_0 and M_0 denote the boson and fermion mass constants in the absence of interactions, and g_0 denotes the unrenormalized coupling constant. In terms of the renormalized Heisenberg operators the equations of motion can be written

$$(\Box-m^2)\phi(x) = \tfrac{1}{2}igZ_1Z_3^{-1}[\bar{\psi}, \gamma_5\psi]-\delta m^2\phi+\lambda Z_3\phi^3, \tag{2}$$

$$\left(\gamma\frac{\partial}{\partial x}+M\right)\psi(x) = -igZ_1Z_2^{-1}\gamma_5\phi\psi+\delta M\psi. \tag{3}$$

The interaction Lagrangian corresponding to the eqs. (2) and (3) is

$$L_I = -\tfrac{1}{2}igZ_1[\bar{\psi}, \gamma_5\psi]\phi+\tfrac{1}{2}\delta MZ_2[\bar{\psi}, \psi]+\tfrac{1}{2}Z_3\delta m^2\phi^2-\tfrac{1}{4}\lambda Z_3^2\phi^4. \tag{4}$$

The term $\lambda\phi^4$ in (4) is well-known [3,4,5]).

For pseudoscalar mesons the fourth order square graphs in perturbation theory give an infinite contribution. Mass and coupling constant renormalization eliminates all divergences except those due to the square graph, which requires a $\lambda\phi^4$ term in the Lagrangian. The coefficient λ has an infinite part $\delta\lambda$, which plays the role of a counter term. In addition, we may give λ a finite part corresponding to a finite effect in the limit of low energy mesons. Thus, $\lambda = \lambda_1-\delta\lambda$, and λ_1 is a finite coupling constant to be determined by experiment.

The combination of $\lambda\phi^4$ and the square graph will lead to a finite physical effect [5]). Thus, in perturbation theory there will be non-vanishing diagrams corresponding to finite effects proportional to λ_1. Although perturbation theory is the motivation for introducing a $\lambda\phi^4$ term in the Lagrangian, the whole of the coefficient λ (i.e. including the counter term $\delta\lambda$) may be finite in the Lehmann formalism. The commutation relations for equal times are

$$[\phi(\mathbf{x}, t), \dot{\phi}(\mathbf{x}', t)] = -i\delta(\mathbf{x}-\mathbf{x}')Z_3^{-1},$$
$$\{\psi_\alpha(\mathbf{x}, t), \bar{\psi}_\beta(\mathbf{x}', t)\} = \gamma^0_{\alpha\beta}\delta(\mathbf{x}-\mathbf{x}')Z_2^{-1}. \tag{5}$$

The other commutation (anti-commutation) relations vanish for $t = t'$.

We shall use vacuum expectation values of the Heisenberg operators. In the representation to be used the state vector Ψ is an eigenfunction of the energy-momentum operator P_μ. For the vacuum expectation value of two boson operators, we have

$$\begin{aligned}\langle\phi(x)\phi(x')\rangle_0 &= (\Psi_0, \phi(x)\phi(x')\Psi_0) \\ &= \sum_k (\Psi_0, \phi(x)\Psi_k)(\Psi_k, \phi(x')\Psi_0) \\ &= \sum_k a_{0k}a^*_{0k}\exp[ik(x-x')],\end{aligned} \tag{6}$$

where

$$(\Psi_0, \phi(x)\Psi_k) = a_{0k}\exp(ikx). \tag{7}$$

We introduce the spectral function ρ obtained by Källen [6]) and Lehmann [2]):

$$\rho(-k^2) = (2\pi)^3\sum' a_{0k}a^*_{0k} = (2\pi)^3\sum' |(\Psi_0, \phi(0)\Psi_k)|^2 \geqq 0. \tag{8}$$

In terms of the vacuum expectation values we have

$$\langle\phi(x)\phi(x')\rangle_0 = i\Delta'^{(+)}(x-x'), \tag{9}$$

$$\langle[\phi(x), \phi(x')]\rangle_0 = i\Delta'(x-x'). \tag{10}$$

From the well-known properties of the free-field propagators it follows that [2])

$$\Delta'^{(+)}(x) = \int_0^\infty \Delta^{(+)}(\kappa^2; x)\rho(\kappa^2)\mathrm{d}(\kappa^2), \tag{11}$$

where we have used the property that

$$\rho(-k^2) = \int_0^\infty \rho(\kappa^2)\delta(k^2+\kappa^2)\mathrm{d}(\kappa^2). \tag{12}$$

Here $\rho(\kappa^2)$ is the probability for finding the bare particle in a state with total mass κ and $\rho(\kappa^2) \geqq 0$ for pseudoscalar mesons [7]). Lehmann [2]) has expressed $\rho(\kappa^2)$ in the form

$$\rho(\kappa^2) = \delta(\kappa^2-m^2)+\sigma(\kappa^2), \tag{13}$$

where

$$\sigma(\kappa^2) = 0 \quad \text{for} \quad 0 \leqq \kappa^2 < (2m)^2. \tag{14}$$

From the commutation relations (5) and the vacuum expectation values, Källen and Lehmann have derived the following expressions for the renormalization constants Z_3 and Z_2:

$$Z_3^{-1} = \int_0^\infty \rho(\kappa^2)\mathrm{d}(\kappa^2), \quad Z_2^{-1} = \int_0^\infty \rho_1(\kappa^2)\mathrm{d}(\kappa^2), \tag{15}$$

where $\rho_1(\kappa^2)$ is connected with the vacuum expectation values of the spinor operators $\psi(x)$ [2]). We have

$$0 \leqq Z_3 < 1, \quad 0 \leqq Z_2 < 1, \tag{16}$$

for pseudoscalar mesons †.

3. The Boson Mass Renormalization Constants

Let us now turn to an investigation of the boson renormalization constants δm^2 and m_0^2. (The fermion renormalization constant δM has been determined by Lehmann [2]) for pseudoscalar coupling. This derivation will not be affected by the addition of a ϕ^4 term in the Lagrangian.) We have

$$\begin{aligned}(\Box - m_0^2)\langle[\phi(x), \phi(x')]\rangle_0 &= \langle[\tfrac{1}{2}igZ_1Z_3^{-1}[\bar{\psi}(x), \gamma_5\psi(x)] + Z_3\lambda\phi^3(x), \phi(x')]\rangle_0 \\ &= i\int_0^\infty (\kappa^2 - m_0^2)\Delta(x-x'; \kappa^2)\rho(\kappa^2)\mathrm{d}(\kappa^2). \end{aligned} \tag{17}$$

Making use of the relation

$$\frac{\partial}{\partial x^0}\Delta(x)|_{t=t'} = -\delta(\mathbf{x}), \tag{18}$$

we obtain, for $t = t'$,

$$\begin{aligned}&\langle[\tfrac{1}{2}igZ_1Z_3^{-1}[\bar{\psi}(x), \gamma_5\psi(x)] + Z_3\lambda\phi^3(x), \dot{\phi}(x')]\rangle_0 \\ &\qquad = +i\int_0^\infty (\kappa^2 - m_0^2)\delta(\mathbf{x}-\mathbf{x}')\rho(\kappa^2)\mathrm{d}(\kappa^2). \end{aligned} \tag{19}$$

For equal times, we have

$$\langle[[\bar{\psi}(x), \gamma_5\psi(x)], \dot{\phi}(x')]\rangle_0|_{t=t'} = 0. \tag{20}$$

Eq. (19) then reduces to

$$Z_3\lambda\langle[\phi^3(x), \dot{\phi}(x')]\rangle_0|_{t=t'} = i\int_0^\infty (\kappa^2 - m_0^2)\delta(\mathbf{x}-\mathbf{x}')\rho\mathrm{d}(\kappa^2). \tag{21}$$

The commutator on the left-hand side gives

$$[\phi^3(\mathbf{x}, t), \dot{\phi}(\mathbf{x}', t)] = -3i\delta(\mathbf{x}-\mathbf{x}')Z_3^{-1}\phi^2(x). \tag{22}$$

From (21) we obtain

$$3\lambda\langle\phi^2(x)\rangle_0 = -\int_0^\infty (\kappa^2 - m_0^2)\rho(\kappa^2)\mathrm{d}(\kappa^2). \tag{23}$$

We can express $\langle\phi^2(x)\rangle_0$ by means of the vacuum expectation value

$$\langle\phi(x)\phi(x')\rangle_0 \underset{x\to x'}{=} i\Delta'^{(+)}(x-x'). \tag{24}$$

We have

$$\langle\phi^2(x)\rangle_0 \underset{x\to x'}{=} \int_0^\infty \Delta^{(+)}(\kappa^2; x-x')\rho(\kappa^2)\mathrm{d}\kappa^2. \tag{25}$$

By expanding $\Delta'^{(+)}(x)$ near the light cone we find that the modified propa-

† In electrodynamics $\rho(\kappa^2) \geqq 0$, but $\rho_1(\kappa^2)$ may be negative owing to the use of an indefinite metric.

gator is at least as singular as the free field propagator [2]) and $\langle\phi^2\rangle_0$ is divergent.

The expression obtained for δm^2 is

$$\delta m^2 = -Z_3\left(\int_0^\infty (\kappa^2-m^2)\rho\mathrm{d}(\kappa^2)+3\lambda\langle\phi^2\rangle_0\right) \tag{26}$$

and for $m_0{}^2$ we get

$$m_0{}^2 = Z_3\left(\int_0^\infty \kappa^2\rho\mathrm{d}(\kappa^2)+3\lambda\langle\phi^2\rangle_0\right). \tag{27}$$

If we set $m_0 = 0$, we obtain

$$3\lambda\langle\phi^2\rangle_0 = -\int_0^\infty \kappa^2\rho(\kappa^2)\mathrm{d}(\kappa^2) \leqq 0. \tag{28}$$

Owing to $\langle\phi^2\rangle_0 > 0$, we see that in this case $\lambda \leqq 0$. Putting $\lambda = 0$ in (26) gives

$$\delta m^2 = -Z_3\int (\kappa^2-m^2)\rho\mathrm{d}(\kappa^2) \leqq 0, \tag{29}$$

where the inequality holds because $\kappa^2 > m^2$. This is Lehmann's theorem [2]). It corresponds to the condition $m_0{}^2 > \delta m^2$, which maintains the positive nature of the observable meson masses. If λ is different from zero the condition $\delta m^2 \leqq 0$ is no longer necessarily true, because λ may be negative.

4. Concluding Remarks

In our field equations there is no effective source of a fermion field mass term, whereas the ϕ^3 term can serve this purpose for the bosons. Schwinger [8]) has suggested that the ϕ^4 term in the Lagrangian creates most of the mass of the mesons. The bare mass of the meson is taken to be zero. The uncoupled Lagrangian is then invariant to within a divergence under the spin 0 transformation $\phi \to \phi+\Lambda$, where Λ is an arbitrary constant. Provided that $\lambda < 0$ in (26) this argument can be justified. Lehmann's condition no longer holds true, and we are free to put $m_0=0$. The ϕ^4 term is the predominant field mass term and the mesons can be treated as elementary particles †. It must be kept in mind that second order perturbation theory will give a negative δm^2 for pseudoscalar mesons, because the ϕ^4 term in $\mathscr{L}_\mathrm{I}$ will not yield contributions to the S-matrix until the next order. This indicates that for bosons it is misleading to use second order perturbation theory to describe self-mass renormalization effects, because the important contributions due to the square diagrams do not appear in the lowest order.

We have indicated that the pion renormalization constant is perhaps infinite. Thus, assigning finite properties to the physical pion mass implies

† Although we can now conjecture that the mesons are elementary particles it is still an open question which type of model i.e., elementary or compound, corresponds to nature.

that the bare mass is characterized by infinite quantities independently of perturbation theory. This result raises the interesting question whether or not pion renormalization theory provides a consistent scheme when based on a local interaction Lagrangian. This problem requires further investigation.

I should like to express my gratitude to Dr. P. Schwed, Dr. T. Fulton and Dr. G. Feldman for stimulating discussions and criticism. My thanks are due to Dr. F. Gürsey, Professor A. Salam and Professor A. S. Wightman for advice and criticism.

References

1) A. Salam and J. Tiomno, Nuclear Physics **9** (1959) 585
2) H. Lehmann, Nuovo Cimento **11** (1954) 342;
M. Gell-Mann and F. E. Low, Phys. Rev. **95** (1954) 1300
3) P. T. Matthews, Phil. Mag. **42** (1951) 221
4) A. Salam, Phys. Rev. **82** (1951) 217; **84** (1951) 426
5) S. S. Schweber, H. A. Bethe and F. de Hoffmann, Mesons and Fields (Row, Peterson and Co., Evanston, 1955) Vol. 1, Sec. 22.
6) G. Källen, Helv. Phys. Acta **25** (1952) 417
7) P. T. Matthews and A. Salam, Phys. Rev. **112** (1958) 283
8) J. Schwinger, Ann. of Physics **2** (1957) 407

1.C *Nuclear Physics* **13** (1959) 156—163; © *North-Holland Publishing Co., Amsterdam*
Not to be reproduced by photoprint or microfilm without written permission from the publisher

ON THE INCLUSION OF HOLE-HOLE SCATTERING IN THE BRUECKNER *t*-MATRIX

J. S. R. CHISHOLM
University College, Cardiff
and
E. J. SQUIRES
A.E.R.E., *Harwell Didcot, Berks.*

Received 29 April 1959

Abstract: A discussion is given of the effect of including hole-hole scattering terms in the Brueckner *t*-matrix method applied to large fermion systems with attractive separable potentials. The nature of the singularity in the *t*-matrix equation is considerably altered, and, for the infinite system, the new *t*-matrix can be written as the sum of a non-singular form and a δ-function.

1. Introduction

Much progress has recently been made in the study of large fermion systems by the use of the Brueckner method [1]). It has, however, been pointed out that, for separable attractive potentials, the Brueckner t matrix is singular for infinite systems no matter how weak the potential [2]). Similar singularities also arise for more general potentials [3]), in particular for those which are often used in the atomic nucleus. The physical significance of these singularities is not yet understood and it is not known, for example, whether they reflect a divergence of the complete perturbation series or whether they merely indicate that a bad selection of terms has been made [4]). We would especially point out that there is little evidence for any connection between the singularity in the t matrix and the alleged existence of energy gaps in the spectrum of excited state energy levels.

In this paper we study the effect of adding an additional set of terms to the usual Brueckner theory, with an attractive separable potential. These extra terms can be described as hole-hole scattering in the usual convention. Since they are of the same sign as the terms of the original series, they do not prevent the series from diverging. However, when the new t matrix is written formally as the solution of an integral equation, it turns out that it has a solution which is very different in form to the solution of the corresponding integral equation in the Brueckner theory.

We shall use the notation of Hugenholtz [5]), in which lines with arrows

to the left represent particles and those with arrows to the right represent holes. A t matrix interaction will be represented by a dot at the vertex. Momenta above the Fermi surface will be denoted by $\mathbf{k}$ and those below by $\mathbf{m}$.

2. The Inclusion of Hole-Hole Scattering

The Brueckner t matrix is the iterated interaction of two nucleons in the nuclear medium. Diagrammatically, the equation for the matrix element $\langle \mathbf{k}_1\mathbf{k}_2|t|\mathbf{m}_1\mathbf{m}_2\rangle$ is

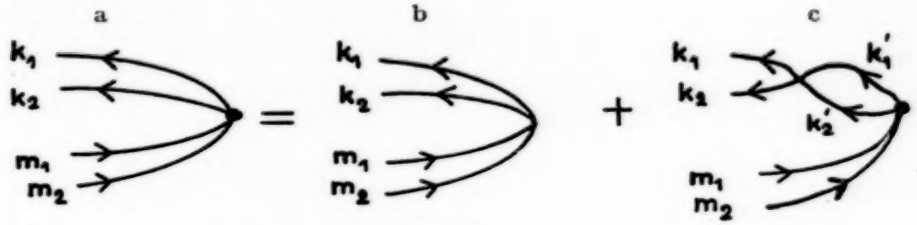

The ground state energy is given by

$$E = \sum_{\mathbf{m}} m^2 + \tfrac{1}{2} \sum_{\mathbf{m}_1,\,\mathbf{m}_2} \langle \mathbf{m}_1\mathbf{m}_2|t|\mathbf{m}_1\mathbf{m}_2\rangle \tag{1}$$

where

$$\langle \mathbf{m}_1\mathbf{m}_2|t|\mathbf{m}_1\mathbf{m}_2\rangle = \langle \mathbf{m}_1\mathbf{m}_2|v|\mathbf{m}_1\mathbf{m}_2\rangle_{\mathrm{A}} + \tfrac{1}{2} \sum_{\mathbf{k'}_1,\,\mathbf{k'}_2} \frac{\langle \mathbf{m}_1\mathbf{m}_2|v|\mathbf{k'}_1\mathbf{k'}_2\rangle_{\mathrm{A}} \langle \mathbf{k'}_1\mathbf{k'}_2|t|\mathbf{m}_1\mathbf{m}_2\rangle}{(m_1^2 + m_2^2 - k_1^2 - k_2^2)}. \tag{2}$$

In eq. (2) the suffix A means that the matrix element is to be antisymmetrised. In the energy denominator we have, for simplicity, used just the kinetic energies, with units such that $\hbar^2/2M = 1$.

In this treatment, the expression for the ground state energy includes all diagrams of the type of fig. 1. We now modify the definition of the t matrix to include all diagrams of the type of fig. 2, i.e. all particle-particle and all

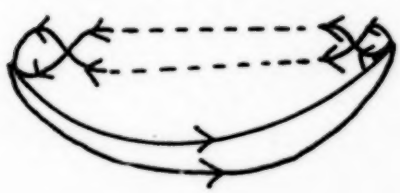

Fig. 1.

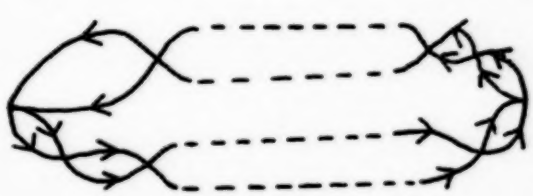

Fig. 2.

hole-hole interactions. This does not include all possible terms since hole-particle and pair creation diagrams are still omitted. Hole particle terms could be included in the integral equation at the cost of greatly complicating the equation.

To include these extra hole-hole scattering terms we retain eqs. (1) and (2) but modify the definition of $\langle \mathbf{k}_1\mathbf{k}_2|t|\mathbf{m}_1\mathbf{m}_2\rangle$ by including in the diagrammatic equation the extra term

d

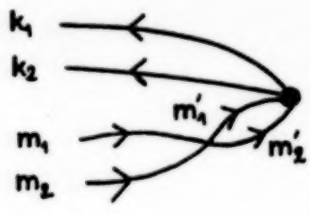

Iteration of the new diagrammatic equation will obviously give the desired sum of terms (we are assuming convergence at present). The equation for $\langle \mathbf{k}_1\mathbf{k}_2|t|\mathbf{m}_1\mathbf{m}_2\rangle$ can be written

$$\langle \mathbf{k}_1\mathbf{k}_2|t|\mathbf{m}_1\mathbf{m}_2\rangle = \langle \mathbf{k}_1\mathbf{k}_2|v|\mathbf{m}_1\mathbf{m}_2\rangle_A + \tfrac{1}{2}\sum_{\mathbf{k}'_1,\mathbf{k}'_2} \frac{\langle \mathbf{k}_1\mathbf{k}_2|v|\mathbf{k}'_1\mathbf{k}'_2\rangle_A \langle \mathbf{k}'_1\mathbf{k}'_2|t|\mathbf{m}_1\mathbf{m}_2\rangle}{(m_1^2+m_2^2-k_1'^2-k_2'^2)}$$
$$+\tfrac{1}{2}\lambda \sum_{\mathbf{m}'_1,\mathbf{m}'_2} \frac{\langle \mathbf{k}_1\mathbf{k}_2|t|\mathbf{m}'_1\mathbf{m}'_2\rangle\langle \mathbf{m}'_1\mathbf{m}'_2|v|\mathbf{m}_1\mathbf{m}_2\rangle_A}{(m_1'^2+m_2'^2-k_1^2-k_2^2)} \qquad (3)$$

where, in eq. (3), we have included the hole-hole scattering terms multiplied by a factor λ, which will help to locate these terms in the subsequent work. It is important to note the energy denominator in the last term of eq. (3); in particular, it is not $m_1^2+m_2^2-m_1'^2-m_2'^2$, which would become zero. In the linked cluster expansion of the ground state energy there are no terms for which the energy denominator becomes zero (though of course it approaches zero on the Fermi surface for the infinite system).

Eq. (3) is an extremely complicated integral equation in $\mathbf{k}$ and $\mathbf{m}$. In order to study its solution we shall make two simplifications, namely, we shall consider only states for which $\mathbf{m}_1+\mathbf{m}_2 = 0$, and we shall use a separable potential. When $\mathbf{m}_1+\mathbf{m}_2 = 0$ we can work in relative momentum space and eq. (3) becomes, with $\mathbf{m}$ and $\mathbf{k}$ denoting the relative momenta,

$$\langle \mathbf{k}|t|\mathbf{m}\rangle = \langle \mathbf{k}|v|\mathbf{m}\rangle_A + \tfrac{1}{2}\sum_{\mathbf{k}'} \frac{\langle \mathbf{k}|v|\mathbf{k}'\rangle_A\langle \mathbf{k}'|t|\mathbf{m}\rangle}{(m^2-k'^2)}$$
$$+\tfrac{1}{2}\lambda\sum_{\mathbf{m}'} \frac{\langle \mathbf{k}|t|\mathbf{m}'\rangle\langle \mathbf{m}'|v|\mathbf{m}\rangle_A}{(m'^2-k^2)}. \qquad (4)$$

For the potential we take

$$\langle \mathbf{l}'|v|\mathbf{l}\rangle = -v(l')v(l). \qquad (5)$$

The solution to eq. (4) can be written in the form

$$\langle \mathbf{k}|t|\mathbf{m}\rangle = -[v(k)t_1(m)+t_2(k)v(m)], \qquad (6)$$

where $t_1(m)$ and $t_2(k)$ satisfy the coupled equations

$$t_1(m)\left[1-\sum_{k'}\frac{|v(k')|^2}{k'^2-m^2}\right]-\sum_{k'}\frac{v(m)v(k')t_2(k')}{k'^2-m^2}=v(m) \tag{7}$$

and

$$t_2(k)\left[1-\lambda\sum_{m'}\frac{|v(m')|^2}{k^2-m'^2}\right]-\lambda\sum_{m'}\frac{v(k)v(m')t_1(m')}{k^2-m'^2}=0. \tag{8}$$

3. Solution of the Integral Equation for an Infinite System

For an infinite system, eqs. (7) and (8) are two coupled integral equations. Since $\int d\mathbf{k}'v|(k')|^2/(k'^2-m^2)$ is logarithmically divergent as m tends to k_F it follows that, for a sufficiently weak potential, the coefficient of $t_1(m)$ vanishes for some value of $m < k_F$. It is this zero that gives rise to the singularity in the usual Brueckner theory [2]). It has been pointed out to us by Emery [6]) that it also prevents us from using Fredholm theory directly on these integral equations. However, we shall show that, by separating out a Dirac δ-function from $t_1(m)$ we can reduce the equations to a Fredholm equation of the second kind, which, in general, will have a good solution.

The coefficient of $t_2(k)$ in eq. (8) is also likely to have a zero. In this case it is necessary to separate out a δ-function from $t_2(k)$ also. Since this can be done in an analogous way to our treatment of $t_1(m)$ we shall assume, for simplicity, that this singularity does not arise: say, by assuming it occurs for a large value of k for which we can take $v(k)$ equal to zero.

We eliminate $t_2(k)$ between eqs. (7) and (8) to obtain

$$t_1(m)[1-a(m)]-\lambda\int d\mathbf{m}'b_\lambda(m_1m')t_1(m')=v(m), \tag{9}$$

$$a(m)=\int d\mathbf{k}'\frac{|v(k')|^2}{k'^2-m^2}, \tag{10}$$

$$b_\lambda(m,m')=\int\frac{v(m)v(m')|v(k')|^2d\mathbf{k}'}{(k'^2-m^2)^2\left[1-\lambda\int d\mathbf{m}'\dfrac{|v(m')|^2}{k'^2-m'^2}\right]}. \tag{11}$$

From its definition we see that $a(m)$ is a monotonically increasing function. Thus $1-a(m)$ can only have one zero and we can put

$$1-a(m)=(m-M)e(m) \tag{12}$$

where $e(m)$ has no zeros. We also define

$$k_\lambda(m,m')=\frac{b_\lambda(m_1m')}{e(m)}, \tag{13}$$

$$c(m)=\frac{v(m)}{e(m)}. \tag{14}$$

The quantities k_λ and c have no singularities.

Eq. (9) becomes

$$(m-M)t_1(m) = c(m)+\lambda \int \mathbf{dm}' k_\lambda(m, m')t_1(m'). \tag{15}$$

We try a solution of the form

$$t_1(m) = \alpha\delta(m-M)+f(m) \tag{16}$$

where we shall require $f(m)$ to be non-singular. If we substitute eq. (16) into eq. (15) we obtain

$$\alpha = -\frac{c(M)+\lambda \int \mathbf{dm}' k_\lambda(M, m')f(m')}{\lambda k_\lambda(M, M)} \tag{17}$$

and

$$f(m) = \frac{c(m)k_\lambda(M, M)-c(M)k_\lambda(m, M)}{(m-M)k_\lambda(M, M)} + \lambda \int \mathbf{dm}' \frac{k_\lambda(m, M)k_\lambda(M, m')-k_\lambda(m, m')k(M, M)}{(m-M)k(M, m)} f(m'). \tag{18}$$

The equation for $f(m)$ is a non-singular Fredholm equation of the second kind which can be solved by normal methods to give a non-singular solution. The solution can then be substituted into eq. (17) to give α.

From eq. (17) we see that the solution is not valid for $\lambda = 0$. In fact, of course, for $\lambda = 0$ eq. (15) has the usual Brueckner singular solution

$$t_1(m) = \frac{c(m)}{m-M}. \tag{19}$$

Clearly this is not the limit as $\lambda \to 0$ of the solution to eq. (15) for $\lambda \neq 0$. Thus, the Brueckner approximation is obtained by taking what is in effect a singular point of the more general integral equation.

The methods which lead to both the Brueckner and the new integral equations are based on a rearrangement of perturbation theory. However, we can easily see that the t-matrix series diverges for infinite systems, for any value of the potential (we are still considering separable attractive potentials only). This is well known for the Brueckner t-matrix and follows for the new t-matrix since it is obtained from the former by adding terms all of the same sign as the original series. This means that the rearrangements which have been carried out are not legitimate. A possible way of justifying the results would be to consider a system of fermions enclosed in a large finite box; for a sufficiently small potential v, the t-matrix series would converge. We could then allow v to become complex and possibly justify the use of the integral equations outside the radius of convergence by the methods of analytical continuation. Finally we would have to take the limit as the volume tends to infinity. However, we shall see in the next section that

both approximations to the energy have no limit for λ tending to infinity. In fact the energies obtained oscillate infinitely as the volume tends to infinity.

The methods which have been used to derive the Brueckner integral equation without using perturbation theory do not overcome these difficulties. This is because these methods depend upon certain correction terms being small, and the arguments used to suggest that they are small certainly do *not* work in general for a finite system, the correction terms being infinite for certain values of the volume.

4. Solution of the Matrix Equation for a Finite System

The Brueckner solution to the matrix analogue of eq. (9) is

$$t(m) = \frac{c(m)}{m-M} \tag{20}$$

and the ground state energy shift is

$$\Delta E = \sum_m \langle m|t|m\rangle = \sum_m \frac{c(m)v(m)}{m-M}. \tag{21}$$

We see that the sum oscillates infinitely as the volume increases, becoming infinite when any of the m is equal to M. Thus the Brueckner method is quite inadequate for dealing with finite systems. The result for an infinite system, with a principal value at the pole, can be obtained as a "limit" if we restrict the volumes such that M always lies half way between the two nearest values of m.

In order to study the effect of the extra term in eq. (15) we make a further simplification by assuming $k(m', m)$ is separable. We see from eqs. (11) and (13) that this would happen if we just include one particular value of k' in the sum of the hole-hole scattering corrections. However, our only object in using this property is that it makes discussion of eq. (15) much simpler, without, we feel, greatly affecting its properties. The sign of $k(m', m)$ does not affect the following analysis; we can therefore take

$$k(m', m) = k(m')l(n). \tag{22}$$

Eq. (15) becomes

$$(m-M)t_1(m) = c(m)+\lambda k(m)R, \tag{23}$$

where

$$R = \frac{\sum_m \dfrac{l(m)c(m)}{m-M}}{1-\lambda \sum_m \dfrac{l(m)k(m)}{m-M}}. \tag{24}$$

We see that the solution is singular wherever

$$\lambda \sum \frac{l(m)k(m)}{m-M} = 1. \tag{25}$$

Thus, the new t matrix still gives an answer which oscillates infinitely as the volume varies. The singularities arise at different values of the volume in the new method and the Brueckner method and, in fact, as the volume varies the two methods become singular alternately [7]). If we consider one of the m, say m_1, to be near to M, for which case the Brueckner result becomes very large, we have

$$R = -\frac{l(m_1)c(m_1)+\sum_{m\neq m_1}\frac{m_1-M}{m-M}\,l(m)c(m)}{\lambda l(m_1)k(m_1)+\sum_{m\neq m_1}\frac{m_1-M}{m-M}\,l(m)k(m)-(m_1-M)} \tag{26}$$

so, as $m_1-M \to 0$,

$$R\to -\frac{c(m_1)}{\lambda k(m_1)}\left[1+\frac{m_1-M}{l(m_1)}\left(\sum_{m\neq m_1}\frac{l(m)\{c(m)/c(m_1)-k(m)/k(m_1)\}}{m-M}+\frac{1}{k(m_1)}\right)\right]. \tag{27}$$

Hence, for $m \neq m_1$,

$$t_1(m) \to \frac{c(m)-k(m)c(m_1)k(m_1)}{(m-M)} \tag{28}$$

and

$$t_1(m_1) \to -\frac{c(m_1)}{l(m_1)}\left(\sum_{m\neq m_1}\frac{l(m)\{c(m)/c(m_1)-k(m)/k(m_1)\}}{m-M}+\frac{1}{k(m_1)}\right). \tag{29}$$

The limit of *this solution* as the volume tends to infinity gives the result which we have used in section 3 for the infinite system.

We can now see why the two methods give entirely different results for the infinite system. In neither case does the solution to the equations have a limit as the volume tends to infinity, and the results for the infinite system are obtained by taking "limits" for certain sequences of volumes — in the Brueckner case such that M is symmetrically placed between the two nearest m values and in the new t matrix case such that M is always equal to one of the m.

In conclusion, then, the inclusion of hole-hole scattering terms removes the pole from the solution of the integral equation and gives an unambiguous answer, which differs from the answer given by Brueckner theory taking, say, the principal value at the pole. There appears, however, at present to be no way of choosing between the two answers and, in fact, no reasons for believing that either of them gives an approximation to the actual energy of the system.

Finally, we note that the singularities in the approximate expressions for the energy occur at different values of the volume in the Brueckner and the new methods. In fact the Brueckner result diverges when the sum in eq. (21) is infinite, whereas our new result diverges when a similar sum is equal to one. If we consider a finite system and allow the volume or the potential to increase from a region where both series converge, it is obvious from the sign of the terms involved (see remarks at the end of section 3) that the new matrix series diverges before the Brueckner series. Thus, for this situation, the Brueckner series would give a finite answer but some of the correction terms would sum to infinity. This shows the danger of estimating the validity of the approximations by just considering the lowest order corrections.

We are grateful to Drs. J. S. Bell and T. H. R. Skyrme for discussions on the content of this paper. The work was commenced while one of us (J.S.R.C.) was consultant at the A.E.R.E.

References

1) Reviews of the method and further references are given by H. A. Bethe, Phys. Rev. **103** (1956) 1353; and R. J. Eden in Nuclear Reactions (North Holland Publishing Co., Amsterdam, 1958)
2) L. N. Cooper, Phys. Rev. **104** (1956) 1189;
J. Goldstone, Thesis, Cambridge (1958);
K. Gottfried, unpublished CERN report
3) V. J. Emery, Nuclear Physics **12** (1959) 69
4) J. S. Bell, Proc. Phys. Soc. **73** (1959) 118
5) N. M. Hugenholtz, Physica **23** (1959), 481
6) V. J. Emery, private communication
7) M. L. Mehta, Nuclear Physics **12** (1959) 333

1.B:2.L *Nuclear Physics* **13** (1959) 164—166; © *North-Holland Publishing Co., Amsterdam*
Not to be reproduced by photoprint or microfilm without written permission from the publisher

POLARIZATION OF 2- TO 4-MeV NEUTRONS SCATTERED BY DEUTERONS

W. P. BUCHER †, W. B. BEVERLY, G. C. COBB and F. L. HEREFORD

Department of Physics, University of Virginia, Charlottesville, Virginia ††

Received 2 July 1959

Abstract: The polarization of 2 to 4-MeV neutrons scattered by deuterons has been measured by observation of the right-left asymmetry induced in the scattering of polarized neutrons. Results at several energies and scattering angles yield negligibly small values (less than 7 %) in agreement with theoretical estimates.

1. Introduction

Several recently reported experiments on the elastic scattering of 2- to 4-MeV neutrons by deuterons yield conflicting results for the deuteron polarization efficiency $P_d(E_n, \theta)$ (i.e., the neutron polarization induced upon scattering initially unpolarized neutrons of energy E_n through a centre of mass angle θ). This quantity can be inferred from the measured right-left asymmetry induced upon scattering neutrons of initial polarization P_n through the relation

$$P_n P_d(E_n, \theta) = \frac{R-L}{R+L} \tag{1}$$

where R and L denote the neutron intensity scattered at angle θ to the right and left.

White *et al.*[1]) observed this asymmetry by detecting recoil deuterons in a deuterium filled directional counter exposed to partially polarized D(d, n) neutrons and reported values of $P_d(E_n, 90°)$ of 0.58 ± 0.05 for 2.26-MeV and 0.86 ± 0.19 for 3.1-MeV. Brullman *et al.*[2]) measured the asymmetry, counting scattered neutrons in coincidence with the recoil deuterons in a scintillating scatterer (C_6D_6) and obtained negligible polarization effects for 3.27-MeV neutrons. Cranberg [3]) also found values of P_d less than 7 % for 2.1-MeV neutrons using a-time-of-flight technique.

In addition to the above experimental results, theoretical estimates [4]) indicate the deuteron polarization efficiency for neutrons in the 2- to 4-MeV range should be of the order of the D-state mixing in the deuteron (a few

† Now at Bartol Research Foundation, Swarthmore, Pennsylvania.

†† Supported jointly by U.S.A.E.C. and O.O.R., U.S. Army.

percent) at the most. The work described here was undertaken to obtain more complete data and to resolve the discrepancies among previous measurements.

2. Experimental Procedure

The experimental arrangement is shown in fig. 1. Magnetically analyzed deuterons struck a heavy ice target yielding partially polarized neutrons from the D(d, n) reaction. Both thin and thick ice targets were employed, the thickness being determined by two methods: (1) observation of the shift

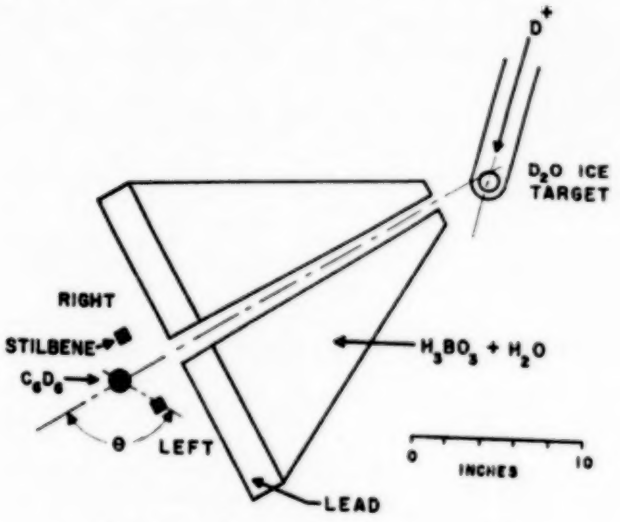

Fig. 1. Experimental arrangement.

in the Al^{27} (p, γ)993-keV resonance using an aluminium backing behind the heavy ice, and (2) comparison of thick and thin target yields. After collimation the neutrons struck a deuterated benzene scintillating scatterer and recoil deuterons were detected in coincidence with neutrons scattered both to the right and left. Stilbene crystals detected the scattered neutrons. Pulses from these latter detectors were counted only when in coincidence (0.1 μsec resolving time) with recoil deuteron pulses. The coincidence circuit incorporated differential pulse height analysis of both recoil deuteron and scattered neutron pulses, the pulse height windows being set in accordance with conservation of momentum and energy in the n—d collision. Accidental coincidence rates amounted to only a few percent of the genuine rates. As a check on the experimental set-up, recoil deuteron spectra were recorded throughout the measurements by a 20-channel analyzer gated by the final output of either the right or left coincidence circuit. These spectra shifted as expected on varying the incident neutron energy and the scattering angle.

Instrumental asymmetries were eliminated by a previously described method [5]) in which the sign of the incident neutron polarization was reversed.

Also the C_6D_6 scatterer was replaced by a stilbene crystal and n—p scattering asymmetry observed, which measurement yielded zero asymmetry.

3. Results

In extracting P_d from the observed asymmetries by means of eq. (1), the values of the D(d, n) neutron polarization reported by Levintov *et al.*[6]) and Pasma [7]) were employed. These workers used the known He^4 (n, n) polarization in analysis of the neutron polarization. The degree of polarization of the neutrons employed in our measurements was 10 to 14 % depending on the neutron energy. The values of P_d obtained from our measurements are shown in table 1. The values are not corrected for finite geometry nor

TABLE 1

d(n, n) neutron polarization (P_d)

E_n (MeV)	ΔE_n (MeV)	θ(CM)	P_d (%)
2.3	0.2	90°	-2 ± 7
3.1	0.2	60°	2 ± 5
3.1	0.2	90°	9 ± 8
3.1	0.2	135°	10 ± 7
3.9	0.1	60°	1 ± 5
3.9	0.1	90°	-2 ± 6
3.9	0.1	135°	4 ± 8

accidental coincidences since these corrections are quite small relative to the indicated statistical errors. Positive polarization corresponds to neutron spin orientation in the direction of $\mathbf{k}_n \times \mathbf{k}'_n$, where $\mathbf{k}_n$ and $\mathbf{k}'_n$ are the incident and scattered neutron momenta. It is clear that the results indicate polarization of several percent at the most.

References

1) R. E. White, A. Chisholm and D. Brown, Nuclear Physics **7** (1958) 233
2) M. Brullmann, H. J. Gerber and D. Meier, Helv. Phys. Acta **31** (1958) 318
3) L. Cranberg, Phys. Rev. Letters **2** (1959) 324
4) R. S. Christian and J. L. Gammel, Phys. Rev. **91** (1953) 100
5) B. M. McCormac, M. F. Steuer, C. D. Bond and F. L. Hereford, Phys. Rev. **104** (1956) 718
6) I. I. Leventov, A. V. Miller, E. Z. Tarumov and V. N. Shamshev, Nuclear Physics **3** (1957) 237
7) P. J. Pasma, Nuclear Physics **6** (1958) 141

1.E.3 *Nuclear Physics* **13** (1959) 167—176; © *North-Holland Publishing Co., Amsterdam*

Not to be reproduced by photoprint or microfilm without written permission from the publisher

HARD CORE CORRELATIONS AND NUCLEAR MOMENTS

J. S. BELL and J. M. SOPER

Atomic Energy Research Establishment, Harwell, Didcot, Berks.

Received 5 June 1959

Abstract: The influence of hard core correlations, introduced in the manner of Jastrow, on several shell model matrix elements has been considered. The corrections are all found to be very small, and in a number of cases identically zero.

1. Introduction

We consider the effect on some simple matrix elements of multiplying shell model states by a Jastrow type correlation function [1])

$$F = \prod_{n>m} f(r_{nm}) \tag{1}$$

where f is a real function zero for small r and unity for r much larger than the hard core radius of the internucleon potential. This is thought of as the minimum correlation that must be allowed for if a hard core exists, and not as an adequate account of the whole correlation structure. First a result of Amado [2]) is established in a simple way, namely that (1) causes no correction to the ordinary (as distinct from interaction) magnetic moments and beta decay matrix elements of nuclei with LS-closed cores plus or minus one particle (i.e. N^{15}, O^{17}, K^{39}, Ca^{41}). It is observed that in an LS-coupling approximation this is also true, sometimes accurately and always in first order cluster expansion, for nuclei with LS-closed cores plus or minus two equivalent particles and for all p-shell nuclei. Corrections in Li^6 and N^{14} associated with departure from LS-coupling are estimated by cluster expansion in § 4. In this same approximation corrections to quadrupole effects in O^{17} and F^{17} are calculated in § 5. All these corrections are found to be very small.

2. Magnetic Moments and Beta Decay Matrix Elements

Denoting shell model states by single brackets, and letting double brackets denote the result of multiplying these by (1) and normalizing, we are interested in matrix elements

$$\langle\langle \mathrm{f}|\sum\mu|\mathrm{i}\rangle\rangle = \frac{\langle \mathrm{f}|F\sum\mu F|\mathrm{i}\rangle}{|\langle \mathrm{f}|F^2|\mathrm{f}\rangle\langle \mathrm{i}|F^2|\mathrm{i}\rangle|^{\frac{1}{2}}} \tag{2}$$

where μ is a single particle operator and the summation is over all particles. In this section μ is either the dipole magnetic moment or one of the operators $\boldsymbol{\tau}$ and $\boldsymbol{\tau}\cdot\boldsymbol{\sigma}$ of allowed beta decay. The final state $|\mathrm{f}\rangle$ may be identical with initial state $|\mathrm{i}\rangle$ as required for magnetic moments, or differ from it only in the values T_3, J_z of the projections of isobaric spin and angular momentum — as required for beta decay of nuclei with LS-closed cores plus or minus one particle, to which at first we restrict attention.

In the identity

$$\langle \mathrm{f}|F\sum\mu F|\mathrm{i}\rangle = \tfrac{1}{2}\langle \mathrm{f}|F^2\sum\mu|\mathrm{i}\rangle + \tfrac{1}{2}\langle \mathrm{f}|\sum\mu F^2|\mathrm{i}\rangle - \tfrac{1}{2}\langle \mathrm{f}|[F,[F,\sum\mu]]|\mathrm{i}\rangle \qquad (3)$$

the last term vanishes because either the operators commute with F, or (in the case of orbital magnetic moment) are at most linear in momentum so that their commutators with F commute with F. The first term is equal to

$$\tfrac{1}{2}\sum\langle \mathrm{f}|F^2|\mathrm{n}\rangle\langle \mathrm{n}|\sum\mu|\mathrm{i}\rangle \qquad (4)$$

where $|\mathrm{n}\rangle$ is the complete set of shell model states. Now the states $|\mathrm{n}\rangle$ generated by $\sum\mu$ from $|\mathrm{i}\rangle$ are very limited because the operators do not change the orbital states of individual particles; for the simple nuclei under consideration this means that $|\mathrm{n}\rangle$ is obtained from $|\mathrm{i}\rangle$ by changing at most the T_3 and J_z of $|\mathrm{i}\rangle$ or of the other member of the spin-orbit doublet. The only such state contained in $F^2|\mathrm{f}\rangle$ is $|\mathrm{f}\rangle$ itself, for F^2 conserves total angular momentum and isobaric spin. The summation over $|\mathrm{n}\rangle$ reduces therefore to the single term $|\mathrm{f}\rangle$, and with the second term in (3) similarly reduced we have

$$\langle\langle \mathrm{f}|\sum\mu|\mathrm{i}\rangle\rangle = \frac{\langle \mathrm{f}|F^2|\mathrm{f}\rangle + \langle \mathrm{i}|F^2|\mathrm{i}\rangle}{2|\langle \mathrm{f}|F^2|\mathrm{f}\rangle\langle \mathrm{i}|F^2|\mathrm{i}\rangle|^{\frac{1}{2}}}\langle \mathrm{f}|\sum\mu|\mathrm{i}\rangle. \qquad (5)$$

Because $|\mathrm{i}\rangle$ and $|\mathrm{f}\rangle$ differ only by rotations in space and isobaric spin, the two matrix elements of F^2 are equal; the first factor in (5) is then unity and

$$\langle\langle \mathrm{f}|\sum\mu|\mathrm{i}\rangle\rangle = \langle \mathrm{f}|\sum\mu|\mathrm{i}\rangle. \qquad (6)$$

As applied to magnetic moments (with $|\mathrm{i}\rangle = |\mathrm{f}\rangle$) this result holds also for nuclei with LS closed cores plus or minus two equivalent particles, in so far as the LS coupling approximation is good. The states of the configuration are then entirely classified by the quantum numbers L, S, J, J_z, T, T_3. Since $\sum\mu$ does not alter the configuration and since F^2 does not alter the quantum numbers, the summation (4) reduces to a single term and (6) follows.

For general p-shell configurations, with the exception of $(\mathrm{s})^4$ $(\mathrm{p})^6$ a complete classification is provided by adding to the above quantum numbers the partition, $[\lambda]$. This also commutes with F^2. Thus in so far as the states are eigenstates of $[\lambda]$, L, S, J, J_z, T, T_3, the correlation function (1) causes no corrections to magnetic moments. The argument works for most states

of $(s)^4(p)^6$, but not for the members of certain pairs which have equal values of the quantum numbers listed. These pairs can be separated by adding to the list the parity under particle-hole conjugation [3, 4]). The theorem then holds in first order cluster expansion (§ 3), when F^2 is replaced by unity plus a two body operator which commutes with the conjugation parity as well as with the other quantum numbers.

For beta decay matrix elements ($|\mathrm{i}\rangle \neq |\mathrm{f}\rangle$) these arguments only allow us to arrive at (5). There is no reason in general for the arithmetic and geometric means of the two normalization factors ($\langle \mathrm{f}|F^2|\mathrm{f}\rangle$ and $\langle \mathrm{i}|F^2|\mathrm{i}\rangle$) to be equal. However, they are equal in first order cluster expansion, and to this order the modified matrix element again equals the unmodified.

All the above remarks on beta decay matrix elements apply equally to magnetic dipole transition matrix elements between states of the given configuration.

It should be remarked that the discussion applies only to the ordinary single body magnetic moment and beta decay operators and not to the interaction contributions [5, 6]).

The argument depends essentially on f being simply a real scalar function of r_{nm}. R. D. Amado (private communication) has withdrawn a suggestion [2]) that a restricted kind of spin dependence could be permitted.

3. Cluster Expansion

The first order cluster expansion is defined as follows. Restricting ourselves to cases where the third term in (3) is zero, the general formula is

$$\langle\langle \mathrm{f}|\sum\mu|\mathrm{i}\rangle\rangle = \frac{\langle \mathrm{f}|F^2\sum\mu+\sum\mu F^2|\mathrm{i}\rangle}{2[\langle \mathrm{f}|F^2|\mathrm{f}\rangle\langle \mathrm{i}|F^2|\mathrm{i}\rangle]^{\frac{1}{2}}}. \tag{7}$$

In this we replace F^2 by the expansion

$$\begin{aligned} F^2 &= \prod_{n>m} f^2(r_{mn}) = \prod_{n>m}\{1-h(r_{mn})\} \\ &= 1-\sum_{n>m} h(r_{mn})+\ldots, \end{aligned} \tag{8}$$

and retain only terms of first order in h:

$$\begin{aligned} \langle\langle \mathrm{f}|\sum\mu|\mathrm{i}\rangle\rangle = \langle \mathrm{f}|\sum\mu|\mathrm{i}\rangle\{1+\tfrac{1}{2}\langle \mathrm{f}|\sum h|\mathrm{f}\rangle+\tfrac{1}{2}\langle \mathrm{i}|\sum h|\mathrm{i}\rangle\} \\ -\tfrac{1}{2}\langle \mathrm{f}|\sum h\sum\mu+\sum\mu\sum h|\mathrm{i}\rangle. \end{aligned} \tag{9}$$

The neglected terms involve the near coincidence of three particles, or two separate pairs, and so are of at least one order higher in the effective volume

$$\int h(r)\mathrm{d}\mathbf{r} \tag{10}$$

of the correlation function. The method therefore depends on this being

sufficiently small—presumably in comparison with the mean volume per nucleon.

For the magnetic moment and beta decay operators, which do not lead out of the configuration, the last term of (9) is conveniently evaluated by introducing as intermediate states the set $|\mathrm{n}\rangle$ of LS coupling states of the configuration, and $|\mathrm{i}\rangle$ and $|\mathrm{f}\rangle$ are expanded in terms of these:

$$|\mathrm{i}\rangle = \sum \alpha_\mathrm{n} |\mathrm{n}\rangle, \quad |\mathrm{f}\rangle = \sum \beta_\mathrm{n} |\mathrm{n}\rangle.$$

As mentioned in § 2 the set $|\mathrm{n}\rangle$ can be so chosen that $\sum h$ has only diagonal elements. Then

$$\langle\langle \mathrm{f}|\sum \mu|\mathrm{i}\rangle\rangle = \sum_{\mathrm{nm}} \beta_\mathrm{n}^* \alpha_\mathrm{m} \langle \mathrm{n}|\sum \mu|\mathrm{m}\rangle$$
$$\{1 + \{\tfrac{1}{2}\sum_\mathrm{l} (\beta_\mathrm{e}^* \beta_\mathrm{e} + \alpha_\mathrm{e}^* \alpha_\mathrm{e}) \langle \mathrm{l}|\sum h|\mathrm{l}\rangle - \tfrac{1}{2}\langle \mathrm{n}|\sum h|\mathrm{n}\rangle - \tfrac{1}{2}\langle \mathrm{m}|\sum h|\mathrm{m}\rangle\}. \quad (11)$$

In evaluating this, only particles outside the LS-closed core need be considered. The filled shells do not of course contribute to the matrix elements of the magnetic moment and beta decay operators. To the matrix elements of $\sum h$ they contribute only diagonal terms equal for all n; the omission of these in (11) causes no error.

In what follows we have for analytical simplicity represented h by a gaussian,

$$h(r) = \mathrm{e}^{-r^2/a^2}, \quad (12)$$

and used oscillator wave functions, whose extension is measured by the parameter b in the common factor $\mathrm{e}^{-r^2/2b^2}$. To obtain a definite range a, where it was needed, we have arbitrarily put the effective volume (10) equal to the volume per nucleon $\frac{4}{3}\pi r_0^3$ in a standard heavy nucleus. With $r_0 = 1.1 \times 10^{-13}$ cm,

$$a = 1.0 \times 10^{-13} \text{ cm}.$$

This is in fact close to the range suggested to Amado [2]) by the work of Brueckner and Gammel [7]), allowing for the fact that his gaussian represents not $(1-f^2)$ but $(1-f)$. On the face of it the cluster expansion parameter is then unity, suggesting large effects and poor convergence. However, our lowest order calculations have produced only very small effects, confirming the idea that nuclear moments are highly insensitive to the short range correlation structure. The magnitude of higher order terms we have not investigated; in the binding energy problems they have been considered by Dąbrowski [8]).

4. Li^6 and N^{14}

The simplest nuclei which will provide non zero correlation effects on magnetic moments and beta decay are those with two odd equivalent particles or holes, departure from LS coupling being allowed for.

Consider first the magnetic moment of Li^6. This involves a configuration of two p particles with total spin 1 and isobaric spin zero. The states n, m, l, in (11) can be restricted to those of isobaric spin zero and only the isobaric scalar part of $\sum\mu$ is operative; this commutes with the complete set of quantum numbers $(LSJJ_zTT_3)$ so that $\sum\mu$ has only diagonal elements. The state $|i\rangle = |f\rangle$ is a mixture of ^{13}S, ^{11}P, and ^{13}D, with expansion coefficients $\beta_1, \beta_2, \beta_3$. Denoting by μ_1, μ_2, μ_3, and h_1, h_2, h_3, the diagonal matrix elements of $\sum\mu$ and $\sum h$, one finds after some rearrangement

$$\begin{aligned}\langle\langle\textstyle\sum\mu\rangle\rangle - \langle\textstyle\sum\mu\rangle = &-|\beta_1\beta_2|^2(\mu_1-\mu_2)(h_1-h_2)\\ &-|\beta_2\beta_3|^2(\mu_2-\mu_3)(h_2-h_3)\\ &-|\beta_3\beta_1|^2(\mu_3-\mu_1)(h_3-h_1).\end{aligned} \tag{13}$$

The matrix elements are

$$(\mu_1, \mu_2, \mu_3) = 0.19(1, -1, -2) \tag{14}$$

in nuclear magnetons, and

$$(h_1, h_2, h_3) = (\tfrac{1}{2}, -\tfrac{3}{4}, -\tfrac{1}{4})X \tag{15}$$

where

$$\begin{aligned}X &= \gamma^3 - 2\gamma^5 + \gamma^7,\\ \gamma &= \left(\frac{a^2}{a^2+2b^2}\right)^{\frac{1}{2}},\end{aligned} \tag{16}$$

and where we have omitted terms which are common to all three μ_i or all three h_i, which evidently do not contribute to (13).

With the values given in (14) and (15), (13) is confined for arbitrary normalized β to the range

$$-\frac{0.19}{4}(1\pm 1.5)X;$$

for all a and b the quantity X is bounded by

$$0 \leqq X \leqq 0.092, \tag{17}$$

so that for all values of the parameters the result is in the range

$$\langle\langle\textstyle\sum\mu\rangle\rangle - \langle\textstyle\sum\mu\rangle = -(1\pm 1.5)4.4\times 10^{-3} \tag{18}$$

and is negligible in comparison with uncertainties in $\langle\mu\rangle$ due to lack of knowledge of the wave functions and to the possible presence of interaction currents [5, 9]) which are of order 0.1.

This result applies equally to N^{14} which has the same J and T but involves two holes rather than two particles. The operation of particle-hole conjugation [3, 4]) shows that the only change in the matrix elements in (11) is an unimportant constant diagonal contribution to those of $\sum h$.

Consider next the beta decays $He^6 \to Li^6$ and $C^{14} \to N^{14}$ which can be

treated together because of the conjugation relation. The initial ($J = 0$ $T = 1$) state is a mixture of ^{31}S and ^{33}P which will be written

$$|\mathrm{i}\rangle = \alpha_4|4\rangle + \alpha_5|5\rangle.$$

The final state we have had above. The correction factors to decay matrix elements due to correlation will be independent of the J_z and T_3 of initial and final states, and equal for all components of the Gamow-Teller operator $\boldsymbol{\tau} \cdot \boldsymbol{\sigma}$. We choose to work with $\mu = \tau_3\sigma_3$, and with $J_z = T_3 = 0$ for all states involved. The matrix elements required in (11) are then

$$\begin{aligned} \mu_{14} &= 1, & \mu_{25} &= -1/\sqrt{3}, \\ h_4 &= h_1, & h_5 &= h_2, \end{aligned} \tag{19}$$

the latter being given by (15).

For the $He^6 \rightarrow Li^6$ case we take the wave functions †

$$\begin{aligned} &\beta_1 = 0.986, \quad \beta_2 = 0.160, \quad \beta_3 = -0.037, \\ &\alpha_4 = 0.933, \quad \alpha_5 = -0.360. \end{aligned} \tag{20}$$

There is little admixture here, the states being almost pure S states. As a result the correlation correction to the decay rate is very small, less using (17) than one per cent of the unmodified value. Again it is possible to calculate the maximum values of the correction by varying the wave function parameters α_i and β_i and the range parameter γ. In no case does the correction exceed 5% of the experimental value and therefore the corrections considered here are always small compared with the uncertainties in the shell model prediction of this quantity.

In the case of $C^{14} \rightarrow N^{14}$, experiment requires almost complete cancellation of the various terms in the matrix element [11, 12]). We consider therefore how much the shell model mixture of states must be altered to restore this when the correlation effect is included. After some rearrangement and the omission of small terms, the required condition is

$$0 = \beta_1^* \alpha_4 - \frac{1}{\sqrt{3}} \beta_2^* \alpha_5 (1 + h_1 - h_2). \tag{21}$$

With $a = 10^{-13}$ cm, $b = 1.6 \times 10^{-13}$ cm, $h_1 - h_2 = 0.06$. Thus cancellation can be restored by for example a 6 % change in $\beta_1^* \alpha_4$ or $\beta_2^* \alpha_5$ from the values suitable before the introduction of correlation. Such a change would not cause any appreciable change in other calculated properties of these nuclei.

5. Quadrupole effects in O^{17} and F^{17}

We consider finally the simplest nuclei which show quadrupole effects, namely O^{17} and F^{17}. In (9) μ is now the quadrupole operator

† Obtained using the force mixture derived in ref. [10]). In the notation of that paper [11]O was taken to be -0.5, a value derived from the spectra of Li^8 and B^{10} (J. M. Soper, unpublished).

$$\mu = 3z^2 - r^2. \tag{22}$$

For the ground state quadrupole moment $|\mathrm{i}\rangle = |\mathrm{f}\rangle$ is the determinantal wave function appropriate to filled s and p shells plus an odd particle in the d state with $j = j_z = \frac{5}{2}$. The operator

$$\sum\mu\sum h + \sum h\sum\mu = 2\sum\mu\sum h$$

in (9) can be separated into a sum of 2- and 3-body terms. The expression can then be expressed in terms of 1- and 2-body matrix elements as follows:

$$\begin{aligned}\langle\langle\mu\rangle\rangle - \langle\mu\rangle &= \tfrac{1}{2}\sum(\mathrm{l}|\mu|\mathrm{l})\sum'(\mathrm{mn}|h'|\mathrm{mn}) \\ &\quad -\tfrac{1}{2}\sum'(\mathrm{mn}|(\mu_1+\mu_2)h'|\mathrm{mn}) \\ &\quad -\tfrac{1}{2}\sum'[(\mathrm{l}|\mu|\mathrm{l})(\mathrm{mn}|h'|\mathrm{mn}) + (\mathrm{l}|\mu|\mathrm{m})(\mathrm{mn}|h'|\mathrm{nl}) + (\mathrm{l}|\mu|\mathrm{n})(\mathrm{mn}|h'|\mathrm{lm})]\end{aligned} \tag{23}$$

where the summations are over all values of the indices (which enumerate the single body states of the determinantal wave function) except that where a prime occurs on the summation sign no two indices are allowed to be equal; h' is defined by

$$h' = h(1 - \mathrm{P}^r\mathrm{P}^\sigma\mathrm{P}^\tau) \tag{24}$$

where the P's are space, spin, and charge exchange operators.

Because of the limited number of states appearing, and because of selection rules associated with μ, the terms in (23) involving off-diagonal elements of μ do not contribute for the present nuclei. There is some cancellation among the remainder, leaving

$$\tfrac{1}{2}\sum'\{(\mathrm{m}|\mu|\mathrm{m}) + (\mathrm{n}|\mu|\mathrm{n})\}(\mathrm{mn}|h'|\mathrm{mn}) - \tfrac{1}{2}\sum'(\mathrm{mn}|\mu_1+\mu_2)h'|\mathrm{mn}). \tag{25}$$

Terms not involving the odd particle state $|\mathrm{o})$ must cancel among themselves, for there can be no correction to the zero quadrupole moment of O^{16}; there remains

$$\sum_{\mathrm{o}<\mathrm{n}}\{-(\mathrm{on}|(\mu_1+\mu_2)h'|\mathrm{on}) + [(\mathrm{o}|\mu|\mathrm{o}) + (\mathrm{n}|\mu|\mathrm{n})](\mathrm{on}|h'|\mathrm{on})\}. \tag{26}$$

This we have evaluated in the extreme short range limit for h; although the shape of h is then unimportant we continue to express results in terms of the gaussian (12). With the unperturbed moment of F^{17} as unit the perturbed moment is found to be

$$e + \frac{7}{8}\left(\frac{a}{\sqrt{2b}}\right)^3(2e-1) \tag{28}$$

where $e = 1$ for F^{17}, $e = 0$ for O^{17}.

The E_2 transition ($2\mathrm{s}_{\frac{1}{2}} \rightarrow 1\mathrm{d}_{\frac{5}{2}}$) can be discussed similarly. To obtain the correction factor for the reduced matrix element it is sufficient to obtain that for the matrix element of $\sum\mu$ between the particular magnetic substates $J_z = \frac{1}{2}$. When (9) is again reduced to 1- and 2-body matrix elements one finds that a particular off diagonal element of μ can now contribute — be-

tween the odd d state of $|\mathrm{f}\rangle$ with magnetic quantum number $\frac{1}{2}$ and one of the s states; denoting the latter by 1,

$$\begin{aligned}\langle\langle \mathrm{f}|\sum\mu|\mathrm{i}\rangle\rangle - \langle \mathrm{f}|\sum\mu|\mathrm{i}\rangle = \sum_{\mathrm{o}<\mathrm{n}} [&-(\mathrm{on}|(\mu_1+\mu_2)h'|\bar{\mathrm{o}}\mathrm{n}) \\ &+(\mathrm{o}|\mu|\bar{\mathrm{o}})\{\tfrac{1}{2}(\mathrm{on}|h'|\mathrm{on})+\tfrac{1}{2}(\bar{\mathrm{o}}\mathrm{n}|h'|\bar{\mathrm{o}}\mathrm{n})\} \\ &+(\mathrm{n}|\mu|\mathrm{n})(\mathrm{on}|h'|\bar{\mathrm{o}}\mathrm{n})+(\mathrm{o}|\mu|1)(1\mathrm{n}|\bar{h}|\bar{\mathrm{o}}\mathrm{n})]\end{aligned} \tag{29}$$

where the use of indices (o, $\bar{\mathrm{o}}$) indicates that the odd particle states are different of the two sides. In the short range limit the unperturbed F^{17} value is found to be multiplied by

$$e+\frac{19}{32}\left(\frac{a}{\sqrt{2b}}\right)^3(2e-1). \tag{30}$$

Numerically, with $b = 1.8\times 10^{-13}$ cm (as suggested by Coulomb energy[13])) and $a = 1\times 10^{-11}$ cm, the correction factors (28) and (30) are

$$e+0.05(2e-1), \quad e+0.04(2e-1).$$

The very small correlation corrections here are no help in explaining the experimental results. Both E2 transition rates are known, and the ground state moment of O^{17}, and all differ considerably from the unmodified shell model predictions [14, 15]). For the O^{17} ground state moment our effect has the wrong sign, and in all three cases is an order of magnitude too small.

Here we have calculated only in the short range limit for h. It might be argued that this is all we are entitled to do when higher order cluster terms have been ignored. On the other hand the terms ignored in the cluster expansion are of relative order $(a/b)^3$, while those ignored in taking the short rangelimit for h are of order (it turns out) $(a/b)^2$. In the case of O^{17} we can restore these terms by using the results of Amado [14]), who calculates in perturbation theory the correlation effect due to a non singular 2-body potential v. The perturbed initial state is

$$|\mathrm{i}\rangle\rangle = \left[1+\frac{\mathrm{Q}_1}{\mathrm{e}_1}\{\sum_{n>m} v_{nm}-\sum_n V_n\}\right]|\mathrm{i}\rangle \tag{31}$$

(and similarly for $|\mathrm{f}\rangle\rangle$) where V is the oscillator potential, e_1 the excess of the unperturbed energy of $|\mathrm{i}\rangle$ over that of the intermediate state, and Q_1 is an exclusion operator removing $|\mathrm{i}\rangle$ as an intermediate state. The perturbed matrix element is

$$\langle\langle \mathrm{f}|\sum\mu|\mathrm{i}\rangle\rangle = \langle \mathrm{f}|\sum\mu\frac{\mathrm{Q}_1}{e_1}(\sum v-\sum V)|\mathrm{i}\rangle+\langle \mathrm{f}|(\sum v-\sum V)\frac{\mathrm{Q}_\mathrm{f}}{e_\mathrm{f}}\sum\mu|\mathrm{i}\rangle. \tag{32}$$

For an oscillator potential V, selection rules associated with $\sum\mu$ result in e_1 and e_f having a certain contant value $-\bar{E}$. In the O^{17} case, where the odd

particle is uncharged, the V in (32) does not in fact contribute. Then (32) is identical with (9) if we put

$$\tfrac{1}{2}h = +V/\bar{E}.$$

In this way we find from Amado that the finite range of h causes a factor

$$\left\{1+\frac{11}{7}\left(\frac{a}{b}\right)^2+\left(\frac{6}{7}\right)\left(\frac{a}{b}\right)^4\right\} \Big/ \left\{1+\frac{1}{2}\left(\frac{a}{b}\right)^2\right\}^{\frac{11}{2}} \approx 0.7.$$

Thus the short range approximation gives an overestimate by some 40%. This is not of much significance for the present exploration of order of magnitude.

6. Conclusion

We have found that in so far as the cluster expansion gives a good estimate, the "holes" punched in nuclear wave functions by a hard core potential have little effect on a number of simple matrix elements. It would of course be desirable to have similar calculations for more elaborate correlation functions, depending on spin, isobaric spin, and possibly on momentum [2]). These will be worth doing when convincing procedures become available for determining such functions from assumed potentials. Our results indicate that the explanation of several failures of the shell model must lie with much more sophisticated short range correlations, or with longer range correlations that cannot be tackled by the Jastrow method. One such difficulty arises in connection with the magnetic moments of N^{15} and O^{17}. That these lie so exactly on the Schmidt lines, despite the probable contributions of interaction moments, suggests the need for small corrections to shell model wave functions. Here our simple hard core correlations have zero effect. On the other hand there are indications [16]) that perturbation theory with a regular pseudo-potential may give contributions of the required order. A clearer failure of the shell model is for the quadrupole effects (to which interaction contributions are usually supposed negligible) in nuclei near O^{16}. Here our correlation effects give contributions which are much too small. Again the pseudo-potential perturbation theory has had some success [14]), but it is incomplete [17]).

For useful discussion we are indebted to G. Barton, A. M. Lane, J. P. Elliott, J. K. Perring (who is particularly thanked for supplying matrix elements of the delta function for § 5), T. H. R. Skyrme and E. J. Squires.

References

1) R. Jastrow, Phys. Rev. **98** (1955) 1479
2) R. D. Amado, Phys. Rev. **111** (1958) 548
3) G. Racah, Phys. Rev. **62** (1942) 438
4) J. S. Bell, Nuclear Physics **12** (1959) 117

5) R. J. Blin-Stoyle, Theories of Nuclear Moments (Oxford Univ. Press, 1957)
6) J. S. Bell and R. J. Blin-Stoyle, Nuclear Physics **6** (1958) 87
7) K. A. Brueckner and J. L. Gammel, Phys. Rev. **107** (1957) 781
8) J. Dabrowski, Proc. Phys. Soc. **72** (1958) 499
9) J. M. Soper, Ph. D. thesis (Cambridge 1958) to be published
10) J. M. Soper, Phil. Mag. **2** (1957) 1219
11) J. P. Elliott, Phil. Mag. **1** (1956) 503
12) W. M. Visscher and R. A. Ferrell, Phys. Rev. **107** (1957) 781
13) J. P. Elliott, private communication
14) R. D. Amado, Phys. Rev. **108** (1957) 1462
15) Lehmann *et al.*, C. R. de L'Acad. Sci. (Paris) **245** (1957) 2259
16) J. S. Bell, Nuclear Physics **4** (1957) 295
17) G. Barton, Nuclear Physics **11** (1959) 466

1.E.4:
3.A:4.E

Nuclear Physics **13** (1959) 177—180; © *North-Holland Publishing Co., Amsterdam*
Not to be reproduced by photoprint or microfilm without written permission from the publisher

LIFETIME OF THE 362-keV E1 TRANSITION IN Tb^{159}

F. R. METZGER and W. B. TODD †

Bartol Research Foundation of the Franklin Institute, Swarthmore, Penna ††

Received 22 June 1959

Abstract: Using the Doppler broadening at elevated temperatures, resonance fluorescence from the 362-keV excited state of Tb^{159} has been observed. From the magnitude of the resonance scattering effect, assuming a spin value of $\frac{5}{2}$ for the excited state and a branching ratio Γ_0/Γ of 0.96, a mean life $\tau_\gamma = (2.0 \pm 0.3) \times 10^{-10}$ s had been determined for the gamma-ray transition to the ground state. Internal conversion measurements confirmed the electric dipole character of the 362-keV transition.

1. Introduction

A recent investigation [1]) of the disintegration scheme of 18-hour Gd^{159} showed that the 362-keV gamma-ray in Tb^{159} is an electric dipole transition. A delayed coincidence measurement [2]) established an upper limit of 5×10^{-10} second for the mean life of this transition, indicating a hindrance factor smaller than 10^5. The determination of the actual mean life appeared to be of interest, and the short upper limit suggested the use of the resonance fluorescence method [3]). The thermal method of compensating for the recoil energy losses was chosen because it presented the least amount of difficulties once the problem of obtaining sufficient scattering material had been solved †††.

While the measured mean life could be easily attributed to a slow E1 transition, it was sufficiently long to be also compatible with an (E2+M1) assignment. Since such a characterization of the 362-keV transition had been made [4]) on the basis of a more recent determination of the conversion coefficient, it was decided that another conversion measurement should be carried out. This was done with a lens spectrometer, using the 265-keV transition in As^{75} and the 412-keV transition in Hg^{198} for comparison purposes.

† Now with RCA Atomic Energy Service, Cherryhill, New Jersey.

†† Assisted by the Joint Program of the U. S. Office of Naval Research and the U. S. Atomic Energy Commission.

††† Three pounds of terbium oxide were made available to us through the courtesy of the Lindsay Chemical Division of the American Potash and Chemical Corporation, West Chicago, Illinois.

2. Resonance Scattering Experiments

2.1. SOURCE PREPARATION

The sources for the resonance scattering experiments were prepared by irradiating 10 mg of gadolinium oxide, enriched in Gd^{158} (92.87 %) †, for approximately one day in the Oak Ridge National Laboratory Research Reactor in a flux of $\approx 5\times 10^{13}$ slow neutrons per cm^2 per second. No chemical separation was performed. A small amount of 9-hour Eu^{152} was found to be present in these sources. Because of the higher energy of its gamma rays and because of geometrical limitations which made it inconvenient to increase the length of the direct beam attenuator, this impurity contributed an appreciable fraction to the total counting rate.

When a Gd^{159} source, prepared in this way, was placed at a distance of 200 cm from a sodium iodide scintillation counter of 3.5 cm diameter and 4 cm length, counting rates of the order of 10^5 per minute were registered in a channel comprising the full width at half maximum of the 362-keV full energy peak. In the most favourable geometry for the scattering experiment (125°) Rayleigh counting rates of 5×10^3 counts/min were observed in the same range of pulse heights.

2.2. ANGULAR DISTRIBUTION OF THE RESONANCE RADIATION

The scattering experiments were carried out in a conventional ring geometry using terbium oxide and neodymium oxide as the scattering materials. Measurements were taken at scattering angles of 125° and 144°, with the source at room temperature and at 1000° C. As the resonance effects at the high source temperature amounted to only ≈ 5 % of the total counting rate, the statistical errors were considerable. Thus it can only be stated that in the expression $W(\theta) = 1+a_2\cos^2\theta$ for the angular distribution †† the coefficient a_2 has the value $a_2 = 0.1\pm 0.4$. For a pure dipole transition in a spin sequence $\frac{3}{2}-\frac{5}{2}-\frac{3}{2}$ the expected value of the coefficient is $a_2 = 0.23$.

2.3. LIFETIME OF THE 362-keV TRANSITION

For the evaluation of the lifetime, the measurements at the 125° scattering angle were used. For a distribution of the form $W = 1+a_2\cos^2\theta$ the differential cross section $d\sigma\,(125°.3)/d\Omega$ is equal to $\sigma_{total}/4\pi$, independent of the value of a_2. For the actual angle of 125° and the upper limit of 0.5 for a_2, the error commited in setting $\sigma_{total} = 4\pi d\sigma/d\Omega$ is smaller than 0.2 %.

Assuming Maxwellian velocity distributions for the nuclei in the source and in the scatterer, the average resonance scattering cross section may be

† Obtained from the Stable Isotopes Division of the U.S. Atomic Energy Commission.

†† A possible $\cos^4\theta$-term was excluded on the basis of the conversion measurements described in section 3.

written in the form

$$\sigma_{av}(T_e, T_a) = \frac{g_2}{g_1} \frac{\lambda^2}{4\pi^{\frac{1}{2}}} \frac{\Gamma_0^2}{\Gamma} \frac{1}{E_\gamma} \left(\frac{Mc^2}{2k(T_e+T_a)}\right)^{\frac{1}{2}} \exp\left(-\frac{E_\gamma^2/Mc^2}{2k(T_e+T_a)}\right) \quad (1)$$

where g_2 and g_1 are the statistical weights of excited state and ground state, respectively, E_γ is the energy of the transition and λ the corresponding wavelength, Γ_0 the partial width of the ground state transition, Γ the total width of the excited level, M the mass of the resonant nuclei, k Boltzmann's constant, T_e and T_a the effective temperatures [5]) of source and scatterer.

According to Ballini and Barloutaud [2]) the sum of the intensities of the 300- and 222-keV transitions originating from the 362-MeV level is 3 % of the intensity of the ground state transition. Adding to this the internal conversion intensity, one arrives at a value $\Gamma_0/\Gamma \approx 0.96$. Insertion of this in eq. (1) results in a linear relationship between Γ_0 and the average resonance scattering cross section. In the actual scattering experiment one measures the difference $[\sigma_{av}(T_e, T_a) - \sigma_{av}(T'_e, T_a)]$ where T_e is the elevated source temperature, T'_e is the effective room temperature.

Assuming a $\frac{3}{2}-\frac{5}{2}-\frac{3}{2}$ spin sequence, i.e. setting $g_2/g_1 = 1.5$, and inserting $T_a = T'_e = 317$, $T_e = 1283$ and the other numerical values into eq. (1), the difference of the cross sections becomes

$$\sigma_{av}(1283,\ 317) - \sigma_{av}(317,\ 317) = 1.92 \times 10^{21} \times (\Gamma_0)_{eV}\ \text{cm}^2. \quad (2)$$

The experimental value for $\sigma_{av}(1283) - \sigma_{av}(317)$ is $(6.4 \pm 0.5) \times 10^{-27}$ cm^2. With eq. (2) this leads to $\Gamma_0 = 3.33 \times 10^{-6}$ eV or a mean life $\tau_\gamma = (1.97 \pm 0.16) \times 10^{-10}$ s. The error quoted here reflects only the statistical uncertainty. Considering the many uncertainties involved in the evaluation of the geometry, it appears to be reasonable to double the error and to quote as the mean life of the 362-keV gamma transition in Tb^{159} the value $\tau_\gamma = (2.0 \pm 0.3) \times 10^{-10}$ s. The mean life of the 362-keV level, $\tau_{level} = (1.9 \pm 0.3) 10^{-10}$ s is close to the upper limit established by Quidort [2]). The hindrance factor is 5×10^4, i.e. falls into the range covered by other E1 transitions in rare earth nuclei [6, 7]).

3. Measurement of the K-Conversion Coefficient

The sources for the lens spectrometer studies were prepared from Gd^{159} with a specific activity of approximately 1 mC/mg by dissolving Gd_2O_3 in acid, depositing a droplet onto a 2 mg/cm^2 Saran foil and evaporating to dryness.

For the determination of the K-conversion coefficient of the 362-keV transition, use was made of two transitions with known conversion coefficients, the 265-keV transition in As^{75} and the 412-keV transition in Hg^{198}. Beta spectrometer sources of Se^{75}, Gd^{159} and Au^{198} of closely the same

physical size were prepared and their respective gamma counting rates were determined with a sodium iodide scintillation counter for which the energy dependence of the detection efficiency was known. The sources were then placed into the lens spectrometer and the K-conversion lines of the three transitions of interest were measured. Using the known conversion coefficients for two of the transitions, two values were obtained for the K-conversion coefficient of the 362-keV transition in Tb^{159}. The fact that these two values differed by less than 10 % was taken as a confirmation of the gamma efficiency curve and an indication of the consistency of the interval conversion date on Se^{75} [8]) and Au^{198} [9]). Using the values $(6.2\pm0.3)\times10^{-3}$ and 2.81×10^{-2} for the K-conversion coefficients of the 265- and the 412-keV transitions, respectively, a value $\alpha_K = (8.1\pm2.0)\times10^{-3}$ was obtained for the 362-keV transition in Tb^{159}. This is in complete agreement with ref. [1]) and in disagreement with ref. [4]). The 362-keV transition is, therefore, an electric dipole transition.

4. Summary

The 362-keV transition in Tb^{159} is shown to be an E1 transition on the basis of K-conversion measurements. From resonance scattering experiments a mean life of $(2.0\pm0.3)\times10^{-10}$ s is found for the 362-keV ground state transition in Tb^{159}. This mean life is 5×10^4 times longer than the theoretical mean life for a single proton transition [10]). This is in accord with the level assignment given in ref. [6]) which characterizes the transition as hindered.

This work would not have been possible without the generous loan of the terbium oxide by the Lindsay Chemical Division of the American Potash and Chemical Corporation; our special thanks go to Mr. Howard E. Kremers, Vice President, for granting the loan and making the necessary arrangements.

References

1) Nielsen, Nielsen and Skilbreid, Nuclear Physics **7** (1958) 561
2) J. Quidort, quoted by R. Ballini and R. Barloutaud, Journ. Phys. Radium **17** (1956) 534
3) For a summary see F. R. Metzger, Progress in Nuclear Physics, Vol. VII, ed. O. R. Frisch (Pergamon Press, London, 1959)
4) Malik, Nath and Mandeville, Phys. Rev. **112** (1958) 262
5) W. E. Lamb, Phys. Rev. **55** (1939) 190
6) B. R. Mottelson and S. G. Nilsson, Mat. Fys. Skr. Dan. Vid. Selsk. **1**, No. 8 (1959)
7) M. E. Voikhanskii, JETP **6** (1958) 771
8) F. R. Metzger and W. B. Todd, Nuclear Physics **10** (1959) 220
9) Wapstra, Nijgh, Salomons-Grobben and Ornstein, Nuclear Physics **9** (1958/59) 538
10) S. Moszkowski, Beta- and Gamma-Ray Spectroscopy, ed. K. Siegbahn (North Holland Publishing Company, Amsterdam) Ch. 13

7.A *Nuclear Physics* **13** (1959) 181—192; © *North-Holland Publishing Co., Amsterdam*
Not to be reproduced by photoprint or microfilm without written permission from the publisher

ON ANALYTIC PROPERTIES OF VERTEX PARTS IN QUANTUM FIELD THEORY

L. D. LANDAU
Institute for Physical Problems, Moscow

Received 27 April 1959

Abstract: A general method of finding the singularities of quantum field theory values on the basis of graph techniques is evolved.

1. Introduction

In recent years many papers have been concerned with dispersion relations. As is known, the latter express the analytic properties of various quantities of quantum field theory. The problem of localizing the singularities of these quantities is therefore highly important. As has become clear recently [1,2]), a direct study of graphs is the most effective method of investigating the location and nature of the singularities of vertex parts. It is often claimed that the graph technique is not sufficiently convincing, since it involves perturbation theory, unlike other, allegedly more rigorous methods. This view is actually based on misunderstanding. Since a rigorous theory which makes use of the Hamiltonian reduces interaction to zero, the sole completely rigorous dispersion relation in this theory is $0 = 0$. By posing the problem of analytic properties of quantum field values, we actually go beyond the framework of the current theory. An assumption is thereby automatically made that there exists a non-vanishing theory in which ψ-operators and Hamiltonians are not employed, yet graph techniques are retained. In evolving dispersion relations, therefore, the employment of the graph technique is, indeed, solely consistent, since the problem becomes meaningless if the graph technique is rejected.

The graph technique is by no means equivalent to perturbation theory, since all particles, stable as regards strong interactions, are considered, whether they are "simple" or "complex". In fact, first steps are thereby taken towards new graph techniques, which will be a generalization of the previous methods and will lay the foundation of the future theory. It stands to reason that the applicability of the graph technique of this type is likewise hypothetical and a test of successive results will be a test of the hypothesis itself.

Unfortunately, expressions obtained in considering more complex graphs are very lengthy. It may be demonstrated, however, that a study may be carried out in general form and be simplified considerably with the help of a corresponding graphic representation.

2. General Method

An arbitrary graph represents a certain integral

$$\int \frac{B\mathrm{d}^4k\mathrm{d}^4l\ldots}{A_1A_2A_3\ldots}\quad . \tag{1}$$

where

$$A_i = m_i^2 - q_i^2, \tag{2}$$

q_i is a certain 4-momentum, corresponding to the given line in a graph, m_i the mass of the particle in question and B a certain polynomial of the vectors q_i. According to the well known Feynman method, one may write

$$\frac{1}{A_1A_2A_3\ldots} = (n-1)!\int_0^1\ldots\int_0^1 \frac{\mathrm{d}\alpha_1\mathrm{d}\alpha_2\ldots\mathrm{d}\alpha_n\,\delta(\alpha_1+\alpha_2+\ldots+\alpha_n-1)}{(\alpha_1A_1+\alpha_2A_2+\ldots+\alpha_nA_n)^n}. \tag{3}$$

The expression $\alpha_1A_1+\alpha_2A_2+\ldots$ in the denominator is a polynomial of second degree with respect to the integration variables $k, l, \ldots$ The terms linear with respect to $k, l, \ldots$ may always be eliminated by transforming integration variables, after which we obtain

$$\alpha_1A_1+\alpha_2A_2+\ldots = \varphi+K(k', l', \ldots). \tag{4}$$

Here K is a homogeneous quadratic form of the new integration variables with coefficients depending only on the parameters α_i, and φ is a heterogeneous quadratic form of the vectors p_i, describing the free ends of the graph under consideration.

Let us confine ourselves to the case of real values of the squares and the scalar products of the vectors p_i. It is easy to verify that if the values of φ are positive the integral with respect to $k, l, \ldots$ is a real quantity (a self-conjugated spinor in the case of spinor functions), since the quadratic form K becomes positive definite (because all α_i are positive) when $k_4 \to i\kappa, l \to i\lambda$ are substituted. The vertex part is real, therefore, if $\varphi > 0$ for all values α_i; if, on the other hand, $\varphi < 0$ for certain values α_i, the vertex part becomes complex. The nearest singularity of the vertex part is obviously located at the values p_i, for which φ vanishes for determined values of all α_i and is positive at all other α_i; in other words, the singularities correspond to the vanishing of the minimum value of φ, treated as a function of α_i. If the singularities in the complex region are meant, any extremum of the function φ should be considered. It will be noted that since φ is a homogeneous function of the first order with respect to the variables α_i, the condition $\sum\alpha_i = 1$

may be excluded when the conditions of the existence of the vanishing extremum are being found.

Let us denote $\alpha_1 A_1+\alpha_2 A_2+ \ldots$ as f. Since K is a quadratic form of the variables k', l', . . ., it is clear that φ is the value of the function f at additional conditions

$$\partial f/\partial k' = \partial f/\partial l' = \ldots = 0,$$

and, since k differs from k' by a constant vector, the latter conditions may be written

$$\partial f/\partial k = \partial f/\partial l = \ldots = 0. \tag{5}$$

The positiveness of the values α_i should be taken into account in finding the conditions of the minimum. Hence it follows that either the condition $\partial\varphi/\partial\alpha_i = 0$ or $\alpha_i = 0$ should take place for every value α_i. In the latter case $\partial\varphi/\partial\alpha_i = 0$ should exist for the nearest singularity. According to the definition we have

$$\frac{\partial\varphi}{\partial\alpha_i} = \frac{\partial f}{\partial\alpha_i} + \frac{\partial f}{\partial k}\frac{\partial k}{\partial\alpha_i} + \frac{\partial f}{\partial l}\frac{\partial l}{\partial\alpha_i} + \cdots.$$

Since all $\partial f/\partial k$ equal zero according to (5), the condition $\partial\varphi/\partial\alpha_i = 0$ is equivalent to the condition $\partial f/\partial\alpha_i = 0$, i.e., according to the definition of f,

$$A_i = 0. \tag{6}$$

Thus, the singularity of the vertex part may be obtained through a joint solution of the equations $A_i = 0$ (or $\alpha_i = 0$) with additional conditions

$$\sum_i \alpha_i \frac{\partial A_i}{\partial k} = \sum_i \alpha_i \frac{\partial A_i}{\partial l} = \ldots = 0. \tag{7}$$

It is essential that these equations should have solutions with positive α_i.

Thus, it may be claimed with respect to every line of the Feynman graph that it either satisfies the condition $q_i^2 = m_i^2$ or passes out of consideration altogether (when $\alpha_i = 0$). In the latter case the singularity under consideration may be ascribed not to the graph in question but to a graph from which the i-line is absent, i.e., the vertices connected by it are fused. In analysing the singularities of the graph, it is sufficient therefore to consider the case when all $\alpha_i \neq 0$.

It can easily be seen that the condition (7) may be written as $\sum\alpha_i q_i = 0$, where summation is carried out not with respect to all lines of the Feynman graph, but with respect to the aggregates of lines forming closed contours, the direction of the vector q_i corresponding to the direction of the contour. The positiveness of the coefficients α_i denotes that if the vectors q_i are regarded as the directions of forces, the possibility of a solution of eq. (7) denotes the possibility of picking such values of these forces as would enable them to preserve equilibrium.

3. Graphs for Green's Functions

It is comparatively easy to interpret the singularities as they arise with the help of the present method. Let us begin with considering the graphs for Green's functions. In this case all vectors q_i obtained from the indicated equations are obviously parallel to the same vector p.

3.1. VERTEX PART WITH TWO EXTERNAL ENDS

Consider the graph in fig. 1. Setting down the formula $\sum \alpha_i q_i = 0$ for the contour formed by any couple of lines and taking into account the positiveness of the quantities α_i, we may infer that all vectors q_i are equally directed with respect to the vertices of the graphs. Noting that the vector lengths are equal to the corresponding masses, we easily obtain the obvious result $p^2 = (\sum m_i)^2$ for the singularities. It will be noted that in the case of Green's functions the consideration of any other graphs, for example graphs of the type shown in fig. 2, is superfluous. The number of equations for determining

Fig. 1.

Fig. 2.

Fig. 3.

the values α_i is, indeed, equal to the number of independent contours in the graph, which is 2 in the example under discussion. Yet, the total number of values α_i equals 5 in this example; hence it is clear that one of them may be taken to equal zero, as a result of which this graph reduces to one of those considered above. It should be mentioned that these arguments likewise hold good for the graphs of the type shown in fig. 3, where a sum of momenta acts as a momentum.

3.2. SIMPLE VERTEX PART WITH THREE EXTERNAL ENDS

Let us proceed to a vertex part with three external ends. Since these represent three vectors lying in the same plane, according to the conservation laws, and the vectors k, l, ... may be obtained from (6) and (7), it is clear that the latter vectors lie in the same plane. Thus, the problem is reduced to a flat system of vectors.

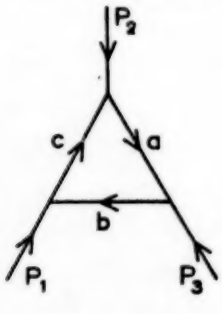

Fig. 4.

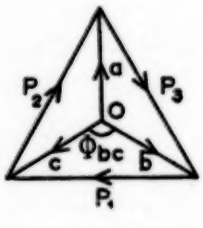

Fig. 5.

First of all, let us consider the simplest example, analysed in detail by R. Karplus, C. M. Sommerfield and E. H. Wichman [3]), as shown in fig. 4. It can easily be seen that the relation between vectors is represented by the scheme of fig. 5. The condition (7) obviously requires the point O to lie inside the triangle. It is implied that all vectors possess the properties of euclidean (not pseudo-euclidean) vectors, which can easily be proved for the nearest singularities.

Preliminarily, let us show how to express analytically the corresponding relations. First consider the scheme of fig. 5 which corresponds to the graph of fig. 4. If unit vectors $n_a = q_a/m_a$, $n_b = q_b/m_b$, $n_c = q_c/m_c$ are introduced, the condition (7) may be written as

$$\beta_a n_a + \beta_b n_b + \beta_c n_c = 0, \tag{8}$$

where $\beta_i = \alpha_i m_i$ are obviously positive quantities also. Projecting these equations on the vectors n_a, n_b, n_c consecutively and introducing the notations $(n_a n_b) = \mu_c = \cos \varphi_{ab}$ etc., we obtain three equations:

$$\begin{aligned} \beta_a + \beta_b \mu_c + \beta_c \mu_b &= 0, \\ \beta_a \mu_c + \beta_b + \beta_c \mu_a &= 0, \\ \beta_a \mu_b + \beta_b \mu_a + \beta_c &= 0. \end{aligned} \tag{9}$$

Making the determinant of this system equal to zero, we obtain the equation

$$1 + 2\mu_a \mu_b \mu_c = \mu_a^2 + \mu_b^2 + \mu_c^2, \tag{10}$$

which determines the situation of a singularity (if all β are simultaneously positive); μ_a, μ_b, μ_c are connected with p_1^2, p_2^2, p_3^2 by the formulae

$$\mu_a = \frac{m_b^2 + m_c^2 - p_1^2}{2m_b m_c}, \quad \mu_b = \frac{m_a^2 + m_c^2 - p_2^2}{2m_a m_c}, \quad \mu_c = \frac{m_a^2 + m_b^2 - p_3^2}{2m_a m_b}. \tag{11}$$

To return to the problem of the properties of vectors for the nearest singularities. Consider any angle, say φ_{bc}. According to (11) μ_a is a real quantity. It is greater than -1, since otherwise $p^2 > (m_b + m_c)^2$, i.e., we

Fig. 6.

would transcend the singularity determined by the graph in fig. 6, which is obtained from the graph under consideration through the elimination of one of the lines. At the same time we can see from (9) that no less than two out of three cosines of the angles should be negative. Now, a real angle corresponds to a negative cosine greater than -1. At least two of the three angles, therefore, are real. Since the sum of them equals 2π, the third angle is real as

well. Thus, fig. 5, which was mentioned in ref.[2]), solves the problem completely.

3.3. MORE COMPLEX GRAPHS WITH THREE EXTERNAL ENDS

Let us turn to more complex graphs. As an example, consider the graph shown in fig. 7. The scheme in fig. 8 corresponds to this graph. The construc-

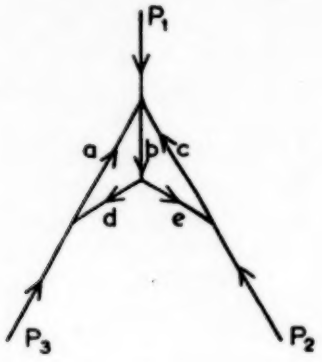

Fig. 7.

Fig. 8.

tion of this scheme is simple enough since every point in the Feynman graph corresponds to a polygon in the scheme with a number of sides equal to that of the rays converging at this point, while every polygon in the Feynman graph corresponds to a point of the scheme. The condition (7) calls for a certain disposition of the vectors a, b and d on the one hand, and b, c and e, on the other. It is not difficult to write an analytic expression of this figure. The triangle bde, as all other parts of the figure, is real, since the graph comprises only stable particles, and the mass of every particle in b, d, e is, therefore, less than the sum of the other two.

If one or several coefficients $\alpha_i = 0$ the graph is simplified. If, for example, $\alpha_c = 0$ the graph of fig. 7 will be reduced to the graph of fig. 9, similar to fig. 4.

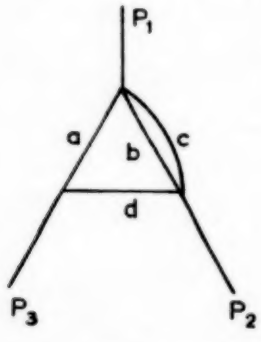

Fig. 9.

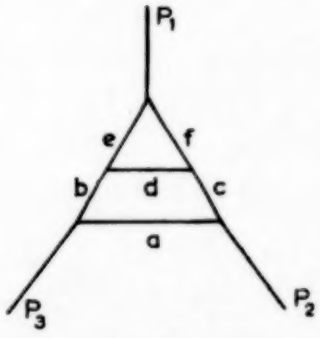

Fig. 10.

As we proceed to more complex Feynman graphs, it becomes apparent that often the case when all $\alpha_i = 0$ is impossible. Let us consider, for exam-

ple, the graph in fig. 10. The number of vector equations for α_i equals two in this case, i.e., we have four equations because the vectors lie in the same plane, while the number of the quantities α_i is six and therefore one of them may be assumed to equal zero. The same applies to the graph of the type shown in fig. 11.

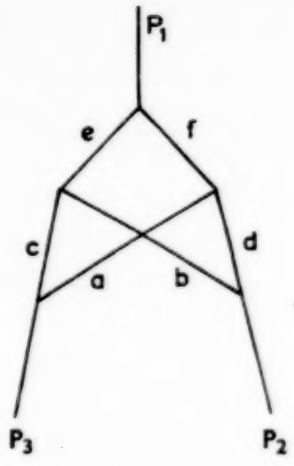

Fig. 11.

It can easily be seen how the above results change when what is meant is not the nearest singularities, that is, the emergence of complex values, but singularities of quantities that are already complex. If the singularity is not the nearest, we cannot, generally speaking, regard all angles as real, as was the case for the nearest singularities considered above.

First of all, consider the scheme of fig. 5 which corresponds to the graph of fig. 4. In the "euclidean" case with all the angles real, all μ_i lie between -1 and $+1$. In the general case a study of eq. (10) shows that the corresponding surface in the space μ_a, μ_b, μ_c consists of four parts intersecting each other at three points: $\mu_a = 1$, $\mu_b = -1$, $\mu_c = -1$, and the points obtained through the permutations of the indices a, b, c. One of these surfaces is limited by the triangle whose apices are the three points mentioned above. This triangle corresponds to the "euclidean" case. The three other surfaces extend to infinity, each starting from the corresponding point of intersection. On each of these surfaces one of the μ's is positive and exceeds 1, while the other two are negative and also exceed 1 in absolute value. As was pointed out, these surfaces always correspond to the non-nearest singular points.

It can easily be seen that the non-euclidean case is possible exclusively in the graph of fig. 4 out of all graphs considered above. In the scheme of fig. 8, for example, which corresponds to the graph of fig. 7, the vectors a, b, c on the one hand and a, b, d on the other, play the role of the vectors b, c, e. But, as was pointed out, the angles of the triangle formed by the vectors

b, d, e are always real. Otherwise, one of the particles b, d, e would not be stable. Yet, as was just mentioned, all cosines in the non-euclidean case should exceed unity in absolute value and consequently all angles should be complex.

3.4. GRAPHS WITH FOUR EXTERNAL ENDS

Let us proceed to the Feynman graphs with four ends. In this case it is obvious that we have to consider schemes which are located not in a plane but in space, which, naturally, complicates the problem a great deal. The most important of such graphs are the graphs with physical ends, i.e., those in which the squares of the corresponding momenta equal the squares of the particle masses. The simplest singularities are connected with the graphs of the type shown in fig. 12. The mean line may here correspond to a single particle or to several of them. The singularities of such a graph obviously correspond to

$$(p_1+p_2)^2 = m_a^2,$$

where m_a is the sum of the masses of the corresponding particles. The case of one particle yields an isolated pole, the case of two particles gives a singular line in the complex region.

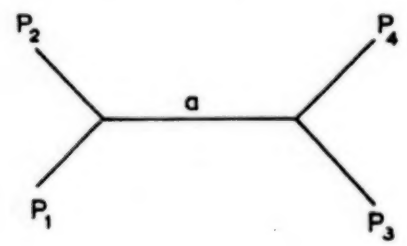

Fig. 12.

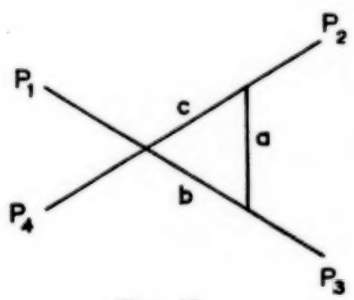

Fig. 13.

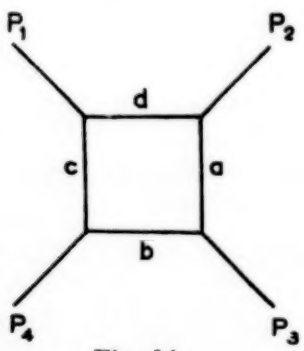

Fig. 14.

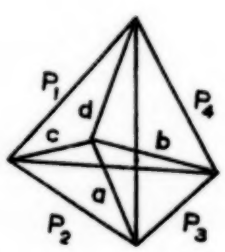

Fig. 15.

The graph in fig. 13 fully corresponds to the graph in fig. 4 and therefore no additional discussion is necessary.

The graph in fig. 14 corresponds to the scheme in fig. 15 where four of the six edges of the tetrahedron are determined by the length of free ends, while the two others equal p_1+p_2 and p_2+p_3 respectively. (It should be noted

that the graphic construction of this graph can be found in the paper of Karplus *et al.* [3].) A detailed analysis shows that here as well, if the nearest singularity is discussed, all angles are real and the condition that the central point should be located within the tetrahedron corresponds to the condition of the positiveness of the coefficients α. A more complex situation, which will not be discussed in the present paper, corresponds to the singularities in the complex region. Just as was done in the analysis of the three-end graphs, it is convenient to introduce four unit vectors in the directions of the vectors a, b, c, d and find an equation connecting the cosines of the angles between them. An equation of the fourth degree arises instead of eq. (10). The following fact is worth mentioning. If graphs with four physical ends are considered, the following condition should be fulfilled for the graph of fig. 13, as is clear from the scheme of fig. 5: the sum of the angle of the triangle abp_3 between the sides a and b, and the angle of the triangle acp_2 between the sides a and c, both of which are fixed by the masses of the corresponding particles, should exceed π. An analogous condition for the graph of fig. 14 evidently is that the sum of the four angles in the triangles, corresponding to the four vertices, should exceed 2π. Hence, it directly follows that a necessary, though certainly not sufficient condition, for the existence of the "non-trivial" nearest singularities is the presence of an obtuse angle in at least one of the triangles, which, in its turn, requires that the virtual decay of at least one particle should be described by an inequality of the type

$$m_2^2 > m_a^2 + m_c^2.$$

This relation obviously cannot be fulfilled either for π-mesons or for nucleons. The nearest singularities in the scattering of these particles on each other, therefore, correspond to the graph of fig. 12. It should be emphasized, however, that this does not apply to the singularities in the complex region.

4. Nature of Singularities

Now we shall consider the nature of the singularities thus obtained. Let us return to the basic formula (1), writing it as

$$\int (\varphi+K)^{-n} B \mathrm{d}^4k' \mathrm{d}^4l' \ldots \mathrm{d}\alpha_1 \mathrm{d}\alpha_2 \ldots \delta(\alpha_1 + \ldots + \alpha_n - 1).$$

Expanding φ with respect to the powers $\alpha'_i = \alpha_i - \alpha_{0i}$ where a_{0i} corresponds to the minimum value of φ, we can write this integral

$$\int (\varphi_0+Q)^{-n} B \mathrm{d}^4k' \mathrm{d}^4l' \ldots \mathrm{d}\alpha'_1 \mathrm{d}\alpha'_2 \ldots \delta(\alpha'_1 + \ldots + \alpha'_n), \qquad (12)$$

where φ_0 is the minimum value of φ_0 equal to zero in the singularity itself (the values of the vectors at the external ends being given), while Q is a quadratic function of the variables k', l', ... and the variables α'_i. To

elucidate the nature of the singularity, it is sufficient to consider the values B at $k' = l' = \ldots = 0$. If the power of the numerator with respect to the integration variables is lower than the power of the expression Q^n, the integral (12) converges at large values of these variables; in other words, its value is determined by the values of the variables corresponding to $Q \approx \varphi_0$, i.e., integration is carried out at small values of the variables, for which (12) has sufficient accuracy. It is evident that in this case (12) may be written as

$$\text{const.} \cdot \varphi_0^{\frac{1}{2}m-n} \tag{13}$$

where m is a number of integrations. If $m \geqq 2n$, the integral (12) does not converge and these arguments do not apply. To determine the nature of a singularity in this case the simplest way is to differentiate (12) with respect to φ_0 as many times as is necessary to make the power of the denominator greater than that of the numerator. After that we can make use of the formula obtained which should be integrated as many times. The integration constants obviously yield integer powers φ_0 which have no singularity at $\varphi_0 = 0$. Accordingly, we again obtain formula (13), with the exception of the case when $\frac{1}{2}m-n$ is zero or a positive integer. In this case, instead of (12) we obviously obtain

$$\text{const.} \cdot \varphi_0^{\frac{1}{2}m-n} \cdot \ln \varphi_0.$$

It should be noted that though the minimum is now discussed, these results may be applied to any extrenum φ as well.

The quantity n equals the number of internal lines in the Feynman graph; the number of vectors k with respect to which integration is carried out, equals the number ν of independent contours which make up the graph under consideration. Accordingly,

$$m = 4\nu+n-1.$$

Hence it follows that the nature of a singularity is determined by the expression $\varphi_0^{2\nu-\frac{1}{2}(n+1)}$ and, if $2\nu-\frac{1}{2}(n+1)$ is zero or a positive integer, by

$$\varphi_0^{2\nu-\frac{1}{2}(n+1)} \ln \varphi_0.$$

The quantity φ_0 is obviously proportional to the distance between the point under consideration and the hypersurface in the space p_i^2, $(p_i+p_k)^2$, in which singular points are situated. The number of contours should also include "biangles" which emerge when not one but several particles are conveyed along one line. For instance, $\nu = 2$ in the graph of fig. 9, and since $n = 4$, the singularity is of the nature of $\varphi_0^{\frac{3}{2}}$.

It will be noted that a more convenient number of vertices may be used than the number of independent contours. The number of independent contours, i.e., the number of independent integrations, equals the number of lines minus the number of additional conditions. The latter equals the

number of vertices less one, since one δ-function goes over into a final answer. Thus,

$$\nu = n - v + 1$$

(where v is a number of vertices) † and the power in the singularity may be written as $\frac{3}{2}(n+1)-2v$.

5. Summary

Let us formulate in brief the general rules for finding singularities. Various graphs with given external ends are considered. An arbitrary number of lines may converge at each vertex of such graphs, in agreement, of course, with the conservation laws (an odd number of π-meson lines cnnot pass through one point, for example). All particle stable in strong interactions may figure as lines. After that, a study is made of the scheme built on the principle of replacing the polygons in the graph by a scheme of vertices. The lengths of all internal lines in the scheme are equal to the corresponding masses. The essential intersections in the schemes (such as are obtained from the polygons in the graph) should satisfy the relation $\sum \alpha_i q_i = 0$, where q_i are the vectors proceeding from this intersection, and all $\alpha_i > 0$. The nearest singularities correspond to a scheme in euclidean space.

6. Application to Scattering Amplitude

A number of facts should be borne in mind in applying the results thus obtained to the scattering amplitude. Let us consider the scattering amplitude as a function of one variable x (which may be, for example, total energy or transferred momentum), regarding all other variables as given. The integrals considered above determine the functions whose values in the upper and lower semi-planes are connected by the relation $f(x^*) = f^*(x)$; in other words, the functions which are considered above and below the axis are actually different functions which are by no means analytic continuations of each other, and, generally speaking, we have a discontinuity if the values x are real. The scattering amplitude which is obtained when the Feynman rules of direction are observed, is in general of the form $a(x+i\delta)+b(x-i\delta)$, where δ is infinitesimal. The analytic properties considered above refer to the function $a(x+i\delta)$, extended by the vriable x into the upper semi-plane, and to the function $b(x-i\delta)$, extended into the lower semi-plane. The behaviour of the analytic continuation of the function $a(x+i\delta)$ into the lower semi-plane and of the function $b(x-i\delta)$ into the upper semi-plane by no means follows from the above.

† This was suggested to me by L. Okun and A. Rudik.

In an "alien" semi-plane the functions a and b may have any singularities located in any manner. Nor can they be determined from any general considerations. As is well-known, the proton-neutron scattering amplitude has, for example, apart from the singularity connected with the formation of a deuteron, another singularity connected with the virtual state of this system, which does not correspond to any real particle and lies precisely in an "alien" semi-plane with respect to the total energy of the system. Another example is the well-known resonance in the scattering of π-mesons on nucleons, which also corresponds to a singularity in an "alien" semi-plane, the total energy of the system being obviously complex. It is clear that such singularities cannot in principle be anticipated from general considerations, but may be obtained only from a theory yielding specific expressions for the scattering amplitude.

The problem is very much simplified in the case when there exists a region of values of x, for which the amplitude in question is real. Then we have two cuts through the real axis in the complex plane, and it is easy to see that the function $a(x+i\delta)$ has only the right cut, while the function $b(x-i\delta)$ has only the left one. If the quantity $a+b^*$ is considered instead of the scattering amplitude, for which it is sufficient to change the sign of the imaginary part of the amplitude in the left cut, we shall obtain a function which has no singularities in the upper semi-plane, which leads to the conventional dispersion relations.

The author is indebted to L. B. Okun, A. P. Rudik and Ya. A. Smorodinsky for numerous valuable comments.

References

1) X. Nambu, Nuovo Cimento **6** (1957) 1064
2) R. Karplus, C. M. Sommerfield and E. H. Wichman, Phys. Rev. **111** (1958) 1187
3) R. Karplus, C. M. Sommerfield and E. H. Wichman (preprint)

7.A *Nuclear Physics* **13** (1959) 193—203; © *North-Holland Publishing Co., Amsterdam*
Not to be reproduced by photoprint or microfilm without written permission from the publisher

A CHECK OF DISPERSION RELATIONS FOR PHOTOPRODUCTION OF π-MESONS

A. M. BALDIN and B. B. GOVORKOV
P. N. Lebedev Physical Institute, Moscow

Received 24 April 1959

Abstract: Experimental data on photoproduction of π-mesons in the near-threshold region are analysed and their essential discrepancy with the photoproduction amplitudes obtained by Chew *et al.* [1]) is revealed. A more detailed study of dispersion relations shows that, apart from these amplitudes, the dispersion relations themselves, obtained in ref. [1,2]) contradict experimental data if one uses the assumption that the amplitudes approach zero sufficiently rapidly at high energies.

1. Introduction

Comparison of the inferences from quantum field theory and the experimental data of π-meson physics is one of the most complex and stimulating problems. Until recently this comparison has not, in fact, been sound, for a great number of rather arbitrary (and often erroneous) assumptions lay between the basic postulates of field theory and the inferences which might be compared with experiment.

Considerable progress has been made following the evolution of methods based on a study of the basic analyticity properties of the scattering matrix. Dispersion relations connecting the imaginary and real parts of the scattering amplitude proved an especially powerful instrument in this respect.

Dispersion relations for π-meson photoproduction were obtained in ref. [1,2]). Explicit formulae for π-meson photoproduction amplitudes were derived from these dispersion relations in the work of Chew *et al.* on the basis of several particular assumptions. These amplitudes were compared with experiment in ref. [3,4,5]). The principal inference from these was that the amplitudes in question agree with experimental data. The assumptions that were made in determining the photoproduction amplitudes were thus justified. It will be noted, however, that usually characteristics comprising a large number of partial amplitudes were compared in this process. Predominant in such comparison are the resonance amplitude $(\frac{3}{2}, \frac{3}{2})$, which requires rather simple models to grasp the main features, and the amplitude connected with the "direct interaction" of the photon and the charged meson.

A more detailed comparison with experiment has been impossible so far,

since polarization experiments are indispensable to obtain more complete information on the partial amplitudes.

The latter observation, however, does not apply to the near-threshold energy region, in which a phase shift analysis of photoproduction is possible without resorting to polarization experiments. Besides, comparison between the amplitudes in this energy region and dispersion relations proves to be the simplest method, as will be shown below. Also, some assumptions used in ref. [1]) can be dispensed with. The present paper is not intended as a full exposition of the method indicated (which will be dealt with later on), nor as an exhaustive treatment of all data on photoproduction in this region. The paper is concerned with experimental data on π^0-mesonphoto-production on hydrogen near the threshold to obtain the principal parameters of the process. These are compared with the results which may be derived from dispersion relations with a few assumptions as possible. In conclusion, there is a short analysis as to the plausible causes of the discrepancy which has been found to exist between experimental data and dispersion relations.

2. Analysis of Experimental Data

Let us consider the data on π^0- meson photoproduction near the threshold. The near threshold region is understood to mean a region for which † $q < 1$, where q is the momentum of a meson in the centre of mass system. This corresponds to energies of photons from the threshold to 220 MeV. In this region, a very effective use can be made of the long-wave approximation. As usual, we assume that s- and p-waves predominate in this process. Let us expand the amplitudes concerned with respect to powers of q, by using the well known connection of photoproduction and π-meson scattering.

The s-wave part of the amplitude may be represented as follows:

$$f_s = f_s^{(0)} + i f_s^{(1)} q + f_s^{(2)} q^2 + i f_s^{(3)} q^3 + \dots \tag{1}$$

and the p-wave part as

$$f_p = f_p^{(1)} q + f_p^{(3)} q^3 + \cdots. \tag{2}$$

The cross section may be written as $d\sigma/d\Omega = q\omega|f|^2$, where $\omega = \sqrt{1+q^2}$.

Below we shall discuss mainly the photoproduction of neutral mesons for which the cross section in the indicated region may be represented with adequate accuracy as follows:

$$\frac{d\sigma}{d\Omega} = A + B\cos\theta + C\cos^2\theta.$$

† Here and in the following $\hbar = c = \mu = 1$, i.e., our cross sections should be multiplied by $(\hbar/\mu c)^2$ to obtain their values in cm².

In the experiment, the coefficients A, B and C are usually measured as functions of energy: A comprises the squares of s and p wave amplitudes, B the interference of s and p waves, C the squares of p wave amplitudes. Hence the coefficients A, B and C assume the form

$$\begin{aligned} A &= q\omega[A^{(0)}+A^{(2)}q^2+A^{(4)}q^4+\ldots], \\ B &= q\omega[B^{(1)}q+B^{(3)}q^3+B^{(5)}q^5+\ldots], \\ C &= q\omega[C^{(2)}q^2+C^{(4)}q^{(4)}+C^{(6)}q^6+\ldots]. \end{aligned} \tag{3}$$

Fig. 1 shows the experimental data for the process $\gamma+\mathrm{p}\to\pi^0+\mathrm{p}$. The graph represents the dependence of the experimental values of $A/\omega q^3$, $B/\omega q^2$, $C/\omega q^3$ upon the square of the momentum of the meson. As is clear

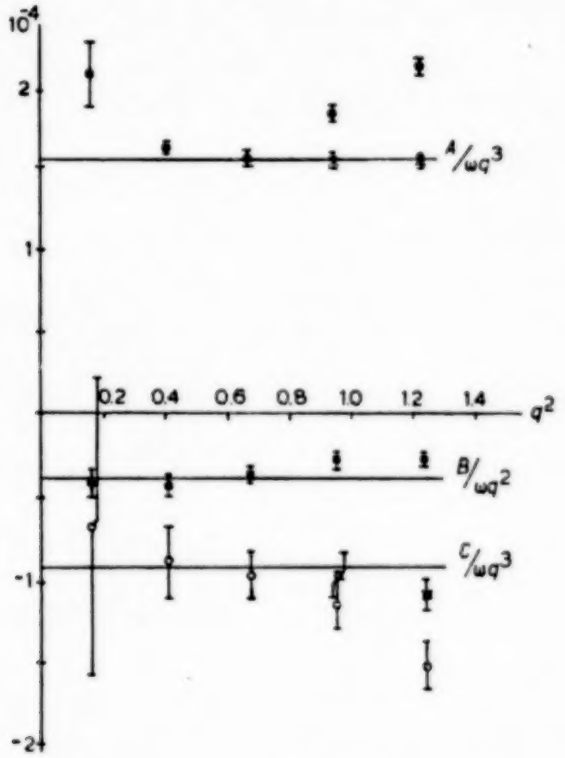

Fig. 1. Dependence of the measured quantities $A/\omega q^3$, $B/\omega q^2$, $C/\omega q^3$ on q^2 (q is the meson momentum).

from the chart, we may confine ourselves to the first terms of the expansion in (3) over a considerable region q^2 (up to $q \approx 0.7$) except for A, for which the first two terms of the expansion are essential in the region of small values of q. For large values of q, the next terms of the expansion become increasingly important. If the latter are calculated by the "resonance" model [7]) for $q>0.7$ and due readjustments are introduced, the values marked by asterisks † are obtained which fairly well agree with the magnitudes $A^{(0)}$, $B^{(1)}$ and $C^{(2)}$ produced for $q < 0.7$.

† These values correspond, not to $A/\omega q^3$ and $C/\omega q^3$, but to $A/\omega q[a_{33}q^2/\sin\delta_{33}]^2$ and $C/\omega q\,[a_{33}q^2/\sin\delta_{33}]^2$, where $a_{33} = \lim_{q\to 0}\delta_{33}/q^3$.

Treatments of the results shown in the graph yields

$$\begin{aligned} A^{(0)} &= \quad |0.085 \pm 0.35| \times 10^{-4}, \quad A^{(2)} = \quad |1.55 \pm 0.03| \times 10^{-4}; \\ B^{(1)} &= -|0.38 \pm 0.04| \times 10^{-4}; \quad C^{(2)} = -|0.91 \pm 0.14| \times 10^{-4}: \end{aligned} \tag{4}$$

$A^{(0)}$ contains the square of the real part of the s-wave, $A^{(2)}$ contains the p-wave part $A_p^{(2)} = A^{(2)} - A_s^{(2)}$, besides the imaginary s-wave part $A_s^{(2)}$. In our approximation, the p-wave amplitudes are purely real. As may easily be proved, the indicated amplitudes may be represented as follows:

$$C^{(2)} = K^2 - A_p^{(2)}, \qquad B^{(1)} = -2\sqrt{A^{(0)}}\, K, \tag{5}$$

where K is a new real parameter.

From (5) $A^{(0)}$ may be obtained independently of $A^{(0)}$ in eq. (4) if $A_s^{(2)}$ is determined on the basis of the data on photoproduction of charged mesons and of s-phase shifts of scattering, and then is subtracted from $A^{(2)}$. The comparison of the values of $A^{(0)}$ found by these two independent methods may serve as a check of our analysis.

As is well known [7]), the photoproduction amplitudes in a state with definite total momentum for the four processes

$$\begin{aligned} &\gamma + p \to \pi^+ + n \quad (+) \\ &\gamma + n \to \pi^- + p \quad (-) \\ &\gamma + p \to \pi^0 + p \quad (p_0) \\ &\gamma + n \to \pi^0 + n \quad (n_0) \end{aligned}$$

may be expressed through three real parameters and phase shifts of scattering. For S-photoproduction we shall take these parameters as follows:

$$\begin{aligned} &-N + i(\delta_1 - \delta_2)\tfrac{2}{3}E \mp \delta E && \text{for processes } (p_0) \text{ and } (n_0), \\ &\sqrt{2}[E + N + \tfrac{1}{3}iE(\delta_3 + 2\delta_1) \pm \delta E] && \text{for processes } (+) \text{ and } (-). \end{aligned}$$

Rough relations between these parameters

$$E : N : \delta E \approx 1 : \frac{1}{2M} : \frac{1}{2M}$$

(where M is the mass of a nucleon) have long been known. Even these relations and the data on the cross sections of the photoproduction of charged mesons are sufficient for the evaluation of $A_s^{(2)} = [(\delta_1 - \delta_3)\tfrac{1}{2}E]^2$. With the help of (5) we find

$$A^{(0)} = |0.08 \pm 0.02| \times 10^{-4} \tag{5}$$

which is in good agreement with

$$A^{(0)} = |0.085 \pm 0.035| \times 10^{-4},$$

obtained through an independent method before.

Let us find the parameters N and δE by using the data that have been obtained on the cross sections of photoproduction of π^+ and π^- mesons and the value $A^{(0)}$ that has been found above. From the experiments [8, 4]) measuring the cross section ratio σ^-/σ^+, this relation is

$$\frac{\sigma^-}{\sigma^+} \approx 1+4\frac{\delta E}{E} = 1.35; \tag{6}$$

E may be found from the cross sections σ^- and σ^+ measured experimentally near the threshold:

$$E \approx \sqrt{\frac{\sigma^+ + \sigma^-}{\omega q}}, \tag{7}$$

so that the parameter δE may be determined from (6). Then from

$$|-N-\delta E|^2 = A^{(0)}$$

it is possible to determine N.

Two possible solutions may be derived for N:

$$N = \begin{cases} -[0.44 \pm 0.04] \times 10^{-2} \\ +[0.123 \pm 0.04] \times 10^{-2}. \end{cases}$$

However, the first solution does not apply since it produces different signs of the interference terms (sign B) in σ^+ and $\sigma^{(p_0)}$, which contradicts the experiment [7, 6]).

Hence the amplitude of s-photoproduction of π^0-meson on neutron near the threshold may be found:

$$\sqrt{A_n^{(0)}} = |0.04 \pm 0.04| + 10^{-2}.$$

Thus this amplitude is near zero. A phase shift analysis of the p-wave is less simple. Yet, if quadrupole absorption is assumed to be absent, the amplitudes of the magnetic dipole transitions $M1_-$ and $M1_+$ may be found. To determine these two real magnitudes, we have indeed two equations

$$[M1_- - M1_+]^2 = (A_p^{(2)} + C^{(2)})q^2, \qquad 2[M1_+]^2 + [M1_-]^2 = (A_p^{(2)} + \tfrac{1}{3}C^{(2)})q^2.$$

Solving this system and utilizing the data (4), we obtain

$$\begin{aligned} |M1_+|^2 &= (0.54 \pm 0.03) \times 10^{-4} q^2, \\ |M1_-|^2 &= (0.0 \pm 0.1) \times 10^{-4} q^2. \end{aligned} \tag{9}$$

Thus, experimental data on the reaction (p_0) agree well with the description, if only those p-wave amplitudes which describe the magnetic dipole transition to the state of total momentum $\frac{3}{2}$ are assumed to differ from zero.

3. Dispersion Relations

Dispersion relations for the process of photoproduction in the c.m. system are written in terms of partial amplitudes [1,2]) as follows:

$$\mathrm{Re}\,\mathcal{F}_i(W,\tau_1) = \mathcal{F}_i^{\mathrm{B}} + \frac{1}{\pi}\int_{M+1}^{\infty} dW'\,\mathrm{Im}\sum_j \mathcal{F}_j(W',\nu_1)Q_{ij}(W,W',\nu_1) \quad (10)$$

where the $\mathcal{F}_i$ are quantities proportional to the individual amplitudes which make up the complete amplitude of the process, $W = \sqrt{M^2+q^2}+\sqrt{1+q^2}$ is the total energy,

$$\nu_1 = \frac{k\sqrt{1+q^2}-\mathbf{k}\cdot\mathbf{q}}{2M},$$

k the momentum of the photon, Q_{ij} known real functions.

We shall not expand equations (10) since they are extremely cumbersome. In deriving them, apart from the fundamental postulates of field theory, the only, yet essential, assumption that is made is that all photoproduction amplitudes vanish sufficiently rapidly for $W \to \infty$. If it were possible to compare these relations directly with experiment, this comparison would, above all, be a check of the assumption under discussion. An attempt at such a comparison and a discussion of the difficulties it involves will be undertaken later. Now, we shall begin by referring to the fact that, having made several assumptions, Chew, Goldberger, Low and Nambu derived explicit photoproduction amplitudes in the low-energy region from these general dispersion relations. These assumptions may in the main be reduced to the following points:

1) the upper limit of the dispersion integral is set at energies just beyond the first resonance in photoproduction;

2) the contribution from the unobservable energy region is assumed to be negligible;

3) the eqs. (10) are regarded as integral equations: the selection of the solutions is made by using the cut off model as a guide;

4) eqs. (10) are expanded with respect to the parameter $1/M$, and only the first terms of this expansion are taken into account.

If the amplitudes derived as a result of these considerations (eqs. (22.5), (22.6), (22.7) of ref. [1])) are used, we obtain the following numerical values for the parameters defined above:

$$N = 0, \qquad \delta E = +0.16\times 10^{-2};$$
$$|M1_-|^2 = 0.25\times 10^{-4}q^2, \qquad |M1_+|^2 = 0.502\times 10^{-4}q^2, \quad (11)$$

or

$$A^{(0)} = 0.026\times 10^{-4}, \quad B^{(1)} = -0.39\times 10^{-4}, \quad A^{(2)} = 1.14\times 10^{-4},$$
$$C^{(2)} = +0.32\times 10^{-4}. \quad (12)$$

Comparison of these values and the corresponding experimental data (cf. the previous section), reveals that the discrepancy reaches several standard deviations. This is an essential discrepancy between the amplitudes of ref. [1]) and experiment.

One's first and natural impulse is to question the four particular assumptions mentioned above. We used a method, therefore, free from these assumptions to a considerable extent. Our approach is an attempt to compare rigorous dispersion relations (10) with experiment. For the general case, this task is at present not feasible, yet for the region under discussion it is essentially simplified, for in our analysis, we in fact, use an expansion of the amplitudes in the neighbourhood of $q = 0$.

From the expression for the bounds of the non-physical region [2] in the c.m. system it will easily be seen that the unobservable energy region at $q=0$ vanishes. Therefore, after the parameters found in section 2 have been substituted into the left-hand side, the integral on the right-hand side will no longer contain any unobservable energy region and assumption (2) is thus eliminated. The amplitudes obtained experimentally are substituted into the integrand on the right-hand side. Therefore, any indeterminacy involved in the solution of integral equations (assumption (3)) is discounted. In our analysis an expansion (assumption (4)) does not result in any substantial simplification and therefore will not be carried out.

The largest discrepancy between theoretical and experimental values is observed in $C^{(2)}$.

In this connection let us consider the exact dispersion relations for the forward photoproduction amplitude. For the sake of simplicity only the part proportional to q will be considered †:

$$\begin{aligned}\sqrt{A_p^{(2)}+C^{(2)}} &= \left[\frac{\partial(\mathcal{F}_1^{(+)}+\mathcal{F}_1^{(0)})}{\partial q}\right]_{q=0} - \left[\frac{\mathcal{F}_2^{(+)}+\mathcal{F}_2^{(0)}}{q}\right]_{q\to 0} \\ &= ef\frac{g_p}{M}\left(\frac{2M+1}{2M}\right)\left(\frac{M}{M+1}\right)^{\frac{3}{2}}+I,\end{aligned} \tag{13}$$

where e, f are the renormalized charge and coupling constant, $g_p = 2.79$ the anomalous magnetic moment of a proton, and I the dispersion integral

† The notations of ref. [1]) are employed.

$$I=\frac{1}{\pi}\frac{2M+1}{M+1}\sqrt{\frac{M}{M+1}}\int_{M+1}^{\infty}dW'\,\frac{W'}{W'-M}\,\mathrm{Im}\left\{\frac{2W'}{(W'+M)^2}[\mathscr{F}'_1]\right.$$

$$\times\left[-\frac{1}{W'-M-1}-\frac{W'+\dfrac{M^2}{M+1}}{W'^2-\dfrac{M(M^2-M-1)}{M+1}}\right]\frac{1}{4M}\,\frac{2M+1}{M+1}-\frac{2W'}{(W'+M)^2}[\mathscr{F}_1]$$

$$\times\left[\frac{-W'^2+W'+\dfrac{M(M^2-1)}{M+1}}{\left(W'^2-\dfrac{M^3-M^2-M}{M+1}\right)^2}\right]\frac{2M+1}{M+1}+[\mathscr{F}'_2]\left[\frac{1}{W'+M+1}+\frac{W'-\dfrac{M^2}{M+1}}{W'^2-\dfrac{M^3-M^2-M}{M+1}}\right]$$

$$\times\frac{1}{4M}\,\frac{2M+1}{M+1}\,\frac{1}{\sqrt{\dfrac{(W'^2-M^2+1)}{4W'^2}}-1}+[\mathscr{F}_2]\,\frac{1}{\sqrt{\dfrac{(W'^2-M^2+1)}{4W'^2}}-1} \tag{14}$$

$$\times\left[\frac{W'^2-\dfrac{M(M^2-1)}{M+1}+W'}{\left(W'^2-\dfrac{M^3-M^2-M}{M+1}\right)^2\dfrac{M+1}{2M+1}}-\frac{1}{2M(W'-M-1)}-\frac{W'+\dfrac{M(M+2)}{M+1}}{2M\left(W'^2-\dfrac{M^3-M^2-M}{M+1}\right)}\right]$$

$$\left.+\frac{1}{2M}\,\frac{2W'}{(W'+M)^2}[\mathscr{F}_1]\times\left[\frac{1}{W'+M+1}+\frac{W'-M(M+2)}{W'^2-\dfrac{M^3-M^2-M}{M+1}}\right]\right\}.$$

Here $[\mathscr{F}_{1,2}]$ denotes the functions $\mathscr{F}^{+}_{1,2}(W',\nu_1)-\mathscr{F}^{(0)}_{1,2}(W',\nu_1)$ for $\nu_1\to$ $\to(2M+1)/4M(M+1)$, while $[\mathscr{F}_{1,2}]'$ denotes the derivatives of these functions with respect to ν_1, for $\nu_1\to(2M+1)/4M(M+1)$.

To estimate I is impossible without setting some upper limit, since at present the photoproduction of single mesons has been studied only in the region up to 1 GeV. As regards assumption (1), therefore, our result will differ from that of ref. [1]) in that the region beyond the first resonance and up to 1 GeV is taken into account.

For the photon energies from the threshold and up to $\approx$ 400 MeV, the main contribution to the integral comes from the resonance $(\frac{3}{2},\frac{3}{2})$; the imaginary parts of other amplitudes will be extremely small, since no such amplitudes have been discovered so far, except for the minor s-wave portion; the imaginary parts of these amplitudes contain still smaller phases as multiples. For this reason the other amplitudes in this region are neglected.

In the region 400—1000 MeV, an essential contribution is only made by the second resonance. In accord with a recent analysis [9]), a $D^{-}_{\frac{1}{2}}$-state is responsible for this resonance. From the above considerations it becomes

clear that the following expressions should be substituted in (13):

$$\operatorname{Im}[\mathscr{F}_1] = 3\,\frac{W'^2-M^2+1-\dfrac{2M+1}{M+1}\,\dfrac{2W'^2}{W'^2-M^2}}{\sqrt{(W^2-M^2+1)^2-4W^2}}\operatorname{Im} \mathrm{M1}_+ + \operatorname{Im}\ \mathrm{E2}_-,$$

$$\operatorname{Im}[\mathscr{F}_2] = 2\operatorname{Im} \mathrm{M1}_+, \tag{15}$$

$$\operatorname{Im}[\mathscr{F}'_1] = -\,\frac{12MW'}{(W'^2-M^2)\sqrt{\dfrac{(W'^2-M^2+1)^2}{4W^2}-1}}\operatorname{Im} M1_+,$$

$$\operatorname{Im}[\mathscr{F}'_2] = 0.$$

The value $\operatorname{Im} \mathrm{M1}_+$ may be obtained from the fact that the total cross section $\sigma_0{}^{\mathrm{t}}$ of the process (p_0) is almost entirely due to the resonance state, and from the relations of the processes of scattering and π-meson photoproduction:

$$\operatorname{Im} \mathrm{M1}_+ = \sqrt{\frac{W'^2-M^2}{16\pi W'}\,\frac{1}{\sqrt{\dfrac{(W'^2-M^2+1)^2}{4W'^2}-1}}\sigma_0{}^{\mathrm{t}}}\ \sin\delta_{33}.$$

The numerical integration of the part of I determined by $\mathrm{M1}_+$ only yields

$$I(\mathrm{M1}_+) = 0.15.$$

The contribution to I from the second resonance

$$\operatorname{Im}(\mathrm{E2}_-) \lesssim \sqrt{\sigma^{\mathrm{II}}},$$

where σ^{II} is the part of the cross section determined by the second resonance.

Taking σ^{II} from ref. [9]), in which all basic data pertaining to the second resonance are analysed, we obtain the rough estimate

$$I(\mathrm{E2}_-) < 0.02\times 10^{-2}.$$

The first term of the right-hand side of eq. (13) for $f^2 = 0.08$ amounts to 0.84×10^{-2}. Hence it follows that the principal contribution to $\sqrt{(A_{\mathrm{p}}{}^{(2)}+C^{(2)})}$ is made by the Born part of the amplitude. The contribution of the second resonance to I lies beyond the accuracy of our calculations.

To sum up, the dispersion relations yield the value

$$\sqrt{A_{\mathrm{p}}{}^{(2)}+C^{(2)}} = 0.99. \tag{16}$$

From the amplitudes of Chew, Goldberger, Nambu and Low it follows that

$$\sqrt{A_{\mathrm{p}}{}^{(2)}+C^{(2)}} = 1.21. \tag{17}$$

For this quantity experiment yields the value

$$\sqrt{A_{\mathrm{p}}{}^{(2)}+C^{(2)}} = 0.68\pm 0.09, \tag{18}$$

which obviously contradicts both theoretical values.

The difference between the theoretical values (16) and (17) may be accounted for by two reasons: a) in obtaining (16), the expansion with respect to $1/M$ was not carried out; b) in obtaining (17) the dispersion integral contained other amplitudes besides the resonance one, and in particular the large amplitude $M1_-$ contradicting our data.

Thus, the main cause of the discrepancy between the theoretical and experimental values of $\sqrt{(A_p^{(2)}+C^{(2)})}$ is not contained in the above particular assumptions.

4. Conclusion

1) A phase shift analysis of the photoproduction of π-mesons on protons has made it possible to determine the s-wave amplitude of this process by two independent methods. One of them, though less accurate, is a direct way of measuring the s-wave part and may safely be recommended for a more accurate evaluation of the parameter $A^{(0)}$ and, thus, of the amplitude of s-photoproduction on neutrons. Besides, it has been established that the contributions of other amplitudes (except for the resonance and s-wave amplitudes) lie beyond the accuracy of experiment.

2) Comparison of the amplitudes obtained by us and the results of ref. [1]) has revealed discrepancy between them.

3) Our method of comparing with the dispersion relations, free from the assumptions of the previous one [1]), has somewhat improved the situation; yet even in this case the discrepancy between the corollary of dispersion relations and experimental data comes up to more than three standard deviations.

Relations (10) will agree with experiment if the contribution of the energy region above 1 GeV not only fully compensates the contribution of the resonance $(\frac{3}{2}, \frac{3}{2})$, but also compensates the Born part of the amplitudes by approximately the same value.

It will be borne in mind, however, that even the second resonance in photoproduction makes a contribution lying beyond the accuracy of our analysis (this is clear from our proof).

References

1) G. Chew, M. Goldberger, F. Low and Y. Nambu, Phys. Rev. **106** (1957) 1345
2) A. Logunov, A. Tavkhelidze and L. Solovyov, Nuclear Physics **4** (1957) 427;
A. Logunov and V. Stepanov, Doklady AN SSSR **110** (1957) 368;
E. Carinoldesi, Nuovo Cimento **4** (1956) 1384
3) Goldwisser and L. Koester, Proc. of 7th Rochester Conf. (1957) 50

4) M. Beneventano, L. Bernardini, L. Stoppini and L. Tau, Nuovo Cimento **10** (1958) 1109
5) A. Lazarus, W. Panofsey and F. Tangherlini, preprint
6) V. Goldansky, B. Govorkov and R. Vassilkov, Nuclear Physics **12** (1959) 327
7) M. Gell-Mann and K. Watson, Amer. Rev. of Nuclear Science **4** (1954) 219
8) M. Adamovich, G. Kuzmicheva, V. Larionova and S. Kharlamov, JETP **35** (1958) 27; A. Baldin, Nuovo Cimento **7** (1958) 569
9) R. F. Peierls, Phys. Rev. Letters **1** (1958) 174

10.D *Nuclear Physics* **13** (1959) 204; © *North-Holland Publishing Co., Amsterdam*

BOOK REVIEW

Proceedings of the International Conference on Low Energy Nuclear Physics (*Paris, July* 1958) (Dunod, Paris 1959. 974 p. 95 fr. nouv.)

In July 1958, an international conference on low energy nuclear physics was held in Paris, under the joint sponsorship of the IUPAP and UNESCO. About 600 physicists participated, submitting more than 100 papers. These were grouped into the following categories: elastic scattering (neutrons, protons, heavier particles, electrons); direct interactions (theoretical, experimental); deuteron stripping; heavy ions; photo-nuclear reactions; shell model; collective model; connection between shell and collective models, nuclear matter; weak interactions. The papers in each category were presented to the Conference by a rapporteur. Their reports, together with transcripts of the lively discussions that followed them, constitute the first part of the Conference Proceedings. The second part consists of the papers themselves.

Most of the rapporteurs used the papers they were presenting as a framework on which to build a survey of the entire field. These surveys should prove valuable to newcomers. First of all, the Conference organizers were able to secure the services of the leading figures in each field, and as a result their reports are authoritative and up-to-date. Moreover they were written to be presented orally, and so are very clear. They have the further advantage over the usual review article that they were delivered to a critical audience, and thus the ensuing discussion emphasized the points in greatest need of further clarification. The actual discussions took place in French, English, and Russian, the three official Conference languages, but the Russian remarks are published here in French translation. This first part of the Proceedings ends with Professor Rosenfeld's summary of the conclusions and mood of the Conference. It is his impression . . . "that there is no spectacular discovery to be excited about, neither were we confronted with any acute contradiction between different experiments or between experiment and theory. . . . The attitude of experimenters and theorists alike in this so-called "low-energy" domain is not the adventurous one that is found at higher energies, but a more sedate one aiming at the consolidation of positions which have been acquired by the work of the preceding years."

The 8-month interval between the Conference and the appearance of the Proceedings seems rather long, especially since one of its principal functions is to provide early publication of the submitted papers. In a few cases expanded versions of these papers had already appeared elsewhere, but most of the material in the Proceedings appears there for the first time. In order to avoid further delay, the book had to go to press before the arrival from Moscow of the translations of 17 papers from their original Russian.

B. F. Bayman

A. DELOFF, Relativistic Coulomb wave function with definite asymptotic momentum and polarization 136

G. M. PROSPERI and A. SCOTTI, On the correspondence principle in quantum electrodynamics 140

JOHN W. MOFFAT, On the boson mass renormalization constants in pseudoscalar meson theory 150

J. S. R. CHISHOLM and E. J. SQUIRES, On the inclusion of hole-hole scattering in the Brueckner t-matrix 156

W. P. BUCHER, W. B. BEVERLY, G. C. COBB and F. L. HEREFORD, Polarization of 2- to 4-MeV neutrons scattered by deuterons 164

J. S. BELL and J. M. SOPER, Hard core correlations and nuclear moments . . . 167

F. R. METZGER and W. B. TODD, Lifetime of the 362-keV E1 transition in Tb^{159} 177

L. D. LANDAU, On analytic properties of vertex parts in quantum field theory 181

A. M. BALDIN AND B. B. GOVORKOV, A check of dispersion relations for photoproduction of π-mesons 193

Book review 204

NUCLEAR PHYSICS

ASSISTANT EDITOR

The Editor of NUCLEAR PHYSICS requires the assistance of a theoretical physicist for the reading and preparation of manuscripts for the press. The main requirements are:

(1) interest in and acquaintance with the methods of field theory and nuclear physics,

(2) interest in obtaining experience in the techniques of typography and editing,

(3) good knowledge of English.

The candidate is expected to reside in Copenhagen and may

(a) either be engaged on a full-time basis

(b) or be given the opportunity of pursuing research on a part-time basis.

The conditions of employment (salary, pension scheme, etc.) will be on the academic level, depending on the status and experience of the candidate.

Applications with details of scientific education and references should be sent to:
Professor L. Rosenfeld, NORDITA, Blegdamsvej 17,
COPENHAGEN, Denmark

NORTH-HOLLAND BOOKS

ASYMPTOTIC METHODS in ANALYSIS

by **N. G. DE BRUIJN** *Professor of Mathematics at the University of Amsterdam*

Asymptotics is that part of analysis which considers problems of the type dealt with in this book

Contents

Ch. I. Introduction
Ch. II. Implicit Functions
Ch. III. Summation
Ch. IV. The Laplace Method for Integrals
Ch. V. The Saddle Point Method
Ch. VI. Applications of the Saddle Point Method
Ch. VII. Indirect Asymptotics
Ch. VIII. Iterated Functions
Ch. IX. Differential Equations

6×9″ XII+200 pages Guilders 20.00 (40s.)